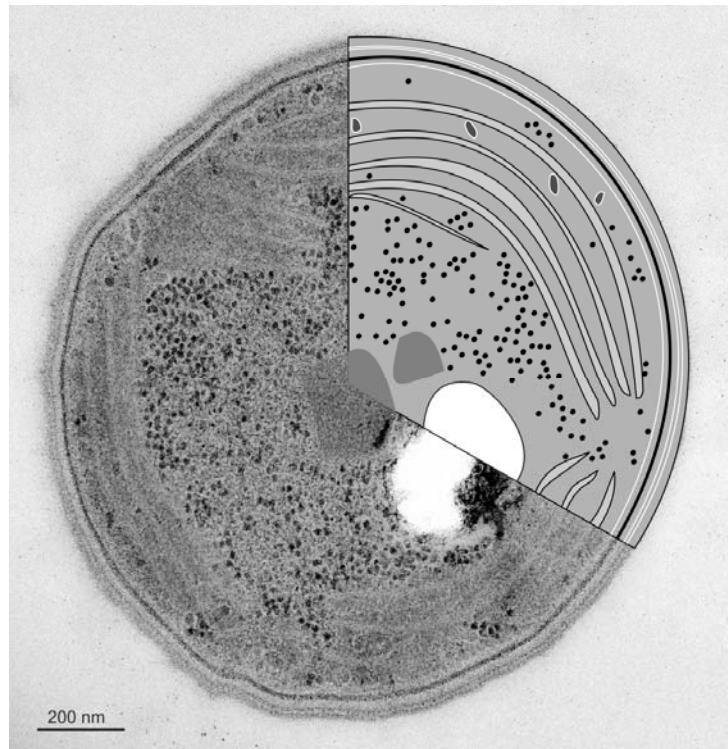


School of Doctoral Studies in Biological Sciences  
University of South Bohemia in České Budějovice  
Faculty of Science

# **Biosynthesis of chlorophyll-binding proteins in cyanobacteria**



Ph.D. Thesis

**Mgr. Lenka Bučinská**

Supervisor: Doc. Ing. Roman Sobotka, Ph.D.  
Institute of Microbiology, Academy of Sciences of the Czech Republic  
Faculty of Science, University of South Bohemia, České Budějovice

České Budějovice 2018



This thesis should be cited as:

Bučinská L (2018): Biosynthesis of chlorophyll-binding proteins in cyanobacteria, Ph.D. Thesis, in English. University of South Bohemia, Faculty of Science, School of Doctoral Studies in Biological Sciences, České Budějovice, Czech Republic, 132 pp.

#### ❖ **Annotation**

In oxygenic phototrophs, the photosynthetic machinery is located in thylakoid membrane (TM), a specialized endogenous membrane system. How TM are synthesized remains however mostly unknown. The aim of this thesis was to clarify a link between the synthesis of chlorophyll (Chl)-binding proteins, the main protein component of TM, and the formation of TM system in the model cyanobacterium *Synechocystis* PCC 6803. During the project, the analysis of TM under various growth conditions and in Chl-deficient mutants has demonstrated that a sufficient amount of de novo produced Chl molecules is crucial for the TM biogenesis. Particularly, the synthesis of the photosystem II subunit CP47 and trimeric photosystem I appeared to be sensitive to a shortage in de novo made Chl molecules. Interestingly, a specialized ribosome-binding protein (Pam68) has been identified to facilitate the insertion of Chl molecules into CP47. The synthesis of Chl-proteins and the biogenesis of TM have been further explored in cells recovering from long-term nitrogen depletion. Using this approach, it was possible to identify a large structure in the cell cytosol, which is very likely the site of TM biogenesis, and to correlate the appearance of this structure with the restored biogenesis of Chl-binding proteins.

### ❖ Declaration [in Czech]

Prohlašuji, že svoji disertační práci jsem vypracovala samostatně pouze s použitím pramenů a literatury uvedených v seznamu citované literatury.

Prohlašuji, že v souladu s § 47b zákona č. 111/1998 Sb. v platném znění souhlasím se zveřejněním své disertační práce, a to v úpravě vzniklé vypuštěním vyznačených částí archivovaných Přírodovědeckou fakultou elektronickou cestou ve veřejně přístupné části databáze STAG provozované Jihočeskou univerzitou v Českých Budějovicích na jejích internetových stránkách, a to se zachováním mého autorského práva k odevzdanému textu této kvalifikační práce. Souhlasím dále s tím, aby toutéž elektronickou cestou byly v souladu s uvedeným ustanovením zákona č. 111/1998 Sb. zveřejněny posudky školitele a oponentů práce i záznam o průběhu a výsledku obhajoby kvalifikační práce. Rovněž souhlasím s porovnáním textu mé kvalifikační práce s databází kvalifikačních prací Theses.cz provozovanou Národním registrem vysokoškolských kvalifikačních prací a systémem na odhalování plagiátů.

České Budějovice, 11.1.2019

.....  
Lenka Bučinská



This thesis originated from a partnership of Faculty of Science, University of South Bohemia, and Algatech Centre, Institute of Microbiology of ASCR. The electron microscopy part of the thesis was performed in the Laboratory of Electron microscopy, Biology centre ASCR and Ing. Jana Nebesářová, CSc. was a consultant outside of the university.



Přírodovědecká  
fakulta  
Faculty  
of Science



### ❖ Financial support

This work was financially supported by the Czech Science Foundation (GACR 17-08755S), and by project Algatech Plus of the Czech Ministry of Education (LO1416). I was also supported by a PhD student grant (GAJU 038/2012/P) of the Grant Agency of the University of South Bohemia and by a scholarship from the Czechoslovak Microscopy Society and FEI company (CSMS/FEI - 2014). The Laboratory of Electron Microscopy, the core facility of Biology Centre of CAS was supported by the MEYS CR (LM2015062 Czech-Biolmaging).

### ❖ Acknowledgements

I am extremely grateful to my supervisor Roman Sobotka. Roman brought me back to the scientific world in the time I was hesitant to proceed with this career. He was inspiring, thoughtful and patient the whole time of my PhD study and I thank him for the support and guidance during these years.

I thank Josef Komenda and Martin Tichý for their ideas, scientific discussion or overall help. I thank Jana Kopečná and Markéta Linhartová as they taught me a lot and never hesitated to answer my curious questions. I thank Eva Prachová, Léňa Moravcová and Baru Zdvihalová for their excellent technician's miracles that keep the lab running. I thank Peter Koník for providing the mass spectroscopy analyses and Honza Pilný for pigment analyses. I thank Vendula Krynická, Adélka Strašková, Pét'a Skotnicová and Helča Hönig-Mondeková for their fruitful discussions in the office, friendship and support not only during the last months. I also thank Iva Mozgová and her group for the collaboration and discussions on scientific or everyday's life topics. I thank our girl's gang "Hloupé buchty" for their friendship and support during everyday's lab routine. It was and still is, a pleasure to be a part of such a great lab and I sincerely thank all of the lab members-students, postdocs or staff for a friendly environment.

I thank Jana Nebesářová for the opportunity to keep working at the Laboratory of electron microscopy, which was always my second home. Even though I have gathered experience elsewhere and in the time shape my own electron microscopy knowledge I have never forgotten, where I have begun. I thank Petra Masařová, Martina Tesařová, Tomáš Bílý and Jirka Vaněček for their friendship and technical assistance whenever I have needed it during my PhD studies.

I am grateful to Heinz Schwarz, Matthias Floetenmeyer and Reza Shahidi for their help and guidance during my stay in Tübingen. They influenced my electron microscopic life, helped me to excel my skills and enlarged my microscopic knowledge.

I am indebted to Iris Maldener and Karl Forchhammer for the great opportunity of staying in their laboratories at Tübingen University.

I thank all my colleagues, collaborators or friends in science that had enriched my life.

I am grateful to all of my friends for their friendship and for making my life happier or sometimes crazier.

I thank my family for their never ending support and love.

## List of papers and author's contributions

The thesis is based on the following papers and manuscript (listed chronologically):

Kopečná J, Komenda J, **Bučinská L**, Sobotka R (2012). Long-term acclimation of the cyanobacterium *Synechocystis* PCC 6803 to high light is accompanied by an enhanced production of chlorophyll that is preferentially channelled to trimeric PSI. *Plant Physiol.* 160 (4): 2239-2250. (DOI:10.1104/pp.112.207274) (IF=6.4).

*L.B. performed ultrastructural analyses by transmission electron microscopy (TEM).*

Hollingshead S, Kopečná J, Armstrong D R, **Bučinská L**, Jackson P J, Chen G E, Dickman M J, Williamson M P, Sobotka R & Hunter C N (2016). Synthesis of Chlorophyll-binding proteins in a fully segregated  $\Delta ycf54$  strain of the cyanobacterium *Synechocystis* PCC 6803. *Front Plant Sci.* 7: 1–15. (DOI:10.3389/fpls.2016.00292) (IF=4.3)

*L.B. performed ultrastructural analyses by TEM.*

Klotz A, Georg J, **Bučinská L**, Watanabe S, Reimann V, Januszewski W, Sobotka R, Jendrossek D, Hess R W, Forchhammer K (2016). Awakening of a dormant cyanobacterium from nitrogen chlorosis reveals a genetically determined program. *Curr Biol.* 26 (21): 2862-2872. (doi:10.1016/j.cub.2016.08.054) (IF=8.8)

*L.B. performed ultrastructural analyses by TEM and the analysis of cell re-greening. L.B. further participated in data processing and contributed to the manuscript preparation.*

**Bučinská L**, Kiss E, Koník P, Knoppová J, Komenda J and Sobotka R (2018). The ribosome-bound protein Pam68 promotes insertion of chlorophyll into the CP47 subunit of Photosystem II. *Plant Physiol.* 176 (4): 2931-2942. (doi:10.1104/pp.18.00061) (IF=6.4)

*L.B. carried all experiments except of MS analyses, radiolabeling and the characterizations of mutants after ferrochelatase inhibition. L.B. also participated in data processing and their evaluation, and contributed equally to writing and reviewing of the manuscript.*

**Bučinská L**, Bílý T, Nebesářová J and Sobotka R Biogenesis of cyanobacterial thylakoid membrane during the recovery from chlorosis. *Manuscript in preparation*

*L.B. carried all experiments except of 3D model rendering by Amira software. L.B. participated in data processing and their evaluation, and contributed equally to writing and reviewing of the manuscript.*

I hereby confirm that Lenka Bučinská contributed to the mentioned publications as described above.

.....

Doc. Ing. Roman Sobotka, Ph.D.

All TEM figures presented in this thesis have been prepared by Lenka Bučinská in Laboratory of Electron Microscopy, Biology Centre ASCR (České Budějovice) or during the scientific visit at Max Planck Institute for Developmental Biology (Tübingen, Germany), if not stated otherwise.

# Contents

List of abbreviations	viii
<b>1. Preface</b>	1
1.1 Oxygenic photosynthesis and biological membrane	1
1.2. Aims of the thesis	5
<b>2. Introduction</b>	7
2.1. Fine ultrastructure of cyanobacteria and chloroplast	7
2.2. The architecture of thylakoid membrane	8
2.2.1. Molecular organization of thylakoid membranes	11
2.2.2. Lateral heterogeneity and micro-domain organization in TM	15
2.3. Biogenesis of photosystems - a current view	17
2.4. The role of cofactors in the synthesis of photosystems	19
2.5. The biogenesis of thylakoid membrane	23
<b>3. Unpublished results</b>	26
3.1. Biogenesis of cyanobacterial TM during the recovery from chlorosis	26
<b>4. Discussion</b>	34
<b>5. Material and methods</b>	40
<b>6. Summary</b>	43
<b>7. Conclusions</b>	46
<b>8. Literature</b>	48
<b>9. Published results</b>	62
9.1. Publication I: Long-term acclimation of the cyanobacterium <i>Synechocystis</i> PCC 6803 to high light is accompanied by an enhanced production of chlorophyll that is preferentially channelled to trimeric PSI.	62
9.2. Publication II: Synthesis of Chlorophyll-binding proteins in a fully segregated $\Delta ycf54$ strain of the cyanobacterium <i>Synechocystis</i> PCC 6803.	76
9.3. Publication III: The ribosome-bound protein Pam68 promotes insertion of chlorophyll into the CP47 subunit of Photosystem II.	92
9.4. Publication IV: Awakening of a dormant cyanobacterium from nitrogen chlorosis reveals a genetically determined program.	106

## List of abbreviations

<i>Synechocystis</i>	<i>Synechocystis</i> sp. PCC 6803
WT	Wild type
PSI	Photosystem I
PSII	Photosystem II
Cyt <i>b<sub>6</sub>f</i>	Cytochrome <i>b<sub>6</sub>f</i>
ATPase	ATP synthase
LHCI	Light-harvesting complexes I
LHCII	Light-harvesting complexes II
RCII	PSII assembly intermediate containing D1, D2, Cyt <i>b-559</i> and PsbI subunits
RC47	RCII with CP47 module attached
CP47m	CP47 assembly module
pD1	Precursor of D1 protein
Chl	Chlorophyll
ChlM	Mg-protoporphyrin IX methyltransferase
MGDG	Monogalactosyldiacylglycerol
DGDG	Digalactosyldiacylglycerol
SQDG	Sulfolipid sulfoquinovosyldiacylglycerol
PG	Phosphatidylglycerol
TM	Thylakoid membrane
PM	Plasma membrane
TC	Thylakoid center
PHB	Poly- $\beta$ -hydroxybutyrate
TEM	Transmission electron microscopy
GFP	Green fluorescent proteins
YFP	Yellow fluorescent proteins
CN-PAGE	Clear-native electrophoresis
HII phase	Hexagonal organization of MGDG
PDM	PratA-defined membrane
Hlips	High light inducible proteins

# 1. Preface

## 1.1 Oxygenic photosynthesis and biological membrane

Photosynthesis is a fundamental biochemical process on Earth evolved by ancient microorganisms around 3 billion years ago to convert the energy of photons into the energy of chemical bonds. Generally, the photosynthesis is a series of biochemical reactions by which organisms utilize light to photo-oxidize certain chemical compounds; the withdrawing of the high-energy electrons powers the cell metabolism. Behind this general description, there is a vast diversity of how the photosynthesis is performed by various groups of phototrophs. Nonetheless, all phototrophs can be divided into two large groups based on their ability to use water as the source of electrons or not. Whereas various (anoxygenic) photosynthetic bacteria utilize reductants such as sulphur or iron that are easier to oxidize than water, cyanobacteria, algae and plants (oxygenic phototrophs) possess photosynthetic machinery that is able to extract electrons from water. Because water is a ubiquitous molecule and thus a never-ending source of electrons, oxygenic phototrophs have spread to all possible habitats and became the dominant group of organisms on our planet (Bar-On et al., 2018). Oxygen, as a by-product of photosynthetic water oxidation, has been released in a massive amount into the atmosphere during aeons shifting the whole planet from a reducing to an oxidative environment. There is no other biochemical process but photosynthesis with such a dramatic impact on Earth geochemistry and, consequently, on the evolution of life.

Three key inventions of nature appear to be crucial for the success of oxygenic photosynthesis: a combination of *two different types of light-powered reaction centers* (Photosystem I and II; PSI and PSII), *chlorophyll (Chl) molecules* providing very strong redox potential, and a unique endogenous (*thylakoid*) *membrane system* (TM). Very likely, the oxygenic photosynthesis was not accommodated in the TM at its earliest time but the invention of TM had certainly a dramatic impact on the performance of photosynthetic cells. As will be discussed later in details, the TM is a specialized galactolipid-rich membrane system that accommodates the entire complicated apparatus for oxygenic photosynthesis – hundreds of proteins and many different cofactors. However, four multi-subunit pigment-protein complexes are particularly abundant. PSI and PSII, cytochrome *b<sub>6</sub>f* (Cyt *b<sub>6</sub>f*) and ATP synthase (ATPase) are submerged in TM (Figure 1) working in parallel like a nano-scaled solar plant, which extracts and utilizes electrons from water to synthesize NADPH and ATP (Blankenship, 2013).

Whereas the Cyt *b<sub>6</sub>f* (more precisely its homologue cytochrome *bc*1) and ATPase are very common in all forms of life, PSI and PSII are complicated, light-powered photo-oxidoreductase enzymes, which are both essential and specific for oxygenic

photosynthesis. PSI and PSII are multi-subunits membrane complexes that contain Chl and carotenoid pigments as well as other cofactors such as quinones or iron-sulfur clusters. The PSII functions as a very strong photo-oxidase, which is able to oxidize water molecules via a special cluster of manganese atoms attached on the luminal side (inside of the TM vesicles). Collected electrons are passed on plastoquinone molecules dissolved in the TM bilayer. Cyt *b<sub>6</sub>f* is a proton pump oxidizing plastoquinol (a reduced form plastoquinone) to generate proton gradient; the resulting low-energy electrons are transferred to soluble electron carriers such as plastocyanin or cytochrome c553 (Figure 1). Here, the unique combination of two different photosystems mentioned earlier comes in play. In heterotrophic organisms, the low-energy electrons cannot be further utilized and must be passed to a terminal acceptor (*e.g.* oxygen). However, PSI is a very strong, light-powered reductase, which is able to take electrons from plastocyanin and to increase their energy enough for the production of NADPH – a crucial molecule providing redox power for the cell (Figure 1). The proton-motive force, established by PSII and Cyt *b<sub>6</sub>f* complexes, is finally consumed by ATPase to synthesize ATP molecules. ATP and NADPH molecules are an outcome of the light reaction of photosynthesis and the produced majority is used to reduce and incorporate CO<sub>2</sub> molecules into carbohydrates (Blankenship, 2013; Figure 1).

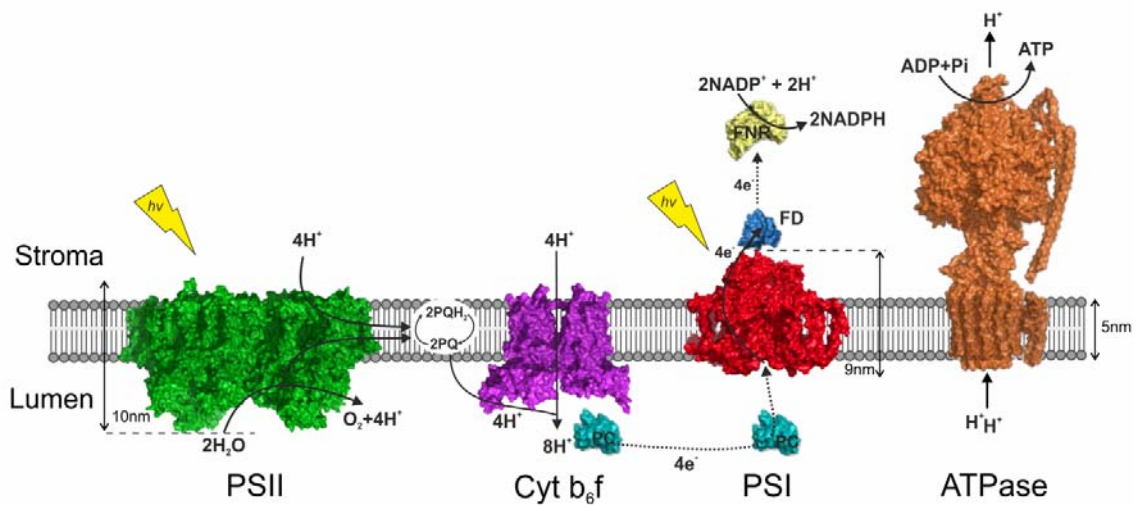


**Figure 1. A model of TM with embedded photosynthetic machinery.** The picture was adopted from Kern et al. (2009) and altered according to MacGregor-Chatwin et al. (2017). Photosystem II - PSII; Cytochrome *b<sub>6</sub>f* - Cyt *b<sub>6</sub>f*; Photosystem I - PSI; ATP synthase – ATPase; Ferredoxin – FD; Plastocyanin - PC.

Chl molecules are essential cofactors of PSI and PSII, almost all photochemistry in photosystems are based on the unique chemical properties of this pigment. Photosystems contain their own apparatus to collect light energy, so-called inner antennas, in which



Chls serve as light-absorbing chromophores. Once a Chl captures light quanta, the energy (exciton) is channelled into the reaction center of the photosystem. Here, a special Chl couple serves a different role. If excited this Chl pair acquires very strong oxidoreduction power, strong enough to extract electrons from the water (in the case of PSII) or to reduce ferredoxin (PSI; see Figure 1). In living systems, such strong oxidoreduction properties are known only for PSI and PSII. Anoxygenic bacteria contain photosynthetic complexes similar to PSII (type II reaction center) or PSI (type I reaction centers), but it is always one type of the reaction center per the cell. Moreover, Chl pigments are replaced by bacteriochlorophylls absorbing in longer wavelengths and the central bacteriochlorophyll pair thus provides weaker redox power than the Chl pair and is not sufficient to oxidize water.

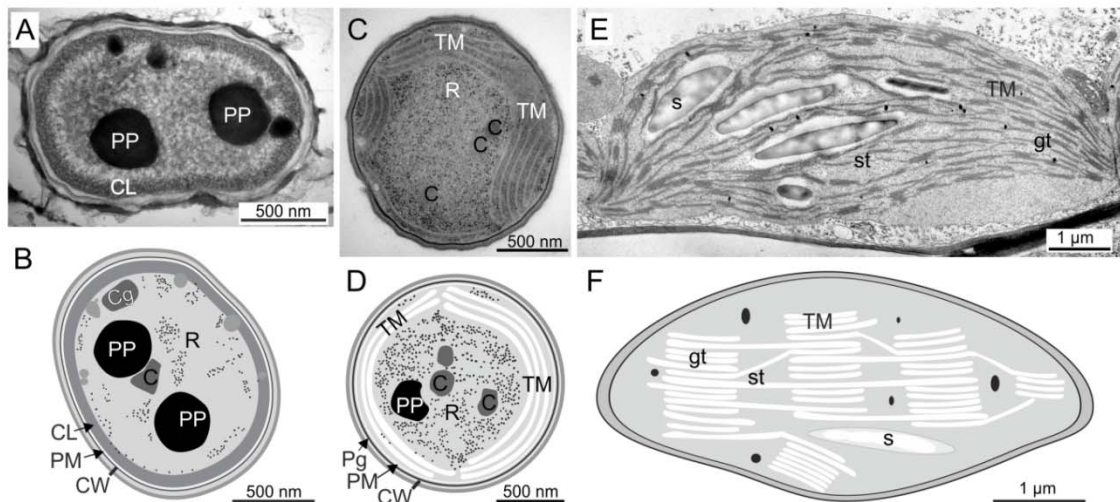


**Figure 2. Organization of TM in cyanobacteria and chloroplast revealed by electron microscopy.** A) A primitive cyanobacterium *Gloeobacter* sp. lacking TM; credit to Jan Mareš (University of South Bohemia) and (B) a model drawn according to Rippka et al. (1974). C) Cyanobacterium *Synechocystis* PCC 6803 grown photoautotrophically under low-stress condition. D) A model of the *Synechocystis* cell. E) Chloroplast of the plant *Arabidopsis thaliana* and a scheme of plant TM (F). Abbreviations used: carboxysome – C; cyanophycin granule – CG; an electron-dense cortical layer of phycobilisomes attached to plasma membrane – CL; Cell wall – CW; polyphosphate granules – PP; ribosomes – R; starch inclusions – S; stacked grana thylakoids – gt; stromal unstacked grana thylakoids – st.

The endogenous TM system dramatically increases the total membrane surface in the cell (Figure 2) and thereby the concentration of photosynthetic complexes and autotrophic performance. The TM probably co-evolved with the oxygenic photosynthesis as the unique TM lipids are also essential structural components of PSI and PSII (see later). It is however very likely that the primitive cyanobacteria had photosynthetic apparatus located entirely in the plasma membrane (PM). This assumption is based on the existence of

‘living fossil’ - the primordial cyanobacterium *Gloeobacter* sp. In contrast to other groups of cyanobacteria, *Gloeobacter* does not possess TM and both photosynthetic and respiratory apparatus are located within the PM (Rippka et al., 1974; Rexroth et al., 2011; Figure 2 A,B). It is worth noting that the proliferation of *Gloeobacter* sp., which has a base position in the phylogeny tree of cyanobacteria (Ponce-Toledo et al., 2017) is extremely slow (Rippka et al., 1974).

The eukaryotic phototrophs, algae and plants, have very probably evolved through endosymbiosis when eukaryotic host cell engulfed the ancestor of a cyanobacterium approximately 1.5 billion years ago (Yoon et al., 2004). This event resulted in the origin of chloroplast (Figure 2 E,F), an organelle that contains TM system resembling the cyanobacterial thylakoids (Figure 2 C,D). Notably, the lipid moiety of TM is highly conserved between cyanobacteria and the eukaryotic phototrophs despite the amount of time that has passed since this primary endosymbiosis. TM is dominated (>70%) by galactolipids - a specific group of glycolipids, whose sugar group is galactose. It contrasts to bacterial and non-photosynthetic eukaryotic membrane systems that are composed mostly of phospholipids (Wada and Murata, 1998).

It should be noted that the cyanobacteria are not the only prokaryotic phototrophs with an inner membrane system. Some bacterial groups, for example, the purple bacteria typified by the model organism *Rhodobacter sphaeroides*, have also evolved specialized intracytoplasmic membrane system in order to increase the cellular concentration of reaction centers and light-harvesting antennae (Golecki and Oelze, 1980). In contrast to the TM, the bacterial inner membranes are not permanent and the formation of these vesicles-like structures (chromatophores) is triggered together with the synthesis of photosynthetic complexes under low-oxygen conditions (Scheuring et al., 2014). Whereas the biogenesis of TM remains enigmatic (see later), the bacterial inner membrane system is clearly derived from the PM by invagination, a process which has been characterized in details (Tucker et al., 2010). The chemical composition of chromatophores is indeed similar to the PM and contains mostly phospholipids. It is however interesting that one particular sulfolipid - sulfoquinovosyldiacylglycerol (SQDG), which is an important TM lipid, is present in many anoxygenic phototrophs though at relatively low concentration (Imhoff et al., 1982). Nonetheless, it is not clear yet if there is any functional link between anoxygenic photosynthesis and SQDG (Benning, 1998; Sato, 2004).

TMs are typically very rich of Chl-binding proteins. Taking into account the fact that Chl molecules are potentially highly phototoxic, the concentration of this pigment in the TM is astonishing. In cyanobacteria and red algae, almost all Chls (> 90%) are localized in PSI and PSII; core protein subunits of both photosystems contain many Chl molecules and without Chl the PSI/PSII synthesis is abolished (Kopečná et al., 2013). It is therefore not surprising that the biogenesis of TM appears to be closely linked (or perhaps

triggered) to the biosynthesis of Chl-binding subunits of photosystems and/or to the process of their assembly (Sobotka et al., 2008; Hollingshead et al., 2016). Unlike cyanobacteria, the most abundant Chl-proteins in green algae and plants are light-harvesting complexes (LHC) II delivering light to PSII. While the lack of LHCII proteins causes indeed defects in the TM organization, the photosystems are produced and plants are viable suggesting that LHCII are not essential for the plant TM biogenesis (Murray and Kohorn, 1991; Kovács et al., 2006). In contrast, the inhibition of the Chl pathway in plants has a devastating impact on the TM system similarly as in cyanobacteria. The formation of TM is practically abolished or drastically delayed (Kirchhoff et al., 1989; Frick et al., 2003; Liu et al., 2007; Sheng et al., 2017). The crucial role of Chl in TM biogenesis is in the line with the fact that the development of chloroplast during photomorphogenesis is synchronized with the activation of protochlorophyllide oxidoreductase (Henningsen and Boynton, 1974), an enzyme in Chl biosynthesis, which is very abundant in etioplasts but requires photons for the activity (Lebedev and Timko, 1998; Yuan et al., 2012).

## **1.2. Aims of the thesis**

Molecular mechanisms, by which the TM is produced and how the synthesis of Chl-protein complexes and biogenesis of the TM are linked, remain enigmatic. In cyanobacteria, there is no clear-cut observation of the connections between TM and PM or a presence of vesicular transport (Liberton et al., 2006; Nevo et al., 2007). The site of PSI/PSII biogenesis is not known. Recently, a model of biogenesis center (thylakoid center) has been elaborated (Rast et al., 2015) but it is not supported yet by conclusive data. In plants, the situation is a bit different because the biogenesis of the TM can be monitored during the transition from non-photosynthetic etioplasts or protoplasts (immature plastid) to chloroplast (Henningsen and Boynton, 1974; Kowalewska et al., 2016; Liang et al., 2018). The developing of the TM in plants is thus better characterized and it is accepted that in plants this process includes (eukaryotic) vesicular transport system (Kroll et al., 2001; Vothknecht and Westhoff, 2001; Kowalewska et al., 2016; Liang et al., 2018). However, there are no further details about the biogenesis of photosystems during development or maintaining the TM in the chloroplasts.

At the starting line of this work, we have proposed that it is probably not possible (or at least not rationale) to separate a putative molecular mechanism called thylakoid biogenesis from the processes related to the biogenesis of photosystems including Chl formation. Based on various bits of data, which are discussed later, we assumed that there is large cellular machinery producing both photosystems and this site is phenomenally identical to the origin of the TM. However, the biogenesis of photosystems and the formation of the TM are historically investigated by researchers from rather distant fields

who are using completely different techniques (molecular and biochemical versus microscopical). It is thus mostly not possible to combine and correlate available data.

The aim of this thesis was to explore the biosynthesis of Chl-protein complexes in cyanobacteria in the context of the biogenesis of the TM system. The ambition was to clarify how the Chl-protein biosynthesis is integrated into the process of the TM formation. In order to study the production of the TM in cyanobacteria from ‘scratch’ (resembling the etioplast – chloroplast transition), we focused on the recovery of cyanobacterial cells from nitrogen starvation. If long-term starved cyanobacteria almost completely lost photosynthetic complexes, the replenishing of nitrogen leads to a quick re-formation of the whole photosynthetic apparatus and the TM. Our specific objective was to monitor this process on both molecular and microscopical levels.

In this thesis, the cyanobacterium *Synechocystis* PCC 6803 (hereafter *Synechocystis*) was used as an experimental organism. *Synechocystis* has become a frequently utilized model in photosynthesis research as it combines the advantage of being a relatively fast growing gram-negative bacterium that is viable even entirely heterotrophically without functional photosynthetic apparatus. *Synechocystis* is also able to survive for months without essential nutrients like nitrogen or sulfur; a feature that is related to this project. The sequenced *Synechocystis* genome is available for a long time (Kaneko et al., 1996), it was several times re-annotated and large sets of transcriptomic data are also available (Kopf et al., 2014). The targeted mutagenesis of *Synechocystis* is relatively easy task thanks to an efficient homologous double recombination and spontaneous uptake of foreign DNA. Thousands of *Synechocystis* mutants have been generated and they are usually available on a request. As cyanobacteria share a common ancestor with a progenitor of chloroplast the photosynthetic processes are conserved and the research performed on *Synechocystis* is often directly applicable to plants and algae (Chidgey et al., 2014; Knoppová et al., 2014).

## 2. Introduction

### 2.1. Fine ultrastructure of cyanobacteria and chloroplast

Since the early 60s cyanobacteria and chloroplast began to be examined by methods of transmission electron microscopy (TEM). The pioneer work of Stanier and Cohen-Bazire started a new era and brought a novel description of cyanobacterial ultrastructure (Stanier and Cohen-Bazire, 1977; Stanier, 1988). Details of chloroplast ultrastructure are available even for a longer period (Menke, 1960). Traditional methods of TEM based on chemical fixatives or using the freeze fracture (etching) techniques were in time replaced by cryo-methods employing high-pressure freezing with freeze-substitution that are considered to preserve the ultrastructure closer to the native arrangement in the cell (Liberton et al., 2006; van de Meene et al., 2006; Nevo et al., 2007) Figure 3B, C). Nowadays, the cryo-TEM methods such as cryo-tomography and its variants are used frequently in ultrastructural research (Engel et al., 2015; Schaffer et al., 2017); yet the „traditional“ TEM protocols can still bring intended results (Noda et al., 2017; Yamane et al., 2018; Figure 5 C,D,E).

Cyanobacteria are classified as gram-negative bacteria as their cell envelope is made by two distinct membranes, an outer membrane and PM that are separated by a periplasmic space with electron-opaque peptidoglycan layer in-between (Figure 3 B,D; Stanier and Cohen-Bazire, 1977). However, regarding the cell morphology, cyanobacteria are a very variable group of prokaryotes, even if we omit a huge diversity of filamentous and heterocyst-forming species. Certain cyanobacterial species have their cells covered by an extra glycoprotein surface layer, organized into a typical hexagonally shaped network (Šmarda et al., 2002). The central part of the cell, devoid of TM, is filled with DNA and ribosomes together with a number of inclusions or storage granules that accumulate here (van de Meene et al., 2006; Gonzalez-Esquer et al., 2016; Figure 2 C,D; Figure 3 A,C,E), for example due to the lack of a certain nutrient or fluctuating growth conditions (Allen, 1984; Kopečná et al., 2012). Storage granules can be electron dense (dark) such as structured cyanophycin granules (Allen and Weathers, 1980) or polyphosphate granules (Liberton et al., 2011). On the other hand, granules of stored carbohydrates, such are large bodies of poly- $\beta$ -hydroxybutyrate (PHB; (Porta et al., 2000) and small rounded granules of glycogen polymer, can be opaque (electron-transparent; Welkie et al., 2013). Interestingly, glycogen granules are often found filling the space between the TM sheets (Figure 3 E,F); particularly when the cells are grown in the presence of glucose or under high light intensities (Kopečná et al., 2012). The content of glycogen and PHB granule is particularly very high under nitrogen-limited conditions (Welkie et al., 2013; Klotz et al., 2016; chapter 3). Other typical structures in cyanobacteria are polyhedral carboxysomes (Orus et al., 1995).

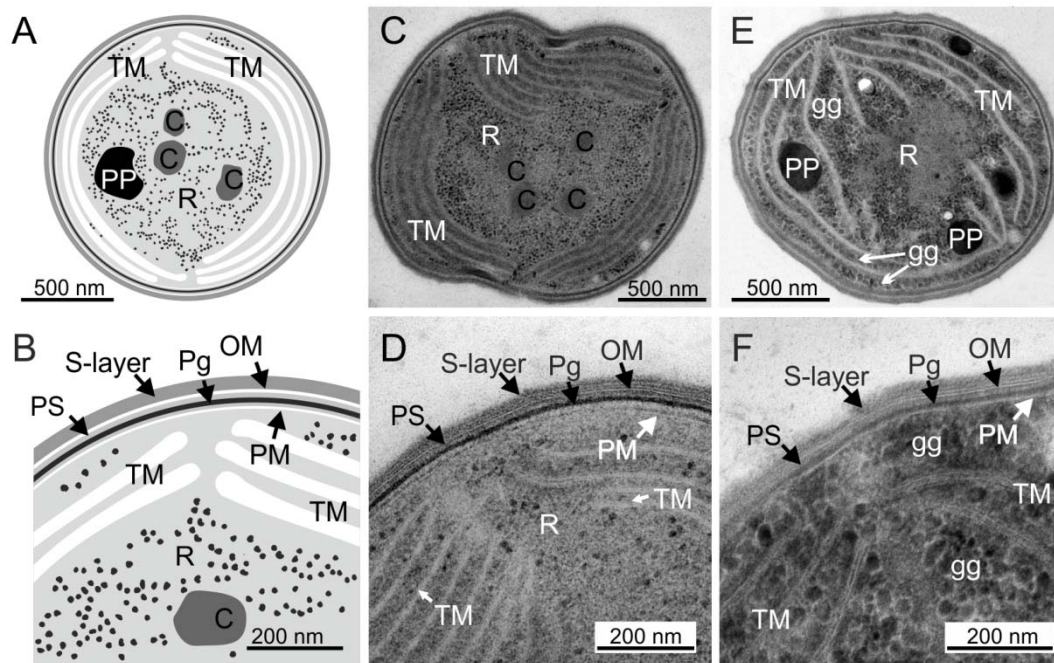


**Figure 3. Fine ultrastructure of *Synechocystis* cells as obtained by TEM.** Wild-type (WT) *Synechocystis* cells (top row) and details of cellular structures (bottom row). A, B) A cartoon presenting the *Synechocystis* ultrastructure. C, D) TEM micrograph of the dividing *Synechocystis* cell grown autotrophically under  $50 \mu\text{mol}$  of photons  $\text{m}^{-2} \text{s}^{-1}$ . E, F) A WT cell that has been grown mixotrophically (supplemented with 5 mM glucose) under  $30 \mu\text{mol}$  of photons  $\text{m}^{-2} \text{s}^{-1}$ . Abbreviations used: carboxysome – C; glycogen granules – gg; outer membrane – OM; peptidoglycan – Pg; polyphosphate granules – PP; periplasmic space – PS; ribosomes – R; surface S-layer - S-layer.

Although the photosynthesis of plants and algae is of the cyanobacterial origin, the ultrastructure of modern chloroplasts show some specific features like grana stacks not presented in cyanobacteria while many original (cyano)bacterial structures have been probably lost. Generally, the chloroplast has a discoid shape about  $5 \mu\text{m}$  long and  $1,5\text{-}2 \mu\text{m}$  wide and it is filled with stroma. The chloroplast is surrounded by an outer and inner envelope and inside there is a highly ordered lamellar TM system (Figure 2 E,F; Figure 5 A).

## 2.2. The architecture of thylakoid membrane

The cyanobacterial TM is described as a network of a flattened “sacs” surrounded by a pair of double layer membranes with aqueous lumen space closed inside (Stanier, 1988). In a close detail, the TM sheet itself is about 12 nm wide in cross-section and two parallel sheets are distant from each other by 30-50 nm due to the phycobilisomes or others inclusions that may be present here (van de Meene et al., 2006). The TMs were at first seen as separate concentric sheets organized inside the cell, at the periphery going parallel to each other following the shape of the cell. It has been originally described in the



cyanobacterium *Synechococcus* sp. (Allen, 1968) and TM sheets were expected to fully enclose the central part of the cytoplasm (Stanier, 1988). Now, thanks to the serial sectioning (Nierzwicki-Bauer et al 1983) and high-resolution TEM combined with tomography (van de Meene et al., 2006; Nevo et al., 2007; Hohmann-Marriott and Roberson, 2009; Liberton et al., 2011) the 3D architecture of TM is shown as a continuous network. TM sheets are however branched or are fused through bridges and contain many perforations, which allow a continuous flow in the cytoplasm (Nevo et al., 2007; Liberton et al., 2011).

*Synechocystis* cells contain usually from 3 to 10 TM sheets depending on the growth conditions (Figure 3). The concentric parallel sheets can also protrude through the cell and or be convexly curved and, in a few places, the sheets tend to converge towards the PM (Liberton et al., 2006; van de Meene et al., 2006; Nevo et al., 2007; Figure 3 B,D,F). Whether there is any connection between TM sheets and the PM is being a matter of discussion during the last decades (Gromov and Mamkaeva, 1976; Nierzwicki-Bauer et al., 1983; Nickelsen et al., 2011). Yet, even though the TM sheets are observed very closely to PM, no direct connections between these two membrane systems have been conclusively demonstrated (Liberton et al., 2006; van de Meene et al., 2006). Indeed, it cannot be excluded that such connections occur only transiently (Nickelsen et al., 2011). Interestingly, tubular membranous structures named thylakoid centers (TC), specifically occurring at the spots, where the TM sheets are approaching PM, have been reported in various cyanobacteria (Kunkel, 1982). In *Synechocystis* the analysis of TCs using cryo-fixation and tomography techniques revealed long (1  $\mu\text{m}$ ) cylindrical structures of 40 – 50 nm in diameter (Figure 4). Along with all their length, TCs are putatively closely associated to the edge of TM sheets although a probable connection with PM was suggested (van de Meene et al., 2006).

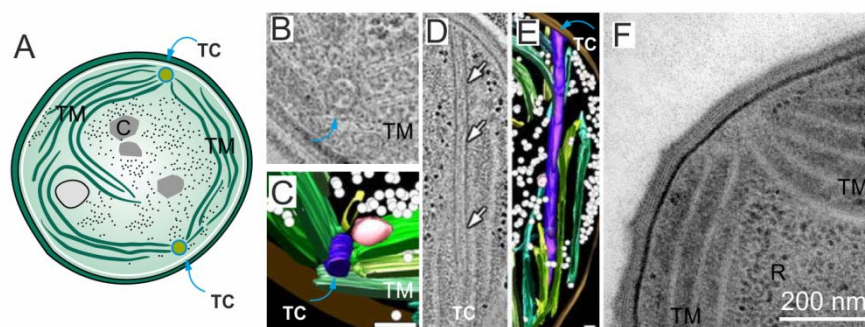


**Figure 4. The observation of thylakoid centers in *Synechocystis*.** A) A model depicting the position of TC inside the cell according to Nickelsen and Zerges (2013). B-E) A tomographic model of TC as presented in the publication of van de Meene et al. (2006). F) The method of fixation by high-pressure freezing that is used in this thesis (see Material and methods section) did not resolve the TC structures in the *Synechocystis* cell.

The architecture of the homologous TM in the chloroplast of plants and some algae appears more complex than in cyanobacteria. The TM continuous lamellar network in plastids is made by two different structural types - grana and stroma (Heslop-Harrison, 1963; Figure 5 B,D,E). The grana are arranged as appressed cylindrical stacks with a disc approximately 300-600 nm in diameter. Grana stacks fill ~80% of the chloroplast volume and are interconnected by stromal non-appressed lamellae that are usually several hundred nm long (Mustardy and Garab, 2003; Staehelin, 2003). The first contours of the complexity of plastid TM have been drawn by standard TEM methods of ultrathin sections and staining with heavy metals (as shown in Figure 2 E; Figure 5). However, the modern advanced microscopical methods such as serial sectioning, cryo-TEM and tomography have become essential to obtain a full 3D picture of the plastid TM network (Daum and Kühlbrandt, 2011). Still, there are three possible models of how lamellae and grana are interconnected (reviewed in Nevo et al., 2012; Pribil et al., 2014; Kirchoff, 2018). In a “helical” (fretwork) model the stroma lamellae connect the grana cylinder in the form of a right-handed helix and enter the grana through small slits, called frets (Paolillo and Falk, 1966; Mustardy and Garab, 2003). Consistently with this model, 3D TEM tomography has provided details of the branching stroma thylakoids spiralling around the grana stacks (Figure 5 B; Austin and Staehelin, 2011). The second model, “the fork/bifurcation” model, proposes that the stroma lamella intersect the whole granum across, lamellae splits into two membranes or connects grana through bridges and fusions at various levels of grana layers (Shimoni et al., 2005). The last model assumes that the TM of the high plant is one continuous membrane sheet that is variously folded, the grana stacks included (Arvidsson and Sundby, 1999).

Plastids of green algae also possess TM stacked into grana though these appressed grana structures could be much longer or stacked differently than in plants (Bertos and Gibbs, 1998). Recently, a novel cryo-TEM method combining freezing with a focused ion beam and cryo-electron tomography has been employed to examine the details of the TM architecture in the green alga *Chlamydomonas reinhardtii* (Engel et al., 2015). Although this method prevails the native structures and has provided new insight on the interconnected network of the TM (Engel et al., 2015), the lamella prepared by milling cells has only a defined thickness and the tomogram thus provides information from a limited volume (Schaffer et al., 2015). Nevertheless, this approach is very powerful and promising tool for the future investigation of cellular ultrastructure.



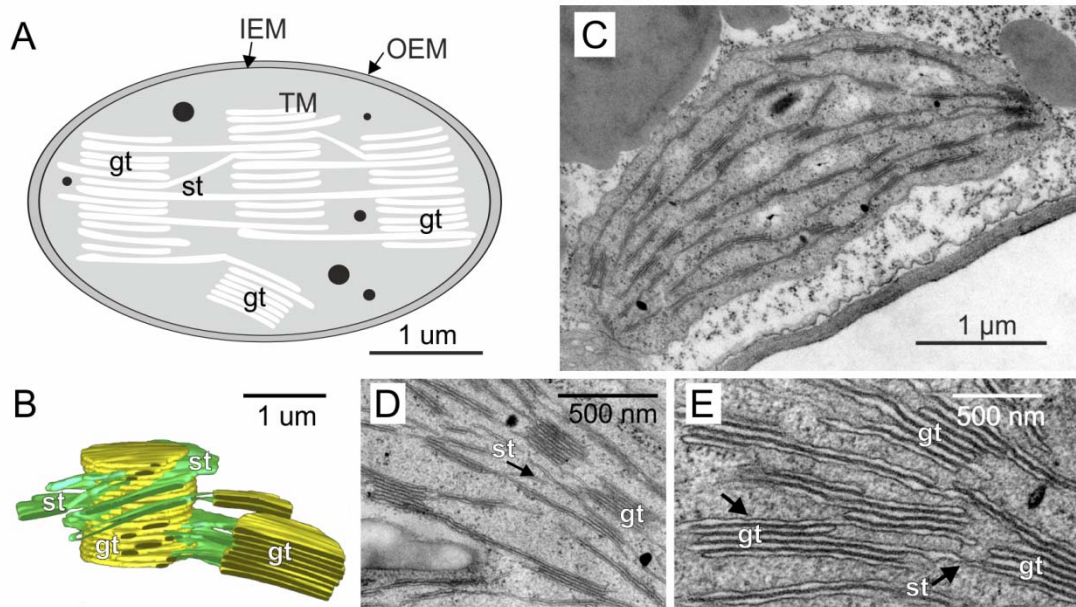


**Figure 5. Ultrastructure of plant (*Arabidopsis*) chloroplast obtained by TEM.** A) A scheme of the chloroplast ultrastructure. B) Detail of 3D helical organisation of plant grana (gt) and its connection with stroma lamellae (st); adopted from Austin and Staehelin (2011). C) A micrograph of chloroplast in *Arabidopsis* plant treated by high light stress. D, E) A detail of TM organization in *Arabidopsis* chloroplast. Abbreviations used: inner envelope membrane – IEM; outer envelope membrane – OEM; stacked grana thylakoids – gt; un-stacked thylakoids – st.

### 2.2.1. Molecular organization of thylakoid membranes

At the molecular level, the TM is a lipid bilayer “frame” densely packed with highly ordered protein assemblies. As mentioned earlier, cyanobacteria and chloroplast TM contains a conserved set of lipids, particularly rich (70-80%) with uncharged galactolipids monogalactosyldiacylglycerol (MGDG) and a digalactosyldiacylglycerol (DGDG). A mixture of both galactolipids is thought to be an optimal component for the forming of flattened membrane vesicles (Demé et al., 2014; Bastien et al., 2016). Less abundant but critical for the functioning of photosynthetic apparatus (see below) are two negatively charged lipids: sulfolipid sulfoquinovosyldiacylglycerol (SQDG) and phospholipid phosphatidylglycerol (PG), which are present only at 15–25% and 5–15% of the total lipid, respectively (Figure 6; reviewed in Kobayashi et al., 2017).

Is it notable that although lipids are typically organized into a lamellar bilayer membrane, the MGDG, very abundant in TM (~ 50%; Figure 6), actually belongs to non-bilayer-forming lipids (Figure 6; Wada and Murata, 2010; Heidrich et al., 2017). The MGDG molecule has a cylindrical shape, which influences the preferable lipid organisation and the tendency of MGDG to be self-organized into the hexagonal arrays (HII phase) with polar heads located in the center of the rod and fatty acids pointing out (Figure 6; reviewed in Lee, 2000 and in Jouhet, 2013). The functional or structural role of the MGDG-driven HII phase is still a matter of discussion but it might be important in the

process of TM biogenesis. In plants chloroplast the MGDG-rich lipoproteic nanostructures accumulate close to the inner envelope together with specialized proteins, potentially stabilizing or triggering the process of TM formation (Bastien et al., 2016). Similarly, the HII phase of MGDG is probably important for the activity of enzymes involved in xanthophyll cycle (Latowski et al., 2004). Nonetheless, it has been experimentally demonstrated that the MGDG mixed with Chl-binding proteins such as the LHCII antennas forms a typical bilayer structure (Simidjiev et al., 2000).

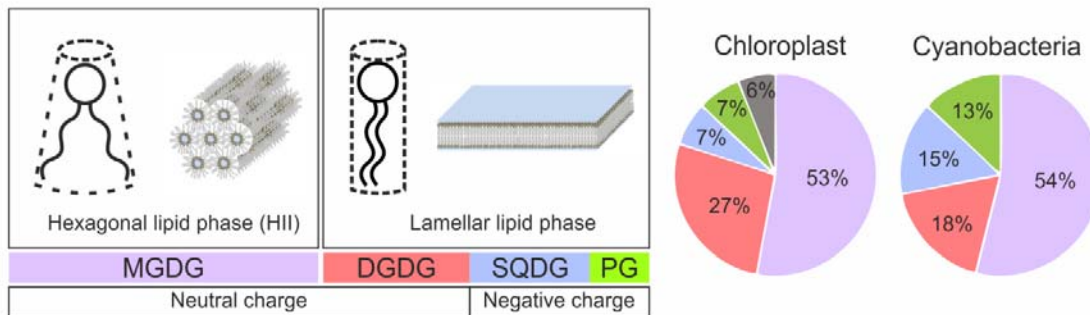


**Figure 6. TM lipids in cyanobacteria and chloroplast.** The left panel shows the characteristics and structural properties of individual TM lipids. Right panel represents lipid distribution in chloroplast and cyanobacteria. Grey colour represents minor lipids, which each contributes to plant TM in less than 2% (phosphatidylinositol, trigalactosyldiacylglycerol, tetragalactosyldiacylglycerol and diacylglycerol) Picture adopted from Heidrich et al. (2017) and Jouhet (2013).

The most abundant protein components embedded in the cyanobacterial TM are PSI and PSII complexes, whereas in green algae and plants the LHCII are dominating on the total protein level. Both PSI/II complexes have been extensively studied for last decades. Their exact protein composition is known and the molecular structure was solved by crystallography methods at various resolution depths (Rhee et al., 1997; Jordan et al., 2001; Ferreira et al., 2004; Amunts et al., 2007; Umena et al., 2011). Recently, these data were also supported by data from EM using methods of single particle analyses (Vacha et al., 2005; Folea et al., 2008) and by AFM studies (Liu and Scheuring, 2013). This long-term effort revealed an astonishing complexity of photosystems (Figure 7) and also an essential role of TM lipids for their functioning and biogenesis.

The structure of PSI has been first solved in 2001 for trimeric complex purified from a thermophilic cyanobacterium (Jordan et al., 2001; Figure 7 A). In each PSI monomer 12 protein subunits, 96 Chl molecules, 3 Fe<sub>4</sub>S<sub>4</sub> clusters, 2 phylloquinones, 22 β-carotenes and 4 lipids have been resolved (3 PG and 1 MGDG; Figure 7 C). The lipid content in PSI monomer has been later determined biochemically to be 2 MGDG, 1 DGDG, 1 SQDG and 2 PG (Kubota et al., 2010). The core of PSI is a heterodimer of two large

PsaA and PsaB proteins subjoined with nine small trans-membrane subunits (Jordan et al., 2001). A docking place for the cytochrome or plastocyanin is located at the lumenal side, while ferredoxin or flavodoxin are attached to the stromal side in a pocket created by PsaC, PsaE and PsaF subunits (Kubota-Kawai et al., 2018). Recently, a new, high-resolution structure of the trimeric PSI from *Synechocystis* has been reported to contain 33 protein subunits, with 72 carotenoids, 285 Chl molecules, 9 iron-sulphur clusters and 6 plastoquinones (Malavath et al., 2018). In this new structure, 51 lipids of all four lipid types have been identified (27 PG, 16 MGDG, 7 SQDG, and 1 DGDG). Notably, the majority of lipids (37 out of 51) were positioned within the trimeric PSI core (Malavath et al., 2018), which suggests an important structural role of lipids in PSI assembly (see below). In addition, several different carotenoid species are also inserted mostly in the space between individual PSI monomers.

The PSII is typically found as a dimer (Figure 7 B). Each monomeric PSII complex consists of 17 transmembrane and 3 peripheral proteins and, together with a number of cofactors, has a total molecular weight ~350 kDa. The monomer comprises 35 Chl molecules, 2 pheophytins, 12 carotenoids, 2 hemes, 1 non-heme iron and 3 plastoquinones. Moreover, 25 lipids have been reported to be stably bound into the PSII (Guskov et al., 2009; Umena et al., 2011; Figure 7 D). The large (> 25 kDa) Chl-binding proteins D1, D2, CP47 and CP43 are key structural parts of PSII; D1 and D2 heterodimer forms a reaction center (RCII), where the charge separation occurs, while the CP47 and CP43 subunits are attached to RCII to serve as inner PSII antennas (Umena et al., 2011). Apart from these main subunits, the PSII contains 13 small, single transmembrane helix subunits. On the lumenal side, the PSII binds a unique  $Mn_4O_5Ca$  cluster that is responsible for the extraction of electrons from water. In cyanobacteria, the manganese cluster is stabilized and protected by lumenal extrinsic proteins PsbO, PsbU and PsbV (Shi and Schroder, 2004; Enami et al., 2008).

Although the eukaryotic photosystems are structurally and functionally fairly similar to their cyanobacterial counterparts, there are some distinct differences. For instance, the cyanobacterial PSI complex is mostly found as a trimer, or a tetramer in a few known cases, while the plant PSI is exclusively monomeric and associated with LHCI antennas (Pan et al., 2018). There are also differences in the presence or absence of some subunits; PsaG and PsaH are present only in plant and green algae PSI, while PsaX and PsaM subunits are specific for cyanobacteria (Scheller et al., 2001; Şener et al., 2005). Similar to PSI, the eukaryotic PSII became surrounded by LHCII and the number and composition of extrinsic lumenal proteins differ in cyanobacteria, algae and plants (Albanese et al., 2017).

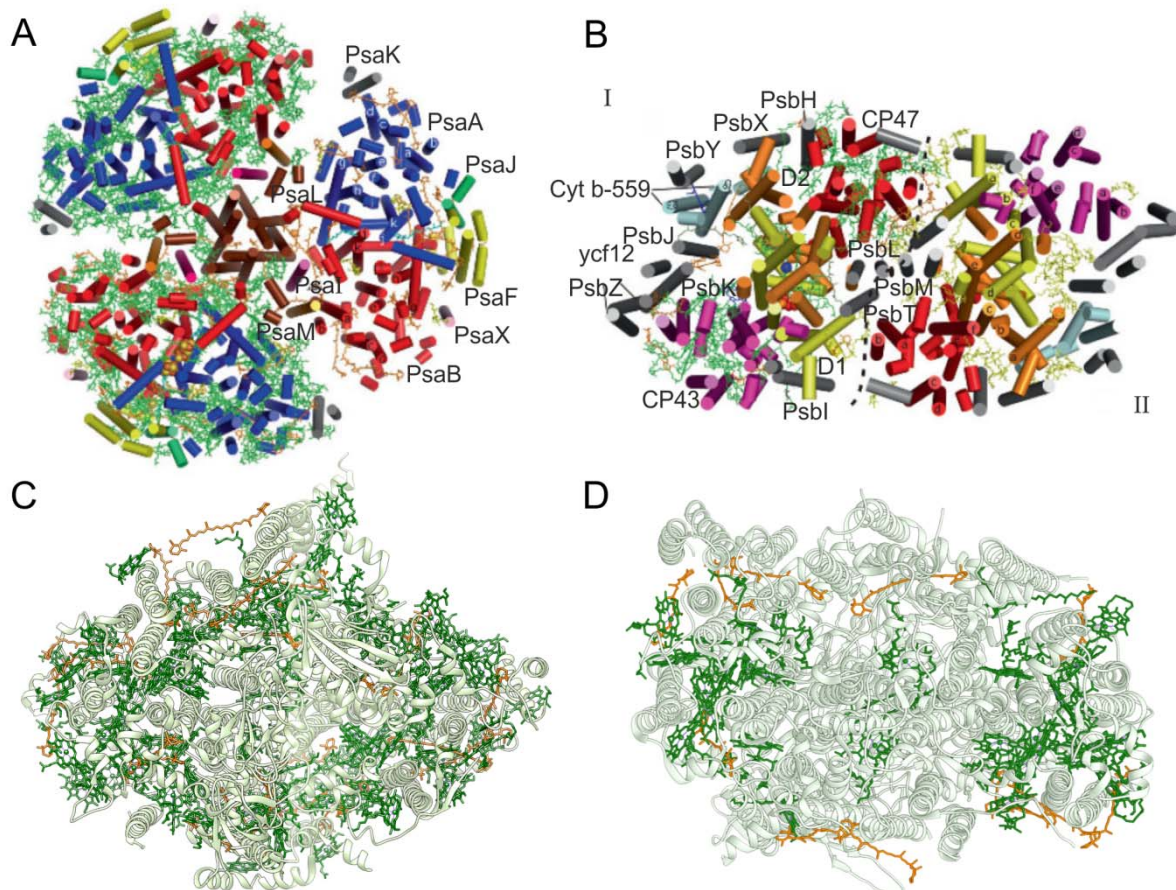


**Figure 7. Protein and pigment compositions of the of PSI and PSII complexes.** A) Protein subunits of the trimeric PSI: PsaA (blue); PsaB (red); PsaF (yellow); PsaI (magenta); PsaJ (green); PsaK (grey); PsaL (brown); PsaM (orange); PsaX (pink). B) The dimeric PSII: D1 (yellow); D2 (orange); CP47 (red); CP43 (magenta); PsbH, PsbI, PsbJ, PsbK, PsbM, PsbT, PsbX, PsbY, PsbZ, Ycf12 (grey); Cyt *b*-559 (blue) picture as presented in Kern et al. (2009) according Jordan et al. (2001) and Umena et al. (2011). C,D) The arrangement of pigment cofactors in the structures of (C) monomeric PSI (PDB:1JB0) and (D) PSII (PDB:3WU2); Chl molecules (green) and  $\beta$ -carotenes (orange).

While often overlooked, lipids are crucial structural and functional components of both photosystems. It is thought that lipids can provide structural flexibility to the core of the complex and allow repair mechanism, during which the damaged protein subunits are replaced with newly synthesized proteins (Loll et al., 2005; Guskov et al., 2009). They might also facilitate an ideal packing during the protein synthesis (reviewed in Lee, 2000) Interestingly, while a low level of MGDG causes defects in the structure of TM in plants (Jarvis et al., 2000) it has only rather a mild effect on the structure of TM in cyanobacteria. However, galactolipids can be partly substituted by glucoselipids, which probably results in retained photosynthetic activity and functional TM (Awai et al., 2007). On the other hand, the depletion in the level of charged lipid species has a drastic impact on viability of oxygenic phototrophs and stability of PS complexes (Kopečná et al., 2015; Nakajima et al., 2018). SQDG is still dispensable, though its lack results in serious



defects (Yu et al., 2002; Aoki et al., 2004; Nakajima et al., 2018). However, the PG is completely essential for the PSII stability; particularly for the binding of inner antenna protein CP43 within the PSII core (Hagio et al., 2000; Babiychuk et al., 2003; Laczko-Dobos et al., 2008). Furthermore, in *Synechococcus* PCC 7942, PG has been reported to play a role in non-linear electron transport as well as in cell division (Kobori et al., 2018). As well as, the loss of PG in *Synechocystis* affects trimerisation of PSI complex (Domonkos et al., 2004) and blocks the Chl biosynthetic pathway at the cyclase step (Kopečná et al., 2015). In this work, Kopečná and co-workers suggested that PG is needed for the integrity of a putative membrane micro-domain, where the synthesis of Chl and PSI complexes are co-localized (Kopečná et al., 2015).

### **2.2.2. Lateral heterogeneity and micro-domain organization in TM**

Photosynthetic complexes are organized in a highly sophisticated and dynamic molecular system, which is able to respond promptly to fluctuations in the environment. In plants, the PSII and PSI complexes have been identified in different regions of TM (Staehelein and Arntzen, 1983). The PSI associated with a half-ring of LHCI antenna is, together with ATPase, allocated to stroma lamellae, while the PSII dimer and LHCII antennas are located in the grana regions (Nelson and Yocum, 2006). This unequal distribution is called lateral heterogeneity (Anderson and Melis, 1983; Kouřil et al., 2012). Only Cyt *b<sub>6</sub>f* complex appears to be equally distributed in both grana and lamellae (Nevo et al., 2012) reviewed by (Pribil et al., 2014). Recently, the advanced techniques of cryo-electron microscopy (EM), tomography and atomic-force microscopy (AFM), have revealed the local arrangement of intact complexes in the isolated grana stacks (Nield and Barber, 2006; Kouřil et al., 2011; Johnson et al., 2014) and in the stroma lamellae (Yadav et al., 2017).

The presence of Chl-binding proteins affects the stacking of grana and the lack of phosphorylation of LHCII alters the arrangement of the plant TM (Fristedt et al., 2009; Kim et al., 2009). Other specific proteins contribute to TM plasticity and influence the grana organisation and bending of TM (Yokoyama et al., 2016; Pribil et al., 2018). Curt1 is a recently identified membrane protein, which is specifically located at the grana margins and it is very likely responsible for their sharp bending (Armbruster et al., 2013). The formation of very large, megadalton protein assemblies could be recognized as another level of the TM organization. Using different EM methods of freeze-fracture (Staehelein and Arntzen, 1983), in situ labelling of PSI and PSII (Mustardy et al., 1992) or single particle analysis in the isolated TM (Kouřil et al., 2005; van Bezouwen et al., 2017), both PSI-LHCI and PSII associated with minor and major LHCII were found to create megacomplexes such as PSI-PSII-LHCs (Yokono et al., 2015). Further

supercomplexes include the PSI associated with NDH or with Cyt *b<sub>6</sub>f* (Kouřil et al., 2014; Yadav et al., 2017; Steinbeck et al., 2018).

The heterogeneity of cyanobacterial TM is less apparent than in the chloroplast but also more challenging to study. Trimeric PSI, dimeric PSII and also dimers of Cyt *b<sub>6</sub>f* and ATPase are so densely packed; the estimated protein crowding in cyanobacterial TM is about 75% (Casella et al., 2017). Historically, the large TM complexes have been first localized using TEM combined with ‘on section’ immunolabelling. Using this approach and the cyanobacterium *Synechococcus* PCC 7942 the PSI and ATPase localized toward the periphery of the cell in the vicinity of PM while the PSII and Cyt *b<sub>6</sub>f* were evenly distributed in the TM (Sherman et al., 1994). Using a hyperspectral fluorescence imaging of *Synechocystis*, (Vermaas et al., 2008) have distinguished PSII, phycobilins and carotenoids in intact cells. Contrary to results of (Sherman et al., 1994), PSII were detected more at the periphery of the cell while PSI complexes were more abundant within the inner rings of thylakoids (Vermaas et al., 2008). In recent studies, PSI, PSII, Cyt *b<sub>6</sub>f* and ATPase subunits were fused with green or yellow fluorescent proteins (GFP or YFP, respectively) and visualized using confocal microscopy (Casella et al., 2017; MacGregor-Chatwin et al., 2017; Strašková et al., Submitted 2018). Interestingly, all these studies demonstrate that the cyanobacterial TM system contains various microdomains. Whereas the PSII is distributed in a distinct spotted fashion, the Cyt *b<sub>6</sub>f* and ATPase complexes had uneven distributions (Casella et al., 2017). Moreover, YFP-tagged PSI expressed in *Synechocystis* accumulates in large membrane segments lacking PSII (MacGregor-Chatwin et al., 2017) as well as in small distinct regions together with phycocyanin and PSII (Strašková et al., Submitted 2018). It is possible that the later regions contain megacomplexes of PSI-PSII and phycobilisome antennas that work as a functional unit (Liu et al., 2013). The heterogeneity of cyanobacterial TM is also supported by proteomic and biochemical studies that employ fractionation of TM on a sucrose gradient (Srivastava et al., 2005; Agarwal et al., 2010; Rengstl et al., 2011). It should be noted that such a domain-like organization can be recognized even in PM of the cyanobacterium *Gloeobacter violaceus* that is devoid of TMs. This heterogeneity of PM has been analyzed using fluorescence of photosynthetic pigments as well as by fractionation of PM followed by a protein mass-spectrometry (Rexroth et al., 2011).

The described organisation of TM is apparently not static but highly dynamic. Light intensity and other important environmental factors like nutrient availability or temperature are fluctuating, thus photosynthetic cells are under constant pressure to rapidly acclimate (Walters and Horton, 1994; Kopečná et al., 2012). The response could be described as an effort to restore optimal metabolic homeostasis (energy input, redox balance, nutrient uptake, carbon fixation) and thus achieve the maximal growth rate. Photosynthetic complexes are a crucial target for the regulatory network; antenna size, the

total levels and stoichiometry of PSI and PSII, and other parameters of the photosynthetic apparatus significantly influence the metabolic homeostasis, as well as the generation of reactive oxygen species (reviewed in Walters, 2005). In cyanobacteria, a typical response to high-light or nutrient limitation is the fast down-regulation of the total TM content per cell together with a reduction of trimeric PSI and antennas (phycobilisomes). On the other hand, the cell is able to maintain a rather constant level of PSII, though it must be intensively repaired. Over the course of just a few hours, the PSI/PSII ratio in cyanobacteria can change remarkably (Kopečná et al., 2012), which should also significantly modify the abundance of TM domains. Almost nothing is known about the mechanism how the cell controls the total content of TMs or the PSI/PSII ratio, however, the available evidence indicates an important role of Chl availability as a key regulatory factor (see Discussion).

### **2.3. Biogenesis of photosystems - a current view**

Despite the known detailed structural characteristics of photosystems, the overall picture of their biogenesis is just being drawn. An important milestone in the understanding of photosystem biogenesis has been achieved by employing *Chlamydomonas reinhardtii* (Wollman et al., 1999; Minai et al., 2006) and *Synechocystis* mutants lacking various subunits of PSI or PSII (Vermaas et al., 1988; Yu and Vermaas, 1990; Eichacker et al., 1996; Komenda et al., 2004). However, in plastids, the biosynthesis of large Chl-binding subunits is tightly controlled on the translation level according to the availability of the partner subunits (Wostrikoff et al., 2004). This regulatory feature, in fact, prevents a detailed study of the unassembled Chl-protein subunits or early photosystem assembly intermediates. In contrast, cyanobacterial mutants lacking a main PSII subunit still accumulate partially assembled PSII complexes (Komenda et al., 2004). This allowed a detailed characterization of assembly steps including the isolation of PSII assembly intermediates, their separation by 2D gel electrophoresis and mass spectroscopic identification of associated proteins (Komenda et al., 2004; Komenda et al., 2005; Knoppová et al., 2014; Tichy et al., 2016; Bučinská et al., 2018). Based mostly on this research, the PSII biogenesis is now considered as a strictly stepwise process, in which individual subunits are first combined into so-called assembly modules and these large building blocks then assemble into PSII (Nixon et al., 2010; Komenda et al., 2012).

There are known four PSII assembly modules (Figure 8) and a key component of each is one large Chl-binding subunit - CP47, CP43, D1 or D2, subjoined with several low molecular mass membrane proteins. Modules appear to be produced independently and already contain Chl molecule and other co-factors (Nixon et al., 2010; Boehm et al., 2011; Komenda et al., 2012; D'Haene et al., 2015). The (p)D1 module is composed of D1 protein and PsbI protein; during the PSII assembly, the pD1 precursor is truncated on its

C-terminus by CtpA protease (Figure 8; (Nixon and Diner, 1992; Dobáková et al., 2007; Komenda et al., 2008). Apart from D2 subunit, the D2 module contains PsbE and PsbF proteins, which together bind a heme molecule and PsbE/F dimer known as cytochrome *b*-559 (Komenda et al., 2004; Komenda et al., 2008). The assembly of PSII is initiated by the association of (p)D1 and D2 modules, which together form RCII assembly intermediate (Figure 8). As a following next step, the CP47 module, which comprises of CP47 protein and several small subunits (PsbH, PsbL, PsbT) associates with the RCII to create the RC47 complex (Boehm et al., 2011). Finally, the CP43 module (CP43 together with PsbK, PsbZ and Psb30), integrates into RC47 to form the core of monomeric PSII. The functional monomeric PSII is finalized by the association of manganese cluster and luminal extrinsic proteins PsbO, PsbU, CyanoQ and PsbV (Figure 8; Bricker et al., 2012). The synthesis/assembly of PSII requires (assembly) factors or auxiliary proteins that are not present in the final PSII complexes (e.g. Ycf48, Psb27, Psb28). It has been generally assumed that assembly factors facilitate protein interactions or stabilize subcomplexes during the assembly process (Komenda et al., 2012; Nickelsen and Rengstl, 2013). However, as we discuss in the following chapter, recent detailed studies showed particular importance of these protein factors for the efficient insertion of cofactors, especially Chl.

The assembly of PSI is fairly much less explored than the PSII. It is assumed though that the process is much faster than for PSII, which brings difficulties to trap the pre-assemble PSI intermediates (Figure 8; (Schöttler et al., 2011), reviewed in (Yang et al., 2015). Nevertheless, the large PsaB protein is probably synthesized and co-translationally inserted into the membrane, where it anchors the PsaA subunit and together they form the central PSI heterodimer (PsaA/B; Wollman et al., 1999). The PsaC attaches to the stromal side of the PsaA/PsaB heterodimer, and the prerequisite for the PSI assembly is a covalent binding of two Fe<sub>4</sub>S<sub>4</sub> clusters to PsaC (Schöttler et al., 2011). The assembly continues by attachment of PsaD and PsaF subunits to PsaC (Jordan et al., 2001). The PsaD is further necessary for the insertion of peripheral PsaE and PsaL subunits and it is also crucial for the stability of the whole PSI complex (Xu et al., 2001). In cyanobacteria, the incorporation of PsaL subunit finally induces trimerization of PSI (Chitnis and Chitnis, 1993). In plants, the remaining small subunits - PsaJ, PsaH, PsaL, PsaG, PsaK, PsaN and LHCI antennas are subsequently attached, the exact mechanism is however not yet fully understood (Yang et al., 2015). A few proteins factors assisting during PSI assembly have been identified (Ycf3, Ycf4; Figure 8), however, their role is not elucidated yet (Boudreau et al., 1997).



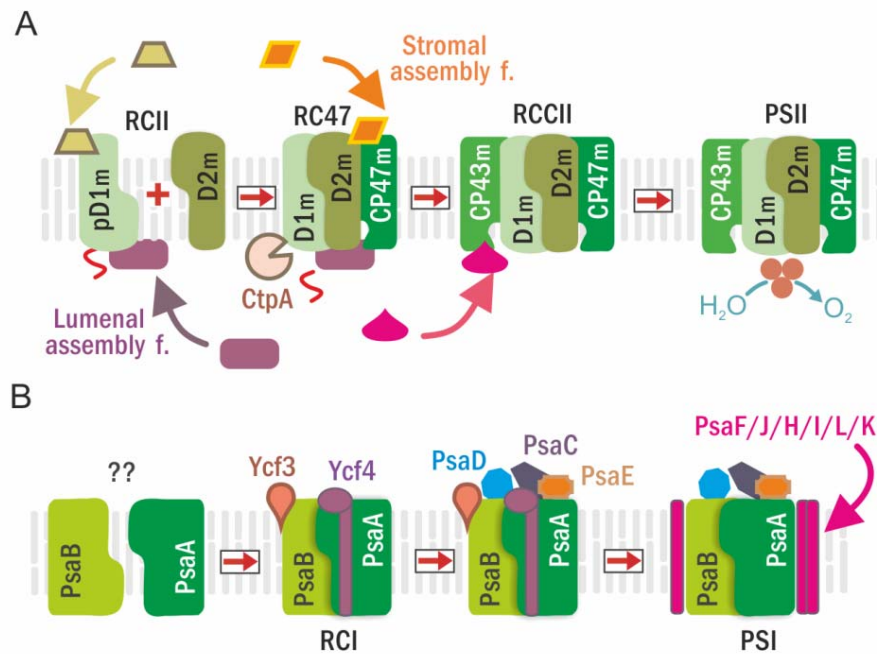


**Figure 8. The modular model of PSII and PSI biogenesis in cyanobacteria with the assistance of lumenal and stromal assembly factors.** A) The PSII is produced in a stepwise manner starting with the synthesis of the pD1 module (pD1m) and continues with the sequential attachment of D2, CP47 and CP43 modules. The formation of RCII complex is accompanied by CtpA-catalyzed pD1 maturation and facilitated by lumenal and stromal assembly factors. B) The PSI assembly putatively starts with the formation of pigmented heterodimer PsaA-PsaB under the assistance of Ycf3 and Ycf4 assembly factors. Then the stromal (cytoplasmic) proteins stabilizing the PSI acceptor side are attached and, finally, the other small subunits associate to generate the active PSI complex.

#### 2.4. The role of cofactors in the synthesis of photosystems

As described earlier, both photosystems bind a high number of cofactors and their synthesis is, in this respect, unique in nature. In cyanobacteria, a single trimeric PSI contains ~ 300 molecules of Chl (the vast majority bound to PsaA/B subunits) and > 70 carotenoids, which are not just  $\beta$ -carotenes but also various xanthophylls reported recently to be important for the trimerization of PSI (Vajravel et al., 2017; Malavath et al., 2018). Since PSI trimers are very abundant in the cyanobacterial TM, more than 80% of the total Chl in *Synechocystis* can be located in PSI (Kopečná et al., 2012). The PSII is however also quite Chl-rich, particularly the inner antenna proteins. CP47 and CP43 contain 16 and 14 molecules of Chl respectively together with 2-3  $\beta$ -carotene molecules each (Ferreira et al., 2004). In fact, the structure of CP47 and CP43 has similar arrangements of the membrane helices compared to PsaA and PsaB (Barber et al., 2000) and these proteins most probably originate from a common ancestor (Cardona, 2016).

Taking into account the phototoxicity of Chl, the synthesis of PSI core proteins and the PSII inner antennas packed with many Chl molecules must be a delicate task. It is known for a long time that Chl is as a prerequisite for the correct folding of PsaA/B proteins as

well as of CP47 and CP43 (Kim et al., 1994a; Eichacker et al., 1996). It means that if the cell fails to deliver enough of Chl for the synthesized Chl-proteins, it can trigger degradation of misfolded proteins and, potentially, releasing of already bound Chl molecules into membrane bilayer (He and Vermaas, 1998). The mechanism preventing such a situation is still not clear but there is remarkable progress in the understanding of Chl-protein biosynthesis achieved during the last decade.

The Chl-binding proteins are synthesized on ribosome bound on TM (Zhang et al., 2000). Possibly all large transmembrane Chl-binding subunits are inserted into the membrane by SecYEG translocon system after emerging from the ribosome; so far, the role of translocon has been conclusively shown for D1 and CP47 (Zhang et al., 2000; Bučinská et al., 2018). The SecY translocase forms a channel through the membrane and is responsible for the insertion of the majority of membrane proteins in bacteria, as well as in chloroplast, into the lipid bilayer (Zhang et al., 2001; Sachelaru et al., 2017). However, a certain subset of membrane proteins requires the assistance of YidC insertase that is probably attached laterally to SecY translocase (reviewed in (Sobotka, 2014). The YidC is highly conserved and its chloroplast homolog (Alb3) is known to assist during the synthesis of D1 and LHC proteins (Klostermann et al., 2002; Ossenbuhl et al., 2004); reviewed in (Hennon et al., 2015). The YidC/Alb3 insertase is indispensable for the biogenesis of photosystems (Pasch et al., 2005; Yang et al., 2015), and is essential for the cell survival in cyanobacteria as the gene coding for YidC cannot be deleted (Spence et al., 2004). Similarly, in algae, the inactivation of plastid Alb3.2 is lethal (Göhre et al., 2006). Indeed, the degradation of YidC and SecY translocase triggered by a defect in the biogenesis of pilins in a *Synechocystis* mutant had the same devastating impact on the *Synechocystis* cell (Linhartová et al., 2014).

While the role of SecY-YidC couple in the insertion of Chl-binding subunits is rather clear, when and how Chl molecules are inserted into apoproteins has been elucidated only recently. As noted above Chl molecules are required for the protein folding, which indicated that the Chl insertion into proteins occurs in the vicinity of translocon before the PSII assembly modules integrate into larger complexes. This has been verified by isolation of CP47 and CP43 assembly modules using His-tagged subunits from *Synechocystis* mutants with blocked PSII assembly; the purified modules contained almost all expected pigments as well as all low molecular mass proteins (PsbH, PsbL, PsbT etc.; Boehm et al., 2011). A physical connection between SecY-YidC translocon and Chl biosynthesis has been discovered a few years ago in *Synechocystis* by isolation of Chl-synthase, the final enzyme of Chl biosynthesis, in a stable complex with YidC (Chidgey et al., 2014). The interaction between Chl-synthase and YidC/Alb3 appears to be evolutionary conserved because the Chl-synthase from *Arabidopsis thaliana* can form a complex with cyanobacterial YidC (Proctor et al., 2018).

Pam68 is an integral membrane protein that has been first described as an auxiliary factor associated with Chl-binding proteins at the early steps of PSII assembly in *Arabidopsis* (Armbruster et al., 2010). In this study, the authors showed that the loss of Pam68 protein is severely affecting the growth and the pigment composition of mutated plants and the accumulation of PSII is impaired. The stability of D1 protein was most affected evoking the conclusion that the Pam68 protein is needed for the formation of RCII (Armbruster et al., 2010). A cyanobacterial Pam68 homolog has been however co-localized with CP47 and CP43 subunits and with the PSII assembly factor Ycf48 in the isolated membrane fractions from *Synechocystis* (Rengstl et al., 2011). Although the deletion of *Synechocystis pam68* gene (*sll0933*) had not such profound effect on the biogenesis of PSII as in plants, it was still assumed that it has a putative role during the formation of RCII (Rengstl et al., 2011). However, the later analyses of the same mutant lacking Pam68 using radioactive pulse labelling and separation of TM complexes by 2D gel electrophoresis linked Pam68 with the synthesis of CP47 (Rengstl et al., 2013). The low accumulation of pD1, which has been demonstrated in plant Pam68 mutant, can be in fact a secondary effect of the impaired synthesis of CP47 (Komenda et al., 2004; Komenda, 2005).

To clarify the role of Pam68 we have engineered a *Synechocystis* strain, which produces the Pam68 protein fused with 3xFlag-tag. This strain has been used to purify Pam68 under native conditions, which confirmed the CP47 protein as a partner of Pam68. However, the elution also contained both large and small ribosomal subunits together with SecY translocase and YidC insertase. Moreover, the Pam68-CP47 complex contained Chl despite the PsbH subunit, a component of CP47 assembly module, was not present in the complex. It signaled that the Pam68 interacts with CP47 very early before the CP47 assembly module is established. We have confirmed the interaction between Pam68 and a 'nascent' CP47 module lacking PsbH protein using another engineered *Synechocystis* strain that accumulates such early assembly intermediate. In addition, we have provided also a negative control that once the PsbH is attached to CP47 the Pam68 is not further present in CP47 assembly module (Bučinská et al., 2018). We have proposed a model that the cyanobacterial Pam68 protein is a ribosomal factor that is in contact with the nascent CP47, in close vicinity of the SecY translocon at the very early stage of PSII assembly, prior the further attachment of PsbH (Figure 9; Bučinská et al., 2018).

*Synechocystis* strain lacking Pam68 had no obvious growth phenotype under low-stress conditions except weaker synthesis of CP47. Under stress conditions such as cold (18°C) the autotrophic growth was significantly slower than in WT but still, the mutant was fairly viable. Similarly, the deletion of *psbH* gene had no drastic effect on the photosynthetic performance. However, when we deleted both *psbH* and *pam68* genes, the

resulted double mutant had practically completely inhibited synthesis of CP47 and its growth was almost completely abolished (Bučinská et al., 2018). Interestingly, the poor phenotype and inability to synthesise the CP47 in the double mutant was rescued by a strongly increased production of Chl. Such upregulation of Chl biosynthesis can be achieved by blocking the activity of ferrochelatase enzyme competing for the same substrate with Mg-chelatase enzyme (Bučinská et al., 2018). These data led us to conclusion that Pam68, and possibly also PsbH, facilitate the loading of Chl molecules into translated CP47 (Figure 9).

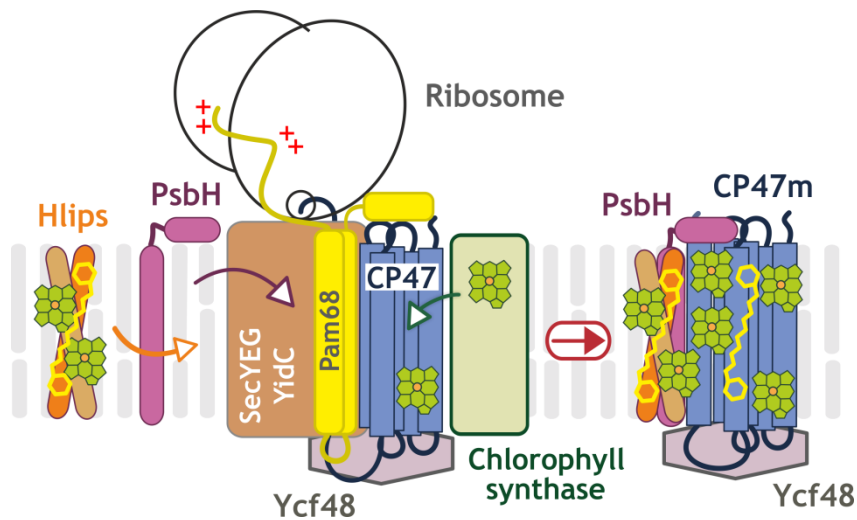


**Figure 9. A working model of CP47m synthesis with Pam68 as a ribosome-interacting factor.** The CP47 protein is translated by membrane-bound ribosomes and inserted into the membrane by the SecYEG translocon together with YidC insertase. Chl is loaded into the nascent polypeptide co-translationally from Chl-synthase when the transmembrane segments are released from the translocase channel to YidC (Chidgey et al., 2014). The Pam68 protein is associated with the translating ribosome as well as with stromal loops of the nascent CP47 chain after it emerges from the translocon. This interaction fixes the CP47 transmembrane segments in a position that facilitates the insertion of Chl molecules (Bučinská et al., 2018). Subsequently, PsbH replaces Pam68 and recruits the photoprotective High-light-inducible proteins (Hlips) that associate with CP47 in the vicinity of PsbH (Promnares et al., 2006).

How other pigments such as carotenoids and pheophytin are integrated into the Chl-binding proteins is still rather unknown. Carotenoids are needed for the PSII assembly and for the stability of PSI trimers but actually not for the synthesis of individual photosystem subunits (Sozer et al., 2010; Vajravel et al., 2017). So far, it is not clear whether specialized auxiliary proteins are required for the insertion of carotenoids or pheophytin into the nascent apoproteins. However, in contrast to Chl molecules, carotenoids are safe, or probably even beneficial, for the cell if occur free in the lipid bilayer and so they do not require such strict control as Chl. Carotenoids could be quite

concentrated in the membrane around the translocon (biogenesis centers; see Discussion) and associate spontaneously with the released proteins (Domonkos et al., 2013).

## **2.5. The biogenesis of thylakoid membrane**

Although there are various attempts to provide a model of TM biogenesis (Rast et al., 2015; Heinz et al., 2016), we have no mechanistic explanation yet how a seemingly independent and very abundant membrane system containing a complicated proteome is built in the cell. However, at least in plants, the TM can be completely restored from prolamellar bodies in etioplasts (Muehlethaler and Frey-Wyssling, 1959; Kowalewska et al., 2016) or in proplastids through vesicle transport originating from the plastid inner envelope (Liang et al., 2018). Thus, the synthesis and transport of lipids via vesicular transport clearly contributes to the biogenesis of TM in chloroplast (Kroll et al., 2001; Westphal et al., 2003; Karim and Aronsson, 2014). Intriguingly, a vesicular-like transport has never been observed in cyanobacteria. All ideas about the biogenesis of cyanobacterial TM are thus still hypothetical rather than supported by experimental data (Nickelsen et al., 2011). The synthesis of the pD1 assembly module of PSII (Figure 8) has been first placed in PM, and thus a physical connection between cyanobacterial TM and PM (or a kind of vesicular transport) has been seen as inevitable (Zak et al., 2001; Nickelsen et al., 2011). However, later, the process of PSII assembly has been completely localized in TM (Selao et al., 2016). A physical connection between cyanobacterial PM and TM has been under close examination for years but it is now more probable that both membranes represent their own closed system (Liberton et al., 2006; Nevo et al., 2007).

The separation of cyanobacterial PM and TM by biochemical methods is a challenging task. Although the purified PM appears fairly pure, the TM is heterogeneous (Norling et al., 1994; Schottkowski et al., 2009; Selao et al., 2016), consistently with the existence of different membrane domains (see Chapter 2.2.2). By a combination of sucrose gradient and two-phase partitioning (Norling et al., 1998), a fraction of TM abundant of PrataA protein has been isolated from *Synechocystis* (Schottkowski et al., 2009). PrataA was connected with the early steps of PSII biogenesis, particularly with the maturation of pD1 (Klinkert et al., 2004). The distinct membrane fraction named PrataA-defined membrane (PDM) contained also other assembly factors involved in the early steps of PSII assembly and also enzymes of the Chl biosynthesis (Rengstl et al., 2011). It has led to the assumption that the PDM represents a micro-domain serving as a specialized (biosynthetic) center for the biogenesis of PSII (Nickelsen et al., 2011; Rengstl et al., 2011; Rast et al., 2015; Heinz et al., 2016). According to this model the PDM domains are serving as a bridge between PM and TM (Nickelsen et al., 2011; Nickelsen and Rengstl, 2013; Heinz et al., 2016) and are somehow equivalent to already mentioned thylakoid centers (TC; Figure 4), a side where the new TMs are hypothetically produced.

It should be noted that this model has been published before the recent data ruled out that any of Chl-proteins is synthesized in PM (Selao et al., 2016). Nonetheless, the *Synechocystis* Prata protein has been co-localized by antibody labelling on ultrathin sections with TCs (Stengel et al., 2012). In fact, the idea that the TCs are linked with biogenesis of TM is much older (Hinterstoisser et al., 1993) and these structures have been described before PDM as a missing link between TM and PM membrane (van de Meene et al., 2006). To summarize our fragmented knowledge, there is a conflict between the expected function of TC and PDM as a biogenetic center for the production of TMs (Komenda et al., 2012) and the ‘traditional’ connection of TC to PM. In cyanobacteria the putative biogenetic center should be however located in the membrane compartment that is co-isolated with TM fraction but this is not the case of Prata localized exclusively in PM (Selao et al., 2016). Interestingly, a specialized biosynthetic center involved in the assembly of photosynthetic apparatus has been identified in green alga *C. reinhardtii*, where a biosynthetically active area, a T-zone, was found close to the pyrenoid (Bohne et al., 2013; Rast et al., 2015).

As noted above, in chloroplast lipid molecules are transported via a vesicular system (Benning, 2008, 2009). Based on the biochemical characterization of a *Arabidopsis* mutant, Vipp1 protein (Vesicle-inducing protein in plastids 1) had been characterized as a factor involved in the transmembrane lipid transport but also in TM formation and/or maintenance (Kroll et al., 2001; Heidrich et al., 2017). In plants, the lack of Vipp1 abolished the photosynthetic capacity and the TM organization is dramatically affected (Kroll et al., 2001). Similar phenotype has been reported in green algae (Nordhues et al., 2012). Interestingly, the gene coding for Vipp1 protein is presented also in cyanobacteria, it is highly conserved and only missing in the TM-lacking cyanobacterium *Gloeobacter* sp. (Vothknecht et al., 2012). Although the vesicular transport has never been observed in cyanobacteria the *Synechocystis* strain lacking Vipp1 exhibits a phenotype similar to that of *Arabidopsis* (Westphal et al., 2001). However, these results have been later questioned. The depletion of Vipp1 in *Synechocystis* appeared to affect the biogenesis of photosystem rather than the formation of TM (Gao and Xu, 2009); later, the Vipp1 has been connected with the PSI biogenesis rather than with TM formation in *Synechococcus* sp. PCC 7002 (Zhang et al., 2014). In a most recent work Gutu et al. (2018) have again shown that, at least in cyanobacteria, the Vipp1 is not specifically required for the TM formation, but it is somehow important during the assembly of photosystems (Gutu et al., 2018).

Regarding the function of Vipp1, this protein can form oligomeric ring structures with a higher affinity towards lipid molecules and *in vitro* is able to facilitate membrane fusing (Hennig et al., 2015; Heidrich et al., 2017; Hennig et al., 2017). In green algae, the Vipp1 forms rods that could serve as a kind of TC resembling cyanobacterial TC and provide structural support for lipids during TM formation or, alternatively, assist during the

protein translocation (Nordhues et al., 2012). In *Synechococcus* sp. PCC 7942 the fluorescently tagged Vipp1 has localized into mobile puncta at the vicinity of PM and TM or in the central cytoplasm (Bryan et al., 2014). Another microscopic work similarly localized the *Synechocystis* Vipp1 as the puncta near PM at highly curved TM or in the cytoplasm (Gutu et al., 2018). Moreover, components of protein synthesis and PSII assembly were found in pull-down experiment using the Vipp1-GFP as bait (Bryan et al., 2014).

### 3. Unpublished results

#### 3.1. Biogenesis of cyanobacterial TM during the recovery from chlorosis

Cyanobacteria sense nitrogen status in the cell via a sophisticated molecular mechanism, which ‘measures’ the level of 2-oxoglutarate – substrate of the glutamate synthase enzyme (MuroPastor et al., 2001). When the level of 2-oxoglutarate is too high the cyanobacterial cell almost immediately upregulates nitrogen uptake systems, mobilizes the stored amino-acid polymers (cyanophycin) and also produces various general stress proteins including Hlips (MuroPastor et al., 2001; Tolonen et al., 2006). If this first response does not improve the nitrogen status, cells start to degrade phycobilisomes, which thus serve also as nitrogen storage (Flores and Herrero, 2005). However, a prolonged nitrogen depletion (days) triggers more complex morphological and metabolic changes described generally as chlorosis (Allen and Smith, 1969). The nitrogen-starved cells gradually degrade the cellular protein content including photosynthetic complexes and the Chl level is thus drastically decreased (Görl et al., 1998). After several weeks such (chlorotic) cells exhibit only traces of metabolic activity resting in a dormant-like stadium (Sauer et al., 2001); Figure 10). Dormant cells of *Synechococcus* PCC 7942 have extremely reduced TM system (Wanner et al., 1986) but contain a lot of stored carbohydrates in glycogen and PHB inclusions (Allen, 1984) Figure 14 A,B). Remarkably, even after a very long period of dormancy (> 1 year) adding of a nitrogen source back to the cell culture induces a quick recovery (~ 3 days; Görl et al., 1998) through a highly organized genetic programme (Klotz et al., 2016). Step by step the cells are able to use energy stored in glycogen granules to re-synthesize Chl and Chl-binding proteins for the assembly of photosynthetic apparatus and for the restart of photoautotrophic metabolism (Schwarz and Forchhammer, 2005; Klotz et al., 2016).

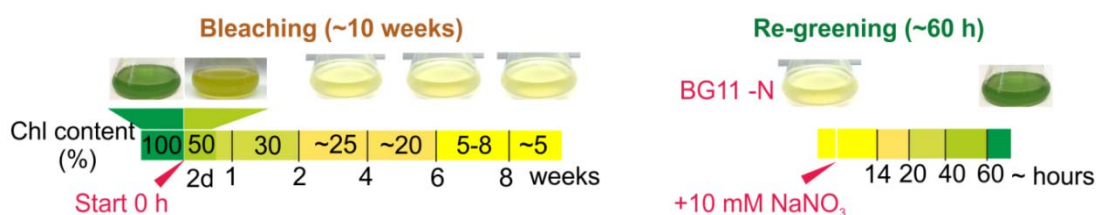


**Figure 10. Bleaching and re-greening of the *Synechocystis* cell culture.** Changes in the Chl cellular content during long-term nitrogen deficiency (left) and a time-course of the recovery from chlorosis (right) after replacing the growth BG11 media with a fresh one containing 10 mM NaNO<sub>3</sub> and 200 μM glutamate.



In order to explore the TM biogenesis and the assembly of the photosynthetic apparatus, we transferred *Synechocystis* wild type cells (WT, GT-P sub-strain; Tichy et al., 2016) into a nitrogen-free BG11 medium and cultivate them on a shaker under  $30 \mu\text{mol photons m}^{-2} \text{s}^{-1}$  for eight weeks. Cellular Chl concentration calculated as a percentage of the initial concentration (time 0) was gradually dropping down to  $\sim 5\%$  (Figure 10). This chlorotic state was reversed by adding of nitrogen sources ( $10 \text{ mM NaNO}_3$ ) back to the culture, assigned here as a re-greening process; the cells reached the WT level of Chl in  $\sim 70$  hours (Figure 10).

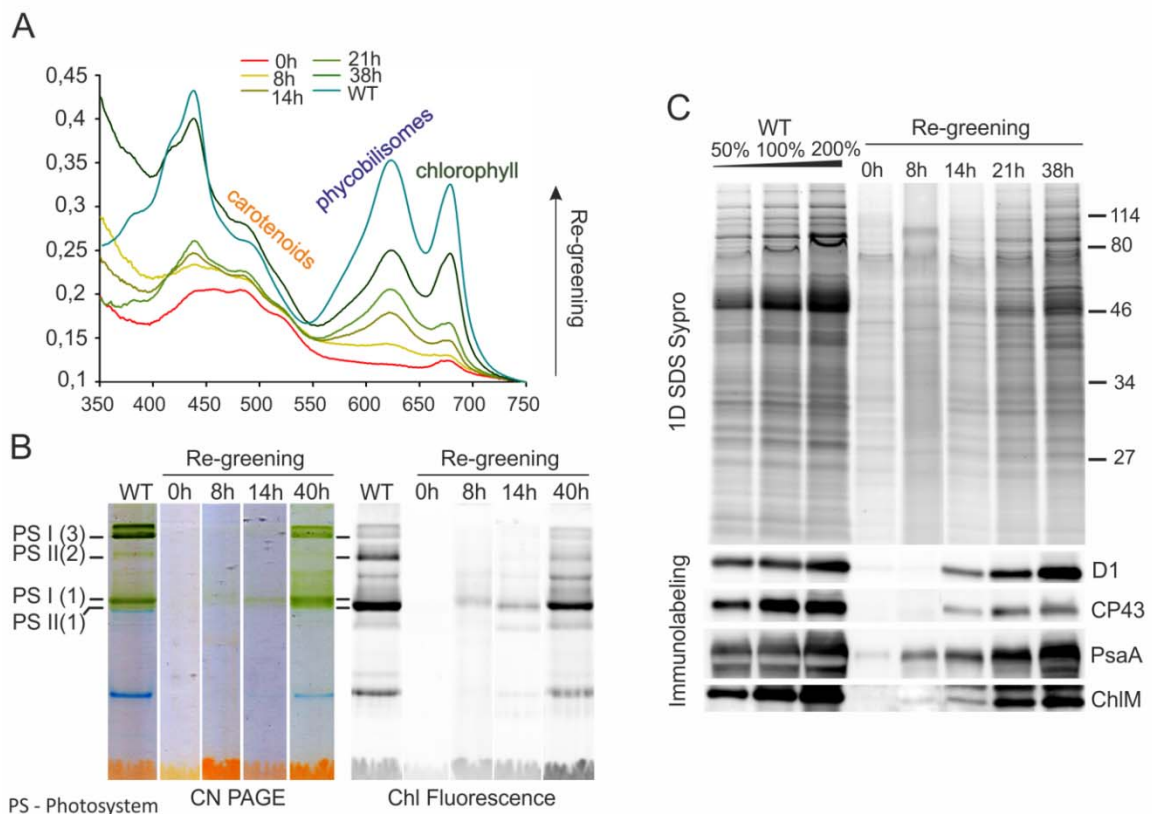


**Figure 11. Accumulation of Chl-protein complexes in *Synechocystis* cells during recovery from the chlorotic state.** A) Whole-cell absorbance spectra of re-greening cells were recorded using Shimadzu 3000 spectrometer and normalized to optical density = 750 nm. Peaks of 620 and 682 represent phycocyanin and Chl, respectively. Carotenoids are detectable as a shoulder around 500. WT – control wild type cells. B) Isolated membranes were solubilized by 1% dodecyl- $\beta$ -maltoside and separated on 4-14% CN-PAGE essentially as described in (Wittig et al., 2007). The native gel was scanned (Scan) and Chl fluorescence measured after illumination with blue light (Chl Fluorescence) using Fuji LAS 4000. Loading of each sample was calculated to correspond to a similar number of cells of the given cell culture.

After replenishing of nitrogen the Chl-protein complexes, as well as the phycobilisome, started to accumulate with first detectable spectroscopic changes in about 8 hours; 30% of the initial Chl content was reached in about 21 hours (Figure 11 A). In order to obtain

details about the content of Chl-binding proteins, we isolated membranes from cells in different time of recovery (0, 8, 14, and 40 h) and solubilized membrane-protein complexes loaded on a clear-native gel (CN-PAGE). The first photosynthetic protein complex detectable in greening cells was monomeric PSI (8 h), later followed by the monomeric PSII complex (14h; Figure 11 B). Although after 40 h the pattern of complexes was already similar to non-stressed WT control (WT control), the amount of dimeric PSII was still significantly lower (Figure 11 B). The re-appearance of Chl-binding proteins were further analyzed by SDS-PAGE and immunodetection (Figure 11 C). Interestingly, the PSI core (PsaA protein) was detected at the earliest time point of recovery at 8h whereas the PSII subunits D1 and CP43 were detectable earliest after 14h. It suggested that the biogenesis of PSII RC is somehow delayed in comparison with PSI.

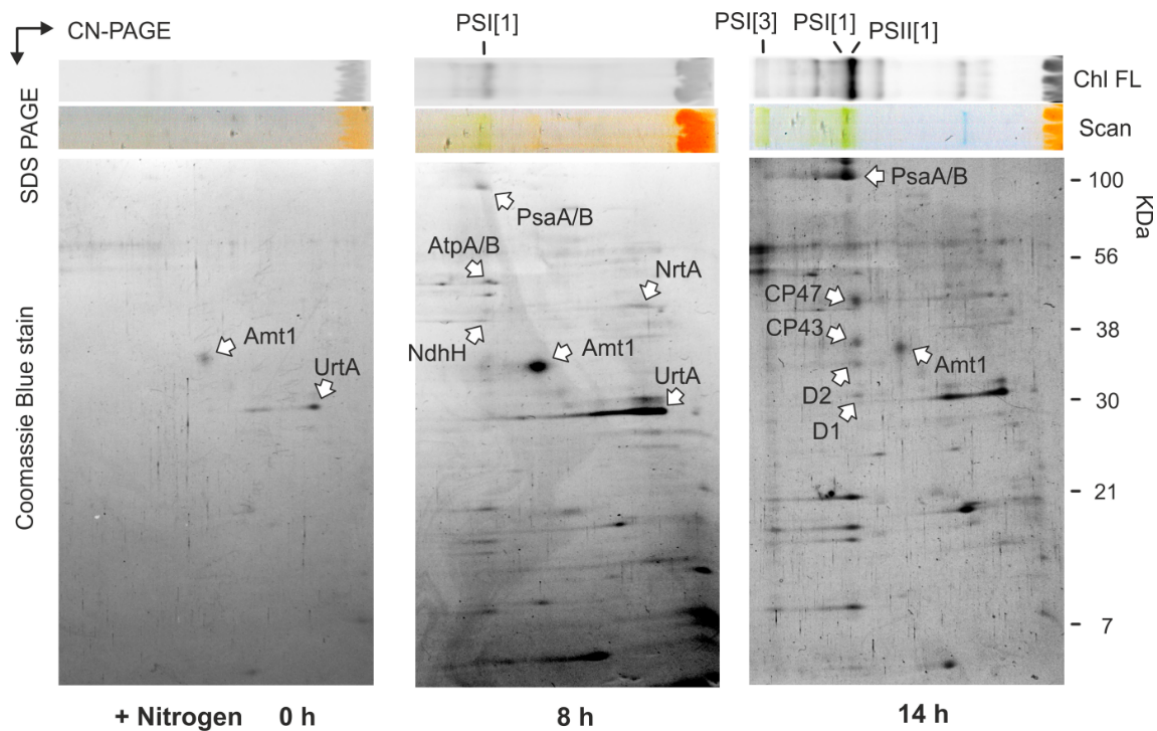


**Figure 12. Two-dimensional CN/SDS-PAGE of membrane-protein complexes** isolated from chlorotic cells (0 h) and during recovery of cells after adding of nitrate (8 and 14 h; see also Figure 11). The gradient 12-20% SDS gel was stained by Coomassie Blue and indicated protein spots identified mass spectrometry.

In order to obtain a detail view on the protein composition of TM during a different stage of re-greening, protein complexes resolved by CN-PAGE were further separated by 2D SDS-PAGE, stained by Coomassie blue and individual protein spot identified by mass spectrometry. At time 0 (the end of nitrogen depletion) the only proteins detectable on the stained gel was ammonium and urea transporters Amt1 and Urt1 (Figure 12, 0 h). In 8 hours of re-greening, the membranes already contained detectable levels of ATPase and

NDH-I complexes together with monomeric PSI that was visible also on the CN-gel. About 6 hours later (14 h) the monomeric PSII and trimeric PSI subunits became detectable, whereas the concentration of nitrogen transporters was visibly reduced (Figure 12).

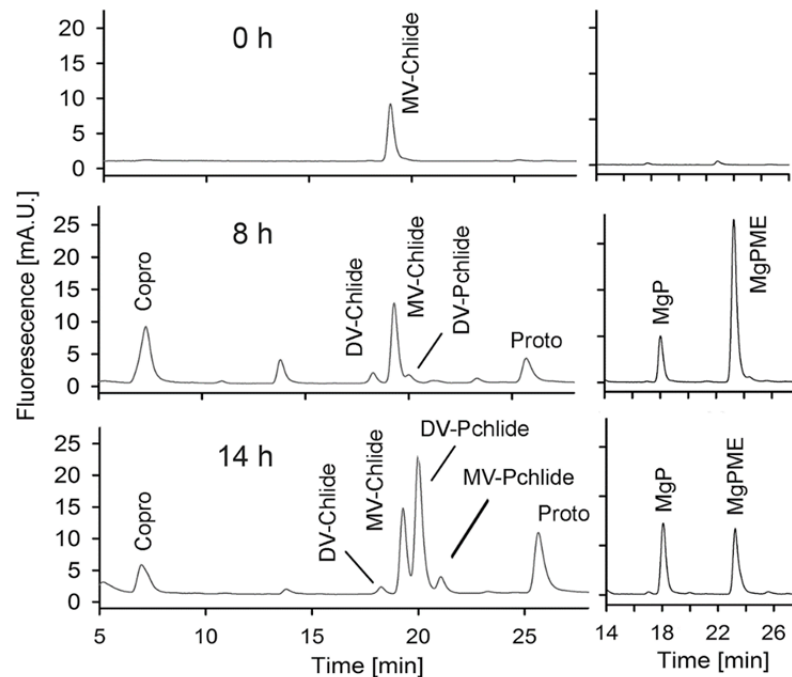


**Figure 13. The level of Chl precursors during first hours of recovery from chlorosis.** Chl precursors were extracted from 2 mL of cells with  $OD_{750nm} = \sim 0.4$  and quantified by HPLC equipped with two fluorescence detectors set on different excitation and emission wavelengths (chromatograms on the right and left side; (Pilný et al., 2015)). Coproporphyrinogen III (detected here as its oxidized form Coproporphyrin III - Copro) and protoporphyrin IX (Proto) are the last common precursors for both Chl and heme synthesis. The first committed intermediate of Chl pathway is Mg-protoporphyrin IX (MgP), which is consequently methylated (MgPME). The MgPME is converted into divinyl protochlorophyllide (DV-Pchlde) and then into divinyl and monovinyl chlorophyllide (DV/MV-Chlide); Chl is finally made by attachment of phytol to the MV-Chlide.

The re-appearance of PSI shortly on the onset of re-greening signaled that the Chl-biosynthetic pathway is quickly activated. Indeed, already in 14 hours of re-greening, we detected by immunoblotting Mg-protoporphyrin IX methyltransferase (ChlM), an enzyme catalyzing a specific step in Chl biosynthesis (Figure 11 C). A more detailed and more sensitive insight into the regulation of Chl biosynthesis provided the measurement of Chl precursors. We used a method based on the HPLC separation of extracted pigments and detection of individual pigments by two very sensitive fluorescence detectors (Pilný et al., 2015). In chlorotic cells, the only detectable Chl precursor is monovinyl-chlorophyllide, which results however almost certainly from dephytylation of

Chl molecules, not from de novo Chl biosynthesis (Kopečná et al., 2015). Already in 8 hours after adding of nitrogen, the cells contain high levels of an early Chl/heme precursor coproporphyrinogen III (detected in its oxidized form) as well as Chl precursors Mg-protoporphyrin IX and Mg-protoporphyrin IX methylester and protochlorophyllide, the later Chl precursor, became detectable (Figure 13). In 14 hours, the pattern of precursors was already similar to (non-stressed) WT cells (Pilný et al., 2015) with a dominating peak of protochlorophyllide eluting from the column in around 20 min (Figure 13). These data clearly demonstrate that the restart of Chl biosynthesis is fast and correlates with the formation of PSI complexes in first hours of re-greening.

For the tracking of TM biogenesis in *Synechocystis* on an ultrastructural basis, we harvested cells at different stages of re-greening (Figure 14 A-J) together with control cells (Figure 14 K,L) and froze them by high-pressure freezer with subsequent freeze substitution procedure. The harvested cell in the pellet was first processed by protocol 1 (see Material and methods) based on the published methodology used previously for the analysis of *Synechocystis* ultrastructure (van de Meene et al., 2006). The obtained samples embedded in Spurr's resin were used for the analysis of cells on 50-60 nm ultra-thin post-stained sections imaged by TEM. We found that the chlorotic cells (0 h; Figure 14 A,B) contain only a few small membrane fragments disorganized through the whole cell volume. Moreover, the cells at time 0 h were packed with glycogen granules about 25 nm in diameter as well with PHB granules - relatively huge 100-400 nm electron-transparent inclusions (Figure 14 A,B). Intriguingly, at an early stage of recovery (14 h) cells possess unusual 'star-like' membrane structures (Figure 14 C-F). In more detailed analyses, these structures appeared as short membrane vesicles grouped around an imaginary center (Figure 14 E,F). Moreover, the cells at the later stage of dividing contained two 'stars' structure, each for one daughter cell (Figure 14 D). At the later stage of recovery (20 h) the number of TM sheets visibly increased and started to be organized around the cell. The concentration of glycogen granules decreased and ribosomes re-appeared in the central part of the cell (Figure 14 G,H). The rest of the granules also diminish in size. After 38 h (Figure 14 I,J) the ultrastructure of cells already resembled the WT control (Figure 14 K,L). The number of glycogen granules was low, TM followed the shape of the cell in concentric sheets and PHB granules were not present, while the cyanophycin granules had accumulated (Figure 14 I,J).



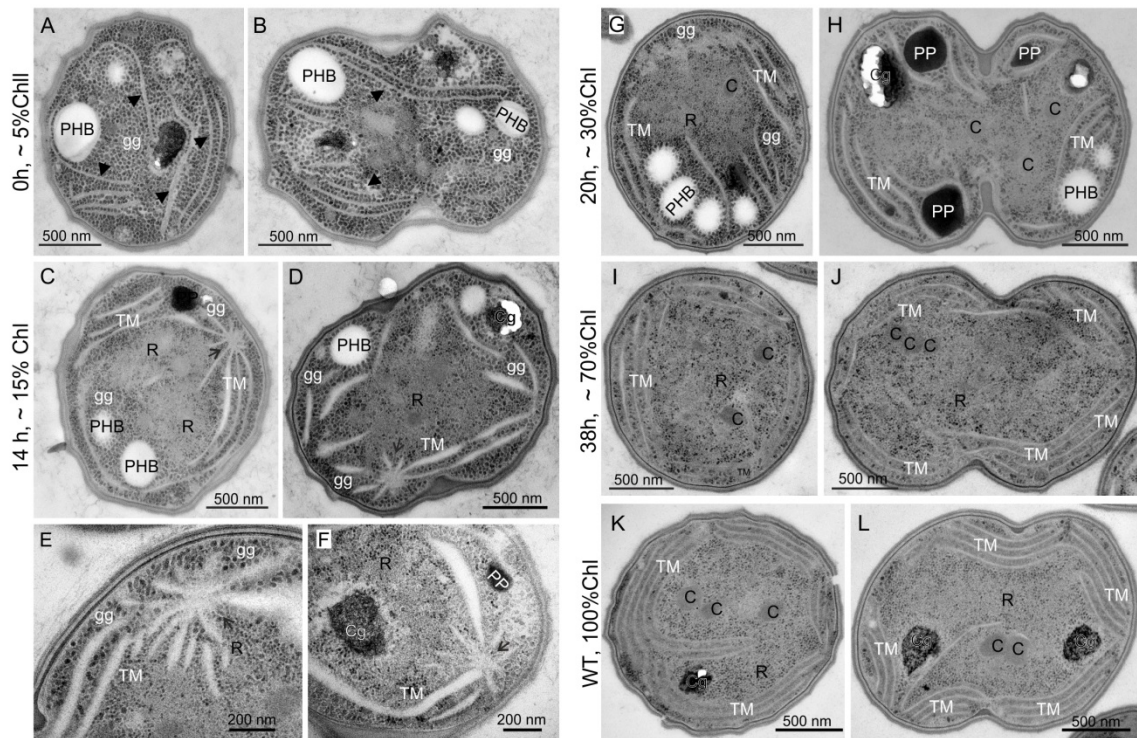


**Figure 14. TEM micrographs of ultrastructural changes during nitrogen starvation and the subsequent recovery.** A,B) Chlorotic *Synechocystis* cells lacking nitrogen for 2 months. C,D) An early stage of recovery in 14 hours after adding of nitrogen. E, F) A detailed image of TM vesicles in “star-like” structures. G,H) The ultrastructure of cells after 20 hours of the recovery and after 38 hours (I,J). K,L) Control WT cells grown in the regular BG11 medium under moderate light intensity ( $30 \mu\text{mol of photons m}^{-2} \text{s}^{-1}$ ). Abbreviations used: carboxysome – C; cyanophycin granules – Cg; glycogen granules – gg; polyhydroxybutyrate granules – PHB; polyphosphate granules – PP; ribosomes – R; thylakoid membrane – TM; Cells are processed by protocol 1 (see text and Material and methods section for details).

To further investigate the ‘star-like’ structures observed during the early phase of recovery (Figure 14 E,F) and to rule out a possibility of an artefact we focused on their detailed ultrastructural analysis. We prepared cells at the same stage of re-greening by an altered freeze substitution protocol (protocol 2). This protocol differs in using of some particular chemicals and also the time of some procedures was reduced (see Method section for details). These modifications improved the preservation of the cell ultrastructure; the TM system became less blurry and better visible as transparent membrane line surrounding the slightly darker lumen both in WT control (Figure 15 A,B) and in recovering cells (Figure 15 C-I). The total resin infiltration of the cell was however insufficient, which is visible as ruptures close to the cell wall (Figure 15 A,C-E). Yet even though some inconvenience during the sectioning, the ultrastructure of unusual ‘star-like’ structures were better preserved and visible as short membrane fragments or short vesicles clustered together toward the common center and vesicles further continued as

the TM sheets (Figure 15 G-I). These results support the model that the ‘star-like’ structures are of the membranous origin but with no obvious connection with PM.

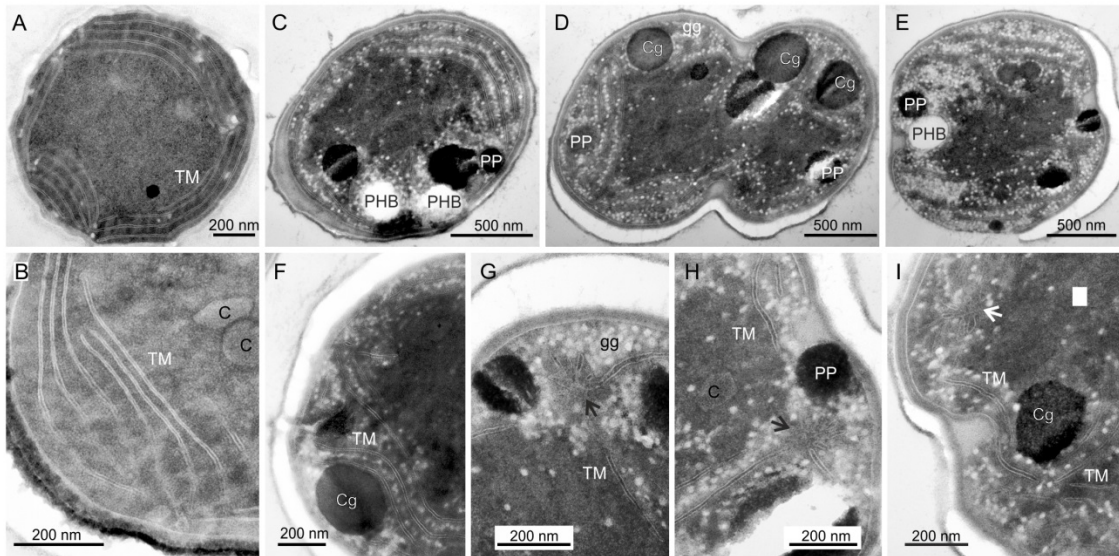


**Figure 15. TEM micrographs of *Synechocystis* cells processed by a modified protocol (#2).** A) Control WT cells grown in the regular BG11 medium under moderate light intensity ( $30 \mu\text{mol}$  of photons  $\text{m}^{-2} \text{s}^{-1}$ ). B) A detail of WT cell showing TMs converging towards the PM. C-E) Images of cells recovering for 14 h from chlorosis. F-I) Details of the TM organization in the recovering cell with visible ‘star-like’ membrane structures (arrow). Abbreviations used: carboxysome – C; cyanophycin granules – Cg; glycogen granules – gg; polyhydroxybutyrate granules – PHB; polyphosphate granules – PP; ribosomes – R.

Serial sectioning was used to investigate the 3D organization of the observed ‘star-like’ structures, which we tentatively recognize as TM biogenesis centers. The resulting picture (Figure 16 D,E) was generated from 23 serial ultra-thin sections of the same dividing cell (Figure 16 A-C). This cell was transversally sectioned showing that the described structures are relatively long (visible length is estimated to about 700 nm) and sheets of TMs are protruding laterally along the entire length and to all directions through at least 12 sections of the analysed cell (Figure 16). These centers are positioned close to cell poles but with no obvious connection to PM. But, in terms of 3D cyanobacterial cell organization, there is a direct connection between the two opposite centers via TM sheets (Figure 16 D,E). Moreover, a high concentration of ribosomes in the vicinity of these centers suggests that these locations in the cell are very active in the translation of new proteins (Figure 16 C,E).

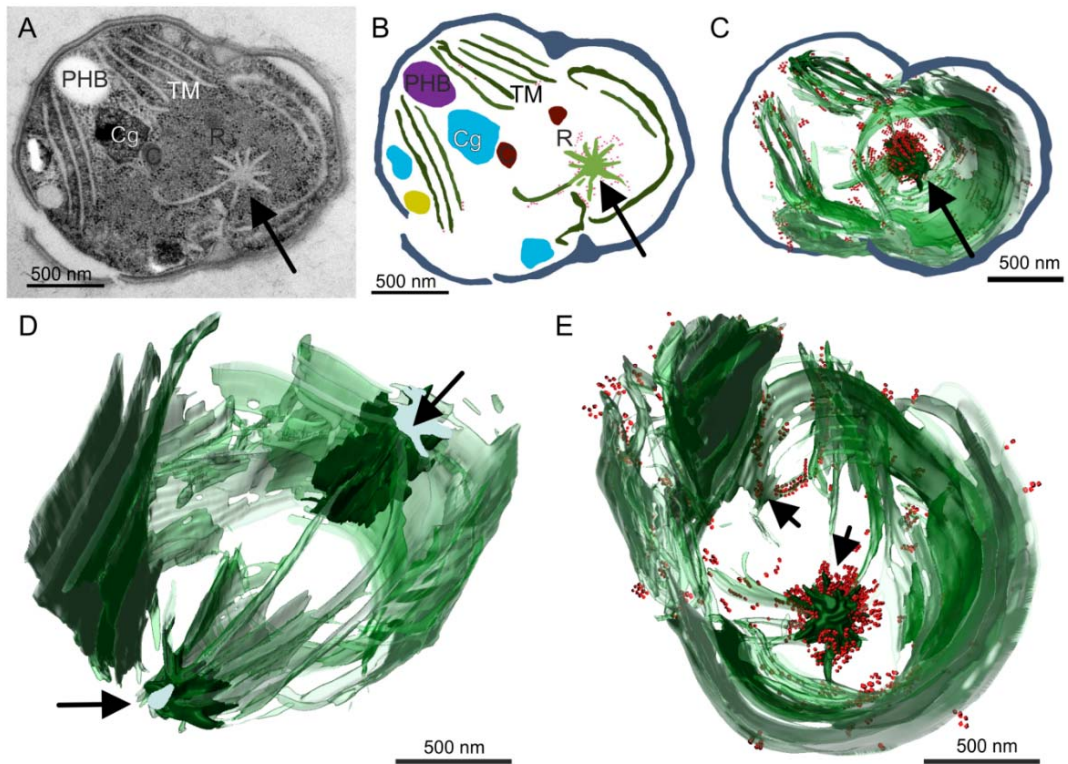


**Figure 16. 3D reconstruction of the recovering cell ultrastructure obtained by ultrathin-serial section TEM.** A) An image of *Synechocystis* dividing cell after 14 h of re-greening. B) A 2D model of the cell based on one of the TEM serial sections. C-E) 3D montage reconstructed produced using Amira software; black arrows show the ‘star-like’ structure observed only during an early stage of the re-greening; TM system is showed in green; Red dots indicate the position of ribosomes associated with TM. Abbreviations used: carboxysome – C; cyanophycin granules – Cg; polyhydroxybutyrate granules – PHB; polyphosphate granules – PP; ribosomes – R

## 4. Discussion

The synthesis of Chl-binding proteins is needed either during the repair of PSII, particularly the D1 subunit of PSII that has the fastest turnover (Komenda and Barber, 1995), or during fluctuating conditions to increase the content of PSI or, simply, for the production of TM during cell proliferation. There is however no technique that would allow to distinguish the newly produced TM from the older 'generation' of TM. Given the expected fast mobility of proteins and lipids in membranes, it is hardly possible anyway. Long-term nitrogen depletion has been shown to cause de-pigmentation of cyanobacteria (decrease/loss of Chl), degradation of photosynthetic complexes and TM; nonetheless after the reintroduction of the lacking nutrient back to the medium the cell quickly recovers (Allen and Smith, 1969; Görl et al., 1998). The recovery is under the control of a developmental programme, which triggers, the biosynthesis of Chl and Chl-binding proteins and the biogenesis of TM at a certain time (Klotz et al., 2016; chapter 3). This provides a chance to monitor the biogenesis of TM in detail by biochemical and microscopic methods.

In *Synechocystis*, when the proteosynthesis is re-established (~8 h) and a low amount of Chl starts to be available (Figure 11 A), perhaps just by converting a pool of chlorophyllide already occurring in the cell (Figure 13), the monomeric PSI is the first complex made by the recovering cell. (Figure 11 B,C). Intriguingly, it is a monomeric PSI and not the much more abundant trimeric PSI, which is in agreement with the report of Majeed et al. (2012) that the monomeric PSIs are produced independently and under different regulation than trimers (Majeed et al., 2012). It is also worth noting that an atypical monomeric PSI (designed PSI[1]\*) has been co-isolated with Chl-synthase (Chidgey et al., 2014). These early PSI monomers might in fact function as components of biosynthetic apparatus (centers) rather than normal photosystems. Moreover, the PSI complexes are known to be longer active in bleaching cells than PSII complexes that are quickly deactivated (Görl et al., 1998). PSIs as the first complexes to re-appear could generate ATP by cyclic electron transport before a sufficient amount of PSII is assembled. A faster re-appearance of PSI complexes has been also observed after recovery from a long-term dark adaptation of *Synechocystis* cells (Vernotte et al., 1992; Barthel et al., 2013). While the PSII activity is completely lost in darkness the PSI has been shown to be partially active (Barthel et al., 2013). Similarly to nitrogen deprivation, during heterotrophic growth cells decrease the Chl content and TMs are less abundant (Vernotte et al., 1992); after illumination levels of both PSI/PSII increased (PSI faster) and new TMs were produced (Barthel et al., 2013).

In our experimental setup, the greening process appears to be faster than that reported previously by Klotz et al. (2016). At the beginning of the recovery, cells start to



catabolise glycogen via parallel operation of the oxidative pentose phosphate cycle and the Entner-Doudoroff pathway to generate ATP (Doello et al., 2018). At this early stage of recovery, the synthesis of photosystems, the biosynthesis of tetrapyrroles and phycobilisome is actively suppressed (Görl et al., 1998; Klotz et al., 2016; Figure 11; Figure 12). Similarly to Spät et al. (2018) and Klotz et al. (2016), we observed a lag phase until 8h, after which the Chl intermediates started to accumulate (Figure 13) and, judging from the cell spectra, the amount of pigments in cells had increased after 14 h (Figure 11 A). In the work of Klotz et al. (2016) the genes involved in Chl biosynthetic pathway and coding for PSI subunits were induced after 12 h, and the central machinery for protein synthesis was fully functioning between 12 to 24 h. However, in our study (chapter 3) the PSI and PSII complexes were already accumulating in TM after 14 h (Figure 11 B,C; Figure 12). Faster re-greening in our case (chapter 3) could be due to the addition of glutamate as another source of nitrogen, which could help to re-establish nitrogen homeostasis, or/and by higher light intensities than used by Klotz et al. (2016).

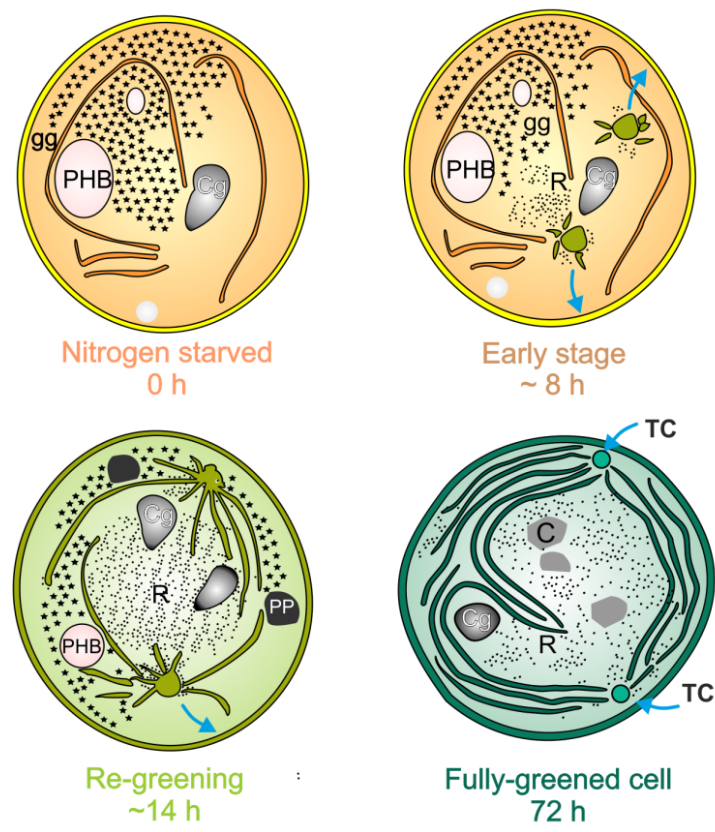


**Figure 17. A working model of the TM biogenesis during recovery from long-term nitrogen starvation.** Very early (~8 hours) after adding of nitrogen a few thylakoid centers are formed in the inner compartment of the cell together with transcription and translation apparatus. These centers contain translocons, enzymes required for the synthesis of lipids and cofactors (Chl, heme) and auxiliary factors involved in the biogenesis of membrane and assembly of photosystems (e.g. Vipp1, Curt1, Ycf3, Ycf48, Ycf39). TMs are produced by these centers that moved later on the periphery of the cell.

The fast induction of Chl pathway in cells that are fully packed with glycogen and containing just a few membrane fragments, strongly indicates that Chl synthesis is occurring in a specific membrane structure. Otherwise, it is hard to imagine how still half-dormant cell co-ordinates Chl synthesis with the translation of Chl-binding apoproteins. Particularly in metabolically ‘fragile’ recovering cells, it must be crucial to prevent any accumulation of unbound phototoxic Chl in membranes and thus further increase oxidative stress (Apel and Hirt, 2004; Wang and Grimm, 2015). Not just Chl but also intermediates of the Chl pathway are very phototoxic; the individual enzymatic steps need to be orchestrated to avoid larger pools of ‘free’ tetrapyrroles. It is, therefore, logical to expect a place in the cell (biosynthetic center), where Chl precursors are passed from enzyme to enzyme, Chl finalized and then loaded into Chl-binding proteins co-translationally as discussed in Sobotka (2014).

Based on data obtained in cyanobacteria (Chidgey et al., 2014; Kopečná et al., 2015; Bučinská et al., 2018; Yu et al., 2018) and algae (Nickelsen and Zerges, 2013), the biosynthetic center could be described as a SecY-YidC translocon embedded in a distinct membrane compartment rich of the lipid PG and equipped with various factors helping assembly of PSI or PSII, as well as enzymes producing Chl. PG (cardiolipin) is known to be essential for the functioning of SecY translocase (Corey et al., 2018) but also for the cyclase step of the Chl biosynthesis (Kopečná et al., 2015). Regarding the assembly factors, the Pam68 protein was co-localized with the translocon apparatus and ribosomes (Bučinská et al., 2018). Recently, the YidC insertase was co-purified with Ycf48, Ycf39 and CyanoP demonstrating that all these PSII auxiliary are located in the vicinity of translocon (Yu et al., 2018). Indeed, the luminal Ycf48 protein has been already suggested to be an interacting partner of the Pam68 protein in *Synechocystis* (Rengstl et al., 2011). Ycf48 and its plant homolog (HCF136) are needed for the formation of pD1m-D2m pre-complex (RCII) (Plücken et al., 2002; Komenda et al., 2008) The cyanobacterial and algal Ycf48 proteins have been crystallized as a seven-bladed beta-propeller with a conserved area interacting probably with pD1, but the *Synechocystis* Ycf48 also interacts with PSI (Yu et al., 2018). The current view is that the Ycf48 facilitates the Chl insertion into Chl-binding subunits, similarly to Pam68. However, the luminal Ycf48 protein is more essential, its absence clearly affects the cell viability even under low-stress conditions. Pam68 is upregulated under cold stress (Kopf et al., 2014) when the lipid bilayer became rigid, the photosynthetic activity is reduced and PSII complexes are prone to photodamage and the repair mechanism is inefficient (Wada and Murata, 1998). Yet cyanobacteria are able to acclimate to these conditions. In *Synechocystis* a various ribosomal genes are either up or down-regulated supporting the existence of a special pool of stress-induced ribosomes needed for the viability under cold stress. Pam68, as a ribosome-bound factor, might be locked close to the translocon machinery to stabilize

CP47 nascent chain while the Chl availability is limited and/or the membrane fluidity is restricted (Bučinská et al., 2018; Figure 9). There is also an interesting possibility that Chl-binding proteins contain amino-acid motifs causing ribosome pausing. It has been suggested that such delays in translation could provide time for the correct incorporation of Chl into the nascent apoproteins (Kim et al., 1994b; Manuell et al., 2007).

Other components of the cyanobacterial biosynthetic center should be High light-inducible proteins (Hlips), small, single helix proteins containing Chl-binding motif. Hlips are functionally connected with re-utilization of Chl molecules (reviewed in Komenda and Sobotka, 2016). This process is well documented as Chl molecules have a much longer lifetime in the cell than Chl-proteins (Vavilin and Vermaas, 2007) and the PSII D1 and D2 subunits are normally synthesized even when the Chl biosynthesis is drastically reduced (Hollingshead et al., 2016). Hlips are attached to Chl-synthase, the CP47 assembly module (Figure 9) and also to Ycf39 factor, which is probably responsible for the delivery of recycled Chl into the synthesised D1 protein (Knoppová et al., 2014). Finally, it is quite likely that a PSI complex is structural component of the center. PSI[1]\*-Chl-synthase complex has already been mentioned above and a complex of PSI with the physically attached RC47 assembly intermediate has been purified using the PSII assembly factor Psb28 as a bait (Bečková et al., 2017). Association to PSI could provide a photoprotective role during the PSII assembly (Komenda et al., 2012) as a trap for the excitation energy. Moreover, the PSI could serve as a source of Chl molecules for the PSII biogenesis during stress conditions (Kopečná et al., 2012).

There is no doubt that the availability of de novo Chl is a critical factor for the organization of TM (Sobotka et al., 2008; Hollingshead et al., 2016; Chapter 3). The ultrastructure of *Synechocystis* mutants deficient in Chl biosynthesis shows the whole TM network completely disrupted (Sobotka et al., 2008; Hollingshead et al., 2016). The deletion of *ycf54* gene that is required for the formation of protochlorophyllide caused a drastic reduction of TMs; the mutant contains only a few short membrane fragments randomly scattered throughout the cell (Hollingshead et al., 2016). The deletion of *gun4* gene, which is needed for another step in Chl biosynthesis, had a similar effect (Sobotka et al., 2008). Interestingly, an aberrant upregulation of Chl biosynthesis in a mutant of *Synechocystis* led to the formation of extra TM sheets; in addition to concentric, new centric membranes atypically crossed the mutant cells (Sobotka et al., 2005). This indicates that the production of de novo Chl (PSI subunits) could be a driving force for the abundance of TM in the cell. It should be however noted that the deletion of genes coding for Chl-binding proteins does not necessarily lead to such drastic ultrastructural changes as low Chl availability (Nilsson et al., 1992). The lack of PSI or PSII complexes indeed alters the organization of membranes within the cell and the number of membrane sheets is reduced (van de Meene et al., 2012). But still, these mutants exhibit normal

concentric TM sheets. PSI/PSII mutants grow however only heterotrophically utilizing glucose and TMs serve in fact as a normal bacterial membrane harbouring the respiratory protein complexes (Mullineaux, 2014). The heterotrophic mode could have a huge and still completely unknown impact on the membrane architecture. For instance, dark-grown *Synechocystis* cells contain only fragments of membranes (Barthel et al., 2013) and authors of this work suggest that the biogenesis of TM is linked to PSII activation.

What is the location of the biosynthetic apparatus (center) in the cyanobacterial cell remains a matter of discussion. As the cyanobacterium *Gloeobacter* sp. must have all components for the biogenesis of photosystems located in the PM (Rexroth et al., 2011), it has been assumed that the PSII assembly starts in PM also in modern cyanobacteria (Zak et al., 2001). This has been later ruled out (Selao et al., 2016) and thus biosynthetic centers should be located somewhere in the intracellular membrane system (Gutu et al., 2018). The specialize PDM fraction assumed having a role in the PSII biogenesis (Schottkowski et al., 2009) has been immuno-localised at the periphery of *Synechocystis* cells and co-localized with pD1 (Stengel et al., 2012). Similarly, the Vipp1 protein has been found in distinct puncta close to the periphery, in the TM regions of high curvature in *Synechocystis* (Gutu et al., 2018). Gutu et al. (2018) further showed that Vipp1 puncta are co-localized with Curt1 enrichments - special zones connected with photosystem biogenesis (Heinz et al., 2016).

Vipp1 and Curt1 proteins somehow affect the structural properties of TM. Vipp1 is able to form large oligomeric structures with tendencies to influence lipid composition in TM. This protein could thus support membrane properties required for the efficient translation or assembly of photosystems (Gutu et al., 2018) or, alternatively, the overall arrangement of TM sheets in the cell. Also, Curt1 could be needed for the optimal membrane plasticity and curvature and contributing to the ultrastructural reorganization (Pribil et al., 2018). Curt1 has not been localized in a photosynthetically active TM (Heinz et al., 2016) but it is co-localized with Vipp1 (Gutu et al., 2018). According to unpublished results of Petra Skotnicová from our laboratory, the *Synechocystis* Curt1 is specifically located in a separated membrane domain lacking completely PSI or PSII complexes. We do not know whether this Curt1 membrane domain is rich in translocons but regarding the observed ribosomes association with the newly established thylakoid centers (Figure 16 E) it would be a logical assumption. Interestingly, when *curt1* gene is deleted in *Arabidopsis* the PSII biogenesis and repair mechanism as well as state transitions in grana are impaired (Armbruster et al., 2013). *Synechocystis* mutant lacking Curt1 has TM atypically winded as spirals or circles inside of the cell without any hypothetical attachment to the cell periphery (Heinz et al., 2016).

We hypothesize that 'star' structures observed during the early stage of recovery from chlorosis represent cellular machinery engaged in the biogenesis of TM (see a working

model Figure 17). Together with the obtained biochemical data, we are tempting to speculate that PSI, and later also PSII complexes, are produced by these structures as the ribosomes are clearly observed close to the protruding TM sheets. According to our model (Figure 17) the biosynthetic center is de novo assembled in the central part of the cell, as this is the place where glycogen granules are first dissolved. Later, centers are moved to cell poles, where TCs have been located. Indeed, the long, tube-like structure of the proposed biosynthetic centers (Figure 16) resembles the shape of thylakoid centers characterized previously by TEM tomography (van de Meene et al., 2006). Apparently, there are two visible biosynthetic centers in the analyzed cells, which signals that each center is inherited by one daughter cell. The large oligomers of Vipp1 or Curt1 could be structural components providing the stability and shape of the TC or/and the produced TM sheets. The question remains, what is the origin of lipids in the produced TMs. So far, it is assumed that the synthesis of lipids occurs, similarly to the chloroplast, both in PM and TM (Selao et al., 2016). Close to inner chloroplast envelope, an MGDG-rich lipoproteic structure has been identified serving a role in non-vesicular lipid transport to TM; an interaction with Vipp1 has been also suggested (Bastien et al., 2016). Whether a similar specialized lipid-rich structure is present in cyanobacteria is not known. In a normally grown *Synechocystis* cell, the protein/lipid composition of TCs could differ from the TC established early during the re-greening process; it might explain why these structures are difficult to investigate and they were scarcely reported (Kunkel, 1982; van de Meene et al., 2006).

## 5. Material and methods

### **Cultivation conditions**

The *Synechocystis* glucose tolerant WT strain (GT-P sub-strain; Tichy et al., 2016) was grown photoautotrophically in liquid BG-11 medium on a rotary shaker under normal continuous light conditions ( $40 \mu\text{mol photons m}^{-2} \text{ s}^{-1}$ ) at  $28^\circ \text{C}$ . After reaching a logarithmic growth phase ( $\text{OD}_{730\text{nm}} = \sim 0.4\text{-}0.5$ ) the cells were gently harvested ( $5,000 \times g$ , 10 min), washed once with BG-11 lacking sodium nitrate (BG-11 -N) and re-suspended in BG-11 -N to obtain a similar cell density ( $\text{OD}_{730\text{nm}} = \sim 0.4\text{-}0.5$ ). Cells were kept at these conditions for 8 weeks; the BG-11 -N medium was replaced weekly with a fresh one. The recovery was triggered by adding the sodium nitrate (10 mM), glutamic acid (200  $\mu\text{M}$ ) and TES (10 mM) into the BG-11 -N medium at an  $\text{OD}_{750}$  of 0.2-0.4.

### **Absorption spectra and determination of Chl content**

Absorption spectra of whole cells were measured at room temperature with a Shimadzu UV 3000 spectrophotometer. Chl was extracted from cell pellets (3 mL,  $\text{OD}_{730\text{nm}} =$  approximately 0.4) with 100% methanol, and its concentration was measured spectrophotometrically according to (Porra et al., 1989).

### **Preparation of cellular membranes**

Cell cultures were harvested at various time-points after adding the nitrogen sources back to the culture. Pellet of cells was washed and re-suspended with buffer A (25 mM MES/NaOH, pH 6.5, 10 mM  $\text{CaCl}_2$ , 10 mM  $\text{MgCl}_2$ , 25% glycerol). Cells were disrupted by glass beads and the membrane fraction was separated from the soluble proteins by centrifugation at high speed ( $65,000 \times g$ , 20 min).

### **Electrophoresis and immunoblotting**

The protein composition of purified complexes was analyzed by electrophoresis in a denaturing 12 to 20% linear gradient polyacrylamide gel containing 7 M urea (Dobáková et al., 2009). Proteins were stained either by Coomassie Brilliant Blue or by SYPRO Orange stain. In the latter case, the proteins were subsequently transferred onto a polyvinylidene fluoride (PVDF) membrane for immunodetection (see below). Membranes were incubated with specific primary antibodies and then with secondary antibody conjugated with horseradish peroxidase (Sigma-Aldrich). The positive signal of chemiluminescence was read by LAS 4000 imager (Fuji, Japan). The following primary antibodies were used in the study: anti-CP43 and anti-D1 (Komenda et al., 2005), anti-PsaA/B (Agrisera, Sweden), and anti-Ycf48, which was raised in rabbit against recombinant *Synechocystis* Ycf48 (provided by Peter Nixon, Imperial College, London). The antibody against ChlM has been provided by Neil Hunter (University of Sheffield).

For clear native electrophoresis, solubilized membrane proteins or isolated complexes were separated on 4 to 12% native gel according to (Wittig et al., 2007). To resolve individual components of protein complexes the gel strips from the native electrophoresis were at first incubated in 2% SDS and 1% dithiothreitol for 30 min at room temperature and then placed on the top of 12 to 20% SDS-polyacrylamide gel containing 7 M urea (Dobáková et al., 2009). After separation, the 2D gel was stained by Coomassie Brilliant Blue. Mass-spectrometry identification of protein spots cut from the Coomassie-stained gel was performed essentially as described in (Bučinská et al., 2018).

### **Transmission electron microscopy**

Cells of *Synechocystis* WT cells that were starved for 8 weeks in BG-11 -N medium or WT cells at various time points of re-greening were pelleted by centrifugation (5,000  $\times$  g, 10 min). Pelleted cells were processed for TEM according to two different protocols:

**Protocol 1:** Pelleted cells were transferred to planchettes (200  $\mu$ m deep, Leica) pre-treated with 1% lecithin dissolved in chloroform (McDonald et al., 2010) and ultra-rapidly frozen by Leica EM PACT2 high-pressure freezer. Samples were processed similarly as described elsewhere (van de Meene et al., 2006) with some modifications. Samples were freeze-substituted in an automatic substitution unit (Leica EM AFS) at -85°C in a solution of 1% tannic acid and 0.5% glutaraldehyde dissolved in acetone. After 3 days the samples were 3 times rinsed in pure acetone for 1 h and the substitution medium was replaced by acetone with 1% osmium; the temperature was kept at -85°C. After 4 hours the temperature started to be gradually increased (5°C per hour) to -25°C and this temperature remained constant for the next 12h. Finally, samples thaw to 4°C (5°C per hour). At room temperature samples without planchettes were 3 times rinsed in pure acetone. Then over the 4-12 h samples were infiltrated by the increasing mixtures of Spurr in acetone (10%, 30%, 50%, 75%) and 2x 100% pure Spurr resin (Spurr, 1969).

**Protocol 2:** Pelleted cells were loaded into nitrate capillaries, placed into aluminium specimen carrier under hexadecane or loaded straight into the specimen carrier and frozen by HPM010 high-pressure freezing device (Bal-Tec). The frozen samples were freeze-substituted in a substitution unit (Leica EM AFM2) at -90°C in acetone containing 1% tannic acid. After 24 h samples were 3 times rinsed in acetone for 1 h and then the substitution medium was replaced with 2% osmium and 0.5% uranyl acetate in acetone. After 24 hours at -90°C the samples were gradually thawed to -60°C (10°C per hour), where they were kept for 6 h and then the temperature was increased to -40°C and glutaraldehyde (0,5%) was added to the mixture. After an additional 6 h, the temperature was finally increased to -20°C (5°C per hour). At this temperature, the samples were rinsed in acetone and infiltration with 20% and 40% mixture of EPON dissolved in

acetone was done over 1-2 h. The infiltration with 75% mixture of EPON/Acetone and with pure EPON resin was completed at room temperature over the 4-6 h.

Processed samples embedded in pure resin by either of the protocols were polymerized in an oven at 60°C for 48 h. Ultra-thin sections (50-70 nm) were cut using Leica UCT ultramicrotome, collected on meshed copper grids (100 or 300; EMS, Hatfield, USA) or on slot grids (EMS, Hatfield, USA) with the formvar coating. Sections were stained with 1% aqueous uranyl acetate for 10 minutes and with Sato's lead citrate for 3 min (Hanaichi et al., 1986). Images were acquired using a Jeol 1010 operated at 80 kV equipped with a Mega View III camera (SIS) at Laboratory of electron microscopy (Biology Centre, CAS, České Budějovice) or at Tecnai G2 Spirit BioTWIN operating at 120 kV equipped with a Gatan USC4000 CCD-camera at MPI for Developmental Biology (Tübingen, Germany). Images were processed with ImageJ software (Abramoff et al., 2004). The serial sections were processed in 3d Imod and render in Amira software.



## 6. Summary

Oxygenic phototrophs rely on Chl-binding protein complexes (photosystems) embedded in a specialized endogenous TM. To build TM the cell needs to coordinate the synthesis and assembly of proteins, Chl and other cofactors and also different lipids into large complexes. The role of Chl-binding subunits of photosystems in the TM biogenesis is crucial but what is the mechanism or cellular machinery that produces the photosynthetic TM system, remains unclear.

The aim of this thesis was to explore the biogenesis of Chl-binding proteins and TM in the model cyanobacterium *Synechocystis* PCC 6803 (hereafter *Synechocystis*) by combining molecular and electron microscopic techniques.

The first publication Kopečná et al. (2012) deals with the distribution of Chl molecules into individual Chl-binding proteins and how the distribution modulates the overall TM architecture. PSI and PSII are complicated, light-powered photo-oxidoreductase enzymes, and Chl-binding proteins are their major protein-building blocks. However, the ratio between PSI and PSII is responding to changes in light conditions. Particularly, the PSI content must be reduced under high light together with phycobilisomes to prevent over-excitation of photosynthetic apparatus and production of reactive oxygen species. This work has shown that most of the newly made Chl molecules are directed to PSI complexes, suggesting that PSII complexes can be synthesized by utilizing ‘old’ Chl released from the degraded proteins. During acclimation to high light, the decrease in PSI is accompanied by lowered content of TMs in cells, which indicates that there is a link between Chl availability, synthesis of PSI complexes and the total number of TMs maintained in the cell.

The second publication Hollingshead et al. (2016) demonstrates that the impaired synthesis of de novo Chl molecules has a selective effect on the synthesis of individual Chl-binding subunits of PSI and PSII. We characterized *Synechocystis ycf54* mutant, which possesses a defect in the Chl biosynthetic pathway and produces < 10% of Chl when compared to WT. Interestingly, while the synthesis of PSI (PsaA/B) and also the PSII subunit CP47 was almost abolished in the mutant, the synthesis of D1 and D2 appeared unaffected and the RCII complex of PSII was assembled. It is in line with the previous publication Kopečná et al. (2012) reporting that the PSII complexes, or at least the central D1 and D2 subunits, can be produced just recycling the same pool of Chl molecules. Chl deficiency in the *ycf54* mutant had a dramatic impact on the structure of TM - this strain contains only fragments of disorganized short membranes dispersed throughout the cell. Thus a sufficient amount of de novo produced Chl is crucial for the TM biogenesis.

As reported in Hollingshead et al. (2016) the synthesis and accumulation of CP47 protein is more sensitive to a shortage in de novo made Chl molecules than the structurally similar CP43. In the third publication Bučinská et al. (2018) we described Pam68 as a ribosome-associated protein, which facilitates the insertion of Chl molecules into CP47. The deletion of *pam68* gene in *Synechocystis* affected the CP47 synthesis under stress conditions such as low temperature, light fluctuation or nitrogen deficiency. Using a strain expressing Flag-tagged Pam68 we co-purified this protein with CP47 but also with ribosomal subunits and other components of translocation apparatus. We have further demonstrated that the Pam68 binds to newly synthesized CP47 before another PSII subunit, PsbH, associates with CP47 to form the CP47 assembly module. When both Pam68 and PsbH were eliminated the synthesis of CP47 was almost completely abolished causing the loss of autotrophy. Interestingly, blocking the heme synthetic pathway, which is known to stimulate Chl biosynthesis, rescued the synthesis of CP47 in the *pam68/psbH* double mutant. Based on these data, we concluded that the Pam68 is an assisting factor, which facilitates the loading of Chl molecules into CP47.

The Chl availability dictates what Chl-binding proteins are synthesised and the insertion of Chl molecules into the translating apoproteins requires the assistance of auxiliary factors. However, how the biogenesis of photosystem is linked to the development of TM is unknown. *Synechocystis* cells kept for two months in growth media without nitrogen remain viable but lost almost completely photosynthetic complexes (chlorosis). After adding nitrogen, cells fully re-green in a few days, which allow monitoring the development of a 'green' cell. In fourth publication Klotz et al. (2016), the recovery from chlorosis has been followed on the RNA and metabolomic levels, as well as by microscopic techniques. This work demonstrates that cyanobacteria possess a specialized genetic program initiated during the resuscitating from the chlorosis. After adding of nitrogen the glycogen stored in granules is progressively catabolized and the generated energy utilized for the re-starting of proteosynthesis. During the second phase (12-24 h), Chl is massively synthesized, which is followed by the reconstitution of photosynthetic apparatus. The *Synechocystis* cell completely recovers from the chlorosis in 48 h.

In a manuscript (chapter 3), we focused on the biogenesis of photosystems and TM in cells recovering from the chlorosis. We found that the Chl pathway is in fact restarted in a few hours after adding of nitrogen and produced Chl is built into monomeric PSI complex, the first Chl-complex that re-appeared in the recovering cells. The biogenesis of TM after nitrogen depletion was tracked on electron-micrographs showing increasingly growing TM sheets that were originating from an atypical 'star-like' membranous structure occurring close to the periphery of the cell. We also observed the high concentration of ribosomes in the vicinity of these structures. We proposed that these

structures serve as biosynthetic centers called before thylakoid centers as they seem to be biosynthetically active with the close association of the ribosomes.

The assembly of photosystems starts with the biosynthesis of Chl-binding proteins which seems to be affected by the availability of Chl and its lack causes their instability and degradation. Many assisting factors facilitating the assembly of photosystems have been identified. However, the synthesis of Chl-binding proteins, its insertion in the TM and incorporation of the cofactors into nascent proteins still needs to be explored. This process involves many steps and it is highly probable that it needs to be co-regulated with the biosynthesis of Chl and also with the formation of TM itself. Therefore, it is logical to presume the existence of putative biosynthetic centers as sites, where the whole biogenesis of TM is coordinated.

## 7. Conclusions

The PhD thesis expands the current view of the biogenesis of TM in cyanobacteria. The presented results demonstrate the interconnectivity of the Chl-binding proteins synthesis and the TM formation. Furthermore, we elaborated on the role of auxiliary protein factors such as Pam68 in the insertion of Chl into PSII subunits. The shortage of Chl, particularly under stress conditions, causes its incorrect/inefficient insertion into apoproteins and affects the biogenesis of photosynthetic membrane, as well as photosynthetic complexes. The thesis consists of one first author publication, three co-author publications and one first author manuscript.

The main conclusions are as follows:

- The lower formation of de novo Chl in the cyanobacterium *Synechocystis* PCC 6803 not only inhibits the synthesis of Chl-binding proteins but clearly affects the structure TM and its organization in the cell.
- Pam68 is a ribosome-bound protein that very probably stabilizes the nascent CP47 chain in a conformation that facilitates Chl insertion. Together with the canonical PSII subunit PsbH, the Pam68 protein is essential for the synthesis of CP47.
- Re-greening of the *Synechocystis* nitrogen-depleted cells is a promising approach to study the biogenesis of TM in cyanobacteria.
- The biogenesis of TM is connected to distinct ‘star-like’ structures that could serve as a biosynthetic center. It might represent the same molecular machinery as the already described thylakoid center. Closely associated with ribosomes, the translation of Chl-binding subunits of both photosystems could be established here and co-localized with the biosynthesis of Chl molecules.



## 8. Literature

- Abramoff MD, Magalhães PJ, Ram SJ** (2004) Image processing with ImageJ. *Biophotonics Intern* **11**: 36–42
- Agarwal R, Matros A, Melzer M, Mock HP, Sainis JK** (2010) Heterogeneity in thylakoid membrane proteome of *Synechocystis* 6803. *J Proteomics* **73**: 976-991
- Albanese P, Melero R, Engel BD, Grinzato A, Berto P, Manfredi M, Chiodoni A, Vargas J, Sorzano CÓS, Marengo E, Saracco G, Zanotti G, Carazo J-M, Pagliano C** (2017) Pea PSII-LHCII supercomplexes form pairs by making connections across the stromal gap. *Sci Rep* **7**: 10067-10067
- Allen MM** (1968) Photosynthetic membrane system in *Anacystis nidulans*. *J Bacteriol* **96**: 836-841
- Allen MM** (1984) Cyanobacterial cell inclusions. *Annu Rev Microbiol* **38**: 1-25
- Allen MM, Smith AJ** (1969) Nitrogen chlorosis in blue-green algae. *Arch Mikrobiol* **69**: 114-120
- Allen MM, Weathers PJ** (1980) Structure and composition of cyanophycin granules in the cyanobacterium *Aphanocapsa* 6308. *J Bacteriol* **141**: 959-962
- Amunts A, Drory O, Nelson N** (2007) The structure of a plant photosystem I supercomplex at 3.4 Å resolution. *Nature* **447**: 58
- Anderson JM, Melis A** (1983) Localization of different photosystems in separate regions of chloroplast membranes. *Proc Natl Acad Sci USA* **80**: 745-749
- Aoki M, Sato N, Meguro A, Tsuzuki M** (2004) Differing involvement of sulfoquinovosyl diacylglycerol in photosystem II in two species of unicellular cyanobacteria. *Eur J Biochem* **271**: 685-693
- Apel K, Hirt H** (2004) Reactive oxygen species: Metabolism, oxidative stress, and signal transduction. *Annu Rev Plant Biol* **55**: 373-399
- Armbruster U, Labs M, Pribil M, Viola S, Xu WT, Scharfenberg M, Hertle AP, Rojahn U, Jensen PE, Rappaport F, Joliot P, Dormann P, Wanner G, Leister D** (2013) *Arabidopsis* CURVATURE THYLAKOID1 proteins modify thylakoid architecture by inducing membrane curvature. *Plant Cell* **25**: 2661-2678
- Armbruster U, Zuhlke J, Rengstl B, Kreller R, Makarenko E, Ruhle T, Schunemann D, Jahns P, Weisshaar B, Nickelsen J, Leister D** (2010) The *Arabidopsis* thylakoid protein PAM68 is required for efficient D1 biogenesis and photosystem II assembly. *Plant Cell* **22**: 3439-3460
- Arvidsson P-O, Sundby C** (1999) A model for the topology of the chloroplast thylakoid membrane. *Funct Plant Biol* **26**: 687-694
- Austin JR, Staehelin LA** (2011) Three-dimensional architecture of grana andstroma thylakoids of higher plants as determined by electron tomography. *Plant Physiol* **155**: 1601
- Awai K, Watanabe H, Benning C, Nishida I** (2007) Digalactosyldiacylglycerol is required for better photosynthetic growth of *Synechocystis* sp. PCC6803 under phosphate limitation. *Plant Cell Physiol* **48**: 1517-1523
- Babiychuk E, Muller F, Eubel H, Braun HP, Frentzen M, Kushnir S** (2003) *Arabidopsis* phosphatidylglycerophosphate synthase 1 is essential for chloroplast differentiation, but is dispensable for mitochondrial function. *Plant J* **33**: 899-909
- Bar-On YM, Phillips R, Milo R** (2018) The biomass distribution on Earth *Proc Natl Acad Sci USA* **115**: 6506
- Barber J, Morris E, Buchel C** (2000) Revealing the structure of the photosystem II chlorophyll binding proteins, CP43 and CP47. *BBA - Bioenergetics* **1459**: 239-247
- Barthel S, Bernat G, Seidel T, Rupprecht E, Kahmann U, Schneider D** (2013) Thylakoid membrane maturation and PSII activation are linked in greening *Synechocystis* sp PCC 6803 cells. *Plant Physiol* **163**: 1037-1046
- Bastien O, Botella C, Chevalier F, Block MA, Jouhet J, Breton C, Girard-Egrot A, Maréchal E** (2016) New insights on thylakoid biogenesis in plant cells. *In* KW Jeon, ed, *Int Rev Cell Mol Biol* Vol 323. Academic Press, pp 1-30

- Bečková M, Gardian Z, Yu J, Koník P, Nixon PJ, Komenda J** (2017) Association of Psb28 and Psb27 proteins with PSII-PSI supercomplexes upon exposure of *Synechocystis* sp. PCC 6803 to high light. *Mol Plant* **10**: 62-72
- Benning C** (1998) Membrane lipids in anoxygenic photosynthetic bacteria. In S Paul-André, M Norio, eds, *Lipids in Photosynthesis: Structure, Function and Genetics*. Springer Netherlands, Dordrecht, pp 83-101
- Benning C** (2008) A role for lipid trafficking in chloroplast biogenesis. *Prog Lipid Res* **47**: 381-389
- Benning C** (2009) Mechanisms of lipid transport involved in organelle biogenesis in plant cells. *Annu Rev Cell Dev Biol* **25**: 71-91
- Bertos NR, Gibbs SP** (1998) Evidence for a lack of photosystem segregation in *Chlamydomonas reinhardtii* (*Chlorophyceae*). *J Phycol* **34**: 1009-1016
- Blankenship RE** (2013) *Molecular mechanisms of photosynthesis*. Wiley- Blackwell, pp-336
- Boehm M, Romero E, Reisinger V, Yu J, Komenda J, Eichacker LA, Dekker JP, Nixon PJ** (2011) Investigating the early stages of photosystem II assembly in *Synechocystis* sp. PCC 6803 isolation of CP47 and CP43 complexes. *J Biol Chem* **286**: 14812-14819
- Bohne A-V, Schwarz C, Schottkowski M, Lidschreiber M, Piotrowski M, Zerges W, Nickelsen J** (2013) Reciprocal regulation of protein synthesis and carbon metabolism for thylakoid membrane biogenesis. *PLoS Biol* **11**: e1001482
- Boudreau E, Takahashi Y, Lemieux C, Turmel M, Rochaix JD** (1997) The chloroplast *ycf3* and *ycf4* open reading frames of *Chlamydomonas reinhardtii* are required for the accumulation of the photosystem I complex. *EMBO J* **16**: 6095-6104
- Bricker TM, Roose JL, Fagerlund RD, Frankel LK, Eaton-Rye JJ** (2012) The extrinsic proteins of Photosystem II. *Biochim Biophys Acta* **1817**: 121-142
- Bryan SJ, Burroughs NJ, Shevela D, Yu J, Rupprecht E, Liu L-N, Mastroianni G, Xue Q, Llorente-Garcia I, Leake MC, Eichacker LA, Schneider D, Nixon PJ, Mullineaux CW** (2014) Localisation and interactions of the Vipp1 protein in cyanobacteria. *Mol Microbiol* **94**: 1179-1195
- Bučinská L, Kiss E, Koník P, Knoppova J, Komenda J, Sobotka R** (2018) The ribosome-bound protein Pam68 promotes insertion of chlorophyll into the CP47 subunit of photosystem II. *Plant Physiol* **176**: 2931-2942
- Cardona T** (2016) Reconstructing the origin of oxygenic photosynthesis: Do assembly and photoactivation recapitulate evolution? *Front Plant Sci* **7**: 1-13
- Casella S, Huang F, Mason D, Zhao G-Y, Johnson GN, Mullineaux CW, Liu L-N** (2017) Dissecting the native architecture and dynamics of cyanobacterial photosynthetic machinery. *Mol Plant* **10**: 1434-1448
- Chidgey JW, Linhartová M, Komenda J, Jackson PJ, Dickman MJ, Canniffe DP, Koník P, Pilný J, Hunter CN, Sobotka R** (2014) A cyanobacterial chlorophyll synthase-HliD complex associates with the Ycf39 protein and the YidC/Alb3 insertase. *Plant Cell* **26**: 1267-1279
- Chitnis VP, Chitnis PR** (1993) PsaL subunit is required for the formation of photosystem I trimers in the cyanobacterium *Synechocystis* sp. PCC 6803. *FEBS Lett* **336**: 330-334
- Corey RA, Pyle E, Allen WJ, Watkins DW, Casiraghi M, Miroux B, Arechaga I, Politis A, Collinson I** (2018) Specific cardiolipin-SecY interactions are required for proton-motive force stimulation of protein secretion. *Proc Natl Acad Sci USA* **115**: 7967-7972
- D'Haene SE, Sobotka R, Bučinská L, Dekker JP, Komenda J** (2015) Interaction of the PsbH subunit with a chlorophyll bound to histidine 114 of CP47 is responsible for the red 77K fluorescence of Photosystem II. *Biochim Biophys Acta* **1847**: 1327-1334
- Daum B, Kühlbrandt W** (2011) Electron tomography of plant thylakoid membranes. *J Exp Bot* **62**: 2393-2402
- Demé B, Cataye C, Block MA, Maréchal E, Jouhet J** (2014) Contribution of galactoglycerolipids to the 3-dimensional architecture of thylakoids. *FASEB J* **28**: 3373-3383

- Dobáková M, Sobotka R, Tichý M, Komenda J** (2009) Psb28 protein is involved in the biogenesis of the photosystem II inner antenna CP47 (*psbB*) in the cyanobacterium *Synechocystis* sp. PCC 6803. *Plant Physiol* **149**: 1076-1086
- Dobáková M, Tichý M, Komenda J** (2007) Role of the PsbI protein in photosystem II assembly and repair in the cyanobacterium *Synechocystis* sp. PCC 6803. *Plant Physiol* **145**: 1681-1691
- Doello S, Klotz A, Makowka A, Gutekunst K, Forchhammer K** (2018) A specific glycogen mobilization strategy enables rapid awakening of dormant cyanobacteria from chlorosis. *Plant Physiol* **177**: 594
- Domonkos I, Kis M, Gombos Z, Ughy B** (2013) Carotenoids, versatile components of oxygenic photosynthesis. *Prog Lipid Res* **52**: 539-561
- Domonkos I, Malec P, Sallai A, Kovacs L, Itoh K, Shen G, Ughy B, Bogos B, Sakurai I, Kis M, Strzalka K, Wada H, Itoh S, Farkas T, Gombos Z** (2004) Phosphatidylglycerol is essential for oligomerization of photosystem I reaction center. *Plant Physiol* **134**: 1471-1478
- Eichacker LA, Helfrich M, Rüdiger W, Müller B** (1996) Stabilization of Chlorophyll a-binding Apoproteins P700, CP47, CP43, D2, and D1 by Chlorophyll *a* or Zn-pheophytin *a*. *J Biol Chem* **271**: 32174-32179
- Enami I, Okumura A, Nagao R, Suzuki T, Iwai M, Shen JR** (2008) Structures and functions of the extrinsic proteins of photosystem II from different species. *Photosyn Res* **98**: 349-363
- Engel BD, Schaffer M, Kuhn Cuellar L, Villa E, Plitzko JM, Baumeister W** (2015) Native architecture of the *Chlamydomonas* chloroplast revealed by in situ cryo-electron tomography. *eLife* **4**: e04889
- Ferreira KN, Iverson TM, Maghlaoui K, Barber J, Iwata S** (2004) Architecture of the photosynthetic oxygen-evolving center. *Science* **303**: 1831-1838
- Flores E, Herrero A** (2005) Nitrogen assimilation and nitrogen control in cyanobacteria. *Biochem Soc Trans* **33**: 164-167
- Folea IM, Zhang P, Nowaczyk MM, Ogawa T, Aro EM, Boekema EJ** (2008) Single particle analysis of thylakoid proteins from *Thermosynechococcus elongatus* and *Synechocystis* 6803: Localization of the CupA subunit of NDH-1. *FEBS Lett* **582**: 249-254
- Frick G, Su QX, Apel K, Armstrong GA** (2003) An *Arabidopsis porB porC* double mutant lacking light-dependent NADPH:protochlorophyllide oxidoreductases B and C is highly chlorophyll-deficient and developmentally arrested. *Plant J* **35**: 141-153
- Fristedt R, Willig A, Granath P, Crevecoeur M, Rochaix JD, Vener AV** (2009) Phosphorylation of photosystem II controls functional macroscopic folding of photosynthetic membranes in *Arabidopsis*. *Plant Cell* **21**: 3950-3964
- Gao H, Xu X** (2009) Depletion of *Vipp1* in *Synechocystis* sp. PCC 6803 affects photosynthetic activity before the loss of thylakoid membranes. *FEMS Microbiol Lett* **292**: 63-70
- Göhre V, Ossenbuhl F, Crevecoeur M, Eichacker LA, Rochaix JD** (2006) One of two Alb3 proteins is essential for the assembly of the photosystems and for cell survival in *Chlamydomonas*. *Plant Cell* **18**: 1454-1466
- Golecki JR, Oelze J** (1980) Differences in the architecture of cytoplasmic and intracytoplasmic membranes of three chemotrophically and phototrophically grown species of the *Rhodospirillaceae*. *J Bacteriol* **144**: 781-788
- Gonzalez-Esquer CR, Smarda J, Rippka R, Axen SD, Guglielmi G, Gugger M, Kerfeld CA** (2016) Cyanobacterial ultrastructure in light of genomic sequence data. *Photosyn Res* **129**: 147-157
- Görl M, Sauer J, Baier T, Forchhammer K** (1998) Nitrogen-starvation-induced chlorosis in *Synechococcus* PCC 7942: adaptation to long-term survival. *Microbiol* **144**: 2449-2458
- Gromov BV, Mamkaeva KA** (1976) Connection of thylakoids with plasmalemma in the *Synechococcus* cyanobacterium. *Microbiol* **45**: 920-922
- Guskov A, Kern J, Gabdulkhakov A, Broser M, Zouni A, Saenger W** (2009) Cyanobacterial photosystem II at 2.9-Å resolution and the role of quinones, lipids, channels and chloride. *Nat Struct Mol Biol* **16**: 334



- Gutu A, Chang F, O'Shea EK** (2018) Dynamical localization of a thylakoid membrane binding protein is required for acquisition of photosynthetic competency. *Mol Microbiol* **108**: 16-31
- Hagio M, Gombos Z, Varkonyi Z, Masamoto K, Sato N, Tsuzuki M, Wada H** (2000) Direct evidence for requirement of phosphatidylglycerol in photosystem II of photosynthesis. *Plant Physiol* **124**: 795-804
- Hanaichi T, Sato T, Iwamoto T, Malavasi-Yamashiro J, Hoshino M, Mizuno N** (1986) A stable lead by modification of Sato's method. *J Electron Microsc* **35**: 304-306
- He QF, Vermaas W** (1998) Chlorophyll a availability affects *psbA* translation and D1 precursor processing in vivo in *Synechocystis* sp. PCC 6803. *Proc Natl Acad Sci USA* **95**: 5830-5835
- Heidrich J, Thurotte A, Schneider D** (2017) Specific interaction of IM30/Vipp1 with cyanobacterial and chloroplast membranes results in membrane remodeling and eventually in membrane fusion. *Biochim Biophys Acta - Biomembranes* **1859**: 537-549
- Heinz S, Liauw P, Nickelsen J, Nowaczyk M** (2016) Analysis of photosystem II biogenesis in cyanobacteria. *Biochim Biophys Acta* **1857**: 274-287
- Heinz S, Rast A, Shao L, Gutu A, Gügel IL, Heyno E, Labs M, Rengstl B, Viola S, Nowaczyk MM, Leister D, Nickelsen J** (2016) Thylakoid Membrane Architecture in *Synechocystis* Depends on CurT, a Homolog of the Granal CURVATURE THYLAKOID1 Proteins *Plant Cell* **28**: 2238- 2260
- Hennig R, Heidrich J, Saur M, Schmäser L, Roeters SJ, Hellmann N, Woutersen S, Bonn M, Weidner T, Markl J, Schneider D** (2015) IM30 triggers membrane fusion in cyanobacteria and chloroplasts. *Nature Commun* **6**: 7018
- Hennig R, West A, Debus M, Saur M, Markl J, Sachs JN, Schneider D** (2017) The IM30/Vipp1 C-terminus associates with the lipid bilayer and modulates membrane fusion. *Biochim Biophys Acta* **1858**: 126-136
- Henningsen KW, Boynton JE** (1974) Macromolecular physiology of plastids. IX. Development of plastid membranes during greening of dark-grown barley seedlings. *J Cell Sci* **15**: 31-55
- Hennon SW, Soman R, Zhu L, Dalbey RE** (2015) YidC/Alb3/Oxa1 Family of Insertases. *J Biol Chem* **290**: 14866-14874
- Heslop-Harrison J** (1963) Structure and morphogenesis of lamellar systems in grana-containing chloroplasts. *Planta* **60**: 243-260
- Hinterstoisser B, Cichna M, Kuntner O, Peschek GA** (1993) Cooperation of plasma and thylakoid membranes for the biosynthesis of chlorophyll in cyanobacteria: the role of the thylakoid centers. *J Plant Physiol* **142**: 407-413
- Hohmann-Marriott MF, Roberson RW** (2009) Exploring photosynthesis by electron tomography. *Photosyn Res* **102**: 177-188
- Hollingshead S, Kopečná J, Armstrong DR, Bučinská L, Jackson PJ, Chen GE, Dickman MJ, Williamson MP, Sobotka R, Hunter CN** (2016) Synthesis of chlorophyll-binding proteins in a fully segregated  $\Delta ycf54$  strain of the cyanobacterium *Synechocystis* PCC 6803. *Front Plant Sci* **7**: 1-15
- Imhoff JF, Kushner DJ, Kushwaha SC, Kates M** (1982) Polar lipids in phototrophic bacteria of the *Rhodospirillaceae* and *Chromatiaceae* families. *J Bacteriol* **150**: 1192-1201
- Jarvis P, Dormann P, Peto CA, Lutes J, Benning C, Chory J** (2000) Galactolipid deficiency and abnormal chloroplast development in the *Arabidopsis* MGD synthase 1 mutant. *Proc Natl Acad Sci USA* **97**: 8175-8179
- Johnson MP, Vasilev C, Olsen JD, Hunter CN** (2014) Nanodomains of cytochrome *b6f* and photosystem II complexes in spinach grana thylakoid membranes. *Plant Cell* **26**: 3051
- Jordan P, Fromme P, Witt HT, Klukas O, Saenger W, Krauss N** (2001) Three-dimensional structure of cyanobacterial photosystem I at 2.5 Å resolution. *Nature* **411**: 909-917
- Jouhet J** (2013) Importance of the hexagonal lipid phase in biological membrane organization. *Front Plant Sci* **4**: 1-5
- Kaneko T, Sato S, Kotani H, Tanaka A, Asamizu E, Nakamura Y, Miyajima N, Hirose M, Sugiura M, Sasamoto S, Kimura T, Hosouchi T, Matsuno A, Muraki A,**

- Nakazaki N, Naruo K, Okumura S, Shimpo S, Takeuchi C, Wada T, Watanabe A, Yamada M, Yasuda M, Tabata S** (1996) Sequence analysis of the genome of the unicellular cyanobacterium *Synechocystis* sp. strain PCC6803. II. Sequence determination of the entire genome and assignment of potential protein-coding regions. *DNA res* **3**: 109-136
- Karim S, Aronsson H** (2014) The puzzle of chloroplast vesicle transport – involvement of GTPases. *Front Plant Sci* **5**: 472
- Kern J, Zouni A, Guskov A, Krauss N** (2009) Lipids in the structure of photosystem I, photosystem II and the cytochrome *b6f* complex. *In* H Wada, N Murata, eds, *Lipids in Photosynthesis: Essential and Regulatory Functions*, Vol 30. Springer, Dordrecht, pp 203
- Kim EH, Li XP, Razeghifard R, Anderson JM, Niyogi KK, Pogson BJ, Chow WS** (2009) The multiple roles of light-harvesting chlorophyll a/b-protein complexes define structure and optimize function of *Arabidopsis* chloroplasts: a study using two chlorophyll *b*-less mutants. *Biochim Biophys Acta* **1787**: 973-984
- Kim J, Eichacker LA, Rudiger W, Mullet JE** (1994a) Chlorophyll regulates accumulation of the plastid-encoded chlorophyll proteins P700 and D1 by increasing apoprotein stability. *Plant Physiol* **104**: 907-916
- Kim J, Klein PG, Mullet JE** (1994b) Synthesis and turnover of photosystem II reaction center protein D1. Ribosome pausing increases during chloroplast development. *J Biol Chem* **269**: 17918-17923
- Kirchhoff H** (2018) Structure-function relationships in photosynthetic membranes: Challenges and emerging fields. *Plant Sci* **266**: 76-82
- Kirchhoff WR, Hall AE, Thomson WW** (1989) Gas exchange, carbon isotope discrimination, and chloroplast ultrastructure of a chlorophyll-deficient mutant of cowpea. *Crop Sci* **29**: 109-115
- Klinkert B, Ossenhuhl F, Sikorski M, Berry S, Eichacker L, Nickelsen J** (2004) PrtA, a periplasmic tetratricopeptide repeat protein involved in biogenesis of photosystem II in *Synechocystis* sp. PCC 6803. *J Biol Chem* **279**: 44639-44644
- Klostermann E, Helling ID, Carde JP, Schunemann D** (2002) The thylakoid membrane protein ALB3 associates with the cpSecY-translocase in *Arabidopsis thaliana*. *Biochem J* **368**: 777-781
- Klotz A, Georg J, Bučinská L, Watanabe S, Reimann V, Januszewski W, Sobotka R, Jendrossek D, Hess Wolfgang R, Forchhammer K** (2016) Awakening of a dormant cyanobacterium from nitrogen chlorosis reveals a genetically determined program. *Curr Biol* **26**: 2862-2872
- Knoppová J, Sobotka R, Tichý M, Yu J, Koník P, Halada P, Nixon PJ, Komenda J** (2014) Discovery of a chlorophyll binding protein complex involved in the early steps of photosystem II assembly in *Synechocystis*. *Plant Cell* **26**: 1200-1212
- Kobayashi K, Endo K, Wada H** (2017) Specific distribution of phosphatidylglycerol to photosystem complexes in the thylakoid membrane. *Front Plant Sci* **8**: 1-7
- Kobori TO, Uzumaki T, Kis M, Kovacs L, Domanos I, Itoh S, Krynická V, Kuppusamy SG, Zakar T, Dean J, Szilak L, Komenda J, Gombos Z, Ughy B** (2018) Phosphatidylglycerol is implicated in divisome formation and metabolic processes of cyanobacteria. *J Plant Physiol* **223**: 96-104
- Komenda J** (2005) Autotrophic cells of the *Synechocystis psbH* deletion mutant are deficient in synthesis of CP47 and accumulate inactive PSII core complexes. *Photosyn Res* **85**: 161-167
- Komenda J, Barber J** (1995) Comparison of *psbO* and *psbH* deletion mutants of *Synechocystis* PCC 6803 indicates that degradation of D1 protein is regulated by the QB site and dependent on protein synthesis. *Biochemistry* **34**: 9625-9631
- Komenda J, Nickelsen J, Tichý M, Prášil O, Eichacker LA, Nixon PJ** (2008) The cyanobacterial homologue of HCF136/YCF48 is a component of an early photosystem II assembly complex and is important for both the efficient assembly and repair of photosystem II in *Synechocystis* sp. PCC 6803. *J Biol Chem* **283**: 22390-22399

- Komenda J, Reisinger V, Muller BC, Dobáková M, Granvogl B, Eichacker LA** (2004) Accumulation of the D2 protein is a key regulatory step for assembly of the photosystem II reaction center complex in *Synechocystis* PCC 6803. *J Biol Chem* **279**: 48620-48629
- Komenda J, Sobotka R** (2016) Cyanobacterial high-light-inducible proteins--Protectors of chlorophyll-protein synthesis and assembly. *Biochim Biophys Acta-Bioenergetics* **1857**: 288-295
- Komenda J, Sobotka R, Nixon PJ** (2012) Assembling and maintaining the photosystem II complex in chloroplasts and cyanobacteria. *Curr Opin Plant Biol* **15**: 245-251
- Komenda J, Tichý M, Eichacker LA** (2005) The PsbH protein is associated with the inner antenna CP47 and facilitates D1 processing and incorporation into PSII in the cyanobacterium *Synechocystis* PCC 6803. *Plant Cell Physiol* **46**: 1477-1483
- Kopečná J, Komenda J, Bučinská L, Sobotka R** (2012) Long-term acclimation of the cyanobacterium *Synechocystis* sp. PCC 6803 to high light is accompanied by an enhanced production of chlorophyll that is preferentially channeled to trimeric photosystem I. *Plant Physiol* **160**: 2239-2250
- Kopečná J, Pilný J, Krynická V, Tomčala A, Kis M, Gombos Z, Komenda J, Sobotka R** (2015) Lack of phosphatidylglycerol inhibits chlorophyll biosynthesis at multiple sites and limits chlorophyllide reutilization in the cyanobacterium *Synechocystis* 6803. *Plant Physiol* **169**: 1307-1317
- Kopečná J, Sobotka R, Komenda J** (2013) Inhibition of chlorophyll biosynthesis at the protochlorophyllide reduction step results in the parallel depletion of photosystem I and photosystem II in the cyanobacterium *Synechocystis* PCC 6803. *Planta* **237**: 497-508
- Kopf M, Klahn S, Scholz I, Matthiessen JK, Hess WR, Voss B** (2014) Comparative analysis of the primary transcriptome of *Synechocystis* sp. PCC 6803. *DNA Res* **21**: 527-539
- Kouřil R, Dekker JP, Boekema EJ** (2012) Supramolecular organization of photosystem II in green plants. *Biochim Biophys Acta* **1817**: 2-12
- Kouřil R, Oostergetel GT, Boekema EJ** (2011) Fine structure of granal thylakoid membrane organization using cryo electron tomography. *Biochim Biophys Acta* **1807**: 368-374
- Kouřil R, Strouhal O, Nosek L, Lenobel R, Chamrad I, Boekema EJ, Šebela M, Ilík P** (2014) Structural characterization of a plant photosystem I and NAD(P)H dehydrogenase supercomplex. *Plant J* **77**: 568-576
- Kouřil R, Yermenko N, D'Haene S, Oostergetel GT, Matthijs HC, Dekker JP, Boekema EJ** (2005) Supercomplexes of IsiA and photosystem I in a mutant lacking subunit Psal. *Biochim Biophys Acta* **1706**: 262-266
- Kovács L, Damkjær J, Kerešiče S, Iliaia C, Ruban AV, Boekema EJ, Jansson S, Horton P** (2006) Lack of the light-harvesting complex CP24 affects the structure and function of the grana membranes of higher plant chloroplasts. *Plant Cell* **18**: 3106
- Kowalewska Ł, Mazur R, Suski S, Garstka M, Mostowska A** (2016) Three-dimensional visualization of the tubular-lamellar transformation of the internal plastid membrane network during runner bean chloroplast biogenesis. *Plant Cell* **28**: 875
- Kroll D, Meierhoff K, Bechtold N, Kinoshita M, Westphal S, Vothknecht UC, Soll J, Westhoff P** (2001) VIPP1, a nuclear gene of *Arabidopsis thaliana* essential for thylakoid membrane formation. *Proc Natl Acad Sci USA* **98**: 4238-4242
- Kubota-Kawai H, Mutoh R, Shinmura K, Setif P, Nowaczyk MM, Rogner M, Ikegami T, Tanaka H, Kurisu G** (2018) X-ray structure of an asymmetrical trimeric ferredoxin-photosystem I complex. *Nat Plant* **4**: 218-224
- Kubota H, Sakurai I, Katayama K, Mizusawa N, Ohashi S, Kobayashi M, Zhang PP, Aro EM, Wada H** (2010) Purification and characterization of photosystem I complex from *Synechocystis* sp PCC 6803 by expressing histidine-tagged subunits. *Biochim Biophys Acta* **1797**: 98-105
- Kunkel DD** (1982) Thylakoid centers: Structures associated with the cyanobacterial photosynthetic membrane system. *Arch Microbiol* **133**: 97-99
- Laczko-Dobos H, Ughy B, Toth SZ, Komenda J, Zsiros O, Domonkos I, Parducz A, Bogos B, Komura M, Itoh S, Gombos Z** (2008) Role of phosphatidylglycerol in the function and assembly of Photosystem II reaction center, studied in a *cdsA*-inactivated PAL mutant

- strain of *Synechocystis* sp. PCC6803 that lacks phycobilisomes. *Biochim Biophys Acta* **1777**: 1184-1194
- Latowski D, Åkerlund H-E, Strzalka K** (2004) Violaxanthin de-epoxidase, the xanthophyll cycle enzyme, requires lipid inverted hexagonal structures for its activity. *Biochemistry* **43**: 4417-4420
- Lebedev N, Timko MP** (1998) Protochlorophyllide photoreduction. *Photosyn Res* **58**: 5-23
- Lee AG** (2000) Membrane lipids: It's only a phase. *Curr Biol* **10**: R377-R380
- Liang Z, Zhu N, Mai KK, Liu Z, Tzeng D, Osteryoung KW, Zhong S, Staehelin LA, Kang B-H** (2018) Thylakoid-bound polysomes and a dynamin-related protein, FZL, mediate critical stages of the linear chloroplast biogenesis program in greening *Arabidopsis* cotyledons. *Plant Cell* **30**: 1476
- Liberton M, Austin JR, 2nd, Berg RH, Pakrasi HB** (2011) Unique thylakoid membrane architecture of a unicellular N<sub>2</sub>-fixing cyanobacterium revealed by electron tomography. *Plant Physiol* **155**: 1656-1666
- Liberton M, Berg RH, Heuser J, Roth R, Pakrasi HB** (2006) Ultrastructure of the membrane systems in the unicellular cyanobacterium *Synechocystis* sp strain PCC 6803. *Protoplasma* **227**: 129-138
- Linhartová M, Bučinská L, Halada P, Ječmen T, Šetlík J, Komenda J, Sobotka R** (2014) Accumulation of the Type IV prepilin triggers degradation of SecY and YidC and inhibits synthesis of Photosystem II proteins in the cyanobacterium *Synechocystis* PCC 6803. *Mol Microbiol* **93**: 1207-1223
- Liu H, Zhang H, Niedzwiedzki DM, Prado M, He G, Gross ML, Blankenship RE** (2013) Phycobilisomes supply excitations to both photosystems in a megacomplex in cyanobacteria. *Science* **342**: 1104-1107
- Liu L-N, Scheuring S** (2013) Investigation of photosynthetic membrane structure using atomic force microscopy. *Trends Plant Sci* **18**: 277-286
- Liu W, Fu Y, Hu G, Si H, Zhu L, Wu C, Sun Z** (2007) Identification and fine mapping of a thermo-sensitive chlorophyll deficient mutant in rice (*Oryza sativa* L.). *Planta* **226**: 785-795
- Loll B, Kern J, Saenger W, Zouni A, Biesiadka J** (2005) Towards complete cofactor arrangement in the 3.0 angstrom resolution structure of photosystem II. *Nature* **438**: 1040-1044
- MacGregor-Chatwin C, Sener M, Barnett SFH, Hitchcock A, Barnhart-Dailey MC, Maghlaoui K, Barber J, Timlin JA, Schulten K, Hunter CN** (2017) Lateral segregation of photosystem I in cyanobacterial thylakoids. *Plant Cell* **29**: 1119-1136
- Majeed W, Zhang Y, Xue Y, Ranade S, Blue RN, Wang Q, He Q** (2012) *RpaA* regulates the accumulation of monomeric photosystem I and *psbA* under high light conditions in *Synechocystis* sp. PCC 6803. *PLoS one* **7**: e45139-e45139
- Malavath T, Caspy I, Netzer-El SY, Klaiman D, Nelson N** (2018) Structure and function of wild-type and subunit-depleted photosystem I in *Synechocystis*. *Biochim Biophys Acta* **1859**: 645-654
- Manuell AL, Quispe J, Mayfield SP** (2007) Structure of the chloroplast ribosome: novel domains for translation regulation. *PLoS Biol.* **5**: 1785-1797
- McDonald K, Schwarz H, Muller-Reichert T, Webb R, Buser C, Morpew M** (2010) "Tips and tricks" for high-pressure freezing of model systems. *Methods Cell Biol* **96**: 671-693
- Menke W** (1960) Das allgemeine Bauprinzip des Lamellarsystems der Chloroplasten. *Experientia* **16**: 537-538
- Minai L, Wostrikoff K, Wollman FA, Choquet Y** (2006) Chloroplast biogenesis of photosystem II cores involves a series of assembly-controlled steps that regulate translation. *Plant Cell* **18**: 159-175
- Muehlethaler K, Frey-Wyssling A** (1959) Development and structure of proplastids. *J biophys biochem cy* **6**: 507-512
- Mullineaux CW** (2014) Co-existence of photosynthetic and respiratory activities in cyanobacterial thylakoid membranes. *Biochim Biophys Acta* **1837**: 503-511

- MuroPastor MI, Reyes JC, Florencio FJ** (2001) Cyanobacteria perceive nitrogen status by sensing intracellular 2-oxoglutarate levels. *J Biol Chem* **276**: 38320-38328
- Murray DL, Kohorn BD** (1991) Chloroplasts of *Arabidopsis thaliana* homozygous for the ch-1 locus lack chlorophyll b, lack stable LHCP II and have stacked thylakoids. *Plant Mol Biol* **16**: 71-79
- Mustardy L, Cunningham FX, Jr., Gantt E** (1992) Photosynthetic membrane topography: quantitative in situ localization of photosystems I and II. *Proc Natl Acad Sci USA* **89**: 10021-10025
- Mustardy L, Garab G** (2003) Granum revisited. A three-dimensional model-where things fall into place. *Trends Plant Sci* **8**: 117-122
- Nakajima Y, Umena Y, Nagao R, Endo K, Kobayashi K, Akita F, Suga M, Wada H, Noguchi T, Shen J-R** (2018) Thylakoid membrane lipid sulfoquinovosyl-diacylglycerol (SQDG) is required for full functioning of photosystem II in *Thermosynechococcus elongatus*. *J Biol Chem* **293**: 14786-14797
- Nelson N, Yocum CF** (2006) Structure and function of photosystems I and II. *Annu Rev Plant Biol* **57**: 521-565
- Nevo R, Charuvi D, Shimon E, Schwarz R, Kaplan A, Ohad I, Reich Z** (2007) Thylakoid membrane perforations and connectivity enable intracellular traffic in cyanobacteria. *EMBO J* **26**: 1467-1473
- Nevo R, Charuvi D, Tsabari O, Reich Z** (2012) Composition, architecture and dynamics of the photosynthetic apparatus in higher plants. *Plant J* **70**: 157-176
- Nickelsen J, Rengstl B** (2013) Photosystem II assembly: from cyanobacteria to plants. *Annu Rev Plant Biol* **64**: 609-635
- Nickelsen J, Rengstl B, Stengel A, Schottkowski M, Soll J, Ankele E** (2011) Biogenesis of the cyanobacterial thylakoid membrane system-an update. *FEMS Microbiol Lett* **315**: 1-5
- Nickelsen J, Zerges W** (2013) Thylakoid biogenesis has joined the new era of bacterial cell biology. *Front Plant Sci* **4**: 458
- Nield J, Barber J** (2006) Refinement of the structural model for the Photosystem II supercomplex of higher plants. *Biochim Biophys Acta* **1757**: 353-361
- Nierzwicki-Bauer SA, Balkwill DL, Stevens SE, Jr.** (1983) Three-dimensional ultrastructure of a unicellular cyanobacterium. *J Cell Biol* **97**: 713-722
- Nilsson F, Simpson DJ, Jansson C, Andersson B** (1992) Ultrastructural and biochemical characterization of a *Synechocystis* 6803 mutant with inactivated *psbA* genes. *Arch Biochem Biophys* **295**: 340-347
- Nixon PJ, Diner BA** (1992) Aspartate 170 of the photosystem II reaction center polypeptide D1 is involved in the assembly of the oxygen-evolving manganese cluster. *Biochemistry* **31**: 942-948
- Nixon PJ, Michoux F, Yu JF, Boehm M, Komenda J** (2010) Recent advances in understanding the assembly and repair of photosystem II. *Ann Bot* **106**: 1-16
- Noda J, Mühlroth A, Bučinská L, Dean J, Bones AM, Sobotka R** (2017) Tools for biotechnological studies of the freshwater alga *Nannochloropsis limnetica*: antibiotic resistance and protoplast production. *J Appl Phycol* **29**: 853-863
- Nordhues A, Schöttler MA, Unger A-K, Geimer S, Schönfelder S, Schmollinger S, Rütgers M, Finazzi G, Soppa B, Sommer F, Mühlhaus T, Roach T, Krieger-Liszskay A, Lokstein H, Crespo JL, Schroda M** (2012) Evidence for a role of VIPP1 in the structural organization of the photosynthetic apparatus in *Chlamydomonas*. *Plant Cell* **24**: 637
- Norling B, Mirzakhani V, Nilsson F, Morre DJ, Andersson B** (1994) Subfractional analysis of cyanobacterial membranes and isolation of plasma membranes by aqueous polymer two-phase partitioning. *Anal Biochem* **218**: 103-111
- Norling B, Zak E, Andersson B, Pakrasi H** (1998) 2D-isolation of pure plasma and thylakoid membranes from the cyanobacterium *Synechocystis* sp. PCC 6803. *FEBS Lett* **436**: 189-192

- Orus MI, Rodriguez ML, Martinez F, Marco E** (1995) Biogenesis and ultrastructure of carboxysomes from wild type and mutants of *Synechococcus* sp. strain PCC 7942. *Plant Physiol* **107**: 1159-1166
- Ossenbuhl F, Gohre V, Meurer J, Krieger-Liszky A, Rochaix JD, Eichacker LA** (2004) Efficient assembly of photosystem II in *Chlamydomonas reinhardtii* requires Alb3.1p, a homolog of *Arabidopsis* ALBINO3. *Plant Cell* **16**: 1790-1800
- Pan X, Ma J, Su X, Cao P, Chang W, Liu Z, Zhang X, Li M** (2018) Structure of the maize photosystem I supercomplex with light-harvesting complexes I and II. *Science* **360**: 1109
- Paolillo DJ, Falk RH** (1966) The ultrastructure of grana in mesophyll plastids of *Zea mays*. *Am J Bot* **53**: 173-180
- Pasch JC, Nickelsen J, Schunemann D** (2005) The yeast split-ubiquitin system to study chloroplast membrane protein interactions. *Appl Microbiol Biotechnol* **69**: 440-447
- Pilný J, Kopečná J, Noda J, Sobotka R** (2015) Detection and quantification of heme and chlorophyll precursors using a High Performance Liquid Chromatography (HPLC) system equipped with two fluorescence detectors. *Bio-protocol* **5**: e1390
- Plücken H, Muller B, Grohmann D, Westhoff P, Eichacker LA** (2002) The HCF136 protein is essential for assembly of the photosystem II reaction center in *Arabidopsis thaliana*. *FEBS Lett* **532**: 85-90
- Ponce-Toledo RI, Deschamps P, López-García P, Zivanovic Y, Benzerara K, Moreira D** (2017) An early-branching freshwater cyanobacterium at the origin of plastids. *Curr Biol* **27**: 386-391
- Porra RJ, Thompson WA, Kriedemann PE** (1989) Determination of accurate extinction coefficients and simultaneous equations for assaying chlorophylls *a* and *b* extracted with four different solvents: verification of the concentration of chlorophyll standards by atomic absorption spectroscopy. *Biochim Biophys Acta* **975**: 384-394
- Porta D, Rippka R, Hernandez-Marine M** (2000) Unusual ultrastructural features in three strains of *Cyanothece* (cyanobacteria). *Arch Microbiol* **173**: 154-163
- Pribil M, Labs M, Leister D** (2014) Structure and dynamics of thylakoids in land plants. *J Exp Bot* **65**: 1955-1972
- Pribil M, Sandoval-Ibáñez O, Xu W, Sharma A, Labs M, Liu Q, Galgenmüller C, Schneider T, Wessels M, Matsubara S, Jansson S, Wanner G, Leister D** (2018) Fine-tuning of photosynthesis requires CURVATURE THYLAKOID1-mediated thylakoid plasticity. *Plant Physiol* **176**: 2351
- Proctor MS, Chidgey JW, Shukla MK, Jackson PJ, Sobotka R, Hunter CN, Hitchcock A** (2018) Plant and algal chlorophyll synthases function in *Synechocystis* and interact with the YidC/Alb3 membrane insertase. *FEBS Lett* **592**: 3062-3073
- Promnares K, Komenda J, Bumba L, Nebesarova J, Vacha F, Tichy M** (2006) Cyanobacterial small chlorophyll-binding protein ScpD (HliB) is located on the periphery of photosystem II in the vicinity of PsbH and CP47 subunits. *J Biol Chem* **281**: 32705-32713
- Rast A, Heinz S, Nickelsen J** (2015) Biogenesis of thylakoid membranes. *Biochim Biophys Acta* **1847**: 821-830
- Rengstl B, Knoppová J, Komenda J, Nickelsen J** (2013) Characterization of a *Synechocystis* double mutant lacking the photosystem II assembly factors YCF48 and Sll0933. *Planta* **237**: 471-480
- Rengstl B, Oster U, Stengel A, Nickelsen J** (2011) An intermediate membrane subfraction in cyanobacteria is involved in an assembly network for photosystem II biogenesis. *J Biol Chem* **286**: 21944-21951
- Rexroth S, Mullineaux CW, Ellinger D, Sendtko E, Rögner M, Koenig F** (2011) The plasma membrane of the cyanobacterium *Gloeobacter violaceus* contains segregated bioenergetic domains. *Plant Cell* **23**: 2379-2390
- Rhee KH, Morris EP, Zheleva D, Hankamer B, Kuhlbrandt W, Barber J** (1997) Two-dimensional structure of plant photosystem II at 8-angstrom resolution. *Nature* **389**: 522-526
- Rippka R, Waterbury J, Cohen-Bazire G** (1974) A cyanobacterium which lacks thylakoids. *Arch Microbiol* **100**: 419-436

- Sachelaru I, Winter L, Knyazev DG, Zimmermann M, Vogt A, Kuttner R, Ollinger N, Siligan C, Pohl P, Koch H-G** (2017) YidC and SecYEG form a heterotetrameric protein translocation channel. *Sci Rep* **7**: 101
- Sato N** (2004) Roles of the acidic lipids sulfoquinovosyl diacylglycerol and phosphatidylglycerol in photosynthesis: their specificity and evolution. *J Plant Res* **117**: 495-505
- Sauer J, Schreiber U, Schmid R, Volker U, Forchhammer K** (2001) Nitrogen starvation-induced chlorosis in *Synechococcus* PCC 7942. Low-level photosynthesis as a mechanism of long-term survival. *Plant Physiol* **126**: 233-243
- Schaffer M, Engel BD, Laugks T, Mahamid J, Plitzko JM, Baumeister W** (2015) Cryo-focused ion beam sample preparation for imaging vitreous cells by cryo-electron tomography. *Bio-protocol* **5**: e1575
- Schaffer M, Mahamid J, Engel BD, Laugks T, Baumeister W, Plitzko JM** (2017) Optimized cryo-focused ion beam sample preparation aimed at in situ structural studies of membrane proteins. *J Struct Biol* **197**: 73-82
- Scheller HV, Jensen PE, Haldrup A, Lunde C, Knoetzel J** (2001) Role of subunits in eukaryotic Photosystem I. *Biochim Biophys Acta* **1507**: 41-60
- Scheuring S, Nevo R, Liu L-N, Mangenot S, Charuvi D, Boudier T, Prima V, Hubert P, Sturgis JN, Reich Z** (2014) The architecture of *Rhodobacter sphaeroides* chromatophores. *Biochim Biophys Acta* **1837**: 1263-1270
- Schottkowski M, Gkalypoudis S, Tzekova N, Stelljes C, Schunemann D, Ankele E, Nickelsen J** (2009) Interaction of the periplasmic PrtA Factor and the *PsbA* (D1) protein during biogenesis of photosystem II in *Synechocystis* sp PCC 6803. *J Biol Chem* **284**: 1813-1819
- Schöttler MA, Albus CA, Bock R** (2011) Photosystem I: Its biogenesis and function in higher plants. *J Plant Physiol* **168**: 1452-1461
- Schwarz R, Forchhammer K** (2005) Acclimation of unicellular cyanobacteria to macronutrient deficiency: emergence of a complex network of cellular responses. *Microbiology* **151**: 2503-2514
- Selao TT, Zhang L, Knoppova J, Komenda J, Norling B** (2016) Photosystem II assembly steps take place in the thylakoid membrane of the cyanobacterium *Synechocystis* sp. PCC6803. *Plant Cell Physiol* **57**: 95-104
- Şener MK, Jolley C, Ben-Shem A, Fromme P, Nelson N, Croce R, Schulten K** (2005) Comparison of the light-harvesting networks of plant and cyanobacterial photosystem I. *Biophys J* **89**: 1630-1642
- Sheng Z, Lv Y, Li W, Luo R, Wei X, Xie L, Jiao G, Shao G, Wang J, Tang S, Hu P** (2017) Yellow-Leaf 1 encodes a magnesium-protoporphyrin IX monomethyl ester cyclase, involved in chlorophyll biosynthesis in rice (*Oryza sativa* L.). *PLOS ONE* **12**: e0177989
- Sherman DM, Troyan TA, Sherman LA** (1994) Localization of Membrane Proteins in the Cyanobacterium *Synechococcus* sp. PCC7942 (Radial Asymmetry in the Photosynthetic Complexes). *Plant Physiol* **106**: 251-262
- Shi LX, Schroder WP** (2004) The low molecular mass subunits of the photosynthetic supracomplex, photosystem II. *Biochim Biophys Acta* **1608**: 75-96
- Shimoni E, Rav-Hon O, Ohad I, Brumfeld V, Reich Z** (2005) Three-dimensional organization of higher-plant chloroplast thylakoid membranes revealed by electron tomography. *Plant Cell* **17**: 2580
- Simidjiev I, Stoylova S, Amenitsch H, Javorfi T, Mustardy L, Laggner P, Holzenburg A, Garab G** (2000) Self-assembly of large, ordered lamellae from non-bilayer lipids and integral membrane proteins in vitro. *Proc Natl Acad Sci USA* **97**: 1473-1476
- Šmarda J, Šmajš D, Komrska J, Krzyžánek V** (2002) S-layers on cell walls of cyanobacteria. *Micron* **33**: 257-277
- Sobotka R** (2014) Making proteins green; biosynthesis of chlorophyll-binding proteins in cyanobacteria. *Photosyn Res* **119**: 223-232
- Sobotka R, Komenda J, Bumba L, Tichý M** (2005) Photosystem II assembly in CP47 mutant of *Synechocystis* sp PCC 6803 is dependent on the level of chlorophyll precursors regulated by ferrochelatase. *J Biol Chem* **280**: 31595-31602

- Sobotka R, McLean S, Žuberová M, Hunter CN, Tichý M** (2008) The C-terminal extension of ferrochelatase is critical for enzyme activity and for functioning of the tetrapyrrole pathway in *Synechocystis* strain PCC 6803. *J Bacteriol* **190**: 2086-2095
- Sozer O, Komenda J, Ughy B, Domonkos I, Laczko-Dobos H, Malec P, Gombos Z, Kis M** (2010) Involvement of carotenoids in the synthesis and assembly of protein subunits of photosynthetic reaction centers of *Synechocystis* sp PCC 6803. *Plant Cell Physiol* **51**: 823-835
- Spät P, Klotz A, Rexroth S, Maček B, Forchhammer K** (2018) Chlorosis as a developmental program in cyanobacteria: The proteomic fundament for survival and awakening. *Mol Cell Proteomics* **17**: 1650
- Spence E, Bailey S, Nenninger A, Moller SG, Robinson C** (2004) A homolog of Albino3/OxaI is essential for thylakoid biogenesis in the cyanobacterium *Synechocystis* sp. PCC6803. *J Biol Chem* **279**: 55792-55800
- Spurr AR** (1969) A low-viscosity epoxy resin embedding medium for electron microscopy. *J Ultra Mol Struct R* **26**: 31-43
- Srivastava R, Pisareva T, Norling B** (2005) Proteomic studies of the thylakoid membrane of *Synechocystis* sp PCC 6803. *Proteomics* **5**: 4905-4916
- Stachelin LA** (2003) Chloroplast structure: from chlorophyll granules to supra-molecular architecture of thylakoid membranes. *Photosynth Res* **76**: 185-196
- Stachelin LA, Arntzen CJ** (1983) Regulation of chloroplast membrane function: protein phosphorylation changes the spatial organization of membrane components. *J Cell Biol* **97**: 1327-1337
- Stanier G** (1988) Fine structure of cyanobacteria. *In Methods Enzymol.*, Vol 167. Academic Press, pp 157-172
- Stanier RY, Cohen-Bazire G** (1977) Phototrophic prokaryotes: the cyanobacteria. *Annu Rev Microbiol* **31**: 225-274
- Steinbeck J, Ross IL, Rothnagel R, Gabelein P, Schulze S, Giles N, Ali R, Drysdale R, Sieracki E, Gambin Y, Stahlberg H, Takahashi Y, Hippler M, Hankamer B** (2018) Structure of a PSI-LHCI-cyt *b<sub>6</sub>f* supercomplex in *Chlamydomonas reinhardtii* promoting cyclic electron flow under anaerobic conditions. *Proc Natl Acad Sci USA* **115**: 10517-10522
- Stengel A, Gugel IL, Hilger D, Rengstl B, Jung H, Nickelsen J** (2012) Initial steps of photosystem II de novo assembly and preloading with manganese take place in biogenesis centers in *Synechocystis*. *Plant Cell* **24**: 660-675
- Strašková A, Steinbach G, Kotabova E, Komenda J, Tichý M, Kaňa R** (Submitted 2018) Pigment-protein complexes are organized into stable microdomains in cyanobacterial thylakoids. *BBA - bioenergetics*
- Tichý M, Beckova M, Kopecna J, Noda J, Sobotka R, Komenda J** (2016) Strain of *Synechocystis* PCC 6803 with aberrant assembly of photosystem II contains tandem duplication of a large chromosomal region. *Front Plant Sci* **7**: 648
- Tolonen AC, Aach J, Lindell D, Johnson ZI, Rector T, Steen R, Church GM, Chisholm SW** (2006) Global gene expression of *Prochlorococcus* ecotypes in response to changes in nitrogen availability. *Mol Syst Biol* **2**: 53
- Tucker JD, Siebert CA, Escalante M, Adams PG, Olsen JD, Otto C, Stokes DL, Hunter CN** (2010) Membrane invagination in *Rhodobacter sphaeroides* is initiated at curved regions of the cytoplasmic membrane, then forms both budded and fully detached spherical vesicles. *Mol Microbiol* **76**: 833-847
- Umena Y, Kawakami K, Shen J-R, Kamiya N** (2011) Crystal structure of oxygen-evolving photosystem II at a resolution of 1.9 Å. *Nature* **473**: 55
- Vacha F, Bumba L, Kaftan D, Vacha M** (2005) Microscopy and single molecule detection in photosynthesis. *Micron* **36**: 483-502
- Vajravel S, Kis M, Klodawska K, Laczko-Dobos H, Malec P, Kovács L, Gombos Z, Toth TN** (2017) Zeaxanthin and echinenone modify the structure of photosystem I trimer in *Synechocystis* sp. PCC 6803. *Biochim Biophys Acta* **1858**: 510-518



- van Bezouwen LS, Caffarri S, Kale RS, Kouřil R, Thunnissen A-MWH, Oostergetel GT, Boekema EJ** (2017) Subunit and chlorophyll organization of the plant photosystem II supercomplex. *Nat Plant* **3**: 17080
- van de Meene AM, Sharp WP, McDaniel JH, Friedrich H, Vermaas WF, Roberson RW** (2012) Gross morphological changes in thylakoid membrane structure are associated with photosystem I deletion in *Synechocystis* sp. PCC 6803. *Biochim Biophys Acta* **1818**: 1427-1434
- van de Meene AML, Hohmann-Marriott MF, Vermaas WFJ, Roberson RW** (2006) The three-dimensional structure of the cyanobacterium *Synechocystis* sp PCC 6803. *Arch Microbiol* **184**: 259-270
- Vavilin D, Vermaas W** (2007) Continuous chlorophyll degradation accompanied by chlorophyllide and phytol reutilization for chlorophyll synthesis in *Synechocystis* sp PCC 6803. *Biochim Biophys Acta* **1767**: 920-929
- Vermaas WFJ, Ikeuchi M, Inoue Y** (1988) Protein composition of the photosystem II core complex in genetically engineered mutants of the cyanobacterium *Synechocystis* sp. PCC 6803. *Photosyn Res* **17**: 97-113
- Vermaas WFJ, Timlin JA, Jones HDT, Sinclair MB, Nieman LT, Hamad SW, Melgaard DK, Haaland DM** (2008) *In vivo* hyperspectral confocal fluorescence imaging to determine pigment localization and distribution in cyanobacterial cells. *Proc Natl Acad Sci USA* **105**: 4050
- Vernotte C, Picaud M, Kirilovsky D, Olive J, Ajlani G, Astier C** (1992) Changes in the photosynthetic apparatus in the cyanobacterium *Synechocystis* sp. PCC 6714 following light-to-dark and dark-to-light transitions. *Photosynth Res* **32**: 45-57
- Vothknecht UC, Otters S, Hennig R, Schneider D** (2012) Vipp1: a very important protein in plastids?! *J Exp Bot* **63**: 1699-1712
- Vothknecht UC, Westhoff P** (2001) Biogenesis and origin of thylakoid membranes. *Biochim Biophys Acta Molecular Cell Research* **1541**: 91-101
- Wada H, Murata N** (1998) Membrane lipids in cyanobacteria. In S Paul-André, M Norio, eds, *Lipids in Photosynthesis: Structure, Function and Genetics*. Springer Netherlands, Dordrecht, pp 65-81
- Wada H, Murata N** (2010) Lipids in thylakoid membranes and photosynthetic cells. In H Wada, N Murata, eds, *Lipids in Photosynthesis: Essential and Regulatory Functions*. Springer Netherlands, Dordrecht, pp 1-9
- Walters RG** (2005) Towards an understanding of photosynthetic acclimation. *J Exp Bot* **56**: 435-447
- Walters RG, Horton P** (1994) Acclimation of *Arabidopsis thaliana* to the light environment: Changes in composition of the photosynthetic apparatus. *Planta* **195**: 248-256
- Wang P, Grimm B** (2015) Organization of chlorophyll biosynthesis and insertion of chlorophyll into the chlorophyll-binding proteins in chloroplasts. *Photosyn Res* **126**: 189-202
- Wanner G, Henkelmann G, Schmidt A, Köst HP** (1986) Nitrogen and sulfur starvation of the cyanobacterium *Synechococcus* 6301 an ultrastructural, morphometrical, and biochemical comparison. In *Zeitschrift für Naturforschung C*, Vol 41, pp 741
- Welkie DG, Sherman DM, Chrisler WB, Orr G, Sherman LA** (2013) Analysis of carbohydrate storage granules in the diazotrophic cyanobacterium *Cyanothece* sp. PCC 7822. *Photosynth Res* **118**: 25-36
- Westphal S, Heins L, Soll J, Vothknecht UC** (2001) Vipp1 deletion mutant of *Synechocystis*: a connection between bacterial phage shock and thylakoid biogenesis? *Proc Natl Acad Sci USA* **98**: 4243
- Westphal S, Soll J, Vothknecht UC** (2003) Evolution of chloroplast vesicle transport. *Plant Cell Physiol* **44**: 217-222
- Wittig I, Karas M, Schagger H** (2007) High resolution clear native electrophoresis for in-gel functional assays and fluorescence studies of membrane protein complexes. *Mol Cell Proteomics* **6**: 1215-1225
- Wollman FA, Minai L, Nechushtai R** (1999) The biogenesis and assembly of photosynthetic proteins in thylakoid membranes1. *Biochim Biophys Acta* **1411**: 21-85

- Wostrikoff K, Girard-Bascou J, Wollman F-A, Choquet Y** (2004) Biogenesis of PSI involves a cascade of translational autoregulation in the chloroplast of *Chlamydomonas*. *EMBO J* **23**: 2696-2705
- Xu W, Tang HD, Wang YC, Chitnis PR** (2001) Proteins of the cyanobacterial photosystem I. *Biochim Biophys Acta* **1507**: 32-40
- Yadav KNS, Semchonok DA, Nosek L, Kouřil R, Fucile G, Boekema EJ, Eichacker LA** (2017) Supercomplexes of plant photosystem I with cytochrome *b<sub>6</sub>*, light-harvesting complex II and NDH. *Biochim Biophys Acta* **1858**: 12-20
- Yamane K, Oi T, Enomoto S, Nakao T, Arai S, Miyake H, Taniguchi M** (2018) Three-dimensional ultrastructure of chloroplast pockets formed under salinity stress. *Plant Cell Environ* **41**: 563-575
- Yang H, Liu J, Wen X, Lu C** (2015) Molecular mechanism of photosystem I assembly in oxygenic organisms. *Biochim Biophys Acta* **1847**: 838-848
- Yokono M, Takabayashi A, Akimoto S, Tanaka A** (2015) A megacomplex composed of both photosystem reaction centres in higher plants. *Nat Commun* **6**: 6675
- Yokoyama R, Yamamoto H, Kondo M, Takeda S, Ifuku K, Fukao Y, Kamei Y, Nishimura M, Shikanai T** (2016) Grana-localized proteins, RIQ1 and RIQ2, affect the organization of light-harvesting complex II and grana stacking in *Arabidopsis*. *Plant Cell* **28**: 2261
- Yoon HS, Hackett JD, Ciniglia C, Pinto G, Bhattacharya D** (2004) A molecular timeline for the origin of photosynthetic eukaryotes. *Mol Biol Evol* **21**: 809-818
- Yu B, Xu C, Benning C** (2002) *Arabidopsis* disrupted in SQD2 encoding sulfolipid synthase is impaired in phosphate-limited growth. *Proc Natl Acad Sci USA* **99**: 5732-5737
- Yu J, Knopová J, Michoux F, Bialek W, Cota E, Shukla MK, Strašková A, Pascual Aznar G, Sobotka R, Komenda J, Murray JW, Nixon PJ** (2018) Ycf48 involved in the biogenesis of the oxygen-evolving photosystem II complex is a seven-bladed beta-propeller protein. *Proc Natl Acad Sci USA* **115**: E7824-E7833
- Yu JJ, Vermaas WFJ** (1990) Transcript levels and synthesis of photosystem II components in cyanobacterial mutants with inactivated photosystem II genes. *Plant Cell* **2**: 315-322
- Yuan M, Zhang D-W, Zhang Z-W, Chen Y-E, Yuan S, Guo Y-R, Lin H-H** (2012) Assembly of NADPH:protochlorophyllide oxidoreductase complex is needed for effective greening of barley seedlings. *J Plant Physiol* **169**: 1311-1316
- Zak E, Norling B, Maitra R, Huang F, Andersson B, Pakrasi HB** (2001) The initial steps of biogenesis of cyanobacterial photosystems occur in plasma membranes. *Proc Natl Acad Sci USA* **98**: 13443-13448
- Zhang L, Paakkarinen V, van Wijk KJ, Aro EM** (2000) Biogenesis of the chloroplast-encoded D1 protein: regulation of translation elongation, insertion, and assembly into photosystem II. *Plant Cell* **12**: 1769-1782
- Zhang LX, Paakkarinen V, Suorsa M, Aro EM** (2001) A SecY homologue is involved in chloroplast-encoded D1 protein biogenesis. *J Biol Chem* **276**: 37809-37814
- Zhang S, Shen G, Li Z, Golbeck JH, Bryant DA** (2014) Vipp1 is essential for the biogenesis of photosystem I but not thylakoid membranes in *Synechococcus* sp. PCC 7002. *J Biol Chem* **289**: 15904-15914



## 9. Published results

**9.1. Publication I:** Long-term acclimation of the cyanobacterium *Synechocystis* PCC 6803 to high light is accompanied by an enhanced production of chlorophyll that is preferentially channelled to trimeric PSI.

Kopečná J, Komenda J, **Bučinská L**, Sobotka R (2012).

*Plant Physiol.* 160(4): 2239-50.

# Long-Term Acclimation of the Cyanobacterium *Synechocystis* sp. PCC 6803 to High Light Is Accompanied by an Enhanced Production of Chlorophyll That Is Preferentially Channeled to Trimeric Photosystem I<sup>1[W]</sup>

Jana Kopečná, Josef Komenda, Lenka Bučinská, and Roman Sobotka\*

Institute of Microbiology, Department of Phototrophic Microorganisms, Academy of Sciences, 37981 Trebon, Czech Republic; and Faculty of Science, University of South Bohemia, 370 05 Ceske Budejovice, Czech Republic

Cyanobacteria acclimate to high-light conditions by adjusting photosystem stoichiometry through a decrease of photosystem I (PSI) abundance in thylakoid membranes. As PSI complexes bind the majority of chlorophyll (Chl) in cyanobacterial cells, it is accepted that the mechanism controlling PSI level/synthesis is tightly associated with the Chl biosynthetic pathway. However, how Chl is distributed to photosystems under different light conditions remains unknown. Using radioactive labeling by <sup>35</sup>S and by <sup>14</sup>C combined with native/two-dimensional electrophoresis, we assessed the synthesis and accumulation of photosynthetic complexes in parallel with the synthesis of Chl in *Synechocystis* sp. PCC 6803 cells acclimated to different light intensities. Although cells acclimated to higher irradiances (150 and 300  $\mu\text{E m}^{-2}\text{s}^{-1}$ ) exhibited markedly reduced PSI content when compared with cells grown at lower irradiances (10 and 40  $\mu\text{E m}^{-2}\text{s}^{-1}$ ), they grew much faster and synthesized significantly more Chl, as well as both photosystems. Interestingly, even under high irradiance, almost all labeled de novo Chl was localized in the trimeric PSI, whereas only a weak Chl labeling in photosystem II (PSII) was accompanied by the intensive <sup>35</sup>S protein labeling, which was much stronger than in PSI. These results suggest that PSII subunits are mostly synthesized using recycled Chl molecules previously released during PSII repair-driven protein degradation. In contrast, most of the fresh Chl is utilized for synthesis of PSI complexes likely to maintain a constant level of PSI during cell proliferation.

Photosynthetic autotrophs are completely dependent on light as the only source of energy for their proliferation. However, light intensity can swiftly change due to variable environmental conditions, sometimes being too low to sufficiently drive photosynthetic reactions, and other times being even higher than can be utilized, or at least safely dissipated, by a photosynthetic apparatus. In the latter case, the excessive part of the absorbed energy can be ultimately transformed into energy of reactive oxygen species, which has a destructive impact on key cellular components: nucleic acids, lipids, pigments, and proteins. To cope with light fluctuations, cyanobacteria as well as algae and plants possess complex regulatory machinery to optimize the utilization of light energy and to protect photosynthetic apparatus against the damage induced by excessive light. This

machinery involves the regulation of size and number of light-harvesting antennas (Anderson et al., 1995; Walters, 2005), dissipation of light energy by non-photochemical quenching (El Bissati et al., 2000; Müller et al., 2001), redistribution of light energy between photosystems by state transition (Mullineaux and Emlyn-Jones, 2005; Fujimori et al., 2005), or adapting the capacity of carbon dioxide (CO<sub>2</sub>) fixation (Demmig-Adams and Adams, 1992).

One of the most prominent responses to light intensity, and also to its spectral quality, is a selective regulation of the abundance of PSI in the thylakoid membrane, which controls the frequency of excitation of photosystems to optimize the entire photosynthetic electron flow (Chow et al., 1990; Muramatsu and Hihara, 2012). Given that the PSII level is much more stable, this process establishes a specific stoichiometry between both photosystems (PSI/PSII ratio) depending on particular light conditions (Neale and Melis, 1986; Murakami and Fujita, 1991; Walters and Horton, 1994). A dynamic adjustment of the PSI/PSII ratio has been shown to be required for maintaining a high quantum efficiency of photosynthesis in plants (Chow et al., 1990) and algae (Melis et al., 1996). In cyanobacteria, a physiological significance of photosystem stoichiometry was demonstrated on mutants of the cyanobacterium *Synechocystis* sp. PCC 6803 (hereafter, *Synechocystis*). The *pmgA* mutant has lost the ability to

<sup>1</sup> This work was supported by projects Algatex (CZ.1.05/2.1.00/03.0110) and RVO61388971 and by projects P501/10/1000 and P501/12/G055 of the Grant Agency of the Czech Republic. L.B. was supported by the Grant Agency of the University of South Bohemia.

\* Corresponding author; e-mail sobotka@alga.cz.

The author responsible for distribution of materials integral to the findings presented in this article in accordance with the policy described in the Instructions for Authors ([www.plantphysiol.org](http://www.plantphysiol.org)) is: Roman Sobotka (sobotka@alga.cz).

<sup>[W]</sup> The online version of this article contains Web-only data.  
[www.plantphysiol.org/cgi/doi/10.1104/pp.112.207274](http://www.plantphysiol.org/cgi/doi/10.1104/pp.112.207274)

selectively decrease the PSI content during acclimation to high light (HL) and its growth is severely inhibited under prolonged HL conditions (Hihara et al., 1998; Sonoike et al., 2001). A similar defect in maintaining reduced PSI content in HL has been demonstrated in a *Synechocystis* strain lacking the putative chlorophyll (Chl)-binding domain of ferrochelatase. The growth of this mutant has been completely abolished by HL (Sobotka et al., 2011). The mechanism responsible for the HL-induced selective decrease in PSI content is not clear; however, the process appears to be under control of the redox state of the cytochrome *b<sub>6</sub>f* complex (Murakami and Fujita, 1993). In a proposed model, a signal from cytochrome *b<sub>6</sub>f* downregulates Chl biosynthesis, particularly formation of an early Chl intermediate aminolevulinic acid (ALA), and it seems to be a limited Chl availability that determines the PSI content (Fujita et al., 1990; Muramatsu et al., 2009). Consistently with this model, transcription of *psaA/B* genes coding for large Chl-binding PSI core subunits is not a rate-limiting step in the PSI accumulation, while *de novo* Chl synthesis is blocked immediately after being transferred to HL conditions (Muramatsu et al., 2009). On the other hand, Chl is required during the repair/replacement of PSII complexes that are photo-damaged much faster than PSI complexes (Nowaczyk et al., 2006; Nixon et al., 2010). Therefore, the synthesis of Chl-binding PSII subunits, especially the fast turning over D1 subunit, should be much faster in comparison with PSI subunits (Yao et al., 2012a, 2012b). It raises the question of how an enhanced synthesis of PSII subunits is achieved if less *de novo*-synthesized Chl is produced under HL conditions to keep PSI at a reduced level. Chl is produced via a quite long and branched pathway together with heme and other tetrapyrroles, and the formation of ALA is a particularly critical step controlling the accumulation of the whole spectrum of phototoxic intermediates of Chl/heme biosynthesis (for review, see Czarnecki and Grimm, 2012; see Supplemental Fig. S1 for a scheme of tetrapyrrole pathway). However, controlling PSI content by the metabolic flow through the whole tetrapyrrole pathway does not seem to be flexible enough to balance the formation of all tetrapyrrole cofactors. The *de novo* Chl biosynthesis is expected to be tightly synchronized with synthesis of Chl-binding proteins (Komenda et al., 2012) but a cross talk between Chl and Chl-protein biosyntheses has to also reflect the fact that the lifetime of Chl molecules is much longer than that of proteins (Vavilin et al., 2005; Vavilin and Vermaas 2007; Yao et al., 2012a, 2012b); therefore, a potential role of the recycled Chl in controlling Chl-protein biogenesis must be addressed as well. In this study, we focused on the correlation between synthesis of both photosystems and Chl biosynthesis in *Synechocystis* cells fully acclimated to different light intensities. Using radioactive labeling of proteins and Chl by <sup>35</sup>S and <sup>14</sup>C, respectively, we found that the rate of *de novo* Chl formation, as well as synthesis of both photosystems, is significantly enhanced in HL, despite the

markedly reduced cellular level of PSI. Our data suggest that there is no simple correlation between the actual synthesis of PSI and PSII core subunits and the synthesis and distribution of *de novo* Chl; *de novo* Chl was found to be predominantly directed to the PSI trimer, whereas the Chl-binding PSII subunits seem to be mostly synthesized using the recycled Chl molecules previously released during Chl-protein degradation. It appears that the particular level of PSI needed for the optimal photosynthetic performance at a given light intensity is reached by a precise equilibrium between the rate of cell proliferation, the rate of Chl biosynthesis, and the distribution of Chl into individual Chl-proteins.

## RESULTS

### Acclimation of the *Synechocystis* Cells to Various Irradiances

To understand how Chl biosynthesis is synchronized with the varying demand for Chl-binding subunits of PSI/PSII, we analyzed the *Synechocystis* wild type acclimated to different light intensities. Cells were first grown for 5 d under continuous illumination at 40  $\mu\text{E m}^{-2} \text{s}^{-1}$  (moderate light [ML]) and subsequently moved for 24 h to either lower light (LL; 10  $\mu\text{E m}^{-2} \text{s}^{-1}$ ) or higher light intensities (HL1, 150  $\mu\text{E m}^{-2} \text{s}^{-1}$ ; HL2, 300  $\mu\text{E m}^{-2} \text{s}^{-1}$ ). Absorption spectra of cells normalized per optical density at 750 nm ( $\text{OD}_{750}$ ) are shown in Figure 1A. Whereas the shift to LL did not result in significant changes in the cell pigmentation (data not shown; see Table I for Chl level), amounts of Chl and phycobilisomes per cell were markedly lowered as a response to higher irradiance (Fig. 1A). Chl concentration at HL2 reached about 50% of that observed at ML (Table I; Supplemental Fig. S2). Levels of carotenoids also decreased, except for myxoxanthophyll, the level of which more than doubled after 24 h at HL2 (Supplemental Fig. S2). Growth rates of the cultures were accelerating with light intensity reaching the maximum at HL2 (Table I), a further increase in light intensity to 600  $\mu\text{E m}^{-2} \text{s}^{-1}$  started to inhibit growth (data not shown), although cell pigmentation did not significantly alter when compared with HL2 (see Supplemental Fig. S3 for the whole-cell spectra). Supplementing growth media with 5 mM  $\text{NaHCO}_3$  did not affect the growth rate or Chl level at HL2 (Table I), implying that under our growth conditions with a higher concentration of  $\text{CO}_2$  in the growth chamber, the proliferation of *Synechocystis* cells was not significantly limited by  $\text{CO}_2$  availability. To gather information about the functional status of PSII during acclimation to HL, we also determined the ratio of variable to maximal fluorescence ( $F_v/F_m$ ). When cells grown at ML were moved to HL2, the  $F_v/F_m$  ratio declined rapidly (Supplemental Fig. S4); nevertheless, in the following 6 h it recovered to the initial value. This suggests that even under HL2, cells coped relatively quickly with the initial damage of PSII, and fully acclimated cells did not contain a significant portion of nonfunctional PSII complexes and grew much faster than at ML.

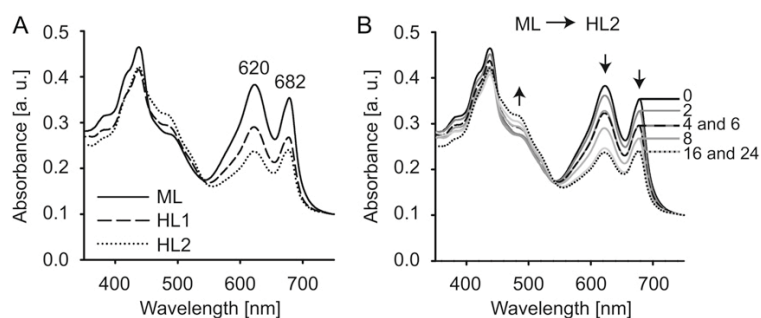


**Figure 1.** Whole-cell absorption spectra of the *Synechocystis* cells acclimated to different light intensities. A, Absorption spectra of *Synechocystis* cells grown photoautotrophically for 24 h under  $40 \mu\text{E m}^{-2} \text{s}^{-1}$  (ML),  $150 \mu\text{E m}^{-2} \text{s}^{-1}$  (HL1), and  $300 \mu\text{E m}^{-2} \text{s}^{-1}$  (HL2). Peaks at 620 and 682 nm represent phycocyanin and Chl absorption, respectively. B, Time course of changes in absorption spectra of cells shifted from ML to HL2 (time 0). Cell spectra measured after 4 (dashed line) and 6 h (solid line) are practically identical, which suggests a lag phase in acclimation to HL2. Spectrum at 24 h is designated by the dotted line. a.u., Absorbance units.

A time-course analysis of changes in whole-cell spectra during acclimation to HL2 showed a rapid decrease in Chl and phycobilisome level in the first 4 h followed by a lag phase between the fourth and sixth hours when no apparent changes were observed (Fig. 1B). The second decrease in Chl and phycobilisome content was observed between the sixth and 16th hour. A prolonged cultivation had no additional effect on the pigment content (Fig. 1B). Observed changes at HL were also reflected in the cell ultrastructure; as shown in Figure 2, cells from HL2 possessed less abundant and less compact thylakoid membrane structures when compared with ML. A distinct feature of HL2 acclimated cells was a very high abundance of glycogen granules that were almost missing in ML grown cells (Fig. 2). Using electron microscopy, we did not observe any significant variability in size among cells from different light conditions even though the growth rate was quite different (Fig. 2). Assessment of cell size and distribution within particular cultures using a cell counter showed that only the cells at HL2 were in average slightly bigger; therefore, their number corresponding to  $\text{OD}_{750} = 1$  was somewhat lower. Nevertheless, cell mass corresponding to  $\text{OD}_{750} = 1$  was quite stable in all cultures grown under various irradiances (data not shown).

#### Accumulation and Synthesis of PSI and PSII in HL-Acclimated Cells

In the *Synechocystis* cells, practically all Chl is associated with photosystems and more than 80% is associated with PSI under ML (Shen et al., 1993). In order to determine how total levels of PSI and PSII are correlated with the drop in the cellular Chl level under HL, we first separated membranes from cultures acclimated to LL, ML, HL1, and HL2 by SDS-PAGE and then probed with antibodies against PSII and PSI subunits (Fig. 3A). As expected, an increase in light intensities

reduced the amount of both PSI and PSII per cell (Fig. 3A). However, a decrease in the PSI level was much more pronounced. The following separation of photosynthetic complexes using clear-native electrophoresis (CN-PAGE) combined with detection of Chl fluorescence in gel allowed us to assess the content of particular oligomeric forms of PSI and PSII (Fig. 3B). Interestingly, the amount of both PSI and PSII monomers per cell was not significantly altered by HL, which contrasts with the dramatically downregulated amount of trimeric PSI and the clearly lowered level of PSII dimer (Fig. 3B).

To assess how de novo synthesis of PSI/PSII complexes corresponds to changes in their accumulation at a cellular level, cells acclimated to ML and HL2 were radioactively labeled using  $[^{35}\text{S}]\text{Met/Cys}$  mixture for 30 min and separated by CN-PAGE. After exposing the CN gel to a phosphor imager plate, we found rather similar labeling of the PSI trimer in both cultures while the labeling of the PSII dimer and both PSI and PSII monomers was at least doubled (Fig. 4A). Taking into account a much lower level of PSI trimer per cell in the HL2 cells, the results indicate significantly faster synthesis of all four complexes at this light intensity. To see how the individual Chl-binding PSII core subunits D1, D2, CP43, and CP47 contributed to the PSII monomer

**Table 1.** Growth rate and Chl content of *Synechocystis* cells under different growth regimes

Values shown represent means  $\pm$  SD from three independent measurements.

Light Intensity	Doubling Time	Chl
	(hours $\pm$ SD)	( $\mu\text{g mL}^{-1} \text{OD}_{750}^{-1}$ )
LL ( $10 \mu\text{E m}^{-2} \text{s}^{-1}$ )	$32.8 \pm 1.3$	$5.9 \pm 0.08$
ML ( $40 \mu\text{E m}^{-2} \text{s}^{-1}$ )	$15.8 \pm 0.8$	$5.5 \pm 0.12$
HL1 ( $150 \mu\text{E m}^{-2} \text{s}^{-1}$ )	$10.4 \pm 1.3$	$3.6 \pm 0.12$
HL2 ( $300 \mu\text{E m}^{-2} \text{s}^{-1}$ )	$7.2 \pm 0.3$	$2.5 \pm 0.09$
HL2 + 5 mM $\text{NaHCO}_3$	$7.1 \pm 0.3$	$2.4 \pm 0.10$



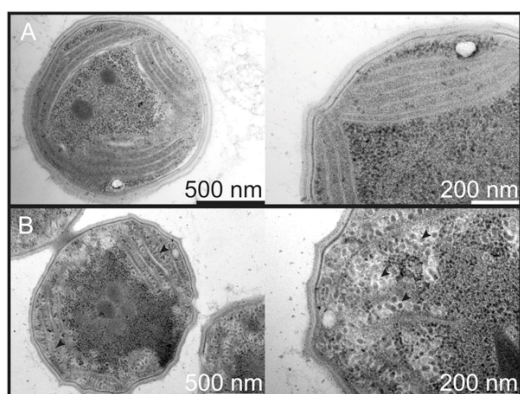


**Figure 2.** Transmission electron microscopy of the *Synechocystis* cells. Representative stained ultrathin sections of cells grown photoautotrophically for 24 h under ML (A) and HL2 (B); black arrows indicate glycogen granules.

and dimer labeling, we separated them in a second dimension using SDS-PAGE (Fig. 4B). Although their total level was lower at HL2, particularly in the dimeric PSII, the synthesis of all four proteins was clearly enhanced in both PSII complexes. We also observed a higher accumulation and synthesis of components of ATPase and FtsH2 and FtsH3 proteases at HL2 (Fig. 4B).

#### Light-Driven Up-Regulation of the Tetrapyrrole Biosynthetic Pathway

Acclimation of the cells to HL2 led to a fast down-regulation of PSI and phycobilisome levels (Fig. 1) and resulted in a reduction of the thylakoid membrane system (Fig. 2). On the other hand, synthesis of Chl-proteins was accelerated (Fig. 4). To evaluate Chl biosynthesis in the acclimated cells, we analyzed this metabolic pathway in detail. First, using a set of specific antibodies, we estimated levels of enzymes involved in the synthesis of heme and Chl in the cells acclimated to the particular light intensities by western blot (Fig. 5; see Supplemental Fig. S1 for a scheme of the tetrapyrrole pathway). Total levels of almost all enzymes, including the heme-producing ferrochelatase, were upregulated by light and light also induced association of enzymes with membranes. The enzymes reached the highest level at HL1 but further increase in irradiance to HL2 resulted in a drop of certain enzymes/enzyme subunits (Mg-protoporphyrin monomethyl ester cyclase, light-dependent protochlorophyllide oxidoreductase, Gun4, and geranylgeranyl reductase). An interesting exception was the D subunit of Mg-chelatase, which exhibited an opposite mode of regulation with the highest concentration reached under LL. Moreover, only at this light intensity was a large portion of the D subunit of Mg-chelatase protein bound to the membranes.

Although these data suggested that the heme/Chl biosynthetic pathway was upregulated after 24 h of

acclimation to increased irradiance, the Chl content per cell started to fall quickly after the light shift and the process finished in 16 h (Fig. 1B). Therefore, the changes in enzyme levels were checked after 2 and 4 h after the shift to HL2 and most of the monitored proteins started to accumulate or at least showed little variation (Fig. 5B). A characteristic feature of Chl biosynthesis up-regulation was an enhanced association of Mg-chelatase subunits H and I with membranes, which was visible after 4 h at HL2 (Fig. 5B). In contrast to the other monitored enzymes, the amount of geranylgeranyl reductase underwent a rapid and significant decline in 2 h after the shift to HL2 and then recovered only very slowly (Fig. 5).

As enzyme levels could not necessarily reflect changes in metabolic flow through the pathway, accumulation of Chl precursors was also quantified. To preserve steady-state levels of precursors, which are probably transient and quickly change during cell handling, we developed a very sensitive method based on HPLC equipped with two fluorescence detectors (see "Material and Methods"). This enabled us to detect very low abundant intermediates of the Chl biosynthesis pathway in extracts from 2-mL cell cultures prepared just in several minutes (Fig. 6A). Employing this method, we observed that the growth at increased irradiance induced an accumulation

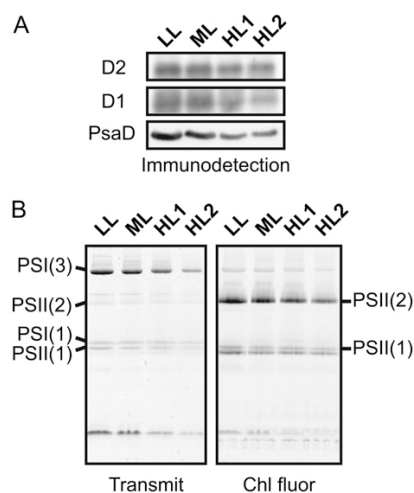


**Figure 3.** Accumulation of PSI and PSII in *Synechocystis* cells acclimated to different light intensities. A, Total amount of PSI and PSII detected using specific antibodies against PSII subunits D1 and D2 and PSI subunit PsaD. Membrane proteins corresponding to 100  $\mu$ L of cells at  $OD_{750} = 1.0$  were loaded per lane, separated by SDS-PAGE, and blotted. B, Separation of monomers and oligomers of PSI and PSII using CN-PAGE. After separation, the gel was scanned in transmittance mode (Transmit) using a LAS 4000 imager (Fuji), and to better visualize PSII complexes, Chl fluorescence in gel (Chl fluor) was detected after excitation by blue light using the same equipment. Proteins were loaded as in A. Designation of complexes: PSI(1) and PSI(3), monomer and trimer of PSI, respectively; PSII(1) and PSII(2), monomer and dimer of PSII, respectively.



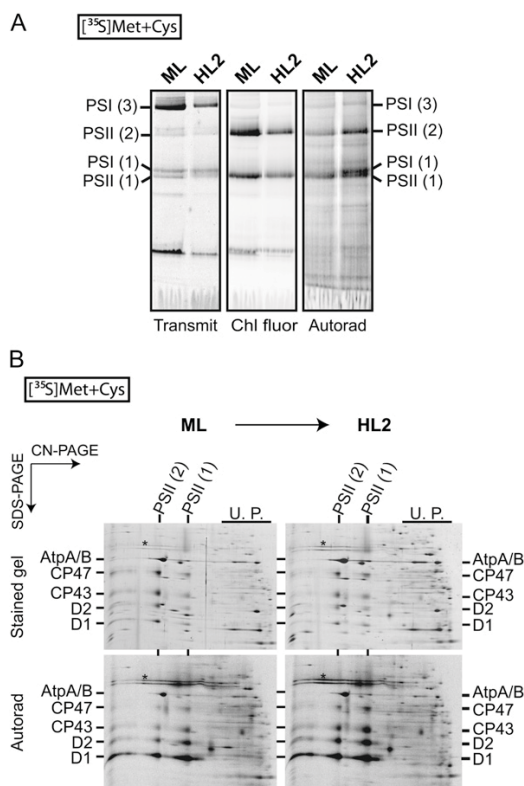


**Figure 4.** Synthesis of PSI and PSII complexes in *Synechocystis* cells acclimated to ML and HL2. A, Cells were radiolabeled with [<sup>35</sup>S]Met/Cys mixture using a 30-min pulse, membrane protein complexes were separated by CN-PAGE, and labeled proteins visualized using a phosphor imager (Autorad). The gel was scanned using a LAS 4000 imager as described in Figure 3B. B, Separation of identical radiolabeled samples by two-dimensional CN/SDS-PAGE. Gel was stained with Coomassie blue and labeled proteins then detected by a phosphor imager (Autorad). Designation of the complexes is as in the legend to Figure 3. U.P., Unassembled proteins. FtsH2/3 proteases are marked with an asterisk.

of Mg-protoporphyrin monomethyl ester and protochlorophyllide, whereas pools of other Chl precursors appeared to be quite stable (Fig. 6B). Finally, to assess the capacity of the whole tetrapyrrole pathway to produce Chl, we followed incorporation of [<sup>14</sup>C]Glu into Chl molecules. Briefly, cells were acclimated to tested light conditions for 24 h and then supplemented with 180 μM [<sup>14</sup>C]Glu for 30 min. Chl (as well as geranylgeranyl-Chl) was immediately extracted by an excess of methanol and converted to Mg-chlorin as described in “Material and Methods.” The solution containing Mg-chlorin was separated on a silica thin-layer chromatography (TLC) plate and exposed to an x-ray film. We found that the incorporation of [<sup>14</sup>C]Glu into Chl is much faster at both HL1 and HL2 than at ML; in contrast, the labeling at LL was very weak (Fig. 6C; see Supplemental Fig. S5 for a color version). Together, these data suggest that the acclimation

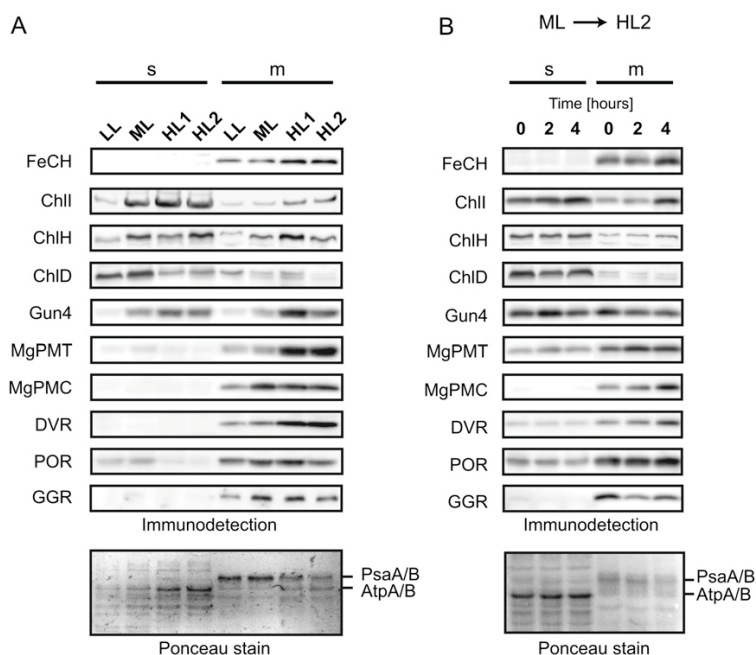
of the *Synechocystis* cells to HL results in a great up-regulation of Chl biosynthesis despite the total relative decline in the cellular level of Chl.

#### Distribution of a Newly Synthesized Chl into Chl-Proteins and Complexes

Formation of an early precursor ALA is accepted as a critical check point controlling the metabolic flow through the whole tetrapyrrole pathway (Czarnecki and Grimm, 2012). Labeling of Chl by [<sup>14</sup>C]Glu then ensures that the total capacity of the pathway can be assessed involving the ALA barrier as well as all other regulatory steps located down the pathway (Supplemental Fig. S1). Moreover, as Glu is also used for protein synthesis, radiolabeling with [<sup>14</sup>C]Glu enabled us to assess the approximate portions of Glu incorporated into the proteins and Chl. Membrane proteins were isolated from HL2 cells, separated by two-dimensional CN/SDS-PAGE and exposed to an x-ray film. Chl migrates on the SDS gel faster than proteins and can be easily distinguished as spots on the bottom of the gel, below the edge of proteins, designated by the arrowheads in Figure 7. We found that the majority of the metabolized [<sup>14</sup>C]Glu was used for the synthesis of Chl. Moreover, even at HL2, most of the labeled Chl was directed to the PSI trimer (Fig. 7A). On the protein side, the strongest radioactive signal was localized in the D1 protein and much less in other PSII subunits; higher molecular mass labeled proteins were probably core subunits of PSI and ATP synthase (Fig. 7A).

To trace the fate of Chl in ML- and HL2-acclimated cells more precisely, we labeled Chl using [<sup>14</sup>C]ALA, and this allowed us to detect new Chl directly in the protein complexes visualized by CN-PAGE. After a 30-min pulse, the Chl labeling in PSII was apparently enhanced in HL2. However, flux of the newly made Chl into the trimeric PSI dominated under both conditions with additional enhancement at HL2 when compared with ML (Fig. 7B). This result contrasted to the very weak [<sup>35</sup>S] labeling of PSI trimer when compared with PSII monomer/dimer and, intriguingly, also to PSI monomer (Fig. 4A), suggesting a specific channeling of labeled Chl into the PSI trimer. However, one has to be careful to assess Chl distribution just according to intensity of Chl labeling in individual PSI/PSII complexes. One PSI trimer contains 288 Chl molecules (Jordan et al., 2001), which is about 4 times more than the sum of Chls and pheophytins in a PSII dimer (Umena et al., 2011) and about 8 times more than number of Chls and pheophytins in a PSII monomer. We used the same methodology as for the [<sup>35</sup>S] labeling to quantify the distribution of labeled Chl in PSI and PSII complexes in cells acclimated to HL2 and labeled by [<sup>14</sup>C]ALA (Table II). As expected, the majority (58%) of Chl was located in trimeric PSI, while only 18% in PSI monomer and 24% in PSII complexes. To take into account different protein/Chl ratios in each complex, we calculated what portion of labeled

**Figure 5.** Accumulation and localization of enzymes of the tetrapyrrole biosynthetic pathway. A, Membrane and soluble protein fractions were prepared from acclimated cells as described in "Materials and Methods," separated by SDS-PAGE, and blotted to a polyvinylidene difluoride membrane. The amount of proteins loaded per lane correspond to 100  $\mu$ L of cells at  $OD_{750} = 1.0$ . These proteins were probed with specific antibodies: FeCH, ferrochelatase; ChII, ChIH, and ChID, subunits of Mg-chelatase; Gun4, a protein required for the activity of Mg-chelatase; MgPMT, Mg-protoporphyrin methyl transferase; MgPMC, Mg-protoporphyrin monomethyl ester oxidative cyclase (Sll1214); DVR, 3,8-divinyl chlorophyllide 8-vinyl reductase; POR, light-dependent protochlorophyllide oxidoreductase; GGR, geranylgeranyl reductase. m, Membrane protein fraction; s, soluble protein fraction. B, Short-term changes in enzyme levels after the shift from ML to HL2. Synechocystis cells were harvested at the indicated time and analyzed as in A. Ponceau-stained proteins blotted onto a membrane are shown as a loading control.



Chl would theoretically be present in each PSI/PSII complex in the case that the protein labeling corresponds to Chl labeling and new Chls are evenly distributed to individual complexes. Less than 10% of labeled Chl should be bound to PSI trimers due to the very weak synthesis of this complex (Table II). The fact that 6 times more of the new Chl is bound to PSI trimer than expected from protein labeling demonstrates a crucial role of a precise distribution of de novo and recycled Chl in the biogenesis of photosystems.

## DISCUSSION

Growth of cyanobacteria under high irradiance induces a fast decrease in harvesting capacity by reducing the number and size of phycobilisomes and abundance of PSI in the thylakoid membranes. However, the total excitation pressure is not the only factor controlling changes in the harvesting capacity. Although an adjustment of PSI and phycobilisome content is characteristic for light acclimation, a regulation of antenna size appears to be initiated by any redox imbalance of the electron transport chain (Wallner et al., 2012), and the actual abundance/ratio of photosynthetic complexes then results from the combined effects of light intensity and quality, temperature, or nutrient availability (Murakami and Fujita, 1991; Murakami et al., 1997; Miskiewicz et al., 2002). Light acclimation can be viewed as a set of regulatory events activated to restore a redox equilibrium in the cell. Indeed, a defect in the mechanism balancing the excitation of PSI and PSII, like the one caused by the *pmgA* mutation, generates a detrimental redox poise (Sonoike et al., 2001)

and presumably locks the mutant cell in a perpetual unsuccessful effort to achieve the redox equilibrium.

The cytochrome *b<sub>6</sub>f* complex was shown to serve as a redox sensor, triggering acclimatory machinery in cyanobacteria (Murakami and Fujita, 1993), though it remains unknown how this signal is transduced and processed in the cell. Undoubtedly, the tetrapyrrole pathway is an important target of this regulation. In cyanobacteria, the main flow of tetrapyrrole biosynthesis intermediates is directed to the synthesis of Chl and phycobilins that serve as the main light-harvesting pigments bound to the PSII-associated phycobilisome antenna. During light acclimation, Chl and intermediates of its biosynthesis deserve special care due to their phototoxic nature and high concentration of Chl in the cell. A tight coordination between synthesis of Chl and Chl apoproteins is expected to be crucial for the viability of the photosynthetic cell as formation of a pool of unquenched Chl or its intermediates would generate harmful reactive oxygen species.

The PSI trimer is the site where the majority of Chl is placed in the cyanobacterial cell, and as we show in this work, this complex is almost an exclusive sink for de novo Chl (Fig. 7B). For the reasons described above, a relatively fast down-regulation of the PSI level during the acclimation to HL has to be reflected by a regulation of Chl biosynthesis or/and Chl trafficking in the cell. A relation between the regulation of the PSI level and Chl biosynthesis is likely to be even more intimate since de novo Chl appears to be a rate-limiting factor for the translation of the PSI core subunits (Eichacker et al., 1996). It is expected that the PSI level is controlled via the regulation of Chl synthesis; thereby, the Chl limitation is the key factor causing the

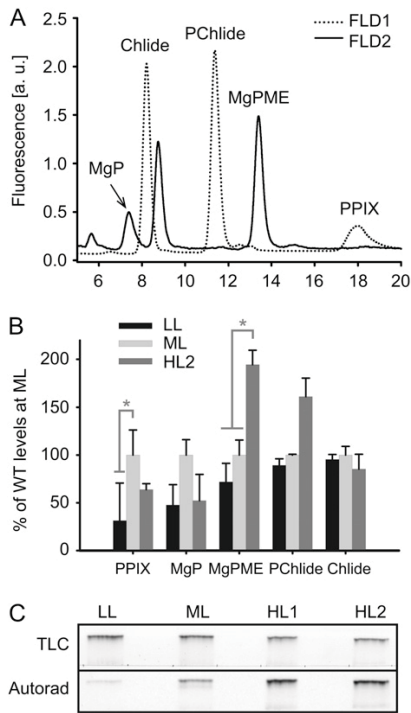


**Figure 6.** Levels of Chl precursors and the rate of Chl formation in cells acclimated to different light intensities. A, Separation and detection of Chl precursors using HPLC equipped with two fluorescence detectors (FLD1 and FLD2). Precursors were extracted from 2 mL of HL2-acclimated cells by a successive extraction using 70% and 80% methanol and immediately injected into the HPLC; for details, see “Materials and Methods.” a.u., Arbitrary units; PP<sub>IX</sub>, protoporphyrin IX; MgP, Mg-protoporphyrin IX; MgPME, Mg-protoporphyrin IX methylester; PChlide, protochlorophyllide; Chlide, chlorophyllide. B, Relative levels of Chl precursors in the *Synechocystis* cells acclimated to LL, ML, and HL2. Values shown represent means  $\pm$  SD from three independent measurements. Asterisks indicate statistically significant differences in precursor levels as tested using a paired Student’s *t* test ( $P = 0.05$ ). WT, The wild type. C, Chl radiolabeled by [<sup>14</sup>C]Glu was extracted using methanol/0.2% NH<sub>4</sub>OH from cells cultivated under different light conditions (LL, ML, HL1, and HL2), converted into Mg-chlorin, and separated on a TLC plate. Radiolabeled Mg-chlorin was detected using an x-ray film (Autorad); amount of Mg-chlorin loaded per TLC lane corresponds to the cellular level of Chl under relevant light conditions.

decrease in PSI level at HL (Fujita et al., 1990; Muramatsu et al., 2009). The proposed mechanism is based on an assumption that a surplus of PsaA/B proteins is continuously translated but finally degraded due to a shortage in Chl. Although it seems to be a waste of energy, it might also provide a crucial function to ensure that there is always a place where Chl molecules can be safely incorporated even when synthesized in excess. Moreover, it is obvious from Figure 2, that *Synechocystis* cells are packed with glycogen when grown at HL2; thus, some energy can be easily sacrificed for a tight control over Chl-(protein) biosynthesis.

Although there is compelling evidence that both the transcription rate and stability of the *psaA/B* transcript are carefully regulated during light acclimation (Hihara et al., 2001; Herranen et al., 2005), the abundance of the *psaA/B* transcript does not appear to limit PSI synthesis consistently with the proposed regulatory role of Chl. In an elegant experiment Muramatsu et al. (2009) demonstrated that a *Synechocystis* strain engineered to have a constantly upregulated *psaA/B* transcript was still able to reduce the PSI level under HL.

Results so far published on an interplay between the Chl biosynthesis and the PSI/PSII stoichiometry concern a time period spanning up to 16 h after the shift to

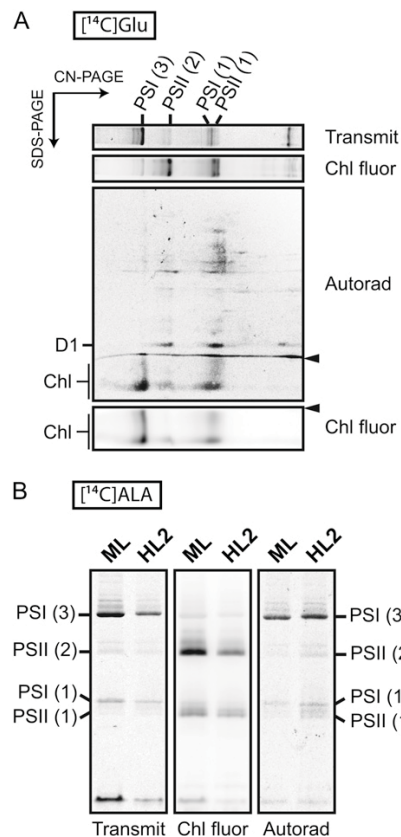


**Figure 7.** Radiolabeling of Chl molecules by [<sup>14</sup>C]Glu and [<sup>14</sup>C]ALA and detection of labeled Chl in Chl-protein complexes. A, *Synechocystis* cells acclimated to HL2 were radiolabeled with [<sup>14</sup>C]Glu in a 30-min pulse and membrane proteins were then separated by two-dimensional CN/SDS-PAGE. Radioactivity was detected by a phosphor imager (Autorad). Position of particular complexes is indicated on the top; Chl molecules running ahead of proteins (below the protein edge line designated by arrowheads) on the SDS gel were also visualized by Chl fluorescence (Chl fluor). B, Cells acclimated to ML and HL2 were radiolabeled with [<sup>14</sup>C]ALA for 30 min, and membrane proteins were separated by CN-PAGE. Proteins loaded in each lane correspond to 200  $\mu$ L of cells at OD<sub>750</sub> = 1.0; all abbreviations used are described in Figure 3.

**Table II.** Quantification of proteins and Chl labeling in individual PSI and PSII complexes

The same *Synechocystis* cell culture acclimated to HL2 was labeled separately by [<sup>35</sup>S]Met/Cys mixture or by [<sup>14</sup>C]ALA for 30 min and isolated cell membranes separated as a dilution series by CN-PAGE (see Figs. 4 and 7; Supplemental Fig. S6). After exposure of gels in a phosphor imager, bands of individual complexes were quantified using ImageQuant TL 7.0 software (GE Healthcare).

Complex	Protein Labeling: [ <sup>35</sup> S]Met+Cys			Chl Labeling: [ <sup>14</sup> C]ALA			
	Protein Labeling <sup>a</sup>	Normalized Labeling <sup>b</sup>	Normalized Labeling <sup>c</sup> (%)	Measured Chl Labeling <sup>a</sup>	Measured Chl Labeling	Expected Chl Labeling <sup>d</sup> (%)	Measured/Expected
PSI trimer	$0.36 \times 10^6$	$0.21 \times 10^6$	2.1	$29.44 \times 10^6$	58.8	9.3	6.31
PSI monomer	$1.46 \times 10^6$	$2.57 \times 10^6$	26.3	$5.92 \times 10^6$	17.5	38.4	0.46
PSII dimer	$2.15 \times 10^6$	$1.86 \times 10^6$	19.0	$8.76 \times 10^6$	11.8	21.9	0.54
PSII monomer	$2.98 \times 10^6$	$5.78 \times 10^6$	52.6	$5.98 \times 10^6$	11.9	30.4	0.39

<sup>a</sup>Absolute values of protein and Chl labeling in PSI and PSII complexes obtained using ImageQuant software and a calibration curve for each complex (Supplemental Fig. S6). <sup>b</sup>[<sup>35</sup>S] labeling normalized to a total number of Met and Cys in D1, D2, CP43, and CP47 core proteins for PSII complexes and PsaA and PsaB core proteins for PSI. Although synthesis rates of individual PSII core proteins are different (see Fig. 5), all four proteins contain a similar number of Met and Cys and then their different syntheses can be neglected. <sup>c</sup>Actual synthesis of PSI/PSII complexes expressed in relative values. <sup>d</sup>Expected Chl labeling simulates a situation when labeled Chls are evenly distributed to individual complexes synthesized in rates determined by [<sup>35</sup>S] labeling. Calculation is based on known number of Chl molecules bound to each complex (see text).

HL when visible changes in the cell pigmentation are observed (for review, see Muramatsu and Hihara, 2012; see also Fig. 1). However, almost no attention has been paid to how an optimal PSI/PSII ratio is maintained in the cyanobacterial cells already acclimated to HL, even though this is the ultimate optimum to which the whole process of acclimation is directed. In this work, we analyzed in detail the *Synechocystis* cells acclimated to four different irradiances; the highest one used (HL2) is close to the saturated (optimal) intensity for *Synechocystis* providing energy for the fastest proliferation that this cyanobacterium is probably able to achieve. Doubling time 7 h (Table 1) for these cells was close to 6 h described by Hihara et al. (2001) for the same light intensity. Taking into account that the cell growth rate was twice and more than 4 times faster at HL2 than at ML and LL, respectively, it is trivial to calculate that cells have to start to produce 4 times more Chl after acclimation at HL2 just to maintain a constant Chl content per cell; it does not matter what exactly the content is. In fact, the rate of Chl formation at HL2 should be elevated more than an order of magnitude since the half-life of Chl molecules was determined by <sup>15</sup>N labeling to be at least 4 times shorter in *Synechocystis* cells growing at HL2 (approximately 50 h) when compared with very stable Chls found in cells acclimated to ML (half-life > 200 h; Vavilin et al., 2007). This expectation corresponds well to the more intensive de novo Chl labeling (Fig. 6C), to the higher level of enzymes of the tetrapyrrole pathway (Fig. 5), and to the significantly increased levels of late Chl precursors Mg-protoporphyrin monomethyl ester and protochlorophyllide in the HL2-acclimated cells (Fig. 6B).

In light of our results and the published data, the process of acclimation to HL could be divided into two phases. In the first moment after the shift to HL, an intensive irradiation catches cells off guard and causes photooxidation demonstrated by a decrease in  $F_v/F_m$  (Supplemental Fig. S4). Cells start to mobilize a broad

spectrum of protective mechanisms, including synthesis of myxoxanthophyll, an acceleration of the PSII repair cycle, and a massive expression of high light-induced proteins (HLIPs) belonging to family of Chl *a/b* binding proteins (for review, see Muramatsu and Hihara, 2012). According to microarray and expression data, the transcription of the *psaA/B* genes is strongly reduced (Hihara et al., 2001; Herranen et al., 2005), and because the ALA formation is also ceased (Muramatsu et al., 2009), it is likely that the PSI synthesis is minimal during an initial phase of acclimation. However, the cells continue dividing and result in the observed fast drop in PSI level in the first 4 h at HL2 caused by a simple dilution (Fig. 1B). Interestingly, levels of enzymes involved in Chl biosynthesis appear to be similar or increasing during this early time of acclimation (Fig. 5B) despite the reported decrease in their transcripts (Hihara et al., 2001). Our results are consistent with the observation of Muramatsu et al. (2009) that glutamyl-tRNA reductase, the first enzyme of Chl biosynthesis, also accumulates after 6 h of cultivating *Synechocystis* cells under HL. An important exception is geranylgeranyl reductase, the level of which is strongly reduced shortly after the shift to HL2 (Fig. 5B), indicating its specific degradation or an unspecific, light-induced destruction. However, the observed decrease in geranylgeranyl reductase level is unlikely a consequence of the regulatory response as this enzyme is essential for the synthesis of phytol and its inactivation in *Synechocystis* resulted in a Chl deficient and light sensitive strain (Shpilyov et al., 2005). A more plausible explanation is that the geranylgeranyl reductase is relatively easily damaged by light and requires a protective mechanism, which, however, is not efficient enough at the time immediately after the shift from ML to HL2. Regarding this possibility, it is interesting that LIL3 protein from the Chl *a/b* binding family is essential for the accumulation of geranylgeranyl reductase in higher plants (Tanaka et al., 2010). As mentioned above, cyanobacteria possess similar Chl *a/b*



binding proteins called HLIPs that are almost absent under LL intensities but very quickly accumulate upon exposure of cells to various stress conditions, including HL (He et al., 2001; see also below).

Based on our data, we propose that the synthesis of PSII subunits does not rely on the availability of the de novo Chl to such an extent as the trimeric PSI (Fig. 7B); thus, the synthesis of the most light-sensitive D1 subunit can be accelerated even when the availability of de novo Chl is limited during the initial phase of the HL acclimation. After this initial emergency phase, the photoprotective mechanisms start to work and in 6 h of the HL2 acclimation the  $F_v/F_m$  returns to the value observed under ML (Supplemental Fig. S4). At that particular moment, cells were already growing rapidly (J. Kopečna and R. Sobotka, unpublished data); thus, the rate of Chl formation has to be boosted to prevent an excessive loss of the thylakoid membranes. The adjustment of the PSI level and the level of phycobilisomes in proceeding approximately 10 h is probably based on a sophisticated regulatory network seeking for a balance among the redox state, Chl availability, growth rate, antenna size, and probably a number of other parameters. The two different phases of the HL acclimation are in line with the phenotype of the *pmgA* mutant; there is no change in the PSI level during the first phase, but in the second phase the PSI accumulates more than it should be (Hihara et al., 1998), indicating that due to the *pmgA* mutation, more Chl than necessary is directed to PSI.

Once the new equilibrium under HL is achieved, the levels of photosystems and phycobilisomes remain constant when the culture is kept at a similar (low) optical density that prevents shading (Fig. 1B; 16 and 24 h). As discussed above, the HL2-acclimated cells have to up-regulate Chl production to support fast growth. Labeling using [ $^{14}\text{C}$ ]Glu or [ $^{14}\text{C}$ ]ALA demonstrated that the main sink for the newly synthesized Chl is the trimeric PSI, a stable, Chl-rich building block of the thylakoid membranes. On the other hand, our study confirmed enhanced synthesis of PSII subunits in comparison with PSI proteins at all studied irradiances (Fig. 4). The HL sensitivity of the PSII complex to the light-induced damage necessitates a higher turnover rate of its protein subunits (especially the D1 protein) than subunits of PSI (Yao et al., 2012b). A significant disproportion between strong protein labeling versus weak Chl labeling in PSII complexes shows that the resynthesis of PSII Chl-proteins largely occurs at the expense of the recycled Chl previously released from degraded Chl-proteins. PSII complexes are completely replaced by new ones in less than a day, but the lifetime of total Chl in *Synechocystis* cells is much longer (see above; Vavilin et al., 2005; Yao et al., 2012a). Moreover, Xu et al. (2004) suggested that the preexisting Chl molecules in a periphery of PSI could be released and redistributed for PSII biosynthesis in the etioloating cyanobacterial cells. The exact mechanism of the Chl recycling process is not known; nevertheless, it seems to include a dissociation of the

phytyl chain and the chlorophyllide ring (Vavilin and Vermaas, 2007) upon PSII protein degradation and their subsequent reassociation before or during their reuse in the biogenesis of new PSII Chl-proteins (Vavilin et al., 2005; Vavilin and Vermaas, 2007). Nonetheless, despite the apparent importance of the Chl recycling, there should always be a certain input of newly synthesized Chl that replaces the lost/degraded Chl released from PSII and that also maintains sufficient Chl quantity for the enhanced de novo/repair-related PSII synthesis under the increased irradiance. The labeling of pigments showed that the input of the newly synthesized Chl into the PSII complex is enhanced after the HL2 acclimation (Fig. 7B).

The input of the de novo Chl into PSII synthesis seems to be largely independent on the main flow of the tetrapyrrole intermediates directed to PSI trimer and might represent a separate branch of the pathway. We speculate that Chl biosynthesis occurs in Chl biosynthesis centers, which contain some common general components, such as Chl biosynthesis enzymes, but may differ in regulatory proteins that are specific for individual Chl proteins (Komenda et al., 2012). In this regard, it is intriguing that the monomeric PSI is synthesized faster than the trimeric PSI but contains much less labeled Chl (Figs. 4A and 7B; Table II). This indicates that cyanobacteria possess a portion of PSI serving perhaps a specific function, which is not assembled into a trimer, has a faster turnover, and is synthesized utilizing recycled Chls. Such separated biogenesis of PSI complexes would be consistent with our idea of protein/complex-specific Chl biosynthesis centers in the cell. The small membrane proteins called HLIPs (also named small chlorophyll *a/b* binding proteins [SCPs]) possessing the conserved Chl *a/b* binding motif are promising candidates for factors controlling a precise distribution of Chl into apoproteins. HLIPs seem to play a crucial role in Chl recycling. In *Synechocystis* HLIP-less mutants, the half-life of Chl molecules is not affected under LL; however, under HL2, Chl is degraded much faster in the mutant than in the wild type (Vavilin et al., 2007). HLIPs also somehow modulate early steps of the Chl biosynthesis (Xu et al., 2002; Yao et al., 2012a) and physically interact with PSII assembly intermediates. Furthermore, cyanobacterial and plastidic ferrochelatase enzymes are fused at the C terminus with a HLIP protein forming the so-called CAB domain. A deletion of this domain in *Synechocystis* has no effect on the ferrochelatase activity or stability, but the resulting mutant accumulates significantly higher Chl level under HL (Sobotka et al., 2011).

In higher plants, particularly in matured leaves, the regulation of the harvesting capacity and the PSI/PSII ratio has to differ from cyanobacteria as plants do not contain phycobilisomes and the dilution of the thylakoid membranes by a slowly dividing chloroplast is minimal compared with fast-growing cyanobacteria. Interestingly, Chl labeling in *Arabidopsis thaliana* was found to be accelerated after a long-term acclimation

to HL (Beisel et al., 2010), which implies that light up-regulates the Chl formation in both plants and cyanobacteria. However, in another radiolabeling experiment carried out on HL-exposed rye (*Secale cereale*) chloroplasts, de novo Chl was localized predominantly in PSII, much less in PSI or in light-harvesting antennas (Feierabend and Dehne, 1996). Thus, opposed to cyanobacteria, most of the Chl produced in plant chloroplasts is probably used to support the PSII repair cycle since the need for synthesis of the new PSI complexes is very limited. Nonetheless, since the tetrapyrrole biosynthesis and the structure of the photosynthetic apparatus is so well conserved in both cyanobacteria and chloroplasts, we expect that, in principle, molecular mechanisms harmonizing the synthesis of Chl and photosystem subunits are shared generally by all oxygenic phototrophs.

## MATERIALS AND METHODS

### Growth Conditions

A nonmotile, Glc-tolerant strain of *Synechocystis* (*Synechocystis* sp. PCC 6803; Williams, 1988) obtained from the laboratory of Peter J. Nixon (Imperial College, London) was grown photoautotrophically in BG11 medium (Rippka et al., 1979). Sixty milliliters of a liquid culture was grown at 28°C in a rotating 250-mL Erlenmeyer flask in a growing chamber under continuous illumination of 40  $\mu\text{E m}^{-2} \text{s}^{-1}$  (ML). For described experiments, cells grown at ML were diluted to  $\text{OD}_{750} = 0.25$  and shifted to 10  $\mu\text{E m}^{-2} \text{s}^{-1}$  (LL), diluted to  $\text{OD}_{750} = 0.1$  and shifted to 150  $\mu\text{E m}^{-2} \text{s}^{-1}$  (HL1), or diluted to  $\text{OD}_{750} = 0.06$  and shifted to 300  $\mu\text{E m}^{-2} \text{s}^{-1}$  (HL2). After 24 h, cells were harvested in an exponential growth phase ( $\text{OD}_{750} = \text{approximately } 0.3$ ). In all experiments, illumination was provided by cool-white fluorescent tubes (Osram).

### Absorption Spectra and Determination of Chl Content

Absorption spectra of whole cells were measured at room temperature with a UV-3000 spectrophotometer (Shimadzu). Chl was extracted from cell pellets (2 mL,  $\text{OD}_{750} = \text{approximately } 0.3$ ) with 100% (v/v) methanol, and its concentration was measured spectrophotometrically according to Porra et al. (1989).

### Radioactive Labeling of Proteins and Preparations of Cell Membranes

Cells (50  $\mu\text{g}$  of Chl) in an exponential growth phase ( $\text{OD}_{750} = \text{approximately } 0.3$ ) were harvested by centrifugation, washed, and resuspended in fresh BG11 with 20 mM TES to a final volume 475  $\mu\text{L}$ . The cell suspension was shaken in 10-mL glass tubes for 30 min at 30°C at the same light conditions as acclimated before for 24 h. [ $^{35}\text{S}$ ]Met/Cys mixture (>1,000 Ci/mmol; Amersham Biosciences) was then added with the final activity of 500  $\mu\text{Ci mL}^{-1}$ , and illumination was continued for another 30 min. After this time period, cells were immediately frozen in liquid nitrogen. To prepare cyanobacterial membranes and cytosolic proteins, harvested cells were washed, resuspended in the thylakoid buffer containing 25 mM MES/NaOH, pH 6.5, 5 mM  $\text{CaCl}_2$ , 10 mM  $\text{MgCl}_2$ , and 20% glycerol, and broken using glass beads. The broken cells were pelleted (20,000g, 15 min). The supernatant represented the soluble fraction, while the sediment was resuspended in the excess volume of the thylakoid buffer, pelleted, and resuspended again in the thylakoid buffer to obtain the membrane fraction.

### Electrophoresis and Immunoblotting

Analysis of membrane proteins under native conditions was performed by CN-PAGE as described by Wittig and Schägger (2008). The isolated membranes were resuspended in 25 mM MES/NaOH, pH 6.5, containing 5 mM  $\text{CaCl}_2$ , 10 mM  $\text{MgCl}_2$ , and 20% glycerol. The membranes were then solubilized in 1% *n*-dodecyl- $\beta$ -maltooside and analyzed at 4°C in a 4% to 14% or 4% to 12% polyacrylamide gel.

Individual proteins in membrane complexes were resolved in the second dimension by SDS-PAGE in a 12% to 20% linear gradient polyacrylamide gel containing 7 M urea (Sobotka et al., 2008). One-dimensional SDS-PAGE and immunodetection was carried out as described by Sobotka et al. (2008). The primary antibodies against subunits of Mg-chelatase and against Mg-protoporphyrin methyltransferase, light-dependent protochlorophyllide oxidoreductase, and geranylgeranyl reductase were kindly provided by Prof. C. Neil Hunter (University of Sheffield), ferrochelatase and Gun4 antibodies were kindly provided by Prof. Annegret Wilde (Justus-Liebig University, Giessen), and antibody against the plant homolog of the cyclase component Sll1214 was purchased from Agrisera.

### Electron Microscopy

A small volume of the *Synechocystis* cells acclimated to ML and HL2 was concentrated in a sealed 200- $\mu\text{L}$  tip by centrifugation at 5,000 rpm for 5 min. The obtained cell pellet was loaded into a specimen carrier (200- $\mu\text{m}$  deep; Leica), pretreated with 1% lecithin in chloroform, and then ultra-rapidly frozen in a high-pressure freezer (EM Pact2; Leica). Samples were freeze-substituted in a solution of 1% tannic acid and 0.5% glutaraldehyde in acetone using an automatic freeze substitution unit (AFS, EM; Leica) as follows: 72 h at  $-85^\circ\text{C}$ , three times rinsed with acetone for 1 h followed by a change of solution to 1% osmium/acetone, 4 h at  $-85^\circ\text{C}$ , 5 h warming up to  $-25^\circ\text{C}$ , 12 h at  $-25^\circ\text{C}$ , and 6 h warming up to  $4^\circ\text{C}$ . Samples were removed from specimen carriers and rinsed three times in acetone at room temperature. Resin infiltration was done stepwise with 20%, 25%, 33%, 50%, 66%, and 80% steps with low viscosity Spurr's resin in acetone (SPI Supplies) for 3 h each. After infiltration with 100% resin overnight, the samples were polymerized for 48 h at  $60^\circ\text{C}$ . Ultrathin sections were cut on an ultramicrotome (UCT; Leica), collected on copper grids with a formvar coating, and stained with uranyl acetate for 5 min followed by lead citrate for 1 min. Sections were examined in a transmission electron microscope (JEOL 1010) equipped with a Mega View III camera (SIS).

### Chl Radiolabeling, Extraction, and Detection Using TLC

The procedure of labeling Chl was identical to the protein labeling except that 180  $\mu\text{M}$  of [ $^{14}\text{C}$ ]Glu or [ $^{14}\text{C}$ ]ALA (specific activity approximately 55 mCi/mmol; American Radiolabeled Chemicals) was used instead of [ $^{35}\text{S}$ ]Met/Cys. Chl was extracted from pelleted cells using 750  $\mu\text{L}$  of methanol/0.2%  $\text{NH}_4\text{OH}$  (v/v), cell debris pelleted by centrifugation, and supernatant collected. This step was repeated and supernatants combined, and NaCl was added to the final concentration of 100 mM. This solution was mixed with 400  $\mu\text{L}$  of hexan and the upper phase taken. The hexan extraction was repeated three times, combined, and completely evaporated in a SpeedVac (Eppendorf). The pellet was resuspended in 0.5% KOH/methanol (v/v) and incubated at room temperature for 15 min to convert Chl to phytol-less Mg-chlorin. The suspension was then washed three times with 200  $\mu\text{L}$  of hexan, concentrated by evaporation to 50  $\mu\text{L}$ , and washed with 100  $\mu\text{L}$  of petroleum ether (boiling range  $45^\circ\text{C}$  to  $60^\circ\text{C}$ ). The solution of Mg-chlorin was dried by evaporation in a SpeedVac, resuspended in 30  $\mu\text{L}$  of methanol/chloroform (1:1, v/v), and loaded on a TLC plate (SIL G-25; Macherey-Nagel). The mobile phase used was methanol/10 mM  $\text{Na}_2\text{H}_2\text{P}_2\text{O}_7$ , pH 6.8 (3:1, v/v); the dried TLC plate was exposed to an x-ray film for 5 d.

### Quantification of Chl Precursors

For quantitative determination of Chl precursors in the cells, 2 mL of culture at  $\text{OD}_{750} = 0.35$  was harvested. Pigments were extracted with 100  $\mu\text{L}$  of 70% methanol, the sample was centrifuged, and the supernatant containing the extracted pigments was collected. The pellet was then extracted again using 100  $\mu\text{L}$  of 80% methanol. Supernatants were combined and immediately separated by HPLC (Agilent 1200) on a reverse-phase column (Nova-Pak C18, 4-mm particle size, 3.9  $\times$  150 mm; Waters) using 30% methanol in 1 M ammonium acetate, pH 6.7, and 100% methanol as solvents A and B, respectively. Porphyrins were eluted with a linear gradient of the solvent B (67%–74% in 20 min) at a flow rate of 0.9 mL  $\text{min}^{-1}$  at  $40^\circ\text{C}$ . Porphyrins were detected by two fluorescence detectors. The first fluorescence detector was set to 435/675 nm (excitation/emission wavelengths) for 0 to 11 min, 435/640 nm for 11 to 14 min, and 400/640 nm for 14 to 25 min, and the second fluorescence detector was set at 416/595 nm throughout the experiment. For retention times of individual precursors, see Figure 5A.

### Supplemental Data

The following materials are available in the online version of this article.

- Supplemental Figure S1.** A scheme of the tetrapyrrole biosynthetic pathway in cyanobacteria.
- Supplemental Figure S2.** Levels of major carotenoids and chlorophyll determined in *Synechocystis* cells acclimated to LL, ML, and HL2.
- Supplemental Figure S3.** Whole-cell spectra of *Synechocystis* wild-type cells grown for 24 h at HL2 ( $300 \mu\text{E m}^{-2} \text{s}^{-1}$ ) and at  $600 \mu\text{E m}^{-2} \text{s}^{-1}$ .
- Supplemental Figure S4.** Time course of changes in  $F_v/F_m$  ratios following shift of *Synechocystis* cells from ML ( $40 \mu\text{E m}^{-2} \text{s}^{-1}$ ) to HL2 ( $300 \mu\text{E m}^{-2} \text{s}^{-1}$ ).
- Supplemental Figure S5.** Color figure of [ $^{14}\text{C}$ ]-labeled Mg-chlorin separated on a TLC plate.
- Supplemental Figure S6.** A dilution series of [ $^{35}\text{S}$ ]-labeled membranes separated by CN-electrophoresis and a calibration curve used for quantification of labeled PSII(2) complex.
- ## ACKNOWLEDGMENTS
- We thank Prof. C. Neil Hunter (Sheffield University, UK) and Prof. Annegret Wilde (Justus-Liebig-University, Giessen, Germany) for antibodies and Ondřej Komárek (Institute of Microbiology, Trebon, Czech Republic) for the measurement of variable Chl fluorescence of *Synechocystis* cells.
- Received September 14, 2012; accepted October 2, 2012; published October 4, 2012.
- ## LITERATURE CITED
- Anderson JM, Chow WS, Park YI** (1995) The grand design of photosynthesis: Acclimation of the photosynthetic apparatus to environmental cues. *Photosynth Res* **46**: 129–139
- Beisel KG, Jahnke S, Hofmann D, Köppchen S, Schurr U, Matsubara S** (2010) Continuous turnover of carotenoids and chlorophyll a in mature leaves of *Arabidopsis* revealed by  $^{14}\text{CO}_2$  pulse-chase labeling. *Plant Physiol* **152**: 2188–2199
- Chow WS, Melis A, Anderson JM** (1990) Adjustments of photosystem stoichiometry in chloroplasts improve the quantum efficiency of photosynthesis. *Proc Natl Acad Sci USA* **87**: 7502–7506
- Czarnecki O, Grimm B** (2012) Post-translational control of tetrapyrrole biosynthesis in plants, algae, and cyanobacteria. *J Exp Bot* **63**: 1675–1687
- Demmig-Adams B, Adams WW** (1992) Photoprotection and other responses of plants to high light stress. *Annu Rev Plant Physiol Plant Mol Biol* **43**: 599–626
- Eichacker LA, Helfrich M, Rüdiger W, Müller B** (1996) Stabilization of chlorophyll *a*-binding apoproteins P700, CP47, CP43, D2, and D1 by chlorophyll *a* or Zn-pheophytin *a*. *J Biol Chem* **271**: 32174–32179
- El Bissati K, Delphin E, Murata N, Etienne AL, Kirilovsky D** (2000) Photosystem II fluorescence quenching in the cyanobacterium *Synechocystis* PCC 6803: involvement of two different mechanisms. *Biochim Biophys Acta* **1457**: 229–242
- Feierabend J, Dehne S** (1996) Fate of the porphyrin cofactors during the light-dependent turnover of catalase and of the photosystem II reaction-center protein D1 in mature rye leaves. *Planta* **198**: 413–422
- Fujimori T, Higuchi M, Sato H, Aiba H, Muramatsu M, Hihara Y, Sonoike K** (2005) The mutant of *sll1961*, which encodes a putative transcriptional regulator, has a defect in regulation of photosystem stoichiometry in the cyanobacterium *Synechocystis* sp. PCC 6803. *Plant Physiol* **139**: 408–416
- Fujita Y, Murakami A, Ohki K** (1990) Regulation of the stoichiometry of thylakoid components in the photosynthetic system of cyanophytes: Model experiments showing that control of the synthesis or supply of Chl *a* can change the stoichiometric relationship between the two photosystems. *Plant Cell Physiol* **31**: 145–153
- He Q, Dolganov N, Bjorkman O, Grossman AR** (2001) The high light-inducible polypeptides in *Synechocystis* PCC6803. Expression and function in high light. *J Biol Chem* **276**: 306–314
- Herranen M, Tyystjärvi T, Aro EM** (2005) Regulation of photosystem I reaction center genes in *Synechocystis* sp. strain PCC 6803 during light acclimation. *Plant Cell Physiol* **46**: 1484–1493
- Hihara Y, Kamei A, Kanehisa M, Kaplan A, Ikeuchi M** (2001) DNA microarray analysis of cyanobacterial gene expression during acclimation to high light. *Plant Cell* **13**: 793–806
- Hihara Y, Sonoike K, Ikeuchi M** (1998) A novel gene, *pmgA*, specifically regulates photosystem stoichiometry in the cyanobacterium *Synechocystis* species PCC 6803 in response to high light. *Plant Physiol* **117**: 1205–1216
- Jordan P, Fromme P, Witt HT, Klukas O, Saenger W, Krauss N** (2001) Three-dimensional structure of cyanobacterial photosystem I at 2.5 Å resolution. *Nature* **411**: 909–917
- Komenda J, Sobotka R, Nixon PJ** (2012) Assembling and maintaining the photosystem II complex in chloroplasts and cyanobacteria. *Curr Opin Plant Biol* **15**: 245–251
- Melis A, Murakami A, Nemson JA, Aizawa K, Ohki K, Fujita Y** (1996) Chromatic regulation in *Chlamydomonas reinhardtii* alters photosystem stoichiometry and improves the quantum efficiency of photosynthesis. *Photosynth Res* **47**: 253–265
- Miskiewicz E, Ivanov AG, Huner NPA** (2002) Stoichiometry of the photosynthetic apparatus and phycobilisome structure of the cyanobacterium *Plectonema boryanum* UTEX 485 are regulated by both light and temperature. *Plant Physiol* **130**: 1414–1425
- Müller P, Li XP, Niyogi KK** (2001) Non-photochemical quenching. A response to excess light energy. *Plant Physiol* **125**: 1558–1566
- Mullineaux CW, Emlyn-Jones D** (2005) State transitions: an example of acclimation to low-light stress. *J Exp Bot* **56**: 389–393
- Murakami A, Fujita Y** (1991) Regulation of photosystem stoichiometry in the photosynthetic system of the cyanophyte *Synechocystis* PCC 6714 in response to light-intensity. *Plant Cell Physiol* **32**: 223–230
- Murakami A, Fujita Y** (1993) Regulation of stoichiometry between PSI and PSII in response to light regime for photosynthesis observed with *Synechocystis* PCC 6714: relationship between redox state of Cyt  $b_{6/f}$  complex and regulation of PSI formation. *Plant Cell Physiol* **34**: 1175–1180
- Murakami A, Kim SJ, Fujita Y** (1997) Changes in photosystem stoichiometry in response to environmental conditions for cell growth observed with the cyanophyte *Synechocystis* PCC 6714. *Plant Cell Physiol* **38**: 392–397
- Muramatsu M, Hihara Y** (2012) Acclimation to high-light conditions in cyanobacteria: from gene expression to physiological responses. *J Plant Res* **125**: 11–39
- Muramatsu M, Sonoike K, Hihara Y** (2009) Mechanism of downregulation of photosystem I content under high-light conditions in the cyanobacterium *Synechocystis* sp. PCC 6803. *Microbiology* **155**: 989–996
- Neale PJ, Melis A** (1986) Algal photosynthetic membrane complexes and the photosynthesis-irradiance curve: a comparison of light-adaptation responses in *Chlamydomonas reinhardtii* (Chlorophyta). *J Phycol* **22**: 531–538
- Nixon PJ, Michoux F, Yu J, Boehm M, Komenda J** (2010) Recent advances in understanding the assembly and repair of photosystem II. *Ann Bot (Lond)* **106**: 1–16
- Nowaczyk MM, Hebel R, Schlodder E, Meyer HE, Warscheid B, Rögner M** (2006) Psb27, a cyanobacterial lipoprotein, is involved in the repair cycle of photosystem II. *Plant Cell* **18**: 3121–3131
- Porra RJ, Thompson WA, Kriedmann PE** (1989) Determination of accurate extinction coefficients and simultaneous equations for assaying chlorophylls *a* and *b* extracted with four different solvents: verification of the concentration of chlorophyll standards by atomic absorption spectroscopy. *Biochim Biophys Acta* **975**: 384–394
- Rippka R, Deruelles J, Waterbury JB, Herdman M, Stanier RY** (1979) Generic assignments, strain histories and properties of pure cultures of cyanobacteria. *J Gen Microbiol* **111**: 1–61
- Shen G, Boussiba S, Vermaas WFJ** (1993) *Synechocystis* sp. PCC 6803 strains lacking photosystem I and phycobilisome function. *Plant Cell* **5**: 1853–1863
- Shpilyov AV, Zinchenko VV, Shestakov SV, Grimm B, Lokstein H** (2005) Inactivation of the geranylgeranyl reductase (ChlP) gene in the cyanobacterium *Synechocystis* sp. PCC 6803. *Biochim Biophys Acta* **1706**: 195–203
- Sobotka R, Dühring U, Komenda J, Peter E, Gardian Z, Tichý M, Grimm B, Wilde A** (2008) Importance of the cyanobacterial Gun4 protein for chlorophyll metabolism and assembly of photosynthetic complexes. *J Biol Chem* **283**: 25794–25802
- Sobotka R, Tichý M, Wilde A, Hunter CN** (2011) Functional assignments for the carboxyl-terminal domains of the ferrochelatase from *Synechocystis* PCC 6803: the CAB domain plays a regulatory role, and region II is essential for catalysis. *Plant Physiol* **155**: 1735–1747
- Sonoike K, Hihara Y, Ikeuchi M** (2001) Physiological significance of the regulation of photosystem stoichiometry upon high light acclimation of *Synechocystis* sp. PCC 6803. *Plant Cell Physiol* **42**: 379–384

- Tanaka R, Rothbart M, Oka S, Takabayashi A, Takahashi K, Shibata M, Myouga F, Motohashi R, Shinozaki K, Grimm B, et al** (2010) LIL3, a light-harvesting-like protein, plays an essential role in chlorophyll and tocopherol biosynthesis. *Proc Natl Acad Sci USA* **107**: 16721–16725
- Umena Y, Kawakami K, Shen JR, Kamiya N** (2011) Crystal structure of oxygen-evolving photosystem II at a resolution of 1.9 Å. *Nature* **473**: 55–60
- Vavilin D, Brune DC, Vermaas WFJ** (2005) <sup>15</sup>N-labeling to determine chlorophyll synthesis and degradation in *Synechocystis* sp. PCC 6803 strains lacking one or both photosystems. *Biochim Biophys Acta* **1708**: 91–101
- Vavilin D, Vermaas WFJ** (2007) Continuous chlorophyll degradation accompanied by chlorophyllide and phytol reutilization for chlorophyll synthesis in *Synechocystis* sp. PCC 6803. *Biochim Biophys Acta* **1767**: 920–929
- Vavilin D, Yao D, Vermaas WFJ** (2007) Small Cab-like proteins retard degradation of photosystem II-associated chlorophyll in *Synechocystis* sp. PCC 6803: kinetic analysis of pigment labeling with <sup>15</sup>N and <sup>13</sup>C. *J Biol Chem* **282**: 37660–37668
- Wallner T, Hagiwara Y, Bernát G, Sobotka R, Reijerse EJ, Frankenberg-Dinkel N, Wilde A** (2012) Inactivation of the conserved open reading frame *ycf34* of *Synechocystis* sp. PCC 6803 interferes with the photosynthetic electron transport chain. *Biochim Biophys Acta* **1817**: 2016–2026
- Walters RG** (2005) Towards an understanding of photosynthetic acclimation. *J Exp Bot* **56**: 435–447
- Walters RG, Horton P** (1994) Acclimation of *Arabidopsis thaliana* to the light environment: changes in composition of the photosynthetic apparatus. *Planta* **195**: 248–256
- Williams JGK** (1988) Construction of specific mutations in photosystem II photosynthetic reaction center by genetic engineering methods in *Synechocystis* 6803. *Methods Enzymol* **167**: 766–778
- Wittig I, Schägger H** (2008) Features and applications of blue-native and clear-native electrophoresis. *Proteomics* **8**: 3974–3990
- Xu H, Vavilin D, Funk C, Vermaas W** (2002) Small Cab-like proteins regulating tetrapyrrole biosynthesis in the cyanobacterium *Synechocystis* sp. PCC 6803. *Plant Mol Biol* **49**: 149–160
- Xu H, Vavilin D, Funk C, Vermaas W** (2004) Multiple deletions of small Cab-like proteins in the cyanobacterium *Synechocystis* sp. PCC 6803: consequences for pigment biosynthesis and accumulation. *J Biol Chem* **279**: 27971–27979
- Yao DC, Brune DC, Vavilin D, Vermaas WF** (2012a) Photosystem II component lifetimes in the cyanobacterium *Synechocystis* sp. strain PCC 6803: small Cab-like proteins stabilize biosynthesis intermediates and affect early steps in chlorophyll synthesis. *J Biol Chem* **287**: 682–692
- Yao DC, Brune DC, Vermaas WF** (2012b) Lifetimes of photosystem I and II proteins in the cyanobacterium *Synechocystis* sp. PCC 6803. *FEBS Lett* **586**: 169–173





**9.2. Publication II:** Synthesis of Chlorophyll-binding proteins in a fully segregated  $\Delta ycf54$  strain of the cyanobacterium *Synechocystis* PCC 6803.

Hollingshead S, Kopečná J, Armstrong D R, **Bučinská L**, Jackson P J, Chen G E, Dickman M J, Williamson M P, Sobotka R & Hunter C N (2016).

*Front Plant Sci.* 7: 1–15.



# Synthesis of Chlorophyll-Binding Proteins in a Fully Segregated $\Delta ycf54$ Strain of the Cyanobacterium *Synechocystis* PCC 6803

Sarah Hollingshead<sup>1,2</sup>, Jana Kopečná<sup>3</sup>, David R. Armstrong<sup>1</sup>, Lenka Bučinská<sup>3,4</sup>, Philip J. Jackson<sup>1,5</sup>, Guangyu E. Chen<sup>1</sup>, Mark J. Dickman<sup>5</sup>, Michael P. Williamson<sup>1</sup>, Roman Sobotka<sup>3,4</sup> and C. Neil Hunter<sup>1\*</sup>

<sup>1</sup> Department of Molecular Biology and Biotechnology, University of Sheffield, Sheffield, UK, <sup>2</sup> Sir William Dunn School of Pathology, University of Oxford, Oxford, UK, <sup>3</sup> Institute of Microbiology, Centre Algatech, Academy of Sciences of the Czech Republic, Třeboň, Czech Republic, <sup>4</sup> Faculty of Science, University of South Bohemia, České Budějovice, Czech Republic, <sup>5</sup> ChELSI Institute, Department of Chemical and Biological Engineering, University of Sheffield, Sheffield, UK

## OPEN ACCESS

### Edited by:

John Love,  
University of Exeter, UK

### Reviewed by:

Peter Jahns,  
University of Düsseldorf, Germany  
Caiji Gao,  
The Chinese University of Hong Kong,  
China

### \*Correspondence:

C. Neil Hunter  
c.n.hunter@sheffield.ac.uk

### Specialty section:

This article was submitted to  
Plant Cell Biology,  
a section of the journal  
Frontiers in Plant Science

Received: 09 November 2015

Accepted: 23 February 2016

Published: 17 March 2016

### Citation:

Hollingshead S, Kopečná J, Armstrong DR, Bučinská L, Jackson PJ, Chen GE, Dickman MJ, Williamson MP, Sobotka R and Hunter CN (2016) Synthesis of Chlorophyll-Binding Proteins in a Fully Segregated  $\Delta ycf54$  Strain of the Cyanobacterium *Synechocystis* PCC 6803. *Front. Plant Sci.* 7:292. doi: 10.3389/fpls.2016.00292

In the chlorophyll (Chl) biosynthesis pathway the formation of protochlorophyllide is catalyzed by Mg-protoporphyrin IX methyl ester (MgPME) cyclase. The Ycf54 protein was recently shown to form a complex with another component of the oxidative cyclase, Sll1214 (Cycl), and partial inactivation of the *ycf54* gene leads to Chl deficiency in cyanobacteria and plants. The exact function of the Ycf54 is not known, however, and further progress depends on construction and characterization of a mutant cyanobacterial strain with a fully inactivated *ycf54* gene. Here, we report the complete deletion of the *ycf54* gene in the cyanobacterium *Synechocystis* 6803; the resulting  $\Delta ycf54$  strain accumulates huge concentrations of the cyclase substrate MgPME together with another pigment, which we identified using nuclear magnetic resonance as 3-formyl MgPME. The detection of a small amount (~13%) of Chl in the  $\Delta ycf54$  mutant provides clear evidence that the Ycf54 protein is important, but not essential, for activity of the oxidative cyclase. The greatly reduced formation of protochlorophyllide in the  $\Delta ycf54$  strain provided an opportunity to use <sup>35</sup>S protein labeling combined with 2D electrophoresis to examine the synthesis of all known Chl-binding protein complexes under drastically restricted *de novo* Chl biosynthesis. We show that although the  $\Delta ycf54$  strain synthesizes very limited amounts of photosystem I and the CP47 and CP43 subunits of photosystem II (PSII), the synthesis of PSII D1 and D2 subunits and their assembly into the reaction centre (RCII) assembly intermediate were not affected. Furthermore, the levels of other Chl complexes such as cytochrome *b<sub>6</sub>f* and the HliD–Chl synthase remained comparable to wild-type. These data demonstrate that the requirement for *de novo* Chl molecules differs completely for each Chl-binding protein. Chl traffic and recycling in the cyanobacterial cell as well as the function of Ycf54 are discussed.

**Keywords:** Ycf54, *Synechocystis* 6803, chlorophyll, photosystem II, protochlorophyllide, Mg-protoporphyrin IX methylester cyclase

## INTRODUCTION

Chlorophylls (Chl) and Chl binding proteins are essential components of the photosynthetic apparatus. Together they act as principal light harvesting and energy transforming cofactors in photosynthetic organisms, as demonstrated by the structures of both photosystem I (PSI) and photosystem II (PSII; Jordan et al., 2001; Zouni et al., 2001; Umena et al., 2011). It is likely that at least for large Chl-binding subunits of PSI (PsaA, PsaB) and PSII (CP43, CP47) Chl molecules must be inserted into these proteins co-translationally as a prerequisite for correct protein folding (Chua et al., 1976; Eichacker et al., 1996; Müller and Eichacker, 1999; Chidgey et al., 2014). As demonstrated recently using a cyanobacterial  $\Delta chlL$  mutant, which is unable to synthesize Chl in the dark, the availability of *de novo* Chl molecules is ultimately essential for synthesis of all central subunits of both photosystems (Kopečná et al., 2013). Nonetheless, there are unexplained aspects of the assembly of PSII subunits, such as the particular sensitivity of the CP47 subunit to the lack of *de novo* Chl (Dobáková et al., 2009; Kopečná et al., 2015).

The Chls are a group of modified tetrapyrrole molecules distinguished by their fifth isocyclic or E ring, the geranylgeranyl/phytyl moiety esterified at C17 and a centrally chelated magnesium ion. The isocyclic ring arises from the cyclisation of the methyl-propionate side-chain at C-13 to the C-15 bridge carbon between rings C and D. In oxygenic phototrophs this biosynthetic reaction is catalyzed by the oxidative Mg-protoporphyrin IX monomethyl ester cyclase (MgPME-cyclase), which incorporates atmospheric oxygen into the C13<sup>1</sup> carbonyl group (Porra et al., 1996). Although studied in some detail, the enzyme responsible for the aerobic cyclisation reaction remains the least understood in the Chl biosynthesis pathway. The first gene identified as encoding an oxidative cyclase component was the *Rubrivivax gelatinosus acsF* (aerobic cyclisation system iron containing protein) locus (Pinta et al., 2002). Subsequently, AcsF homologs have been identified in all studied oxygenic photosynthetic organisms (Boldareva-Nuianzina et al., 2013).

The Ycf54 protein (12.1 kDa) has been shown recently to interact with the AcsF homolog Sll1214 (hereafter CycI; Peter et al., 2009) in the cyanobacterium *Synechocystis* PCC 6803 (hereafter *Synechocystis*; Hollingshead et al., 2012). Demonstrations that partial elimination of Ycf54 strongly impairs the formation of PChlide and causes Chl deficiency in both cyanobacteria and plants (Albus et al., 2012; Hollingshead et al., 2012) led to speculations that this protein is a catalytic subunit of the MgPME cyclase (Bollivar et al., 2014). Here, we clarify this issue by achieving the complete deletion of the *ycf54* gene in *Synechocystis*. Although the Chl content in this strain was very low, the MgPME-cyclase was apparently active, which demonstrated that the Ycf54 protein is not an essential subunit of the MgPME cyclase. On the other hand, the mutant contained a very low level of CycI and lacked a high-mass complex associated with the light-dependent PChlide oxidoreductase enzyme (POR). The greatly limited formation of PChlide in the *ycf54* mutant provided an opportunity to assess

the sensitivity of assembly pathways for all known Chl-proteins in cyanobacteria to the availability of *de novo* Chl. Interestingly, the deletion of the *ycf54* gene almost abolished the synthesis of PsaA/B subunits and PSII antennas CP47 and CP43, whereas the accumulation of other Chl-proteins showed little or no defects.

## EXPERIMENTAL PROCEDURES

### Growth Conditions

*Synechocystis* strains were grown photomixotrophically in a rotary shaker under low light conditions ( $5 \mu\text{mol photons m}^{-2} \text{s}^{-1}$ ) at 30°C in liquid BG11 medium (Rippka et al., 1979) supplemented with 10 mM TES-KOH (pH 8.2) and 5 mM glucose.

### Construction of the $\Delta ycf54$ *Synechocystis* Strain

In order to disrupt open reading frame *slr1780* (*ycf54*), we prepared a construct for replacing the most this gene (bp 64–276) by a Zeocin resistance cassette. The sequences up- and down-stream (~300 bp) of the *ycf54* gene were amplified with the relevant primers and fusion PCR in conjunction with megaprimers (Ke and Madison, 1997) were used to anneal these either side of the Zeocin resistance cassette. The resulting PCR product was transformed into the GT-W *Synechocystis* substrain (Bečková et al., submitted) and transformants were selected on a BG11 agar plate containing  $2 \mu\text{g ml}^{-1}$  Zeocin. Complete segregation was achieved by sequentially doubling the concentration of antibiotic to a final concentration of  $32 \mu\text{g ml}^{-1}$  Zeocin.

### Cell Absorption Spectra and Determination of Chl Content

Absorption spectra of whole cells were measured at room temperature using a Shimadzu UV-3000 spectrophotometer (Kyoto, Japan). To determine Chl levels, pigments were extracted from cell pellets (2 ml,  $\text{OD}_{750} = \sim 0.5$ ) with 100% methanol and the Chl concentration was determined spectroscopically (Porra et al., 1989).

### Analysis of Pigments by HPLC

Pigments were extracted from equal quantities of cells by the method described in Canniffe et al. (2013) and separated on a Phenomenex Aqua C<sub>18</sub> reverse phase column (5  $\mu\text{M}$  particle size, 125 Å pore size, 250 mm  $\times$  4.6 mm) at a flow rate of 1 ml  $\text{min}^{-1}$ . 3-formyl-MgPME was purified on a Fortis Universil C<sub>18</sub> reverse phase column (5  $\mu\text{M}$  particle size, 125 Å pore size, 150 mm  $\times$  10 mm) at a flow rate of 3.5 ml  $\text{min}^{-1}$ . Reverse phase columns were run using a method modified from Sobotka et al. (2011). Solvents A and B were 350 mM ammonium acetate pH 6.9/30% methanol (v/v) and 100% methanol, respectively. Pigments were

eluted over a linear gradient of 65 to 75% buffer A over 35 min.

### Purification of 3-Formyl-MgPME for NMR Analysis

Pigments were extracted by phase partitioning from 6 L of  $\Delta ycf54$  culture grown to an  $OD_{750\text{ nm}}$  1.2. One volume of diethyl ether was added to two volumes of cell culture in a separation funnel and the diethyl ether phase containing 3-formyl-MgPME was separated from the cell culture. Pigments were extracted from the cell culture three times. The diethyl ether was removed by rotary evaporation and the extracted pigments were re-suspended in a small volume of HPLC grade methanol. After centrifugation at  $15,000 \times g$  for 10 min, 3-formyl-MgPME was purified by preparative HPLC. Ammonium acetate was removed from the HPLC purified 3-formyl-MgPME by solid-phase extraction on DSC-18 reverse-phase columns (Supelco). Solvents C, D, and E were  $QH_2O$ , 50% methanol (v/v) and 100% methanol, respectively. After equilibration of the column with 1.0 ml solvent D, the purified 3-formyl-MgPME, diluted 1/3 with  $QH_2O$ , was loaded and allowed to enter the column by gravity flow. The column was washed with 1 ml solvent C, then 1 ml solvent D to remove the ammonium acetate. The pigment was eluted into a glass vial with 300  $\mu$ l methanol. The purified pigment was completely dried in a vacuum centrifuge and stored at  $-20^\circ C$ .

### NMR Assignment of 3-Formyl-MgPME

The dried pigment from HPLC was re-suspended in 500  $\mu$ l methanol- $d_4$  (Sigma), centrifuged to remove any insoluble pigment, transferred to a 5 mm NMR tube and sealed. All NMR experiments were carried out on a Bruker Avance DRX 600 instrument equipped with a cryoprobe at an acquisition temperature of 298 K.

The one-dimensional selective Nuclear Overhauser Enhancement (NOE) experiments were recorded using a double pulsed field gradient spin echo selective NOE experiment (Stott et al., 1995) using an 80 ms  $180^\circ$  Gaussian pulse for the selective excitation and a 1 s mixing time, acquiring 1024 transients at each saturation frequency. The Total Correlation Spectroscopy (TOCSY) experiment was recorded using a 45 ms spin lock at a power of 8.3 kHz. Two carbon Heteronuclear Single Quantum Correlation (HSQC) experiments were recorded with carbon offsets of 60 and 140 ppm.

### 2D Electrophoresis, Immunodetection, and Protein Radiolabeling

Membrane and soluble protein fractions were isolated from 50 ml of cells at  $OD_{750\text{ nm}} \sim 0.4$  according to Dobáková et al. (2009) using buffer A (25 mM MES/NaOH, pH 6.5, 5 mM  $CaCl_2$ , 10 mM  $MgCl_2$ , 20% glycerol). Isolated membrane complexes (0.25 mg/ml Chl) were solubilized in buffer A containing 1% *n*-dodecyl- $\beta$ -D-maltoside.

To assess protein levels by immunodetection, the protein content of *Synechocystis* lysates was quantified spectroscopically (Kalb and Bernlohr, 1977), separated by SDS-PAGE (Novagen) and transferred to a nitrocellulose membrane. The membranes

were probed with specific primary antibodies and then with secondary antibodies conjugated to horseradish peroxidase (Sigma). The primary antibodies used in this study were raised in rabbits as described in Hollingshead et al. (2012), with the exception of CHL27 (anti-CycI), which was purchased from Agrisera (Sweden).

Two-dimensional clear-native electrophoresis was performed essentially as described in Kopečná et al. (2013). Proteins separated in the gel were stained either by Coomassie Blue, or Sypro Orange, followed by transfer onto a PVDF membrane. Membranes were incubated with specific primary antibodies, and then with a secondary antibody conjugated with horseradish peroxidase (Sigma).

Radioactive pulse labeling of the proteins in cells was performed using a mixture of [ $^{35}S$ ]Met and [ $^{35}S$ ]Cys (Translabel; MP Biochemicals). After 30 min incubation of cells with labeled amino-acids, the solubilized membranes isolated from radiolabelled cells were separated by 2D-electrophoresis. The stained 2D gel was finally exposed to a phosphor-imager plate, which was scanned by Storm (GE Healthcare) to visualize labeled protein spots.

### Relative Quantification of FLAG-CycI and Captured Proteins in Pulldown Assays

Pulldown assays using N-terminal FLAG-tagged CycI as bait, with both wild-type (WT) and  $\Delta ycf54$  backgrounds, were carried out according to Hollingshead et al. (2012). FLAG eluates were concentrated to 100  $\mu$ l using Amicon Ultra 0.5 ml 3 kDa MWCO ultrafiltration devices (Millipore). The proteins were then precipitated, reduced and S-alkylated according to Zhang et al. (2015). Proteolytic digestion was carried out with 1:25 w/w (enzyme:substrate) pre-mixed trypsin/Lys-C (1  $\mu$ g/ $\mu$ L, Promega, mass spectrometry grade) at  $37^\circ C$  for 2 h. The samples were then diluted with 75  $\mu$ l 100 mM Tris-HCl, pH 8.5, 10 mM  $CaCl_2$  and the digestion allowed to proceed for a further 18 h at  $37^\circ C$ . After the addition of 5  $\mu$ l 10% TFA, the samples were desalted using  $C_{18}$  spin columns (Thermo Fisher) and analyzed by nano-flow liquid chromatography (Ultimate 3000 RSLCnano system, Dionex) coupled to a mass spectrometer (Maxis UHR-TOF, Bruker or Q Exactive HF Orbitrap, Thermo Scientific). For Maxis data, mass spectra were internally calibrated with the lock-mass ion at  $m/z$  1221.9906 then converted to MGF format using a script provided by Bruker. Q Exactive data-files were converted to MGFs using MSConvert<sup>1</sup>. Protein identification was carried out by searching against the *Synechocystis* PCC 6803 proteome database (release date 02-08-2015, 3507 entries<sup>2</sup> using Mascot Daemon v. 2.5.1 running with Mascot Server v. 2.5 (Matrix Science), specifying trypsin as the enzyme in the search parameters and allowing for one missed cleavage. S-carbamidomethyl-cysteine and methionine oxidation were selected as fixed and variable modifications, respectively. MS and MS/MS tolerances were set to 0.01 Da and false discovery rates determined by searching of a decoy database composed of reversed protein sequences. The data-files and search results have

<sup>1</sup>www.proteowizard.sourceforge.net

<sup>2</sup>www.uniprot.org/proteomes/UP000001425

been uploaded to the ProteomeXchange Consortium<sup>3</sup> via the PRIDE partner repository (identifier DOI 10.6019/PXD003149).

## Electron Microscopy

Wild-type and  $\Delta ycf54$  cells were harvested in the log phase by centrifugation. Cell pellets were loaded into 200  $\mu\text{m}$  deep specimen carriers (Leica Microsystems), pre-treated with 1% lecithin in chloroform and cryo-immobilized by high-pressure freezing using EM PACT2 (Leica Microsystems). Freeze-substitution was carried out as described by van de Meene et al. (2006) using an automatic freeze substitution unit (EM ASF, Leica). Samples were then infiltrated with graded series (1:2, 1:1, 2:1) of Spurr-acetone mixture (6–8 h for each), twice with 100% Spurr's resin (SPI Supplies) and finally embedded in fresh resin. The polymerization was performed at 60°C for 48 h. Ultra-thin 70 nm sections were cut on ultramicrotome (UCT, Leica), collected on formvar-coated copper grids and stained with uranyl acetate (5 min) and lead citrate (3 min). Grids were viewed with a JEOL 1010 transmission electron microscope operating at 80 kV equipped with a Mega View III camera (SIS GmbH).

## RESULTS

### Ycf54 Is Not Essential for Activity of MgPME Cyclase

In our previous report (Hollingshead et al., 2012) we described a  $ycf54^-$  *Synechocystis* strain harboring an insertion of the Erythromycin resistance cassette in the *ycf54* gene. Although prolonged attempts to fully segregate the mutant allele into all copies of the chromosome were unsuccessful, the phenotype of the partially segregated strain was informative nevertheless, and it exhibited an obvious defect in PChlide formation. However, the capability of *Synechocystis* cells to tolerate deletions of important genes also depends on the 'WT' substrain used. For instance, a previous attempt to inactivate *gun4*, another gene crucial for Chl biosynthesis, was achieved in the non-motile *Synechocystis* GT-P substrain but it failed in the motile PCC-M (compare Wilde et al., 2004; Sobotka et al., 2008). Thus, in order to obtain a fully segregated *ycf54* mutant, we prepared a new construct for replacement of the *ycf54* gene and transformed GT-P, GT-S, GT-W and PCC-M substrains; the GT-P substrain has been used in our previous work (Hollingshead et al., 2012). Interestingly, the *ycf54* deletion readily segregated in the GT-W substrain (Figure 1A) under low light (5  $\mu\text{mol photons.m}^{-2}.\text{s}^{-1}$ ) and photomixotrophic conditions; all attempts to segregate the *ycf54* deletion in other substrains failed (not shown). For the purposes of the work reported here the GT-W substrain is designated as the WT; a detailed analysis of GT-P and GT-W including genome sequencing is presented elsewhere in this issue (Bečková et al., submitted).

The fully segregated  $\Delta ycf54$  strain did not grow photoautotrophically, although supplementation of the growth medium with glucose made photomixotrophic growth possible at

light intensities up to 100  $\mu\text{mol photons.m}^{-2}.\text{s}^{-1}$ . Examination of the absorption spectra from cells normalized for optical density at 750 nm ( $OD_{750}$ ), shows that the Chl absorbance maxima at 439 and 679 nm and the carotenoid absorbance maximum at 494 nm are severely depleted in  $\Delta ycf54$ , whilst the absorbance maximum of the phycobiliproteins at 624 nm remains unchanged when compared to the WT (Figure 1B). Mutant cells contained only about 13% of WT Chl (Figure 1B) and the whole cell spectrum showed a large absorbance peak at 422 nm, indicating a substantial accumulation of MgPME (Figure 1B) (Hollingshead et al., 2012).

### Identification of the Chl Precursors that Accumulate in the $\Delta ycf54$ Mutant

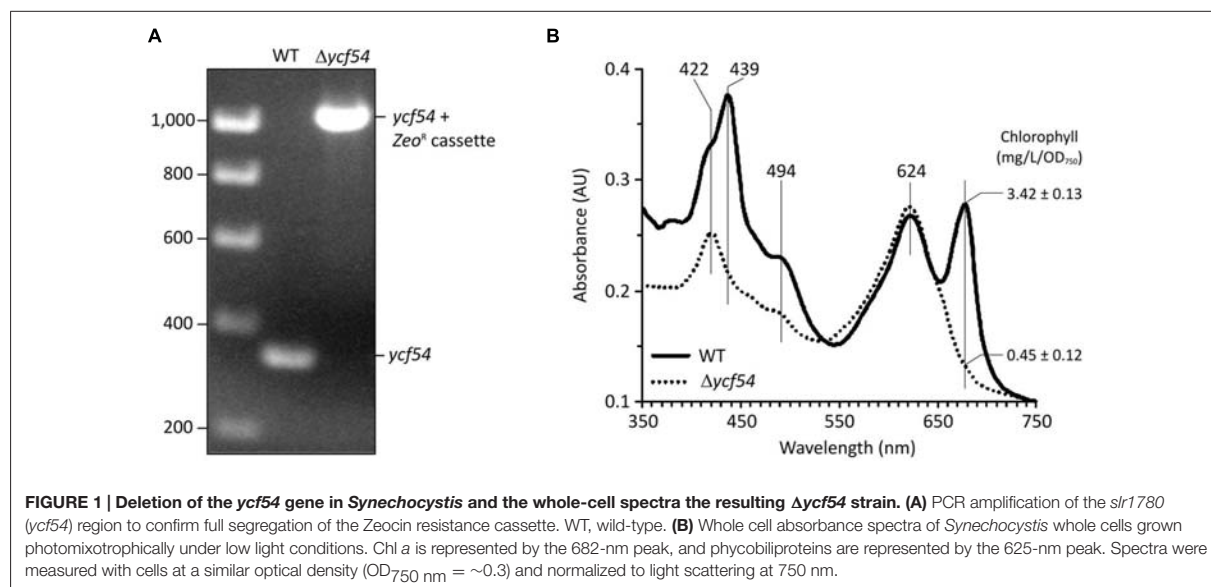
Previously we reported that Chl biosynthesis in a partially segregated  $ycf54^-$  mutant was blocked at the MgPME cyclase step, which causes accumulation of high levels of MgPME, the substrate of the cyclase, and lesser levels of an unknown pigment with a Soret peak at 433 nm (Hollingshead et al., 2012). To examine the photosynthetic precursor pigments present in  $\Delta ycf54$ , methanol extracts from low light grown cells were separated by HPLC (Figure 2A). As with  $ycf54^-$ ,  $\Delta ycf54$  synthesized high levels of MgPME and lesser levels of the unknown pigment. Given that the Soret band of this pigment is situated between the Soret peaks of MgPME at 416 nm and PChlide at 440 nm (Figure 2B) we proposed that it could be an intermediate of the cyclase reaction.

Nuclear magnetic resonance spectroscopy was used to determine the identity and structure of this unknown pigment, which was extracted by diethyl ether/water phase partitioning from the medium of  $\Delta ycf54$  cells grown under very low light conditions. This pigment was purified to homogeneity by preparative HPLC. The one-dimensional  $^1\text{H}$  spectrum (Figure 3A) shows the reasonable degree of purity of the pigment, with impurities indicated by an asterisk; the signals downfield of 5 ppm represent minor contaminants and methanol, whilst the impurity signals upfield of 5 ppm represent solvents, including water. Signals from the unknown pigment were assigned using a combination of  $^1\text{H}$  TOCSY, gradient-selected 1D NOE, and natural abundance  $^{13}\text{C}$  HSQC spectra.

NOE experiments were carried out with selective saturation of all proton peaks downfield from 3 ppm in order to identify protons with through-space correlation (Figure 3A). To cover the full range of  $^{13}\text{C}$  shifts, two  $^{13}\text{C}$  HSQC spectra were run with  $^{13}\text{C}$  offsets of 60 ppm and 140 ppm. Many of the signals have  $^1\text{H}$  and  $^{13}\text{C}$  chemical shifts similar in frequency to those from MgPME (Figure 3B), with the expected TOCSY and NOE connectivities, and can therefore be assigned straightforwardly. The  $^{13}\text{C}$  HSQC spectra (Figure 3C) confirmed the assignments of the four meso protons and the five methyl groups (with the four imidazole methyls having  $^{13}\text{C}$  shifts of around 10 ppm and the propionate methyl having a shift of 50 ppm). The signals from the 3-vinyl protons were absent, but there is a new signal with  $^1\text{H}$  and  $^{13}\text{C}$  shifts of 11.6 and 190 ppm, respectively, which can only come from an aldehyde. This

<sup>3</sup><http://proteomecentral.proteomexchange.org>





signal has NOEs to both the 5-meso and 2-methyl protons, both of which were shifted downfield, and no through-bond connectivity in the TOCSY, verifying that this was a 3-formyl group which had replaced the 3-vinyl group of the MgPME. The NMR data are compiled, together with details of the acquisition parameters, in Supplementary Table 1, including Supplementary Figures S1–S3. Further confirmation that this signal represents a 3-formyl group comes from the  $^1\text{H-NMR}$  spectra of Chl *d* (Fukumami et al., 2012), which has a clear signal at  $\sim 11.5$  assigned as the 3-formyl group. Thus, the unknown pigment is magnesium 3-formyl-protoporphyrin IX monomethyl ester (Figure 2D).

### Effects of Removal of Ycf54 on Other Chl Biosynthesis Enzymes

In order to investigate levels of Chl biosynthetic enzymes, and to verify the loss of Ycf54 in the  $\Delta ycf54$  mutant, lysates from WT and  $\Delta ycf54$  cells were fractionated into membrane and soluble components. The appearance of the cell lysate fractions (Figure 4A) reflects their pigment composition; the WT whole cell lysate and membrane fractions are green, and in  $\Delta ycf54$  whole cell lysate and membrane fractions are blue and orange, respectively, because of the near-absence of Chl. A western blot of each of these extracts was probed with antibodies raised against a wide range of Chl biosynthesis enzymes (Figure 4B). The immunoblot probed with the antibody to Ycf54 shows this protein is distributed evenly between the soluble and insoluble fractions and is not detected in  $\Delta ycf54$ , confirming the full segregation of this mutant. The absence of Ycf54 is also accompanied by a decrease in CycI and geranylgeranyl reductase (ChlP) and increased relative levels of the Mg-chelatase subunits ChII and ChID, although no change was detected in the levels of ChIH (Figure 4B).

Mass spectrometry was used to quantify the effects of *ycf54* deletion, in terms of the ability of CycI to associate with partner proteins *in vivo*. Pulldown assays with FLAG-tagged CycI are already known to retrieve Ycf54 from cell extracts (Hollingshead et al., 2012), so this experiment was repeated using FLAG-CycI in a  $\Delta ycf54$  background. The amounts of PChlide oxidoreductase (POR), 3,8-divinyl (proto)chlorophyllide reductase (DVR) and ChlP captured in pulldown assays by FLAG-CycI/WT and FLAG-CycI in  $\Delta ycf54$  were compared by mass spectrometry. Proteins extracted from FLAG eluates were digested with a combination of endoproteinase LysC and trypsin and the peptide fragments analyzed by nanoLC-MS/MS. The captured proteins were quantified relative to the CycI bait as shown in Figure 5. Captured POR levels had decreased significantly in the  $\Delta ycf54$  strain while DVR was reduced to an undetectable level. ChlP was only just detectable in one  $\Delta ycf54$  replicate and relative to CycI by three orders of magnitude in the other two.

### Lack of PChlide Impairs Synthesis of PsaA/B and Inner PSII Antennae but the Accumulation of Other Chl-Binding Proteins Is Not Affected

To evaluate the effects of greatly reduced Chl on the photosystems in  $\Delta ycf54$  compared to the WT, photosynthetic membranes isolated from an equal biomass were gently solubilized with  $\beta$ -DDM and the membrane complexes were resolved by clear native electrophoresis (CN-PAGE), followed by SDS-PAGE in the second dimension. The resulting 2D CN/SDS-PAGE (Figure 6A) showed that  $\Delta ycf54$  has drastically reduced levels of both photosystems, whilst the levels of other abundant membrane complexes such as ATP synthase, NADH:ubiquinone oxidoreductase and the cytochrome *b<sub>6</sub>f* complex (shown by the western blot) are comparable between the two strains.

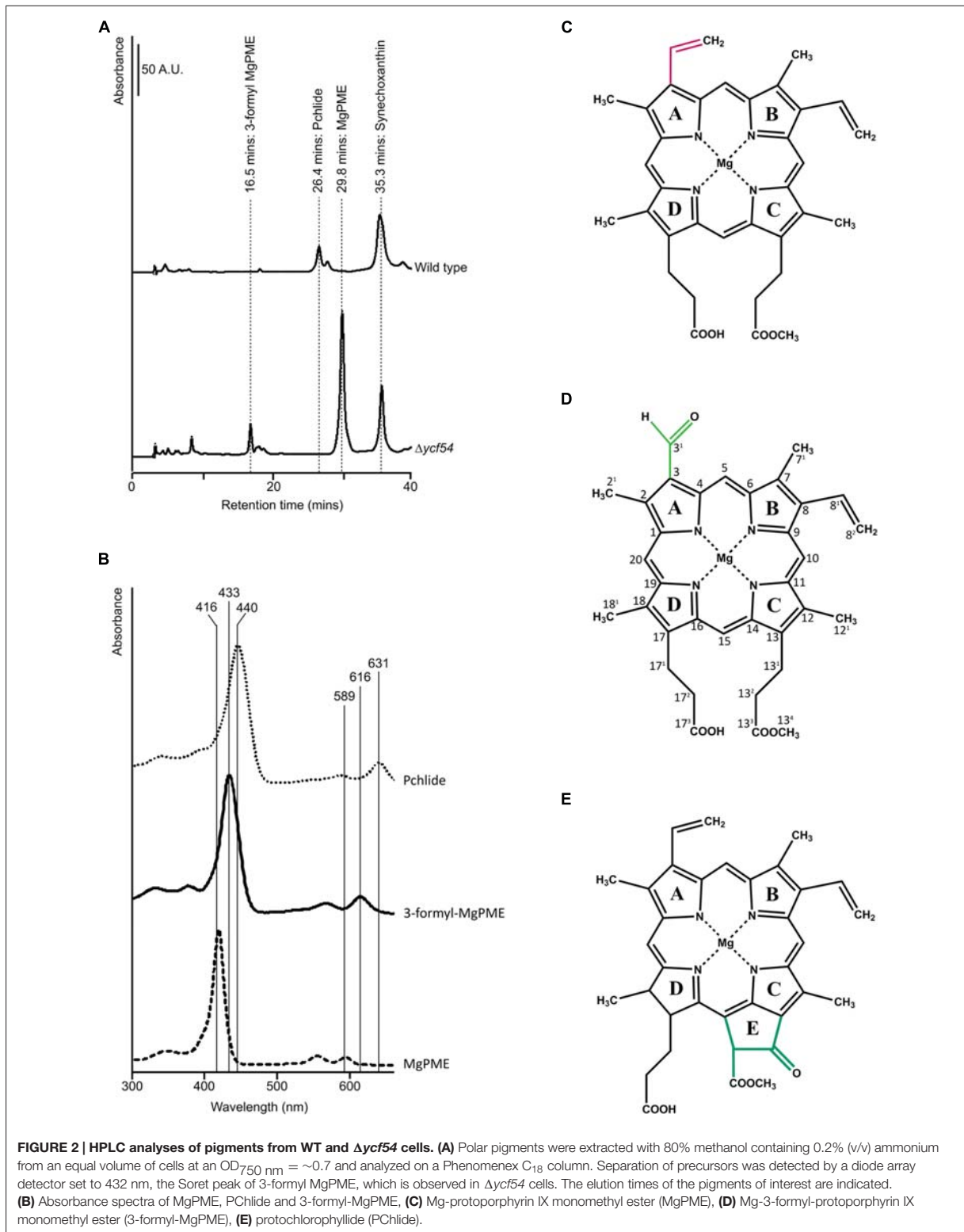
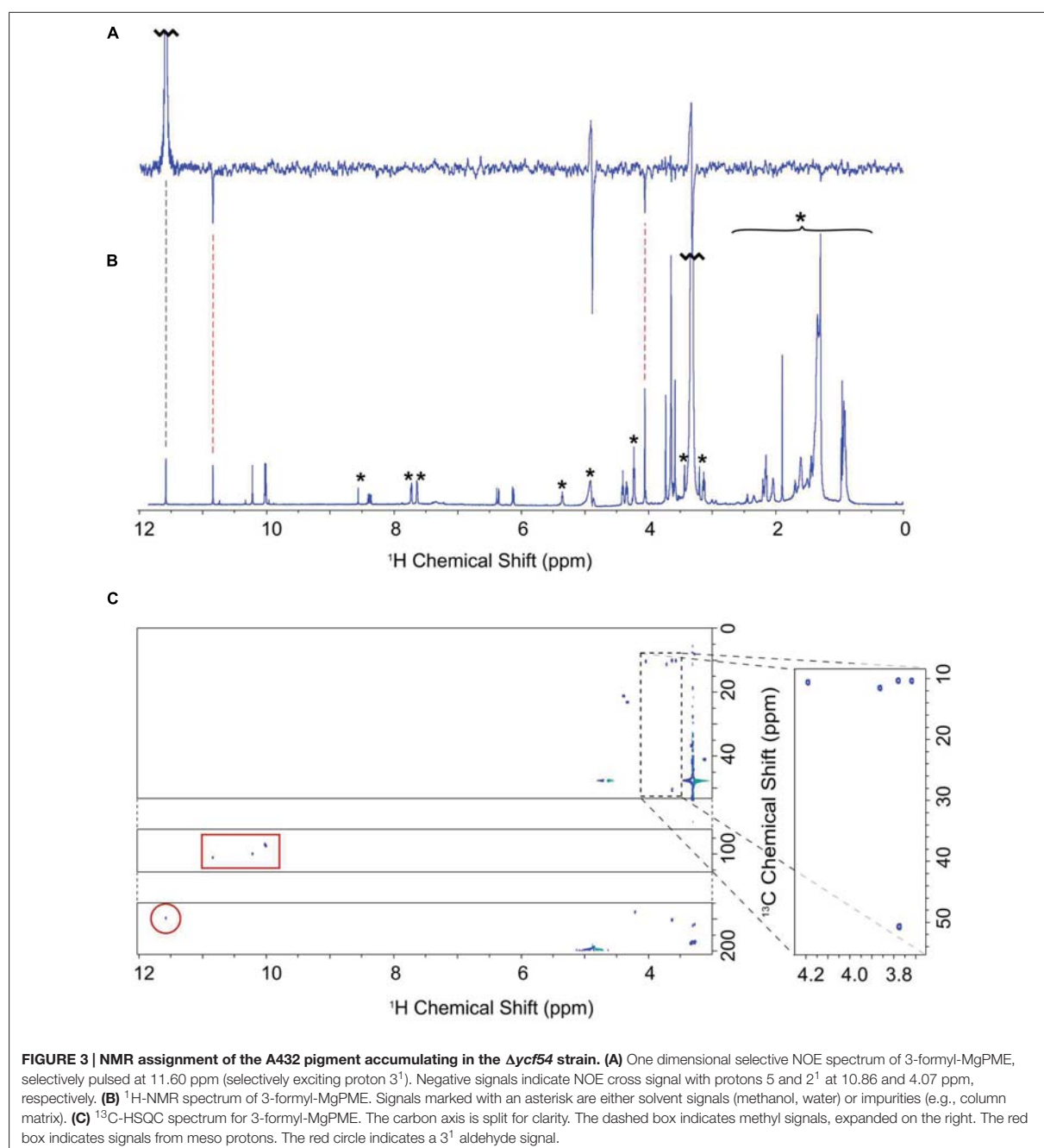


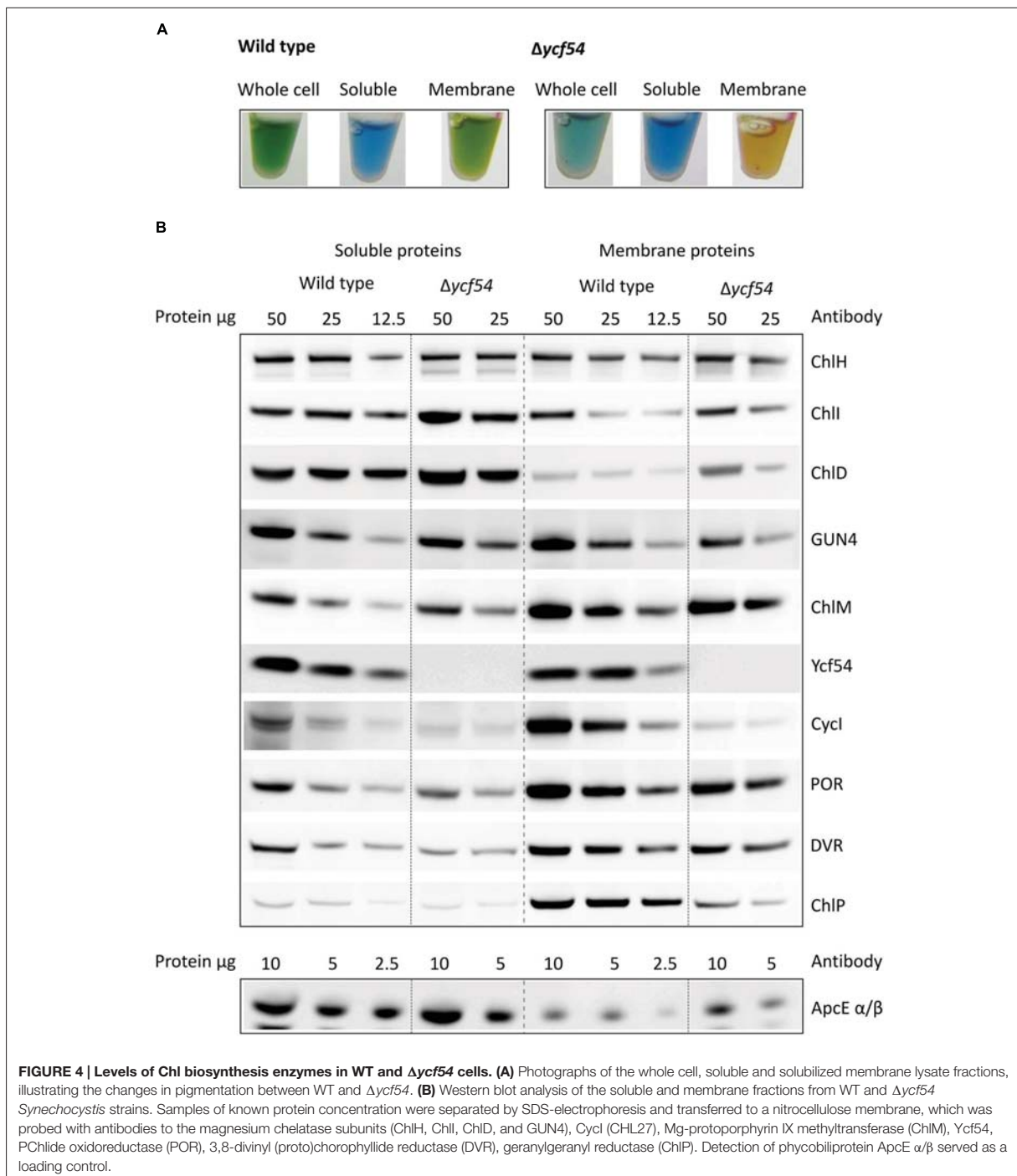
**FIGURE 2 | HPLC analyses of pigments from WT and  $\Delta ycf54$  cells. (A)** Polar pigments were extracted with 80% methanol containing 0.2% (v/v) ammonium from an equal volume of cells at an  $OD_{750\text{ nm}} = \sim 0.7$  and analyzed on a Phenomenex C<sub>18</sub> column. Separation of precursors was detected by a diode array detector set to 432 nm, the Soret peak of 3-formyl MgPME, which is observed in  $\Delta ycf54$  cells. The elution times of the pigments of interest are indicated. **(B)** Absorbance spectra of MgPME, Pchlide and 3-formyl-MgPME, **(C)** Mg-protoporphyrin IX monomethyl ester (MgPME), **(D)** Mg-3-formyl-protoporphyrin IX monomethyl ester (3-formyl-MgPME), **(E)** protochlorophyllide (Pchlide).





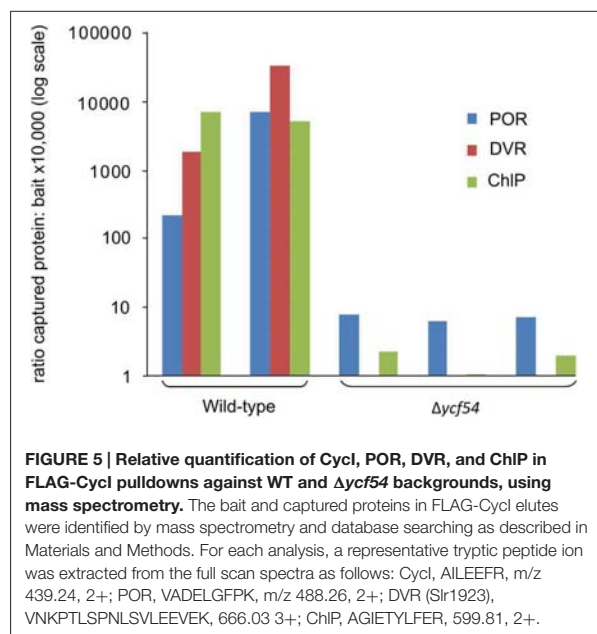
Interestingly, although the fully assembled PSII complexes in the mutant were barely detectable, this strain still accumulated relatively high levels of unassembled CP43 (**Figure 6A**). This observation suggests a block in formation of the early PSII assembly intermediates, which precedes attachment of the CP43 module and finalization of PSII reaction center core assembly (Komenda et al., 2004).

PSII assembly occurs in a stepwise fashion from four preassembled modules. These consist of one large Chl binding subunit (D1, D2, CP47, or CP43) in addition to several low molecular mass membrane polypeptides, bound pigments and other co-factors (Komenda et al., 2012). Assembly is initiated via the association of D1 and D2 to form the intermediate complex RCII\* Knoppová et al. (2014), next the CP47 assembly



module is attached, forming RC47, and finally mature PSII is formed by addition of the CP43 module (Boehm et al., 2011, 2012), attachment of the luminal extrinsic proteins, and light-driven assembly of the oxygen-evolving  $Mn_4CaO_5$

complex (Komenda et al., 2008; Nixon et al., 2010). To further investigate the perturbations in PSII assembly, the levels of individual PSII assembly sub-complexes were ascertained by 2D gel electrophoresis and immunodetection (Figure 6B). To assess



accumulation of the RCII\* complex, the immunoblot was probed with antibodies raised against the RCII\* components D1, Ycf39, and HliD (Knoppová et al. (2014). **Figure 6B** shows that the level of RCII\* is unaffected by the large reduction in cellular Chl levels in the  $\Delta ycf54$  mutant. Next, we investigated if PSII maturation was blocked at CP47 attachment and formation of RC47, by probing the blots with antibodies raised against HliA, a specific component of the CP47 assembly module (Promnares et al., 2006). We found that HliA, and hence the CP47 assembly module, was readily detectable in WT, but could not be detected in  $\Delta ycf54$  (**Figure 6B**), indicating that low Chl abundance in  $\Delta ycf54$  is impairing accumulation of the CP47 assembly module.

Our FLAG-pulldown experiments show that the interactions between Cycl, POR, and DVR are significantly reduced in the  $\Delta ycf54$  strain (**Figure 5**), therefore we compared the co-migration of these enzymes on a 2D gel (**Figure 6C**). Evident in the WT is a putative high-mass complex of ~400 kDa (highlighted by the green box), which contains both Cycl and POR; this complex was not detectable in the mutant (**Figure 6C**). Interestingly, our 2D gel shows that levels of Chl synthase, ChlG, HliD, and Ycf39, components of a chlorophyll biosynthetic/membrane insertase assembly complex (Chidgey et al., 2014), are unaffected in the  $\Delta ycf54$  mutant (**Figure 6C**).

To understand the flux of photosystem biogenesis, we used  $^{35}\text{S}$  pulse radio-labeling coupled with 2D CN/SDS-PAGE (**Figure 7**; a Coomassie stained gel is provided as Supplementary Figure S4), to compare the levels of protein synthesis between the WT and  $\Delta ycf54$  mutant. As demonstrated in **Figure 7**, the ability of  $\Delta ycf54$  to synthesize the Chl-binding PSI subunits PsaA/B is limited and synthesis of CP47 and CP43 subunits is hardly detectable even though 3-times more  $\Delta ycf54$  protein was loaded onto the gel (See Supplementary Figure S4 for overexposed

signal of the CP47). In contrast, there were comparable levels of synthesis of the PSII reaction center core subunits D1 and D2 in the WT and  $\Delta ycf54$  strains. This observation, coupled with the data from our 2D-immunoblot (**Figure 6B**), shows that the D1 and D2 subunits are rapidly assembled into RCII\* in  $\Delta ycf54$ , but given the lack of assembled PSII complexes, these RCII\* are presumably rapidly degraded in the mutant. Interestingly, in the mutant the unassembled CP43 was still detectable on the stained gel, which contrasted to virtually zero level of unassembled CP47 (**Figures 6A,B** and 7; Supplementary Figure S4). This observation indicates that both synthesis and stability of the CP47 are impaired in the mutant, whereas the structurally similar CP43 antenna can still accumulate though the synthesis is also very weak (Supplementary Figure S4). Taken together, our data suggest that the depleted levels of *de novo* Chl in  $\Delta ycf54$  specifically hinder the synthesis of PSI and the inner antennae of the PSII. However, given different stability of CP47 and CP43, it is the lack of CP47 protein that blocks assembly of RC47 and thus PSII maturation, sensitizing the PSII assembly pathway to the availability of *de novo* Chl.

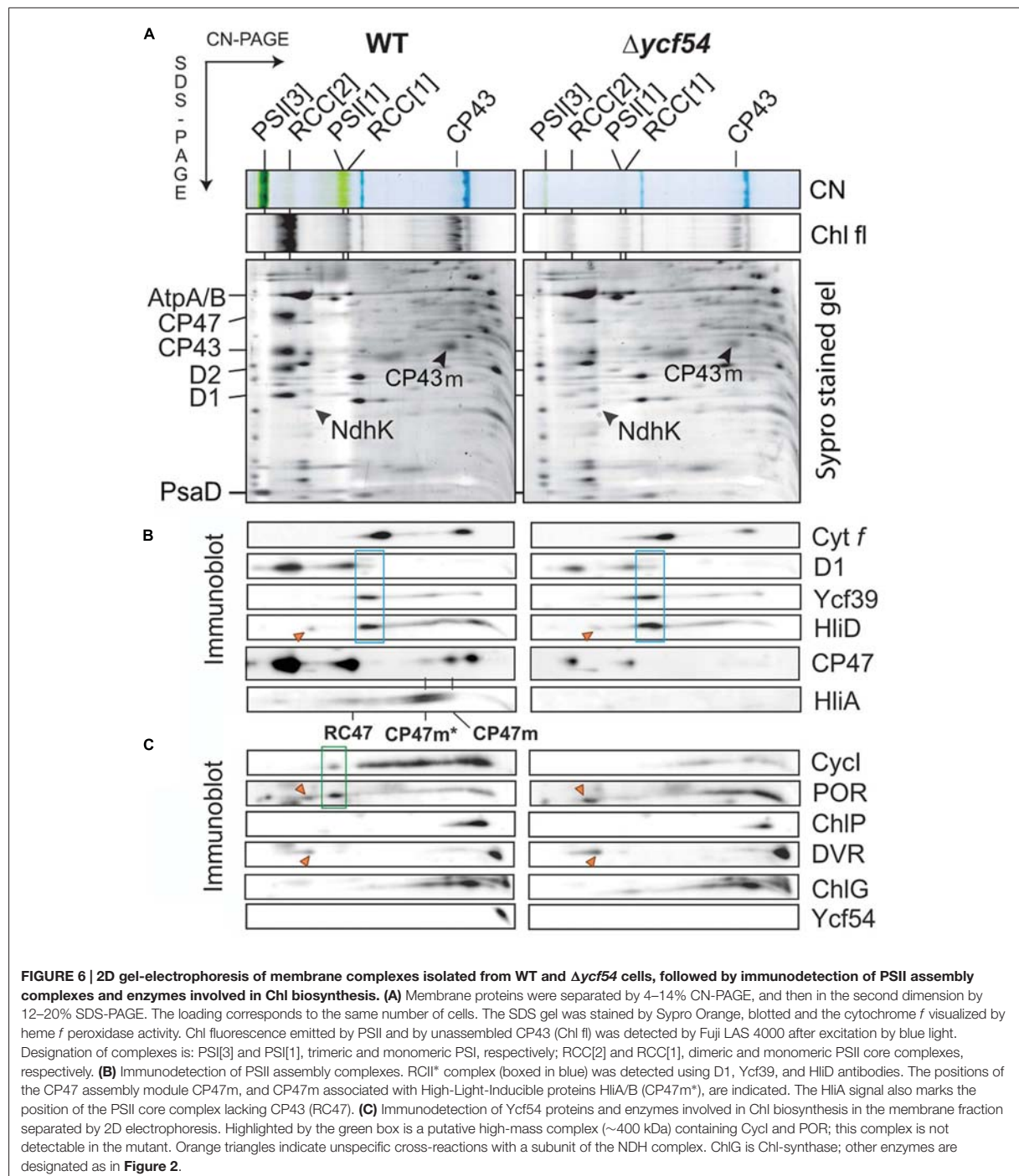
### Lack of *De Novo* Chl Affects Ultrastructure of $\Delta ycf54$ Cells

In order to investigate the effects of removal of 87% of the cellular Chl on the ultrastructure of  $\Delta ycf54$  cells, electron microscopy of negatively stained thin cell sections was performed. Electron micrographs are shown in **Figure 8**. In the WT the thylakoids are observed as parallel stacks of two to five membranes that closely follow the contour of the cell membrane (**Figures 8A–C**), but no such organized thylakoid membranes are visible in micrographs of the  $\Delta ycf54$  mutant (**Figures 8B–D**). Instead, membrane-like structures are dispersed throughout the cytoplasm of the cell. These results suggest key role of photosystems in the formation of the highly ordered thylakoid structures.

## DISCUSSION

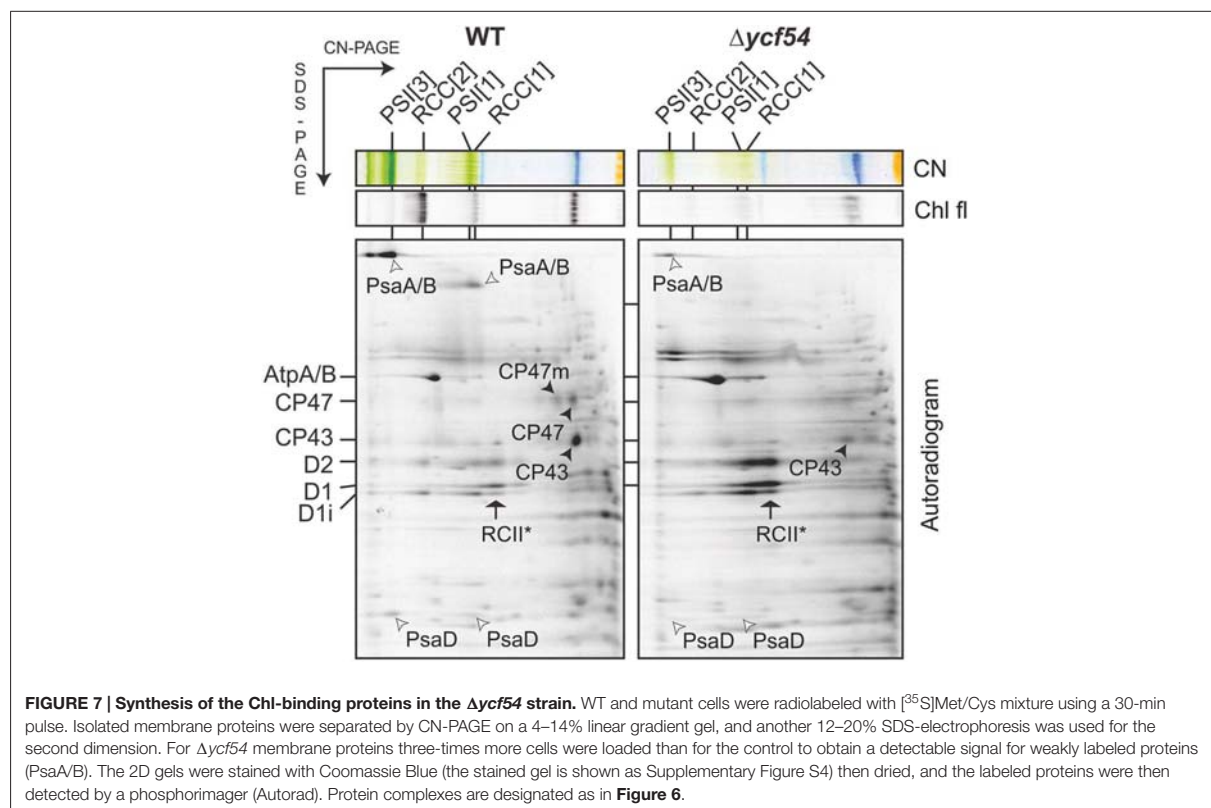
The MgPME-cyclase is the least understood component in the Chl biosynthetic pathway, and current knowledge of the individual components of the MgPME-cyclase had been limited to homologs of the *Rubrivivax gelatinosus* AcsF protein. Previous work identified two genes in *Synechocystis*, *sl1214*, and *sl1874*, as *acsF* homologs, which encode a membrane associated component of the MgPME-cyclase (Minamizaki et al., 2008; Peter et al., 2009). AcsF and its homologs contain a putative di-iron site and are thus viewed as the true catalytic subunit of the MgPME-cyclase (Tottey et al., 2003). The discovery of another gene, *ycf54*, that plays an important role in cyclase activity (Albus et al., 2012; Hollingshead et al., 2012) showed that other components are required, but so far it is not possible to assign a catalytic or assembly-related function to the Ycf54 protein. Further work on the role of Ycf54 required a fully segregated  $\Delta ycf54$  mutant, which is reported herein.

In our efforts to construct a fully segregated  $\Delta ycf54$  mutant, we discovered it was only possible to completely delete the *ycf54* gene in one specific substrain of *Synechocystis* (GT-W).



One possible explanation for this finding was elucidated by analysis of the GT-W genome, which contains a long (~100 kbp) chromosomal duplication that covers one hundred genes, including *cycl* (*sl1214*; Bečková et al., submitted). This

chromosomal duplication is not present in any of the other *Synechocystis* substrains for which a genome sequence is available (Kanesaki et al., 2012; Trautmann et al., 2012). Given the duplication of *cycl* in GT-W, it is likely that *cycl* expression is



increased in this strain. A very low level of CycI is a hallmark of the strains in which we partially or completely inactivated the *ycf54* gene. Thus, we hypothesize that the doubled expression of the *slI1214* gene coding for CycI may suppress the lethality of inactivating the *ycf54* gene. This hypothesis is in agreement with our observation that in the absence of Ycf54 the CycI cyclase component is destabilized (**Figures 4 and 5**) and the remaining CycI content is probably very close to a threshold essential for viability.

Analysis of the pigments that accumulate in the  $\Delta ycf54$  mutant could provide clues regarding the role of the Ycf54 protein, and a previous analysis showed that the partially segregated *ycf54* mutant accumulates MgPME, the substrate of the cyclase. In addition, there was an unknown pigment (**Figure 2**) that was suggested to be an intermediate in the cyclase reaction (Hollingshead et al., 2012), on the basis that the 433 nm Soret absorbance peak falls between the Soret peaks of the cyclase substrate MgPME (416 nm) and the PChlide product (440 nm). Similarly, early work with greening cucumber cotyledons had found pigments with emission maxima between 434 and 436 nm, proposed to be biosynthetic intermediates between MgPME and PChlide (Rebeiz et al., 1975). Identification of the unknown pigment as Mg-3-formyl-PME suggests that this pigment is not an intermediate in the cyclase reaction, as it is highly unlikely that this would produce a Chl pigment modified at the C3 position. Rather, Mg-3-formyl-PME bears a striking resemblance

to Chl *d*, the major light harvesting pigment found in the cyanobacterium *Acaryochloris marina* (Miyashita et al., 1996). The pathway and reaction mechanism of Chl *d* biosynthesis in *Acaryochloris marina* have not yet been elucidated but, based on the genome sequence, Chl *d* is thought to be derived from Chl *a* (Swingley et al., 2008). Previously, Chl *d* has been synthesized in low yields in aqueous acetone from Chl *a* by treatment with papain (Koizumi et al., 2005) and peroxide (Aoki et al., 2011) and in much higher yields from Chl *a* incubated with thiophenol and acetic acid in tetrahydrofuran (Fukusumi et al., 2012). Given the high accumulation of MgPME in  $\Delta ycf54$ , it is likely that reactive oxygen species, including peroxide, convert the MgPME 3-vinyl group, leading to the formation of Mg-3-formyl-PME.

The identification of Mg-3-formyl-PME as an oxidation product of the substrate rather than a catalytic intermediate is not consistent with a catalytic role for Ycf54 in the MgPME-cyclase complex. However, the hypothesis by Hollingshead et al. (2012) that Ycf54 plays a role in the assembly or stabilization of the catalytic MgPME-cyclase enzyme complex remains valid. By using FLAG-CycI as bait in pull-down assays, combined with quantitative MS analysis, we demonstrated that the absence of Ycf54 affects formation of a complex between CycI and enzymes further down the pathway (POR, DVR, and ChlP). In particular, the almost complete absence of DVR in the pull-down from the  $\Delta ycf54$  strain provides a strong evidence that Ycf54 facilitates formation of such a complex; in contrast to POR and ChlP the



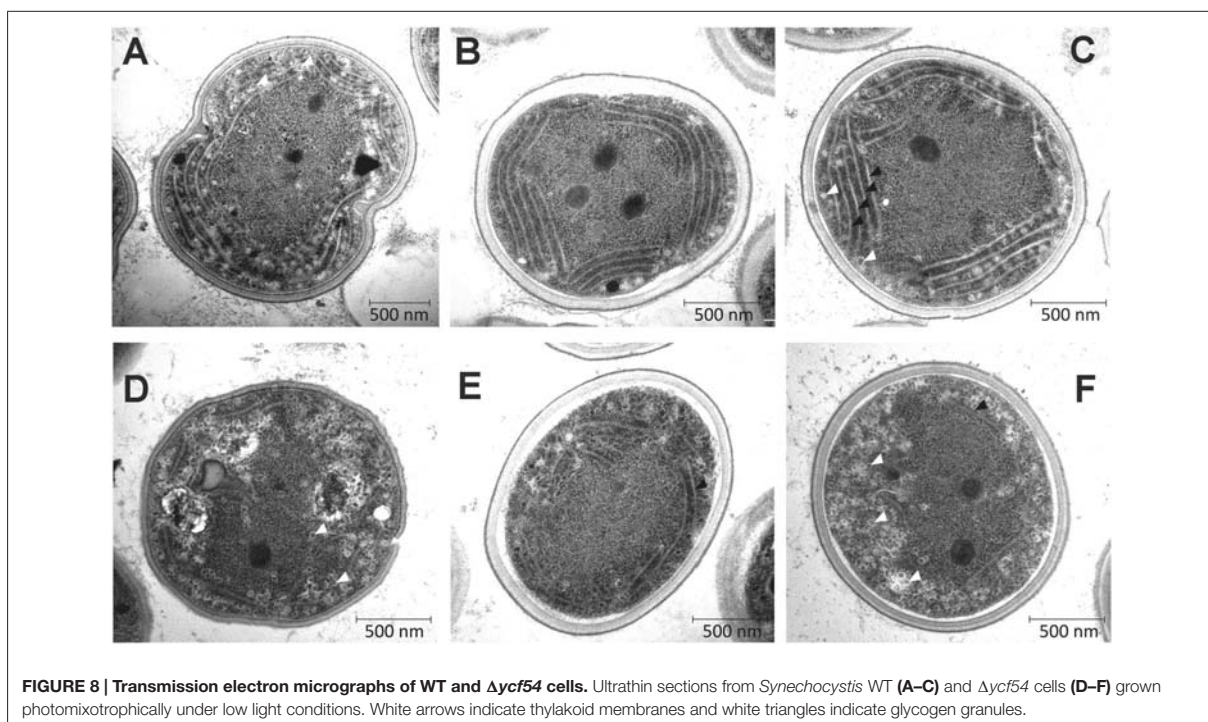


**FIGURE 8 | Transmission electron micrographs of WT and  $\Delta ycf54$  cells.** Ultrathin sections from *Synechocystis* WT (A–C) and  $\Delta ycf54$  cells (D–F) grown photomixotrophically under low light conditions. White arrows indicate thylakoid membranes and white triangles indicate glycogen granules.

stability of DVR in the mutant does not seem to be compromised and thus this result cannot be explained by a hypothetical fast degradation of this enzyme during pulldown assay. Indeed, the present data also provide evidence for an interaction between CycI and POR, DVR, and ChlP, which aligns well with data obtained by Kauss et al. (2012) who performed pulldown experiments with the *Arabidopsis* FLU protein. These analyses found that FLU forms a complex with CHL27, the *Arabidopsis* AcsF homolog, PORB, PORC, and ChlP. In *Synechocystis* at least, it appears that Ycf54 plays no direct catalytic role, and that it is important for the formation and maintenance of a Chl biosynthetic complex, with disruption of this complex possibly triggering degradation of CycI and consequently Chl deficiency. However, a wider role for Ycf54 in governing the whole pathway appears to be excluded by the lack of effect of the  $\Delta ycf54$  on components of the ChlG-HliD-Ycf39 complex that operates at the end of the pathway. This complex likely coordinates Chl delivery to the membrane-intrinsic apparatus for insertion and translocation of apoproteins of the photosynthetic apparatus (Chidgey et al., 2014). It is notable that although the CycI is almost exclusively associated with the membrane fraction under moderate light conditions Ycf54 is distributed equally between membrane and soluble fractions (Figure 4B). It is not known whether membrane-bound or soluble Ycf54 is critical for the CycI stability but there is a possibility that dissociation of Ycf54 from a membrane-bound assembly of CycI, POR, and DVR enzymes triggers degradation of CycI. Such a mechanism might regulate CycI activity at post-translational level and allow the cell to respond quickly to fluctuations in the environment.

Deletion of the *ycf54* gene generated a *Synechocystis* strain with very low levels of Chl, facilitating our studies on the cellular effects of a greatly lowered flux down the Chl biosynthetic pathway. It has long been known that photosystem biosynthesis requires Chl (Mullet et al., 1990; Eichacker et al., 1992; Müller and Eichacker, 1999), so we took advantage of the low Chl levels in the  $\Delta ycf54$  mutant to investigate the effects of Chl depletion on the synthesis and assembly of the photosystems. Although the levels of some Chl biosynthesis enzymes are altered in the  $\Delta ycf54$  mutant the ChlG-HliD-Ycf39 complex is unaffected, allowing the effects of reduced flux down the Chl pathway on Chl binding proteins to be investigated without disrupting ChlG-HliD-Ycf39 interactions with the YidC/Alb3 insertase and the consequent synthesis of nascent photosystem polypeptides. In addition, we were able to investigate the accumulation of “minor” Chl binding proteins, including cytochrome *b<sub>6</sub>f* (Kurusu et al., 2003), the Hli proteins (Staleva et al., 2015) and the Chl-synthase complex (Chidgey et al., 2014). Our findings show that whilst the Chl binding proteins PsaA/B and CP47 are highly sensitive to cellular Chl levels, the accumulation of CP43 and “minor” Chl binding proteins, including cytochrome *b<sub>6</sub>f*, is robust under Chl limiting conditions.

PSI is the main sink for *de novo* Chl (Kopečná et al., 2013); our results (Figure 7) show that synthesis of the core PSI subunits PsaA/B is impaired in the absence of Ycf54, i.e., under *de novo* Chl limiting conditions, suggesting that *Synechocystis* is unable to recycle Chl molecules released from degraded complexes for the synthesis of new PSI complexes. In comparison, the dependence of PSII biogenesis on the availability of *de novo* Chl

modules appears to be more complex, as previous studies show Chl molecules are re-cycled during PSII synthesis and repair (Kopečná et al., 2013, 2015) via re-phytylation of chlorophyllide (Vavilin and Vermaas, 2007). The PSII complex assembles in a modular fashion, starting with the association of D1 and D2 assembly modules, to form the RCII\* complex. This is followed by attachment of a CP47 module, then a CP43 module, then the luminal extrinsic proteins and the oxygen-evolving Mn<sub>4</sub>CaO<sub>5</sub> complex (reviewed in Komenda et al., 2012). Despite the large decrease in cellular Chl levels in  $\Delta ycf54$ , all components of the RCII\* complex are synthesized in adequate amounts and assembled. We hypothesize that synthesis of the RCII\* complex is enabled by the continuous recycling of a relatively stable pool of Chl molecules made available during the RCII\* assembly/degradation cycle. Evidence that RCII\* contains Chl as well pheophytin, carotenoids and heme cofactors has been shown previously (Knoppová et al., 2014). We cannot exclude the possibility that in the  $\Delta ycf54$  mutant there is a pool of the RCII\* complex that lacks Chl. However, we did not observe any shift of electrophoretic mobility even for the <sup>35</sup>S labeled RCII\* that would indicate presence of a hypothetical Chl-less RCII\*. Furthermore,  $\Delta ycf54$  contains some functional PSII complexes, which requires that at least some RCII\* with cofactors has to be synthesized en route to the fully assembled PSII.

Our findings also show that CP43 can accumulate as an unassembled module in  $\Delta ycf54$  even though the synthesis is very limited (Figures 6A and 7). In contrast, CP47 seems to be unstable in  $\Delta ycf54$ , which suggests that CP47 is the *de novo* Chl sensitive component of PSII biogenesis. This observation is consistent with previous work on the accumulation of PSII subunits in  $\Delta por$  (Kopečná et al., 2013) and  $\Delta gun4$  (Sobotka et al., 2008) mutants, disrupted in the PChlide reduction and Mg-chelatase steps, respectively. As also seen for  $\Delta ycf54$ , the  $\Delta por$  and  $\Delta gun4$  strains accumulate the PSII core complex RCII\* and the PSII antenna CP43, but CP47 synthesis is not observed (Sobotka et al., 2008; Kopečná et al., 2013). It is not currently known why CP47 is more sensitive to the availability of *de novo* Chl than the similar CP43 subunit, although it has been recently observed that the newly synthesized CP43, but not CP47, subunit is attached to a PSI complex (Kopečná et al., 2015). We tentatively speculate that the situation in the mutant leads frequently to the synthesis of aberrant CP47 lacking one or more Chl molecules. The synthesis of CP43 might be less error-prone because Chl molecules bound to the periphery of PSI could be used for the assembly of this complex.

## REFERENCES

- Albus, C. A., Salinas, A., Czarnecki, O., Kahlau, S., Rothbart, M., Thiele, W., et al. (2012). LCAA, a novel factor required for magnesium protoporphyrin monomethylester cyclase accumulation and feedback control of aminolevulinic acid biosynthesis in Tobacco. *Plant Physiol.* 160, 1923–1939. doi: 10.1104/pp.112.206045
- Aoki, K., Itoh, S., Furukawa, H., Nakazato, M., Iwamoto, K., Shiraiwa, Y., et al. (2011). “Enzymatic and non-enzymatic conversion of Chl a to Chl d,” in *Proceedings of the 5th Asia and Oceania Conference on Photobiology*, Nara.
- Boehm, M., Romero, E., Reisinger, V., Yu, J., Komenda, J., Eichacker, L. A., et al. (2011). Investigating the early stages of Photosystem II assembly in

In summary, the role of Ycf54 in the MgPME-cyclase complex has been elucidated further. This work shows that whilst Ycf54 is required for stabilization of Cyc1, the known catalytic component of the MgPME-cyclase, the protein itself is unlikely to play a key catalytic role in the formation of the fifth isocyclic ring. Furthermore, Ycf54 does not appear to be directly implicated in Chl phytylation or Chl insertion into proteins. The construction of a  $\Delta ycf54$  mutant has provided a useful tool to investigate the effects of reduced *de novo* Chl on the biosynthesis of cyanobacterial Chl binding proteins, highlighting the differing requirements for Chl exhibited by proteins within the PSI and PSII light harvesting complexes that bind this pigment. Insights into the catalytic cycle of the MgPME-cyclase remain elusive and further work is required to determine the exact molecular mechanisms of this enzyme.

## AUTHOR CONTRIBUTIONS

SH, JK, DA, LB, PJ, and GC performed the research; MD, MW, RS, and CNH designed the experiments, and SH, DA, PJ, MD, MW, RS, and CNH wrote the paper.

## ACKNOWLEDGMENTS

SH, PJ, CNH, and MD gratefully acknowledge financial support from the Biotechnology and Biological Sciences Research Council (BBSRC UK), award numbers BB/G021546/1 and BB/M000265/1. MD acknowledges support from the Biotechnology and Biological Sciences Research Council (UK; BB/M012166/1). CNH was also supported by Advanced Award 338895 from the European Research Council. SH was supported by a doctoral studentship from the University of Sheffield. GC and DA were supported by a BBSRC doctoral studentship. JK, LB, and RS were supported by project 14-13967S of the Czech Science Foundation, and by the National Programme of Sustainability I (LO1416).

## SUPPLEMENTARY MATERIAL

The Supplementary Material for this article can be found online at: <http://journal.frontiersin.org/article/10.3389/fpls.2016.00292>

*Synechocystis* sp PCC 6803: isolation of CP47 and CP43 complexes. *J. Biol. Chem.* 286, 14812–14819. doi: 10.1074/jbc.M110.207944

- Boehm, M., Yu, J., Reisinger, V., Bečková, M., Eichacker, L. A., Schlodder, E., et al. (2012). Subunit composition of CP43-less photosystem II complexes of *Synechocystis* sp PCC 6803: implications for the assembly and repair of photosystem II. *Philos. Trans. R. Soc. B Biol. Sci.* 367, 3444–3454. doi: 10.1098/rstb.2012.0066
- Boldareva-Nuianzina, E. N., Bláhová, Z., Sobotka, R., and Koblížek, M. (2013). Distribution and origin of oxygen-dependent and oxygen-independent forms of Mg-protoporphyrin monomethylester cyclase among phototrophic *proteobacteria*. *Appl. Environ. Microbiol.* 79, 2596–2604. doi: 10.1128/AEM.00104-13

- Bollivar, D., Braumann, I., Berendt, K., Gough, S. P., and Hansson, M. (2014). The Ycf54 protein is part of the membrane component of Mg-protoporphyrin IX monomethyl ester cyclase from barley (*Hordeum vulgare* L.). *FEBS J.* 281, 2377–2386. doi: 10.1111/febs.12790
- Canniffe, D. P., Jackson, P. J., Hollingshead, S., Dickman, M. J., and Hunter, C. N. (2013). Identification of an 8-vinyl reductase involved in bacteriochlorophyll biosynthesis in *Rhodobacter sphaeroides* and evidence for the existence of a third distinct class of the enzyme. *Biochem. J.* 450, 397–405. doi: 10.1042/BJ20121723
- Chidgey, J. W., Linhartová, M., Komenda, J., Jackson, P. J., Dickman, M. J., Canniffe, D. P., et al. (2014). A cyanobacterial chlorophyll synthase-HliD complex associates with the Ycf39 protein and the YidC/Alb3 insertase. *Plant Cell* 26, 1267–1279. doi: 10.1105/tpc.114.124495
- Chua, N. H., Blobel, G., Siekevitz, P., and Palade, G. E. (1976). Periodic variations in the ratio of free to thylakoid-bound chloroplast ribosomes during the cell cycle of *Chlamydomonas reinhardtii*. *J. Cell Biol.* 71, 497–514. doi: 10.1083/jcb.71.2.497
- Dobáková, M., Sobotka, R., Tichý, M., and Komenda, J. (2009). Psb28 protein is involved in the biogenesis of the photosystem II inner antenna CP47 (PsbB) in the cyanobacterium *Synechocystis* sp. PCC 6803. *Plant Physiol.* 149, 1076–1086. doi: 10.1104/pp.108.130039
- Eichacker, L., Paulsen, H., and Rüdiger, W. (1992). Synthesis of chlorophyll a regulates translation of chlorophyll a apoproteins P700, CP47, CP43 and D2 in barley etioplasts. *Eur. J. Biochem.* 205, 17–24. doi: 10.1111/j.1432-1033.1992.tb16747.x
- Eichacker, L. A., Helfrich, M., Rüdiger, W., and Müller, B. (1996). Stabilization of chlorophyll a-binding apoproteins P700, CP47, CP43, D2, and D1 by chlorophyll a or Zn-pheophytin a. *J. Biol. Chem.* 271, 32174–32179. doi: 10.1074/jbc.271.50.32174
- Fukumami, T., Matsuda, K., Mizoguchi, T., Miyatake, T., Ito, S., Ikeda, T., et al. (2012). Non-enzymatic conversion of chlorophyll-a into chlorophyll-d in vitro: a model oxidation pathway for chlorophyll-d biosynthesis. *FEBS Lett.* 586, 2338–2341. doi: 10.1016/j.febslet.2012.05.036
- Hollingshead, S., Kopečná, J., Jackson, P. J., Canniffe, D. P., Davison, P. A., Dickman, M. J., et al. (2012). Conserved chloroplast open-reading frame ycf54 is required for activity of the magnesium protoporphyrin monomethylester oxidative cyclase in *Synechocystis* PCC 6803. *J. Biol. Chem.* 287, 27823–27833. doi: 10.1074/jbc.M112.352526
- Jordan, P., Fromme, P., Witt, H. T., Klukas, O., Saenger, W., and Krauss, N. (2001). Three-dimensional structure of cyanobacterial photosystem I at 2.5 Å resolution. *Nature* 411, 909–917. doi: 10.1038/35082000
- Kalb, V. F., and Bernlohr, R. W. (1977). A new spectrophotometric assay for protein in cell extracts. *Anal. Biochem.* 82, 362–371. doi: 10.1016/0003-2697(77)90173-7
- Kanesaki, Y., Shiwa, Y., Tajima, N., Suzuki, M., Watanabe, S., Sato, N., et al. (2012). Identification of substrain-specific mutations by massively parallel whole-genome resequencing of *Synechocystis* sp. PCC 6803. *DNA Res.* 19, 67–79. doi: 10.1093/dnares/dsr042
- Kauss, D., Bischof, S., Steiner, S., Apel, K., and Meskauskiene, R. (2012). FLU, a negative feedback regulator of tetrapyrrole biosynthesis, is physically linked to the final steps of the Mg<sup>2+</sup>-branch of this pathway. *FEBS Lett.* 586, 211–216. doi: 10.1016/j.febslet.2011.12.029
- Ke, S. H., and Madison, E. L. (1997). Rapid and efficient site-directed mutagenesis by single-tube 'megaprimer' PCR method. *Nucleic Acids Res.* 25, 3371–3372. doi: 10.1093/nar/25.16.3371
- Knoppová, J., Sobotka, R., Tichý, M., Yu, J., Konik, P., Halada, P., et al. (2014). Discovery of a chlorophyll binding protein complex involved in the early steps of photosystem II assembly in *Synechocystis*. *Plant Cell* 26, 1200–1212. doi: 10.1105/tpc.114.123919
- Koizumi, H., Itoh, Y., Hosoda, S., Akiyama, M., Hoshino, T., Shiraiwa, Y., et al. (2005). Serendipitous discovery of Chl d formation from Chl a with papain. *Sci. Technol. Adv. Mater.* 6, 551–557. doi: 10.1016/j.stam.2005.06.022
- Komenda, J., Nickelsen, J., Tichý, M., Prášil, O., Eichacker, L. A., and Nixon, P. J. (2008). The cyanobacterial homologue of HCF136/YCF48 is a component of an early photosystem II assembly complex and is important for both the efficient assembly and repair of photosystem II in *Synechocystis* sp. PCC 6803. *J. Biol. Chem.* 283, 22390–22399. doi: 10.1074/jbc.M801917200
- Komenda, J., Reisinger, V., Müller, B. C., Dobáková, M., Granvogl, B., and Eichacker, L. A. (2004). Accumulation of the D2 protein is a key regulatory step for assembly of the photosystem II reaction center complex in *Synechocystis* PCC 6803. *J. Biol. Chem.* 279, 48620–48629. doi: 10.1074/jbc.M405725200
- Komenda, J., Sobotka, R., and Nixon, P. J. (2012). Assembling and maintaining the Photosystem II complex in chloroplasts and cyanobacteria. *Curr. Opin. Plant Biol.* 15, 245–251. doi: 10.1016/j.pbi.2012.01.017
- Kopečná, J., Pilný, J., Krynická, V., Toměala, A., Kis, M., Gombos, Z., et al. (2015). Lack of phosphatidylglycerol inhibits chlorophyll biosynthesis at multiple sites and limits chlorophyllide reutilization in *Synechocystis* sp. Strain PCC 6803. *Plant Physiol.* 169, 1307–1317. doi: 10.1104/pp.15.01150
- Kopečná, J., Sobotka, R., and Komenda, J. (2013). Inhibition of chlorophyll biosynthesis at the protochlorophyllide reduction step results in the parallel depletion of Photosystem I and Photosystem II in the cyanobacterium *Synechocystis* PCC 6803. *Planta* 237, 497–508. doi: 10.1007/s00425-012-1761-4
- Kurisu, G., Zhang, H. M., Smith, J. L., and Cramer, W. A. (2003). Structure of the cytochrome b6f complex of oxygenic photosynthesis: tuning the cavity. *Science* 302, 1009–1014. doi: 10.1126/science.1090165
- Minamizaki, K., Mizoguchi, T., Goto, T., Tamiaki, H., and Fujita, Y. (2008). Identification of two homologous genes, chlAI and chlAII, that are differentially involved in isocyclic ring formation of chlorophyll a in the cyanobacterium *Synechocystis* sp. PCC 6803. *J. Biol. Chem.* 283, 2684–2692. doi: 10.1074/jbc.M708954200
- Miyashita, H., Ikemoto, H., Kurano, N., Adachi, K., Chihara, M., and Miyachi, S. (1996). Chlorophyll d as a major pigment. *Nature* 383, 402. doi: 10.1038/383402a0
- Müller, B., and Eichacker, L. A. (1999). Assembly of the D1 precursor in monomeric photosystem II reaction center precomplexes precedes chlorophyll a-triggered accumulation of reaction center II in barley etioplasts. *Plant Cell* 11, 2365–2377. doi: 10.2307/3870961
- Mullet, J. E., Klein, P. G., and Klein, R. R. (1990). Chlorophyll regulates accumulation of the plastid encoded chlorophyll apoprotein CP43 and apoprotein D1 by increasing apoprotein stability. *Proc. Natl. Acad. Sci. U.S.A.* 87, 4038–4042. doi: 10.1073/pnas.87.11.4038
- Nixon, P. J., Michoux, F., Yu, J., Boehm, M., and Komenda, J. (2010). Recent advances in understanding the assembly and repair of photosystem II. *Ann. Bot.* 106, 1–16. doi: 10.1093/aob/mcq059
- Peter, E., Salinas, A., Wallner, T., Jeske, D., Dienst, D., Wilde, A., et al. (2009). Differential requirement of two homologous proteins encoded by sll1214 and sll1874 for the reaction of Mg protoporphyrin monomethylester oxidative cyclase under aerobic and micro-oxic growth conditions. *Biochim. Biophys. Acta* 1787, 1458–1467. doi: 10.1016/j.bbabi.2009.06.006
- Pinta, V., Picaud, M., Reiss-Husson, F., and Astier, C. (2002). *Rubrivivax gelatinosus* acsF (previously orf358) codes for a conserved, putative binuclear-iron-cluster-containing protein involved in aerobic oxidative cyclization of Mg-protoporphyrin IX monomethylester. *J. Bacteriol.* 184, 746–753. doi: 10.1128/JB.184.3.746-753.2002
- Porra, R., Thompson, W., and Kriedemann, P. (1989). Determination of accurate extinction coefficients and simultaneous equations for assaying chlorophylls a and b extracted with four different solvents: verification of the concentration of chlorophyll standards by atomic absorption spectroscopy. *Biochim. Biophys. Acta* 975, 384–389. doi: 10.1016/S0005-2728(89)80347-0
- Porra, R. J., Schafer, W., Gadon, N., Katheder, I., Drews, G., and Scheer, H. (1996). Origin of the two carbonyl oxygens of bacteriochlorophyll alpha – Demonstration of two different pathways for the formation of ring E in *Rhodobacter sphaeroides* and *Roseobacter denitrificans*, and a common hydratase mechanism for 3-acetyl group formation. *Eur. J. Biochem.* 239, 85–92. doi: 10.1111/j.1432-1033.1996.0085u.x
- Promnare, K., Komenda, J., Bumba, L., Nebesarova, J., Vacha, F., and Tichý, M. (2006). Cyanobacterial small chlorophyll-binding protein ScpD (HliB) is located on the periphery of photosystem II in the vicinity of PsbH and CP47 subunits. *J. Biol. Chem.* 281, 32705–32713. doi: 10.1074/jbc.M606360200
- Rebeiz, C. A., Mattheis, J. R., Smith, B. B., Rebeiz, C., and Dayton, D. F. (1975). Chloroplast biogenesis. Biosynthesis and accumulation of Mg-protoporphyrin IX monoester and longer wavelength metalloporphyrins by greening cotyledons. *Arch. Biochem. Biophys.* 166, 446–465. doi: 10.1016/0003-9861(75)90408-7
- Rippka, R., Deruelles, J., Waterbury, J., Herdman, M., and Stanier, R. (1979). Generic assignments, strain histories and properties of pure cultures of cyanobacteria. *Microbiology* 111, 1–61. doi: 10.1099/00221287-111-1-1



- Sobotka, R., Duerhring, U., Komenda, J., Peter, E., Gardian, Z., Tichy, M., et al. (2008). Importance of the cyanobacterial GUN4 protein for chlorophyll metabolism and assembly of photosynthetic complexes. *J. Biol. Chem.* 283, 25794–25802. doi: 10.1074/jbc.M803787200
- Sobotka, R., Tichy, M., Wilde, A., and Hunter, C. N. (2011). Functional assignments for the carboxyl-terminal domains of the ferrochelatase from *Synechocystis* PCC 6803: the CAB domain plays a regulatory role, and region II is essential for catalysis. *Plant Physiol.* 155, 1735–1747. doi: 10.1104/pp.110.167528
- Staleva, H., Komenda, J., Shukla, M. K., Šlouf, V., Kaõa, R., Polívka, T., et al. (2015). Mechanism of photoprotection in the cyanobacterial ancestor of plant antenna proteins. *Nat. Chem. Biol.* 11, 287–291. doi: 10.1038/nchembio.1755
- Stott, K., Stonehouse, J., Keeler, J., Hwang, T., and Shaka, A. (1995). Excitation sculpting in high-resolution nuclear magnetic resonance spectroscopy: application to selective NOE experiments. *J. Am. Chem. Soc.* 117, 4199–4200. doi: 10.1021/ja00119a048
- Swingle, W. D., Chen, M., Cheung, P. C., Conrad, A. L., Dejesa, L. C., Hao, J., et al. (2008). Niche adaptation and genome expansion in the chlorophyll d-producing cyanobacterium *Acaryochloris marina*. *Proc. Natl. Acad. Sci. U.S.A.* 105, 2005–2010. doi: 10.1073/pnas.0709772105
- Totter, S., Block, M. A., Allen, M., Westergren, T., Albriex, C., Scheller, H. V., et al. (2003). *Arabidopsis* CHL27, located in both envelope and thylakoid membranes, is required for the synthesis of protochlorophyllide. *Proc. Natl. Acad. Sci. U.S.A.* 100, 16119–16124. doi: 10.1073/pnas.2136793100
- Trautmann, D., Voss, B., Wilde, A., Al-Babili, S., and Hess, W. R. (2012). Microevolution in cyanobacteria: re-sequencing a motile strain of *Synechocystis* sp. PCC 6803. *DNA Res.* 19, 435–448. doi: 10.1093/dnares/dss024
- Umena, Y., Kawakami, K., Shen, J. R., and Kamiya, N. (2011). Crystal structure of oxygen-evolving photosystem II at a resolution of 1.9 Å. *Nature* 473, 55–60. doi: 10.1038/nature09913
- van de Meene, A. M., Hohmann-Marriott, M. F., Vermaas, W. F., and Roberson, R. W. (2006). The three-dimensional structure of the cyanobacterium *Synechocystis* sp. PCC 6803. *Arch. Microbiol.* 184, 259–270.
- Vavilin, D., and Vermaas, W. (2007). Continuous chlorophyll degradation accompanied by chlorophyllide and phytol reutilization for chlorophyll synthesis in *Synechocystis* sp. PCC 6803. *Biochim. Biophys. Acta* 1767, 920–929. doi: 10.1016/j.bbabi.2007.03.010
- Wilde, A., Mikolajczyk, S., Alawady, A., Lokstein, H., and Grimm, B. (2004). The gun4 gene is essential for cyanobacterial porphyrin metabolism. *FEBS Lett.* 571, 119–123. doi: 10.1016/j.febslet.2004.06.063
- Zhang, H., Liu, H., Blankenship, R. E., and Gross, M. L. (2015). Isotope-encoded carboxyl group footprinting for mass spectrometry-based protein conformational studies. *J. Am. Soc. Mass Spectrom.* 27, 178–181. doi: 10.1007/s13361-015-1260-5
- Zouni, A., Witt, H. T., Kern, J., Fromme, P., Krauss, N., Saenger, W., et al. (2001). Crystal structure of photosystem II from *Synechococcus elongatus* at 3.8 Å resolution. *Nature* 409, 739–743. doi: 10.1038/35055589

**Conflict of Interest Statement:** The authors declare that the research was conducted in the absence of any commercial or financial relationships that could be construed as a potential conflict of interest.

Copyright © 2016 Hollingshead, Kopečná, Armstrong, Bučinská, Jackson, Chen, Dickman, Williamson, Sobotka and Hunter. This is an open-access article distributed under the terms of the Creative Commons Attribution License (CC BY). The use, distribution or reproduction in other forums is permitted, provided the original author(s) or licensor are credited and that the original publication in this journal is cited, in accordance with accepted academic practice. No use, distribution or reproduction is permitted which does not comply with these terms.

**9.3. Publication III:** The ribosome-bound protein Pam68 promotes insertion of chlorophyll into the CP47 subunit of Photosystem II.

**Bučinská L,** Kiss E, Koník P, Knoppová J, Komenda J and Sobotka R (2018).

*Plant Physiol.* 176 (4) 2931-2942.

# The Ribosome-Bound Protein Pam68 Promotes Insertion of Chlorophyll into the CP47 Subunit of Photosystem II<sup>1</sup>[OPEN]

Lenka Bučinská,<sup>a,b</sup> Éva Kiss,<sup>a</sup> Peter Koník,<sup>a,b</sup> Jana Knoppová,<sup>a</sup> Josef Komenda,<sup>a</sup> and Roman Sobotka<sup>a,b,2</sup>

<sup>a</sup>Laboratory of Photosynthesis, Centre Algatech, Institute of Microbiology, Academy of Sciences, 37981 Třeboň, Czech Republic

<sup>b</sup>Faculty of Science, University of South Bohemia, 37005 České Budějovice, Czech Republic

ORCID IDs: 0000-0001-8652-5323 (P.K.); 0000-0003-4588-0328 (J.K.); 0000-0002-6359-7604 (J.Kno.); 0000-0001-5909-3879 (R.S.).

Photosystem II (PSII) is a large enzyme complex embedded in the thylakoid membrane of oxygenic phototrophs. The biogenesis of PSII requires the assembly of more than 30 subunits, with the assistance of a number of auxiliary proteins. In plants and cyanobacteria, the photosynthesis-affected mutant 68 (Pam68) is important for PSII assembly. However, its mechanisms of action remain unknown. Using a *Synechocystis* PCC 6803 strain expressing Flag-tagged Pam68, we purified a large protein complex containing ribosomes, SecY translocase, and the chlorophyll-binding PSII inner antenna CP47. Using 2D gel electrophoresis, we identified a pigmented Pam68-CP47 subcomplex and found Pam68 bound to ribosomes. Our results show that Pam68 binds to ribosomes even in the absence of CP47 translation. Furthermore, Pam68 associates with CP47 at an early phase of its biogenesis and promotes the synthesis of this chlorophyll-binding polypeptide until the attachment of the small PSII subunit PsbH. Deletion of both Pam68 and PsbH nearly abolishes the synthesis of CP47, which can be restored by enhancing chlorophyll biosynthesis. These results strongly suggest that ribosome-bound Pam68 stabilizes membrane segments of CP47 and facilitates the insertion of chlorophyll molecules into the translated CP47 polypeptide chain.

Photosystem II (PSII) is a large protein-cofactor complex embedded in the thylakoid membranes of oxygenic phototrophs. The key large structural components of PSII are the chlorophyll (Chl)-binding proteins D1, D2, CP43, and CP47, subjoined with other small and extrinsic subunits (Umena et al., 2011). According to this model, PSII is assembled in a stepwise manner from four preassembled smaller subcomplexes called modules (Komenda et al., 2012). Each module consists of one large Chl-binding subunit (D1, D2, CP43, or CP47) and several low molecular mass membrane polypeptides. PSII assembly is initiated through the association of D1 and D2 modules to form an assembly intermediate, termed the Reaction Center II (RCII) complex. The CP47 assembly module (CP47m) is

then attached to RCII (Boehm et al., 2011), which results in a CP43-less core complex called “RC47” (Boehm et al., 2012). The active, oxygen-evolving PSII is completed by the addition of the CP43 module (Boehm et al., 2011) and attachment of the luminal extrinsic proteins (Nixon et al., 2010). Biogenesis of PSII is a highly complex process requiring many auxiliary proteins that are not present in the fully assembled complex. A number of these assembly factors have been described (Komenda et al., 2012; Heinz et al., 2016). However, their precise functions remain mostly unknown, and only a few of them have been connected with a specific assembly step (Knoppová et al., 2014; Bečková et al., 2017).

The fully assembled PSII contains 35 Chl molecules, most of them bound to the inner PSII antennas CP47 (16) and CP43 (14). According to this model, Chl molecules are integrated directly into synthesized CP47 and CP43, and the insertion of Chl appears to be a prerequisite for the correct folding and stability of these polypeptides (for review, see Sobotka, 2014). However, little is known about how Chl proteins are produced. PSII Chl-binding subunits are integral membrane proteins most likely cotranslationally inserted into the thylakoid membrane with the assistance of the protein translocation apparatus. This process usually includes the SecYEG translocon, which forms a protein-conducting channel, and an associated insertase/foldase YidC (Sachelar et al., 2013). Chl synthase is the last enzyme of Chl biosynthesis, and it was recently shown to physically interact with YidC insertase (Chidgey et al., 2014). This interaction suggests that Chl molecules are

<sup>1</sup> This work was supported by project 17-08755S of the Grant Agency of the Czech Republic and by the Czech Ministry of Education (projects CZ 1.05/2.1.00/19.0392 and LO1416).

<sup>2</sup> Address correspondence to sobotka@alga.cz.

The author responsible for distribution of materials integral to the findings presented in this article in accordance with the policy described in the Instructions for Authors ([www.plantphysiol.org](http://www.plantphysiol.org)) is: Roman Sobotka ([sobotka@alga.cz](mailto:sobotka@alga.cz)).

L.B. constructed the strains and employed most of the biochemical methods under the supervision of R.S.; P.K. performed protein identification by LC-MS/MS; J.K. and J.Kno were responsible for <sup>35</sup>S radiolabeling; E.K. performed various mutant characterizations; R.S., L.B., E.K., and J.K. designed the study and wrote the paper; R.S. supervised the whole study; and all authors discussed the results and commented on the manuscript.

[OPEN] Articles can be viewed without a subscription.

[www.plantphysiol.org/cgi/doi/10.1104/pp.18.00061](http://www.plantphysiol.org/cgi/doi/10.1104/pp.18.00061)

passed directly from Chl synthase to the nascent apo-protein chain in the vicinity of the translocon.

The small PSII subunit PsbH and two assembly factors, hypothetical chloroplast open reading frame 48 (Ycf48) and photosynthesis-affected mutant 68 (Pam68), were found to be important for the accumulation of CP47m (Komenda, 2005; Rengstl et al., 2013). Here, we identified the cyanobacterial Pam68 protein as a ribosomal factor that is in contact with the nascent CP47 in the vicinity of the SecY translocase. Our data suggest that Pam68 stabilizes membrane segments of CP47 during Chl insertion.

## RESULTS

### Pam68 Associates with the CP47 Protein at an Early Stage of PSII Biogenesis

To identify proteins interacting with Pam68, we constructed a *Synechocystis* sp. PCC 6803 strain (hereafter *Synechocystis*) expressing a Flag-tagged Pam68 derivative (Pam68.f protein). This protein was purified from solubilized membranes using an anti-Flag gel, and the obtained elution was analyzed by SDS-PAGE. The identities of prominent protein bands were determined by mass spectrometry (MS; Supplemental Fig. S1A). We identified CP47 and ribosomal subunits, which were missing in the control pull-down, as putative interactors (Supplemental Fig. S1A). Consistent with our previous reports, Photosystem I (PSI) subunits were the only substantial contaminants (Knoppová et al., 2014; Bečková et al., 2017). Furthermore, our control purification of the Flag-tagged ferrochelatase enzyme (FeCh) showed that the 3×Flag-tag does not bind ribosome subunits nonspecifically (Supplemental Fig. S1B).

Because membrane-bound ribosomes were present in the Pam68.f elution, we checked for the presence of SecY translocase and YidC insertase. Indeed, both these proteins coeluted with Pam68.f (Supplemental Fig. S1C). Additionally, our data support the interaction of the luminal Ycf48 protein with Pam68, as previously suggested (Rengstl et al., 2013). Moreover, CP47 was the only PSII subunit detected in the Pam68.f elution. Remarkably, the PsbH subunit was hardly detectable even by specific antibodies, despite a high level of CP47 protein in the elution. PsbH is a component of CP47m (Boehm et al., 2011); hence, the absence of PsbH in the Pam68.f pull-down indicates that the association of CP47 with Pam68 is an early event that occurs before the attachment of PsbH to CP47.

To elucidate whether Pam68.f physically interacts with unassembled CP47 in the absence of PsbH, we purified Pam68.f from the PsbH-less strain, and both elutions (Pam68.f and Pam68.f/ $\Delta$ PsbH) were analyzed by 2D Clear-Native/SDS-PAGE (CN/SDS-PAGE). On the stained gels, we identified large (50S) and small (30S) ribosome subunits and two fractions of Pam68.f comigrating with 50S and with CP47, respectively. The Pam68.f-CP47 complex exhibited Chl fluorescence, and its green pigmentation was visible on the CN gel (Fig. 1A).

In addition to the ribosome subunits, FtsH proteases, and a smeary band of SecY, the Pam68.f elutions also contained two unknown proteins (Sll1830 and Ssr0332). Whereas Sll1830 migrated as a free protein, the small Ssr0332 protein comigrated with the 50S ribosomal subunit. Another identified protein was light-repressed protein A (LrtA, Sll0947), which showed sequence similarity to the bacterial pY factor associated with stalled ribosomes (Galmozzi et al., 2016). A similar pattern of ribosomal proteins, but with higher levels of LrtA, was also obtained in the Pam68.f pull-down isolated from the  $\Delta$ psbB ( $\Delta$ CP47) mutant background (Supplemental Fig. S2). This result implies that Pam68 remains associated with a pool of membrane-bound ribosomes even when no CP47 translocation occurs in the cell. Notably, the electrophoretic mobility of Pam68.f proteins purified from the  $\Delta$ psbH and wild-type backgrounds were slightly different, indicating a posttranslational modification of Pam68.f upon the *psbH* deletion (Fig. 1A). This shift allowed us to distinguish that the spot of Pam68.f comigrating with 50S in the Pam68.f/ $\Delta$ PsbH pull-down (just above the Rpl6 protein) consists of only Pam68.f, with no other (ribosomal) proteins. There is no spot in this position in the Pam68.f elution (Fig. 1A).

To better visualize the pattern of proteins on the 2D gel, the separation of Pam68.f/ $\Delta$ PsbH and the control  $\Delta$ PsbH pull-downs on 2D CN/SDS-PAGE was followed by immunoblotting. The immunodetection determined a fraction of YidC, Ycf48, and SecY comigrating with 50S, as expected for the isolated ribosome-translocon apparatus (Fig. 1B). However, the barely visible (SecY) or invisible (YidC, Ycf48) staining of these proteins on the gel indicates that they are substantially less abundant than Pam68. Hence, it is unlikely that they connect Pam68.f with ribosomes. CP47 was found in a spot that had the same mobility as the dissociated Pam68.f, suggesting a mutual complex.

We used an independent approach to verify the interaction between the unassembled CP47 and Pam68 proteins. We isolated CP47m and a nascent CP47m lacking PsbH (CP47m/ $\Delta$ PsbH) via His-tagged CP47 from *Synechocystis* strains accumulating these complexes due to the absence of the D1 or D1/PsbH PSII subunits, respectively (Boehm et al., 2011; D'Haene et al., 2015). The Pam68 protein was copurified with CP47m/ $\Delta$ PsbH but was not detected in the CP47m elution (Fig. 1C). Therefore, either the binding of PsbH to the CP47-Pam68 complex is considerably weaker than to CP47, or Pam68 and PsbH share a similar binding site.

### N-Terminal Segment of Pam68 Is Required for the Interaction with Ribosomes

To verify that the interaction of Pam68 with ribosomes is not an artifact of the pull-down assay, solubilized membrane complexes from the *pam68.f* strain were separated by 2D CN/SDS-PAGE, stained by SYPRO Orange, and blotted onto a polyvinylidene fluoride (PVDF) membrane. Pam68.f comigrated with the 50S and, unexpectedly, also with the 30S subunit (Fig. 2A). On the other hand, Pam68.f spots in the

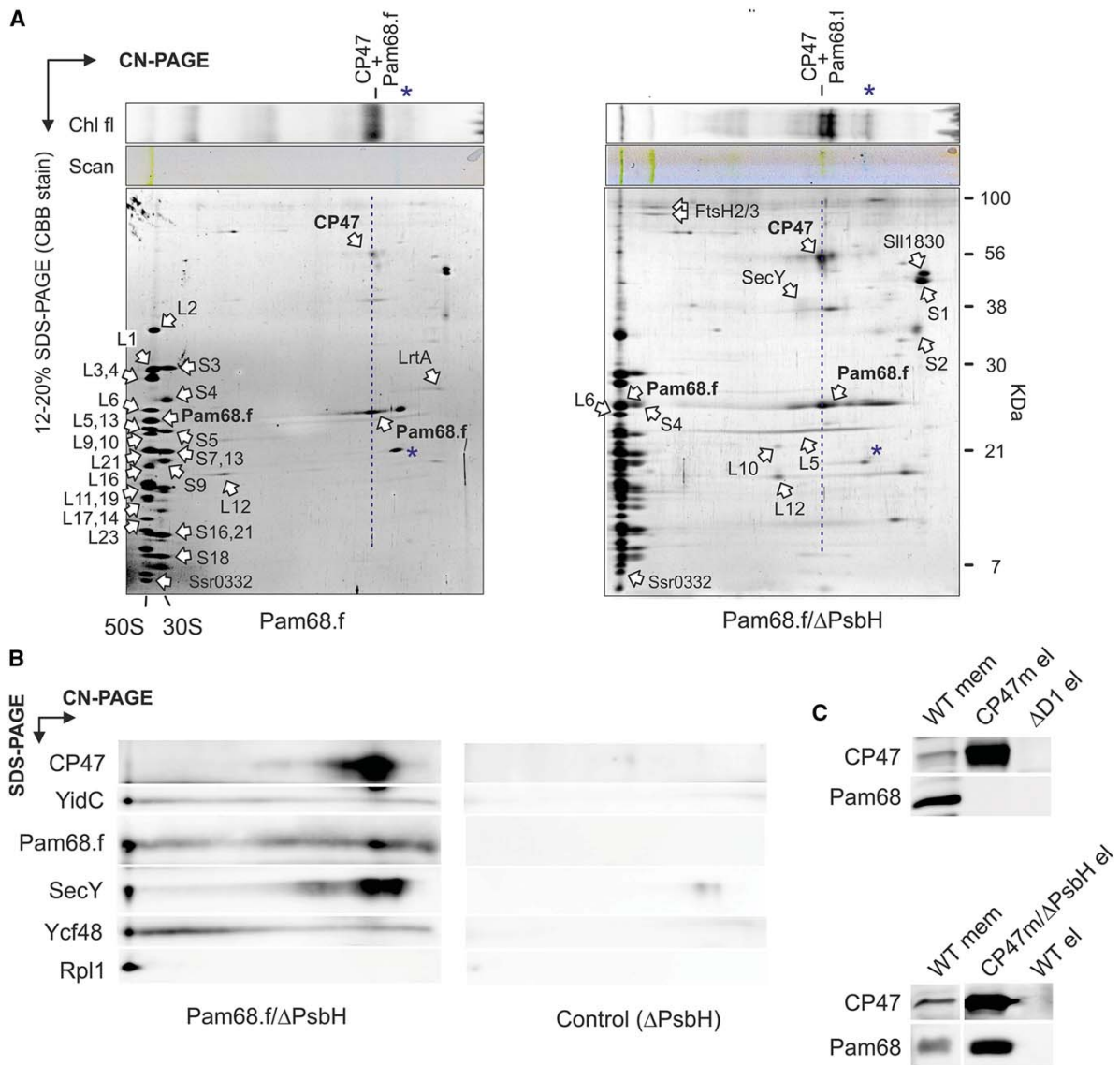


**Figure 1.** Identification of Pam68 as a component of the CP47 assembly module. A, The Pam68.f pull-down (left-hand gel) and the Pam68.f/ΔPsbH pull-down (right-hand gel) were separated by CN-PAGE, whereas SDS-electrophoresis was used for the second dimension. Individual protein spots were cut and identified by MS (Supplemental Dataset). The dashed blue line highlights the comigration of Pam68.f with CP47; note that CP47 exhibits Chl fluorescence demonstrating the presence of Chl molecules. Asterisks mark phycobiliproteins contaminating the elutions. B, The Pam68.f/ΔPsbH pull-down prepared from a different cell culture was separated together with the control ΔPsbH elution by 2D electrophoresis and blotted. The indicated proteins were sequentially detected by specific antibodies and the separate segments of the 2D blot with the individual antibody signals are shown. C, The CP47 assembly modules containing PsbH (CP47m) and lacking PsbH (CP47m/ΔPsbH) were purified on a nickel column. The eluted proteins were separated by SDS-PAGE together with the control pull-downs of wild type and ΔD1. The separated proteins were blotted, and the blot was sequentially probed with the indicated antibodies; the separate segments of the blot with individual antibody signals are shown. Chl fl, Chl fluorescence.

region of smaller complexes did not align with either of the CP47m forms (both are known to contain PsbH; Komenda, 2005). These results suggest that complexes between Pam68.f and the CP47m forms are not

detectable in the 2D gel of the *pam68.f* membranes (Fig. 2A). This observation is consistent with the proposed transient interaction between Pam68 and the newly synthesized CP47; the transient complex pool is



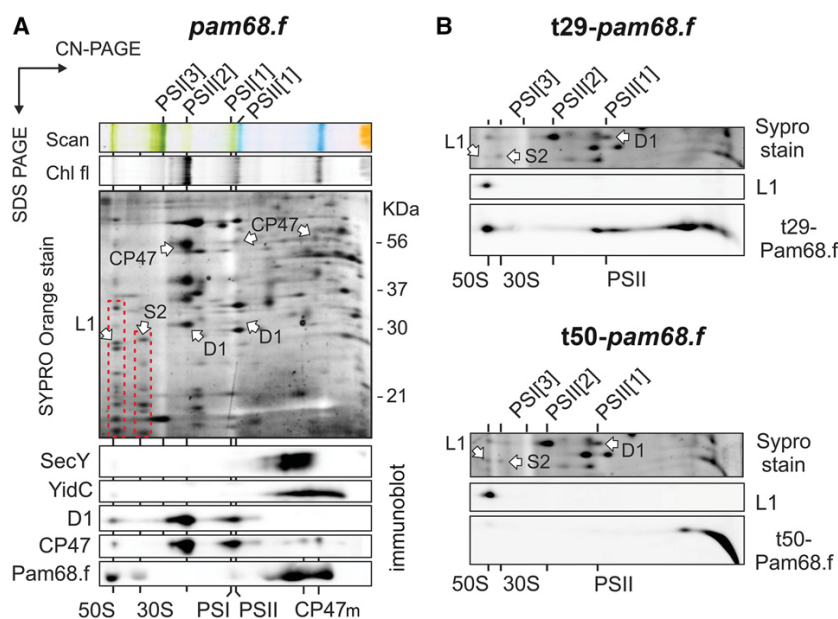


**Figure 2.** 2D CN/SDS-PAGE and immunodetection of membrane protein complexes from strains expressing full-length or truncated Pam68.f. A, Solubilized membrane proteins from the *pam68.f* strain were separated by 2D CN/SDS-PAGE. The 2D gel was stained with SYPRO Orange, blotted, and the 2D blot was sequentially probed by the indicated antibodies. Separate segments of the 2D blot with individual antibody signals are shown. The large and small ribosomal subunits are highlighted on the stained gel by red dashed boxes; protein spots belonging to Rpl1 and Rps2 were identified previously (Chidgey et al., 2014). Chl fluorescence was detected after excitation by blue light. CP47m marks two forms of the CP47 assembly module detected in the *Synechocystis* membrane fraction (Komenda, 2005). B, The same analysis was performed on membranes isolated from strains expressing the truncated variants t29-Pam68.f (top panel) and t50-Pam68 (bottom panel). Only a region of the SYPRO Orange stained gel around the Rpl1 protein (SYPRO stain) and separate segments of the 2D blot with signals of anti-Rpl1 and anti-Flag antibodies are shown. Complexes are designated as in (B). Chl fl, Chl fluorescence; L1, Rpl1; PSI[3], trimer of PSI; PSII[1], monomer of PSII; PSII[2], dimer of PSII; S2, Rps2.

apparently below the detection limit of the immunoblot analysis.

According to this model, ribosomes can be docked to bacterial membranes via interaction with the large subunit and the SecYEG translocon, or alternatively, with YidC insertase (Prinz et al., 2000; Seitel et al., 2014). However, the interaction between the membrane-bound ribosomes and SecY or YidC in isolated thylakoids was not preserved in our 2D gel system (Fig. 2A). Therefore, it is unlikely that SecY/YidC facilitates the observed association of Pam68.f with ribosomes.

It is likely that Pam68 interacts directly with ribosomal proteins from both the 50S and 30S subunits. The 30S subunit of the membrane-docked ribosome is close to the membrane surface (approximately 10 nm; Frauenfeld et al., 2011). Theoretically, the strongly positively charged N terminus of Pam68.f is long enough (65 amino acids, approximately 20 nm; Supplemental Fig. S3) to reach the 30S subunit. To test this possibility, we constructed strains expressing variants of Pam68.f truncated either up to the V29 (t29-*pam68.f* strain) or the S50 amino acid residues (t50-*pam68.f*). The t29-Pam68.f protein still comigrated

with ribosomes on the 2D gel (Fig. 2B), but the more truncated t50-Pam68.f protein was not detectable in any larger complexes, which supports the role of the Pam68 N-terminal segment in the interaction with ribosomes.

A close relationship between the cyanobacterial Pam68 and ribosomes can also be inferred from the existence of an operon of the *pam68* and the *rps15* genes, which is highly conserved among the cyanobacterial genomes. According to the STRING database (<http://string-db.org/>), there are only a few examples of sequenced cyanobacterial genomes (e.g. *Gloeobacter violaceus*) where these two genes are not organized in tandem. In the *Synechocystis* genome, the *pam68* gene is transcribed from the *rps15* promoter as a single mRNA with *rps15* (Mitschke et al., 2011). Interestingly, the *rps15-pam68* mRNA belongs to a small group of ribosomal transcripts that are significantly up-regulated under stress conditions with the strongest expression under low temperature (Kopf et al., 2014; Supplemental Fig. S4). Indeed, we found the Pam68 protein level to be high during high light or chilling stress (Supplemental Fig. S5).

### Enhanced Chl Biosynthesis Rescues the Abolished CP47 Synthesis in the $\Delta psbH/\Delta pam68$ Strain

The results described above imply that Pam68 functions during the synthesis and/or folding of CP47 before it associates with PsbH, which also facilitates CP47 synthesis (Komenda, 2005). To test whether PsbH can compensate for the absence of Pam68, we characterized the *Synechocystis*  $\Delta pam68$  and  $\Delta psbH$  mutants and the  $\Delta psbH/\Delta pam68$  double mutant. Under moderate light intensities ( $40 \mu\text{mol photons m}^{-2} \text{s}^{-1}$ ),  $\Delta pam68$  grew similarly as the wild-type strain and had a similar Chl content (Supplemental Fig. S6, A and B). The  $\Delta psbH$  mutation affected both the growth rate and Chl content; nevertheless, this mutant grew fairly well photoautotrophically (Supplemental Fig. S6, A and B). However, even the single  $\Delta pam68$  mutant stopped proliferating on plates under more severe conditions, such as dark-/high-light fluctuation or low temperature (Fig. 3A). Moreover, the level of PsbH was merely affected in the  $\Delta pam68$  strain and, vice versa, the level of Pam68 in the  $\Delta psbH$  strain remained comparable to wild type (Fig. 3B).

Unlike the strains containing single mutations, the double mutant showed extremely slow autotrophic growth (double time approximately 20 d), accumulated only traces of Chl and died immediately after exposure to mild stress conditions (Fig. 3A; Supplemental Fig. S6). However, photoautotrophy of the  $\Delta psbH/\Delta pam68$  strain can be restored by the expression of Pam68.f (Fig. 3C), which provides evidence that the poor phenotype of the double mutant is not caused by a position effect, e.g. lower levels of Rps15. To obtain enough cells of the poor-growing  $\Delta psbH/\Delta pam68$  mutant, we first grew all strains with Glc supplementation. Then, we characterized the phenotype 2 d after removing Glc from the media. As revealed by the CN-PAGE separation of membrane complexes (Fig. 3D), the levels of PSI and PSII were virtually unchanged in the  $\Delta pam68$  strain, but the  $\Delta psbH$  strain contained much less dimeric PSII. In the double mutant, very little PSI and only traces of the PSII complexes were detectable. Thus, both PsbH and Pam68 play distinct roles in the accumulation of PSII; the parallel elimination of both of these proteins is nearly fatal for cell viability.

For a closer look at the role of PsbH and Pam68 in the synthesis of PSII wild type,  $\Delta pam68$ ,  $\Delta psbH$ , and  $\Delta psbH/\Delta pam68$  cells were pulse-labeled and the isolated membrane complexes analyzed by 2D CN/SDS-PAGE (Fig. 4). Consistent with the previously published analysis of  $\Delta pam68$  (Rengstl et al., 2013), this strain showed less labeled CP47 and CP43 in total, and lacked the labeled unassembled CP47. In addition, we observed severe accumulation of RCIIa and RCII\* assembly intermediates, which is a typical feature of cells deficient in the formation of CP47m (Knoppová et al., 2014). The obtained pattern for  $\Delta psbH$  differed from the  $\Delta pam68$  strain by having only weakly labeled dimeric PSII and also less synthesized D1. A detectable pool of unassembled CP47 was also absent and both RCII complexes accumulated, which implies that the rate of CP47m formation limits the process of PSII assembly. In the  $\Delta psbH/\Delta pam68$  strain, the capacity to

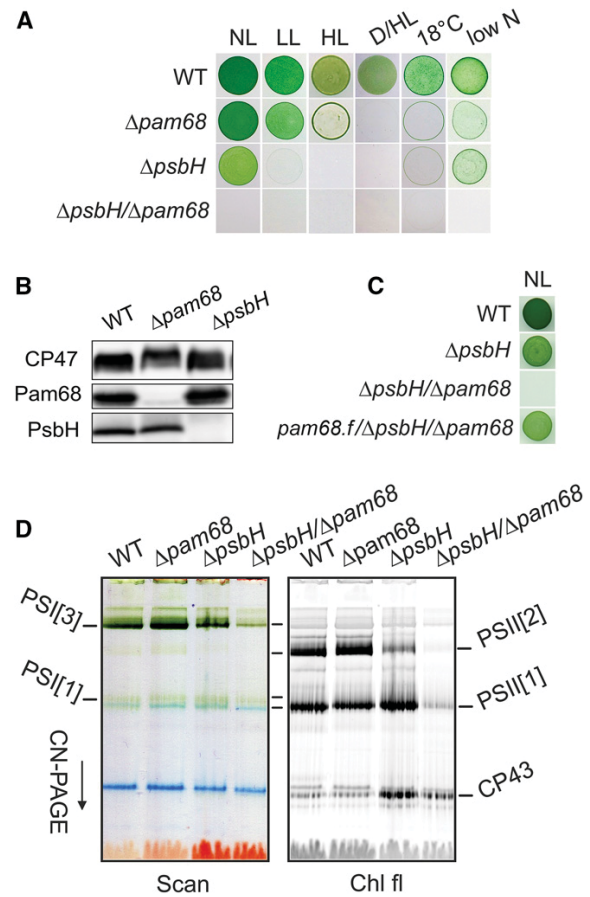


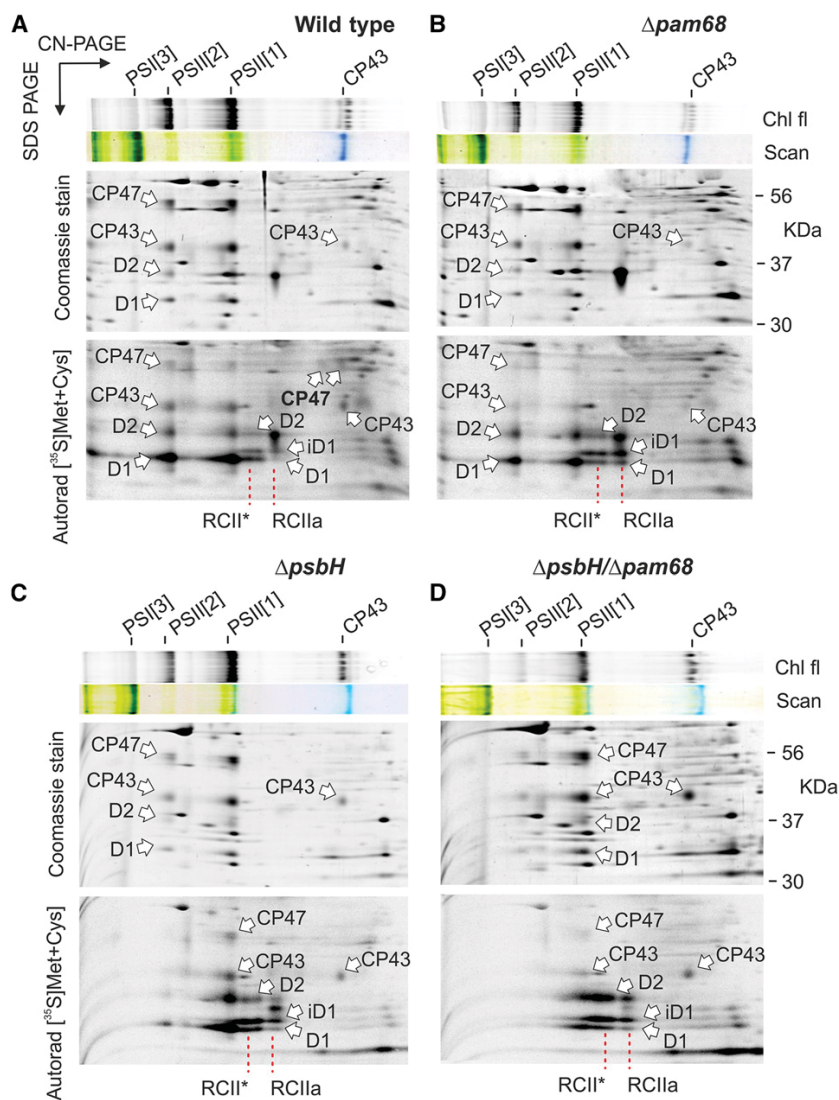
**Figure 3.** Characterization of the *Synechocystis* strains lacking Pam68, PsbH, or both of these proteins. **A**, Autotrophic growth of the wild-type and mutant strains on agar plates under various conditions. Growth for 5 d under normal light ( $40 \mu\text{mol photons m}^{-2} \text{s}^{-1}$ ), low light ( $10 \mu\text{mol photons m}^{-2} \text{s}^{-1}$ ), high light ( $400 \mu\text{mol photons m}^{-2} \text{s}^{-1}$ ), fluctuating dark/high light conditions (5 min dark, 5 min  $400 \mu\text{mol photons m}^{-2} \text{s}^{-1}$ ),  $18^\circ\text{C}$  at  $40 \mu\text{mol photons m}^{-2} \text{s}^{-1}$ , and low nitrogen ( $0.1 \text{ mM NaNO}_3$ ). **B**, Levels of PsbH and Pam68 in the  $\Delta pam68$  and  $\Delta psbH$  strains under normal light conditions. A comparable amount of Chl was loaded for each strain. **C**, Autotrophic growth of the *pam68.f/\Delta pam68/\Delta psbH* strain expressing the Pam68.f protein under the regulation of the *psbAII* promoter. **D**, Membranes, isolated from the wild-type and mutant strains grown as described in (A), were solubilized and separated by CN-PAGE. D/HL, dark/high light; HL, high light; LL, low light; NL, normal light; PSI[3], trimer of PSI; PSII[1], monomer of PSII; PSII[2], dimer of PSII.

synthesize PSII was extremely weak, almost certainly caused by the lack of CP47m because the intensively labeled RCII complexes resembled the canonical pattern of the  $\Delta\text{CP47}$  strain (Fig. 4; Komenda et al., 2004).

Based on the available PSII structure (Umena et al., 2011), the N-terminal segment of PsbH creates a network of hydrogen bonds with the stromal loops connecting the first four helices of CP47 (Supplemental Fig. S7). Therefore, the PsbH protein could fix the nascent CP47 in



**Figure 4.** Synthesis of PSII subunits in the  $\Delta pam68$ ,  $\Delta psbH$ , and  $\Delta psbH/\Delta pam68$  mutant strains. Wild-type (A) and the mutant  $\Delta pam68$  (B),  $\Delta psbH$  (C), and  $\Delta psbH/\Delta pam68$  (D) cells grown for 2 d without Glc were radiolabeled with a mixture of [ $^{35}$ S]Met/Cys using a 30-min pulse. Isolated membrane proteins were separated by CN-PAGE on a 4% to 14% linear gradient gel, whereas 12% to 20% SDS-electrophoresis was used for the second dimension. The same amounts of Chl were loaded for each strain. Note that the  $\Delta psbH/\Delta pam68$  strain contains three-times less Chl per cell than  $\Delta psbH$ , meaning that the membrane proteins from the double mutant were overloaded on a per-cell basis to obtain a detectable radioactivity signal of the assembled PSII. The 2D gels were stained with Coomassie Blue, and the labeled proteins were detected by a phosphorimager (Autorad). Chl fluorescence emitted by Chl was detected by LAS 4000 (Fuji) after excitation by blue light. Chl fl, Chl fluorescence; iD1, incompletely processed form of the D1 precursor; PSI[3], trimer of PSI; PSII[1], monomer of PSII; PSII[2], dimer of PSII; RCII\*, assembly intermediate (reaction center complex) lacking CP47m (Knoppová et al., 2014); RCIIa, PSII assembly intermediate (reaction center complex) lacking CP43m (Knoppová et al., 2014).



a position that facilitates prompt insertion of Chl molecules. Moreover, the C-terminal region of Pam68 may play a similar role. To test the importance of both proteins for Chl insertion into CP47, we removed Glc from the  $\Delta psbH/\Delta pam68$  liquid culture, while supplementing it with 200 nM N-methyl mesoporphyrin IX. This compound is a specific inhibitor of the FeCh enzyme and a partial inhibition of FeCh strongly enhances Chl biosynthesis (Sobotka et al., 2005). Remarkably, the  $\Delta psbH/\Delta pam68$  cells treated with the FeCh inhibitor started to grow much faster than the control cells without the inhibitor (Fig. 5A). The control culture had very low Chl content on a per-cell basis, whereas the treated cells progressively built up new Chl-complexes, and in 4 d reached approximately 85% of the Chl level when compared to wild type (Fig. 5B).

Precursors of the Chl biosynthetic pathway differed dramatically between treated and untreated cells. Whereas monovinyl-chlorophyllide was the only detectable Chl precursor in the untreated cells, the inhibitor-treated cells contained a spectrum of Chl precursors typical for wild type (Piňný et al., 2015; Supplemental Fig. S8). Because the earlier precursors upstream of chlorophyllide were below the detection level in the untreated double mutant, this chlorophyllide pool originated almost certainly from Chl recycling and not from de novo synthesis (Vavilin et al., 2005; Kopečná et al., 2015). We repeated the protein radiolabeling experiment described above using  $\Delta psbH/\Delta pam68$  cells treated with the FeCh inhibitor. The assembly of PSII was restored (Fig. 5C), suggesting that boosting of the ceased Chl

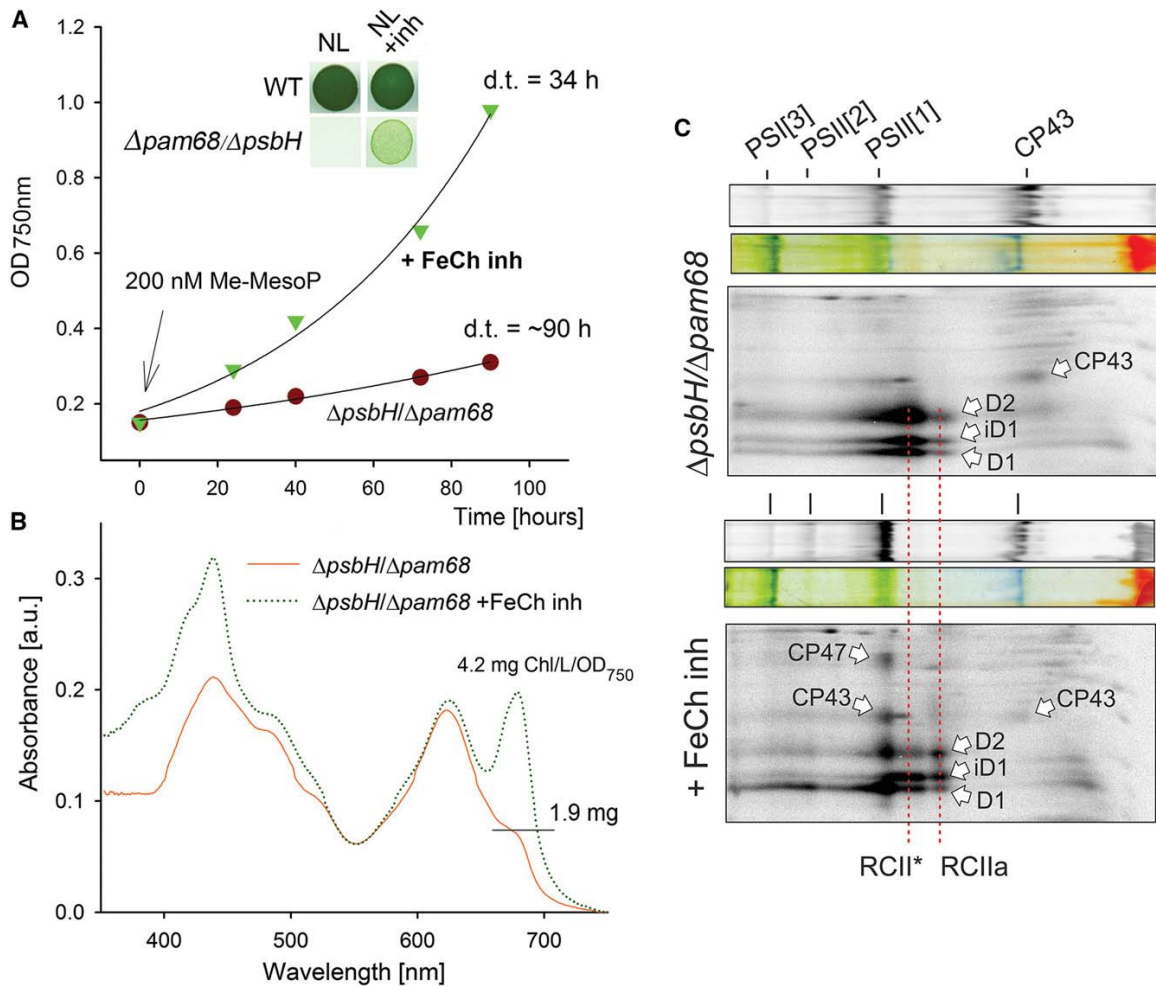


**Figure 5.** Abolished synthesis of CP47 in the  $\Delta psbH/\Delta pam68$  mutant is rescued by enhanced Chl biosynthesis. **A**, The  $\Delta psbH/\Delta pam68$  cells grown mixotrophically were harvested and resuspended in a growth medium without Glc. The obtained culture was divided into two flasks, with one of them supplemented with N-methyl-mesoporphyrin IX (Me-MesoP, FeCh inhibitor). The photoautotrophic growth was then monitored. The inset shows the same growth experiment but with 200 nM Me-MesoP added into the plate. **B**, Absorbance spectra of mutant cells growing for 4 d in the presence or absence of FeCh inhibitor. Spectra were normalized to light scattering at 750 nm. Also shown is the Chl content determined spectroscopically in methanol extract and normalized per OD<sub>750 nm</sub>. **C**,  $\Delta psbH/\Delta pam68$  cells grown for 2 d photoautotrophically in the presence of 200 nM FeCh inhibitor were radiolabeled with a mixture of [<sup>35</sup>S]Met/Cys; incorporation of radioactivity into core PSII subunits was detected after 2D CN/SDS-PAGE. The same amounts of Chl were loaded of each sample. a.u., absorbance units; d.t., doubling time; iD1, incompletely processed form of the D1 precursor; PSII[3], trimer of PSII; PSII[1], monomer of PSII; PSII[2], dimer of PSII; RCII\*, assembly intermediate (reaction center complex) lacking CP47m (Knoppová et al., 2014); RCIIa, PSII assembly intermediate (reaction center complex) lacking CP43m (Knoppová et al., 2014).

biosynthesis restores the formation of CP47m in the mutant lacking both Pam68 and PsbH.

## DISCUSSION

The Pam68 protein was first described in the *Arabidopsis* (*Arabidopsis thaliana*) *pam68*-null mutant, which accumulated only approximately 10% of PSII (Armbruster et al., 2010). The function of Pam68 was

originally linked to the synthesis or maturation of the D1 subunit of PSII (Armbruster et al., 2010); however, a strong relationship between Pam68 and CP47 was also suggested, based on the low level of Pam68 detected in the *Synechocystis* CP47-less strain (Rengstl et al., 2011). Our results agree with a recent study, which demonstrated that the lack of Pam68 in *Synechocystis* limits the synthesis of CP47 and CP43 (Rengstl et al., 2013). Given that the mechanism of PSII biogenesis is highly conserved, it is likely that the eukaryotic Pam68 is involved

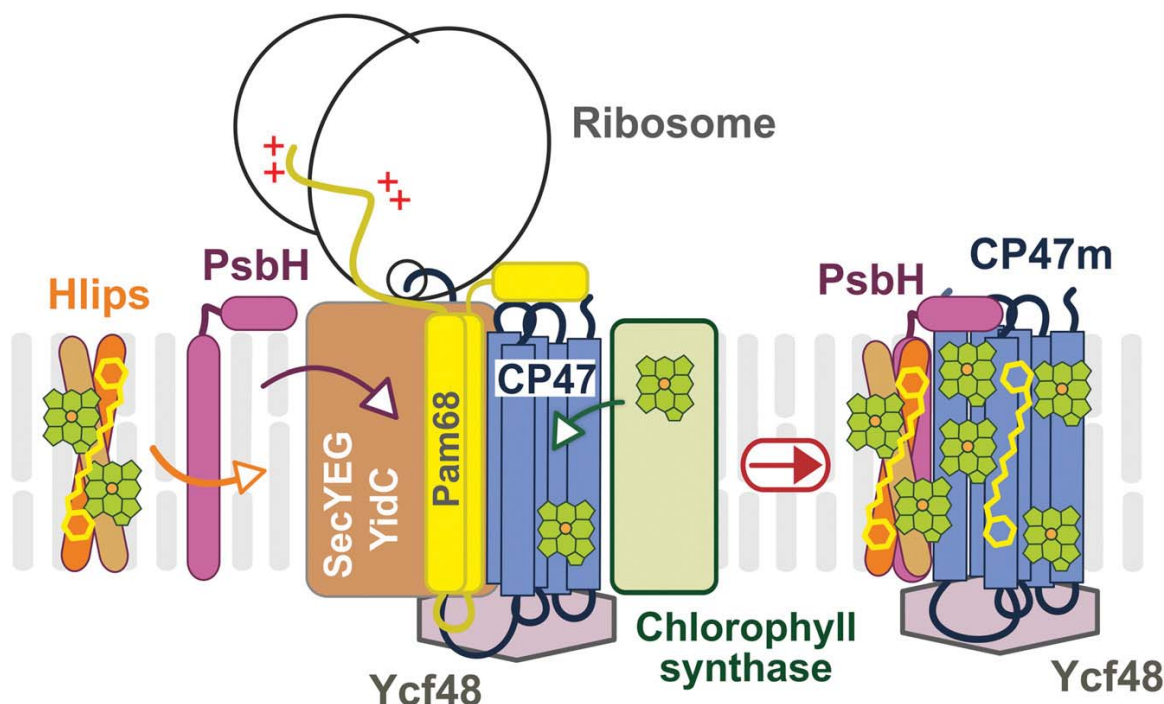


**Figure 6.** A working model of CP47m synthesis with Pam68 as a ribosome-interacting factor. The CP47 protein is translated by membrane-bound ribosomes and inserted into the membrane by the SecYEG translocon together with YidC insertase. Chl is loaded into the nascent polypeptide cotranslationally from Chl-synthase when the transmembrane segments are released from the translocase channel to YidC (Chidgey et al., 2014). The N-terminal region of the Pam68 protein is associated with the translating ribosome, whereas the C terminus segment interacts with stromal loops of the nascent CP47 chain after it emerges from the translocon. This interaction fixes the CP47 transmembrane segments in a position that facilitates the insertion of Chl molecules. A similar role can be played by the Ycf48 protein at the lumenal site of CP47 (Crawford et al., 2016). Subsequently, PsbH replaces Pam68 and recruits the photoprotective high-light-inducible proteins that associate with CP47 in the vicinity of PsbH (Promnares et al., 2006). Hlips, high-light-inducible proteins.

in the synthesis of CP47. Indeed, using a standard methodology ( $^{35}\text{S}$  radiolabeling combined with 2D gel-electrophoresis), the synthesis of CP47 in the Arabidopsis *pam68*-null mutant was hardly detectable (Armbruster et al., 2010).

In contrast to Arabidopsis, the inactivation of *pam68* in *Synechocystis* had no obvious effect on the PSII level under standard growth conditions, although the synthesis of CP47 and CP43 was visibly affected in both organisms (Rengstl et al., 2013; Fig. 4). However, after 3 h of high light treatment ( $2000 \mu\text{mol photons m}^{-2} \text{s}^{-1}$ ), the levels of functional PSII in the  $\Delta\textit{pam68}$  strain decreased by approximately 50% (Rengstl et al., 2013). In addition, we demonstrated the importance of Pam68 under fluctuating light conditions, low temperature, and nitrogen limitation (Fig. 3). These observations imply that Pam68 is essential once the synthesis of CP47 becomes difficult and limits PSII biogenesis.

The PsbH protein is required for sufficient CP47 synthesis in plants as well as in cyanobacteria (Komenda, 2005; Levey et al., 2014); the *Synechocystis*  $\Delta\textit{psbH}$  mutant shows a noticeable growth defect even under nonstress

conditions (Supplemental Fig. S6, A and B). However, the phenotype of this strain is probably quite complex, because PsbH also stabilizes electron transfer processes between  $\text{Q}_\text{A}$  and  $\text{Q}_\text{B}$  in the PSII complex (Komenda et al., 2002). It is further essential for the association of photoprotective high-light-inducible proteins to CP47 (Promnares et al., 2006; Fig. 6), and creates an environment for binding of a red Chl molecule in CP47, which is also supposed to have a protective function (D'Haene et al., 2015). However, we expect that the impaired CP47 synthesis/stability is the major reason for the slow growth of the  $\Delta\textit{psbH}$  mutant (Supplemental Fig. S6A). This conclusion is supported by the fact that the growth rate of this strain can also be improved by the inhibition of FeCh (Supplemental Fig. S6C), and is consistent with the very poor phenotype of the  $\Delta\textit{psbH}/\Delta\textit{pam68}$  double mutant. Therefore, PsbH appears to be more crucial for the biogenesis than for the functioning of fully assembled PSII complexes. Similarly, the PsbI subunit was found to be more important for attachment of CP43m to RCII, rather than for PSII activity (Dobáková et al., 2007). Other small PSII subunits may also play roles in assembly.



We present a working model of CP47m synthesis (Fig. 6). Pam68 is firmly bound to the translating ribosome via the N-terminal segment, whereas its C-terminal end interacts with the stromal loops of the nascent CP47 chain emerging from the translocon. We speculate that the coordination of Pam68 (stromal side), YidC (lateral site; Hennon et al., 2015), and Ycf48 (luminal site; Crawford et al., 2016) fixes the CP47 helix pairs in a position that is amenable to Chl binding. The Pam68 C terminus contains highly conserved charged residues (Supplemental Fig. S3) that can form a network of hydrogen bonds resembling the interaction of the N terminus of PsbH with CP47 (see Supplemental Fig. S7). The synthesis of CP47 is impaired in the  $\Delta pam68$  strain even under nonstressful conditions (Fig. 4), suggesting that Pam68 permanently assists during CP47 synthesis. Because Pam68 is particularly critical for the mutant lacking PsbH, it is probable that both proteins can work similarly as chaperones facilitating the folding of CP47 and/or the loading of Chl into the newly synthesized apolypeptide chain.

Based on previous data and the results of our radiolabeling experiment (Rengstl et al., 2013; Fig. 4), Pam68 appears to also facilitate the synthesis of the CP43 protein and PSI. However, the interaction of Pam68 with these proteins is either too weak to detect, or the lower levels of CP43 and PSI in the absence of Pam68 is a secondary phenotype caused by the feeble CP47 synthesis. The second possibility is more probable, as the mutant lacking CP47 has been shown to contain considerably lower cellular level of Chl in comparison with wild type, implying that the level of CP43 and PSI is lower in the absence of CP47 (Bečková et al., 2017). Although this approach is frequently used, we are aware that arresting particular PSII assembly steps to accumulate specific assembly intermediates may affect other cellular processes, including the synthesis of Chl-binding proteins. The Flag-tag technology used here has the advantage of allowing the purification of PSII assembly intermediates that only exist temporarily in the cell (such as the Pam68.f-CP47m complex) directly from the wild-type background.

The synthesis of CP47 is very sensitive to Chl availability (Hollingshead et al., 2016), which may explain why the lack of Pam68 is not tolerated under stress conditions. The Chl pathway can be temporarily switched-off after a shift to stressful conditions (Kopečná et al., 2012) and when the de novo Chl amount decreases, a fine structural stabilization of the nascent CP47 is likely to be particularly important for the smooth loading of Chls. After addition of the FeCh inhibitor, the pool of available Chl increased, and the impaired CP47 synthesis was rescued (Fig. 5). Thus, a high concentration of Chl molecules around the translated CP47 increases the chance that all Chls are inserted in time even if the orientation of CP47 is not perfect. A similar effect of FeCh inhibition was reported earlier in the *Synechocystis* strain harboring a mutated CP47 protein (Sobotka et al., 2005).

The observed tight binding of Pam68 to the ribosome is intriguing. A high level of LrtA protein, which associates with the 30S ribosomal subunit (Galmozzi et al., 2016), was present in the Pam68.f pull-downs prepared from strains lacking CP47 (Supplemental Fig. S2). As the potential function of LrtA is to stabilize stalled ribosomal 70S particles (Di Pietro et al., 2013), its appearance in the elution indicates that Pam68 interacts with both the SecY-bound idle ribosomes as well as with the actively translating ribosomes. In *Synechocystis*, Pam68 is not an abundant membrane protein (it is not detectable in the stained SDS PAGE gel with separated cellular membrane proteins), and there is only a limited pool of membrane-bound ribosomes associated with Pam68. It is possible that these ribosomes differ structurally from other ribosomes in the cell. The heterogenic nature of ribosomes is demonstrated by the variable stoichiometry among core ribosomal subunits or between the monosome/polysome arrangement of ribosomes according to environmental conditions (Xue and Barna, 2012; Slavov et al., 2015). Similarly, the plastid-encoded Rps15 is not an essential ribosomal subunit in plants, but under chilling stress, the tobacco (*Tobacco nicotiana*)  $\Delta rps15$  knockdown showed a drastic reduction in the number of plastid ribosomes (Fleischmann et al., 2011). In *Synechocystis*, the *rps15-pam68* operon as well as the *rps18*, *rps20*, and *rps25* genes are up-regulated under cold stress, whereas many ribosomal genes are simultaneously down-regulated (Supplemental Fig. S4). This result supports the existence of a pool of modified, stress-induced type of ribosomes in cyanobacteria. It is possible that Pam68 has a higher affinity for the stress-induced type of ribosomes. Once bound to SecY, the ribosome might serve as an anchor to localize Pam68 in the vicinity of the translocon machinery. Under severe conditions with limited Chl availability and/or lowered membrane fluidity (chilling stress), Pam68 can promptly assist during the synthesis of CP47.

## MATERIALS AND METHODS

### *Synechocystis* Strains and Growth Conditions

All the *Synechocystis* strains used are summarized in Supplemental Table S1. The  $\Delta pam68$  strain was kindly provided by Jörg Nickelsen (Ludwig-Maximilians University), and is described in Armbruster et al. (2010). The  $\Delta psbH/\Delta pam68$  double mutant was prepared by transformation of the  $\Delta psbH$  strain (D'Haene et al., 2015) by genomic DNA isolated from the  $\Delta pam68$  strain. The *Synechocystis* strain expressing the Pam68 protein fused with 3×Flag at the C terminus (the *pam68.f* strain) was constructed using pPD-CFLAG plasmid as described in Hollingshead et al. (2012). The *pam68.f* construct was further transformed into the  $\Delta psbH$  and  $\Delta psbB$  cells (Eaton-Rye and Vermaas, 1991) to express the Pam68.f protein in these genetic backgrounds. Derivatives of Pam68.f truncated at the amino acid 29 (the *t29-pam68.f* strain) or 50 (the *t50-pam68.f* strain) were constructed by PCR amplification of the *Synechocystis pam68* gene lacking the 3' part (primers are listed in Supplemental Table S2). The obtained PCR products were cloned into a pPD-CFLAG plasmid and transformed into wild type. To be able to express Pam68.f in the  $\Delta pam68/\Delta psbH$  mutant (already resistant to kanamycin), we replaced the kanamycin-resistance cassette in the pPD-CFLAG plasmid with an erythromycin-resistance cassette, cloned the *pam68* gene into this modified construct, and fully segregated the *pam68.f/\Delta pam68/\Delta psbH* strain.

Unless stated otherwise, strains were grown photoautotrophically in liquid BG-11 medium on a rotary shaker under moderate (normal) light intensities ( $40 \mu\text{E m}^{-2} \text{s}^{-1}$ ) at  $28^\circ\text{C}$ . For purification of the Pam68.f protein under native conditions, 4 L of *pam68.f* and *pam68.f/ΔpsbH* cells were grown in a 10 L flask in BG-11 medium supplemented by 5 mM Glc under normal light conditions and bubbled with air. Strains lacking PSII (*ΔpsbB*) were supplemented with 5 mM Glc and grown under lower light intensities ( $10 \mu\text{E m}^{-2} \text{s}^{-1}$ ).

### Absorption Spectra and Determination of Chl Content

Absorption spectra of the whole cells were measured at room temperature with a UV-3000 spectrophotometer (Shimadzu). Chl was extracted from cell pellets (2 mL,  $\text{OD}_{750} = \text{approximately } 0.3$ ) with 100% (v/v) methanol, and its concentration was measured spectrophotometrically according to Porra et al. (1989).

### Preparation of Cellular Membranes

Cell cultures were harvested at optical densities of  $750 \text{ nm} = \text{approximately } 0.5$  to  $0.7$ . Cells were pelleted, washed, and resuspended with buffer A (25 mM MES/NaOH, pH 6.5, 10 mM CaCl<sub>2</sub>, 10 mM MgCl<sub>2</sub>, 25% [v/v] glycerol) for the preparation of membranes for 2D electrophoresis and purification of Pam68.f. For nickel-affinity chromatography, the membrane fraction was prepared in 25 mM Na-P buffer, pH 7.5, 50 mM NaCl, 10% (v/v) glycerol (buffer B). Cells were broken using glass beads (0.1 mm diameter), and the membrane fraction was separated from soluble proteins by centrifugation at high speed ( $65,000 \times g$ , 20 min).

### Isolation of Protein Complexes by Affinity Chromatography

Cellular membranes containing approximately 1 mg/mL Chl were solubilized for 1 h with 1% (w/v)  $\beta$ -dodecyl-maltoside at  $10^\circ\text{C}$  and centrifuged for 20 min at  $65,000g$  to remove cell debris. The Pam68.f complexes were purified using an anti-Flag-M2 agarose column (Sigma-Aldrich). To remove contaminants, the anti-Flag-resin was washed with 20 resin volumes of buffer A containing 0.04%  $\beta$ -dodecyl-maltoside. The Pam68.f complex was eluted with 2.5 resin volumes of buffer A containing 150  $\mu\text{g/mL}$  3 $\times$ Flag peptide (Sigma-Aldrich) and 0.04%  $\beta$ -dodecyl-maltoside. For purification of the His-tagged proteins, solubilized membrane complexes were loaded onto a nickel-affinity chromatography column (Protino Ni-NTA-agarose; Macherey-Nagel). Proteins bound to the column were washed with buffer B containing 0.04%  $\beta$ -dodecyl-maltoside and increasing concentrations of imidazole (5, 10, 20, and 30 mM); His-tagged proteins were finally eluted with 150 mM imidazole.

### Electrophoresis and Immunoblotting

The protein composition of the purified complexes was analyzed by electrophoresis in a denaturing 12% to 20% linear gradient polyacrylamide gel containing 7 M urea (Dobáková et al., 2009). Proteins were stained either by Coomassie Brilliant Blue or SYPRO Orange stain and subsequently transferred onto a PVDF membrane for immunodetection (see below). For native electrophoresis, solubilized membrane proteins or isolated complexes were separated on 4% to 12% CN-PAGE (Wittig et al., 2007). Individual components of protein complexes were resolved by incubating the gel strip from the first dimension in 2% (w/v) SDS and 1% (w/v) DTT for 30 min at room temperature, and proteins were separated along the second dimension by SDS-PAGE in a denaturing 12% to 20% polyacrylamide gel containing 7 M urea (Dobáková et al., 2009). Proteins were stained by Coomassie Brilliant Blue or by SYPRO Orange; in the latter case, they were subsequently transferred onto a PVDF membrane. Membranes were incubated with specific primary antibodies and then with a secondary antibody conjugated with horseradish peroxidase (Sigma-Aldrich). The following primary antibodies were used in the study: anti-SecY and anti-YidC (Linhartová et al., 2014), anti-CP47, anti-D1 and anti-PsbH (Komenda, 2005), anti-Pam68 (Armbruster et al., 2010), anti-Rp11 (Agrisera), anti-Flag (Sigma-Aldrich), and anti-Ycf48 (which was raised in rabbit against recombinant *Synechocystis* Ycf48 and provided by Peter Nixon, Imperial College, London).

### Protein Radiolabeling

For protein labeling, the cells were incubated with using a mixture of [<sup>35</sup>S]Met and [<sup>35</sup>S]Cys (Translabel; MP Biochemicals) as described in Dobáková et al.

(2009). After separation of labeled proteins by CN-PAGE in the first dimension, the polyacrylamide gel was scanned for Chl fluorescence and then treated for second-dimension separation with 18% SDS-PAGE. The 2D gel was exposed to a Phosphorimager plate (GE Healthcare) overnight and stained by Coomassie Brilliant Blue and scanned by Storm (GE Healthcare).

### Protein Identification by LC-MS/MS Analysis

Gel slices were placed in 200  $\mu\text{L}$  of 40% acetonitrile, 200 mM ammonium bicarbonate and incubated at  $37^\circ\text{C}$  for 30 min, after which the solution was discarded. This procedure was performed twice, and the gel was subsequently dried in a vacuum centrifuge. Ten microliters of 40 mM ammonium bicarbonate in 9% acetonitrile containing 0.4  $\mu\text{g}$  trypsin (proteomics grade; Sigma-Aldrich) were added to the gel slice and left to soak in the solution at  $4^\circ\text{C}$  for 45 min. To digest proteins, 20  $\mu\text{L}$  of 9% (v/v) acetonitrile in 40 mM ammonium bicarbonate was added to the gel and incubated at  $37^\circ\text{C}$  overnight. Peptides were purified using ZipTip C18 pipette tips (Millipore). MS analysis was performed on a NanoAcquity UPLC (Waters) on-line coupled to the ESI Q-ToF Premier mass spectrometer (Waters). One microliter of the sample was diluted in 3% (v/v) acetonitrile/0.1% (v/v) formic acid, and tryptic peptides were desalted on a Symmetry C18 Trapping column (180  $\mu\text{m}$  i.d., 20 mm length, particle size 5  $\mu\text{m}$ , reverse phase; Waters) with a flow rate of 15  $\mu\text{L}/\text{min}$  for 1 min. Trapping was followed by a reverse-phase UHPLC using the BEH300 C18 analytical column (75  $\mu\text{m}$  i.d. 150 mm length, particle size 1.7  $\mu\text{m}$ , reverse phase; Waters). The linear gradient elution ranged from 97% solvent A (0.1% formic acid) to 40% solvent B (0.1% formic acid in acetonitrile) at a flow rate of 0.4  $\mu\text{L}/\text{min}$ . Eluted peptides flowed directly into the ESI source. Raw data were acquired in the data-independent MS<sup>E</sup> identity mode (Waters). Precursor ion spectra were acquired with a collision energy of 5 V and fragment ion spectra with a collision energy of 20 V to 35 V ramp in alternating 1 s scans. Data-dependent analysis mode was used for the second analysis; peptide spectra were acquired with a collision energy of 5 V and peptides with charge states of + 2, +3, and + 4 were selected for MS/MS analysis. Fragment spectra were collected with a collision energy of 20 V to 40 V ramp. In both modes, the acquired spectra were submitted for database search using the PLGS2.3 software (Waters) against *Synechocystis* protein databases from the Cyanobase Web site (<http://genome.microbedb.jp/cyanobase/>). Acetyl N-terminal, deamidation N and Q, carbamidomethyl C, and oxidation M were set as variable modifications. Identification of three consecutive *y*-ions or *b*-ions was required for a positive peptide match.

### Accession Numbers

Pam68, BAA16881.1; CP47, BAA10458.1; PsbH, BAA17629.1, SecY; BAA17331.1, YidC - BAA18244.1.

### Supplemental Data

The following supplemental materials are available.

Supplemental Table S1. A list of *Synechocystis* strains used in this study.

Supplemental Table S2. A list of primers used to clone the *pam68.f* gene and its two truncated variants (*t29-pam68.f* and *t50-pam68.f*) into the pPD-CFLAG plasmid (adding of 3 $\times$ Flag tag at the C terminus).

Supplemental Figure S1. Identification of proteins copurified with Pam68.f.

Supplemental Figure S2. 2D CN/SDS-PAGE of the Pam68.f complex purified from the *pam68.f/ΔpsbB* strain (A) and the control  $\Delta\text{CP47}$  (B).

Supplemental Figure S3. Conservation profile and the prediction of secondary structure of the *Synechocystis* Pam68 protein.

Supplemental Figure S4. Coexpression of the cyanobacterial *pam68-rps15* operon with a subset of ribosomal genes.

Supplemental Figure S5. Accumulation of the Pam68 protein under stress conditions.

Supplemental Figure S6. Growth rate and whole cell spectra of the wild-type and mutant strains.

Supplemental Figure S7. Stromal view of the CP47–PsbH complex with indicated hydrogen bonds between the CP47 and the PsbH N terminus.

- Supplemental Figure S8. Changes in the levels of Chl precursors in the  $\Delta psbH/\Delta pam68$  strain after treatment with FeCh inhibitor.
- Supplemental Dataset. MS data—numbers of identified trypsin peptides for 2D gel protein spots.
- Received January 17, 2018; accepted February 7, 2018; published February 20, 2018.
- ## LITERATURE CITED
- Armbruster U, Zühlke J, Rengstl B, Kreller R, Makarenko E, Rühle T, Schünemann D, Jahns P, Weisshaar B, Nickelsen J, Leister D (2010) The *Arabidopsis* thylakoid protein PAM68 is required for efficient D1 biogenesis and photosystem II assembly. *Plant Cell* **22**: 3439–3460
- Bečková M, Gardian Z, Yu J, Koník P, Nixon PJ, Komenda J (2017) Association of Psb28 and Psb27 proteins with PSII-PSI supercomplexes upon exposure of *Synechocystis* sp. PCC 6803 to high light. *Mol Plant* **10**: 62–72
- Boehm M, Romero E, Reisinger V, Yu J, Komenda J, Eichacker LA, Dekker JP, Nixon PJ (2011) Investigating the early stages of photosystem II assembly in *Synechocystis* sp. PCC 6803: isolation of CP47 and CP43 complexes. *J Biol Chem* **286**: 14812–14819
- Boehm M, Yu J, Reisinger V, Bečková M, Eichacker LA, Schlodder E, Komenda J, Nixon PJ (2012) Subunit composition of CP43-less photosystem II complexes of *Synechocystis* sp. PCC 6803: implications for the assembly and repair of photosystem II. *Philos Trans R Soc Lond B Biol Sci* **367**: 3444–3454
- Chidgey JW, Linhartová M, Komenda J, Jackson PJ, Dickman MJ, Canniffe DP, Koník P, Pilný J, Hunter CN, Sobotka R (2014) A cyanobacterial chlorophyll synthase-HliD complex associates with the Ycf39 protein and the YidC/Alb3 insertase. *Plant Cell* **26**: 1267–1279
- Crawford TS, Eaton-Rye JJ, Summerfield TC (2016) Mutation of Gly195 of the ChlH subunit of Mg-chelatase reduces chlorophyll and further disrupts PS II assembly in a Ycf48-deficient strain of *Synechocystis* sp. PCC 6803. *Front Plant Sci* **7**: 1060
- D'Haene SE, Sobotka R, Bučinská L, Dekker JP, Komenda J (2015) Interaction of the PsbH subunit with a chlorophyll bound to histidine 114 of CP47 is responsible for the red 77K fluorescence of Photosystem II. *Biochim Biophys Acta* **1847**: 1327–1334
- Di Pietro F, Brandi A, Dzeladini N, Fabbretti A, Carzaniga T, Piersimoni L, Pon CL, Giuliodori AM (2013) Role of the ribosome-associated protein PY in the cold-shock response of *Escherichia coli*. *MicrobiologyOpen* **2**: 293–307
- Dobáková M, Sobotka R, Tichý M, Komenda J (2009) Psb28 protein is involved in the biogenesis of the photosystem II inner antenna CP47 (PsbB) in the cyanobacterium *Synechocystis* sp. PCC 6803. *Plant Physiol* **149**: 1076–1086
- Dobáková M, Tichý M, Komenda J (2007) Role of the PsbI protein in photosystem II assembly and repair in the cyanobacterium *Synechocystis* sp. PCC 6803. *Plant Physiol* **145**: 1681–1691
- Eaton-Rye JJ, Vermaas WFJ (1991) Oligonucleotide-directed mutagenesis of psbB, the gene encoding CP47, employing a deletion mutant strain of the cyanobacterium *Synechocystis* sp. PCC 6803. *Plant Mol Biol* **17**: 1165–1177
- Fleischmann TT, Scharff LB, Alkatib S, Hasdorf S, Schöttler MA, Bock R (2011) Nonessential plastid-encoded ribosomal proteins in tobacco: a developmental role for plastid translation and implications for reductive genome evolution. *Plant Cell* **23**: 3137–3155
- Frauenfeld J, Gumbart J, Sluis EO, Funes S, Gartmann M, Beatrix B, Mielke T, Berninghausen O, Becker T, Schulten K, Beckmann R (2011) Cryo-EM structure of the ribosome-SecYE complex in the membrane environment. *Nat Struct Mol Biol* **18**: 614–621
- Galmozzi CV, Florencio FJ, Muro-Pastor MI (2016) The cyanobacterial ribosomal-associated protein LrtA Is involved in post-stress survival in *Synechocystis* sp. PCC 6803. *PLoS One* **11**: e0159346
- Heinz S, Liauw P, Nickelsen J, Nowaczyk M (2016) Analysis of photosystem II biogenesis in cyanobacteria. *Biochim Biophys Acta* **1857**: 274–287
- Hennon SW, Soman R, Zhu L, Dalbey RE (2015) YidC/Alb3/Oxa1 family of insertases. *J Biol Chem* **290**: 14866–14874
- Hollingshead S, Kopečná J, Armstrong DR, Bučinská L, Jackson PJ, Chen GE, Dickman MJ, Williamson MP, Sobotka R, Hunter CN (2016) Synthesis of chlorophyll-binding proteins in a fully segregated  $\Delta ycf54$  strain of the cyanobacterium *Synechocystis* PCC 6803. *Front Plant Sci* **7**: 292
- Hollingshead S, Kopečná J, Jackson PJ, Canniffe DP, Davison PA, Dickman MJ, Sobotka R, Hunter CN (2012) Conserved chloroplast open-reading frame *ycf54* is required for activity of the magnesium protoporphyrin monomethylester oxidative cyclase in *Synechocystis* PCC 6803. *J Biol Chem* **287**: 27823–27833
- Knopková J, Sobotka R, Tichý M, Yu J, Koník P, Halada P, Nixon PJ, Komenda J (2014) Discovery of a chlorophyll binding protein complex involved in the early steps of photosystem II assembly in *Synechocystis*. *Plant Cell* **26**: 1200–1212
- Komenda J (2005) Autotrophic cells of the *Synechocystis psbH* deletion mutant are deficient in synthesis of CP47 and accumulate inactive PS II core complexes. *Photosynth Res* **85**: 161–167
- Komenda J, Lupínková L, Kopecký J (2002) Absence of the *psbH* gene product destabilizes photosystem II complex and bicarbonate binding on its acceptor side in *Synechocystis* PCC 6803. *Eur J Biochem* **269**: 610–619
- Komenda J, Reisinger V, Müller BC, Dobáková M, Granvogl B, Eichacker LA (2004) Accumulation of the D2 protein is a key regulatory step for assembly of the photosystem II reaction center complex in *Synechocystis* PCC 6803. *J Biol Chem* **279**: 48620–48629
- Komenda J, Sobotka R, Nixon PJ (2012) Assembling and maintaining the Photosystem II complex in chloroplasts and cyanobacteria. *Curr Opin Plant Biol* **15**: 245–251
- Kopečná J, Komenda J, Bučinská L, Sobotka R (2012) Long-term acclimation of the cyanobacterium *Synechocystis* sp. PCC 6803 to high light is accompanied by an enhanced production of chlorophyll that is preferentially channeled to trimeric photosystem I. *Plant Physiol* **160**: 2239–2250
- Kopečná J, Pilný J, Krynická V, Tomčala A, Kis M, Gombos Z, Komenda J, Sobotka R (2015) Lack of phosphatidylglycerol inhibits chlorophyll biosynthesis at multiple sites and limits chlorophyllide reutilization in the cyanobacterium *Synechocystis* 6803. *Plant Physiol* **169**: 1307–1017
- Kopf M, Klähn S, Scholz I, Matthiessen JK, Hess WR, Voß B (2014) Comparative analysis of the primary transcriptome of *Synechocystis* sp. PCC 6803. *DNA Res* **21**: 527–539
- Levey T, Westhoff P, Meierhoff K (2014) Expression of a nuclear-encoded *psbH* gene complements the plastidic RNA processing defect in the PSII mutant *hcf107* in *Arabidopsis thaliana*. *Plant J* **80**: 292–304
- Linhartová M, Bučinská L, Halada P, Ječmen T, Setlík J, Komenda J, Sobotka R (2014) Accumulation of the Type IV prepilin triggers degradation of SecY and YidC and inhibits synthesis of Photosystem II proteins in the cyanobacterium *Synechocystis* PCC 6803. *Mol Microbiol* **93**: 1207–1223
- Mitschke J, Georg J, Scholz I, Sharma CM, Dienst D, Bantscheff J, Voss B, Steglich C, Wilde A, Vogel J, Hess WR (2011) An experimentally anchored map of transcriptional start sites in the model cyanobacterium *Synechocystis* sp. PCC 6803. *Proc Natl Acad Sci USA* **108**: 2124–2129
- Nixon PJ, Michoux F, Yu J, Boehm M, Komenda J (2010) Recent advances in understanding the assembly and repair of photosystem II. *Ann Bot* **106**: 1–16
- Pilný J, Kopečná J, Noda J, Sobotka R (2015) Detection and quantification of heme and chlorophyll precursors using a High Performance Liquid Chromatography (HPLC) system equipped with two fluorescence detectors. *Bio Protoc* **5**: e1390
- Porra RJ, Thompson WA, Kriedmann PE (1989) Determination of accurate extinction coefficients and simultaneous equations for assaying chlorophylls a and b extracted with four different solvents: verification of the concentration of chlorophyll standards by atomic absorption spectroscopy. *Biochim Biophys Acta* **975**: 384–394
- Prinz A, Behrens C, Rapoport TA, Hartmann E, Kalies KU (2000) Evolutionarily conserved binding of ribosomes to the translocation channel via the large ribosomal RNA. *EMBO J* **19**: 1900–1906
- Promnares K, Komenda J, Bumba L, Nebesářová J, Vácha F, Tichý M (2006) Cyanobacterial small chlorophyll-binding protein ScpD (HliB) is located on the periphery of photosystem II in the vicinity of PsbH and CP47 subunits. *J Biol Chem* **281**: 32705–32713

- Rengstl B, Knoppová J, Komenda J, Nickelsen J** (2013) Characterization of a *Synechocystis* double mutant lacking the photosystem II assembly factors YCF48 and SII0933. *Planta* **237**: 471–480
- Rengstl B, Oster U, Stengel A, Nickelsen J** (2011) An intermediate membrane subfraction in cyanobacteria is involved in an assembly network for Photosystem II biogenesis. *J Biol Chem* **286**: 21944–21951
- Sachelaru I, Petriman NA, Kudva R, Kuhn P, Welte T, Knapp B, Drepper F, Warscheid B, Koch HG** (2013) YidC occupies the lateral gate of the SecYEG translocon and is sequentially displaced by a nascent membrane protein. *J Biol Chem* **288**: 16295–16307
- Seitl I, Wickles S, Beckmann R, Kuhn A, Kiefer D** (2014) The C-terminal regions of YidC from *Rhodospirella baltica* and *Oceanicaulis alexandrii* bind to ribosomes and partially substitute for SRP receptor function in *Escherichia coli*. *Mol Microbiol* **91**: 408–421
- Slavov N, Semrau S, Airolidi E, Budnik B, van Oudenaarden A** (2015) Differential stoichiometry among core ribosomal proteins. *Cell Reports* **13**: 865–873
- Sobotka R** (2014) Making proteins green; biosynthesis of chlorophyll-binding proteins in cyanobacteria. *Photosynth Res* **119**: 223–232
- Sobotka R, Komenda J, Bumba L, Tichý M** (2005) Photosystem II assembly in CP47 mutant of *Synechocystis* sp. PCC 6803 is dependent on the level of chlorophyll precursors regulated by ferrochelatase. *J Biol Chem* **280**: 31595–31602
- Umena Y, Kawakami K, Shen JR, Kamiya N** (2011) Crystal structure of oxygen-evolving photosystem II at a resolution of 1.9 Å. *Nature* **473**: 55–60
- Vavilin D, Brune DC, Vermaas W** (2005) <sup>15</sup>N-labeling to determine chlorophyll synthesis and degradation in *Synechocystis* sp. PCC 6803 strains lacking one or both photosystems. *Biochim Biophys Acta* **1708**: 91–101
- Wittig I, Karas M, Schägger H** (2007) High resolution clear native electrophoresis for in-gel functional assays and fluorescence studies of membrane protein complexes. *Mol Cell Proteomics* **6**: 1215–1225
- Xue S, Barna M** (2012) Specialized ribosomes: a new frontier in gene regulation and organismal biology. *Nat Rev Mol Cell Biol* **13**: 355–369





**9.4. Publication IV:** Awakening of a dormant cyanobacterium from nitrogen chlorosis reveals a genetically determined program.

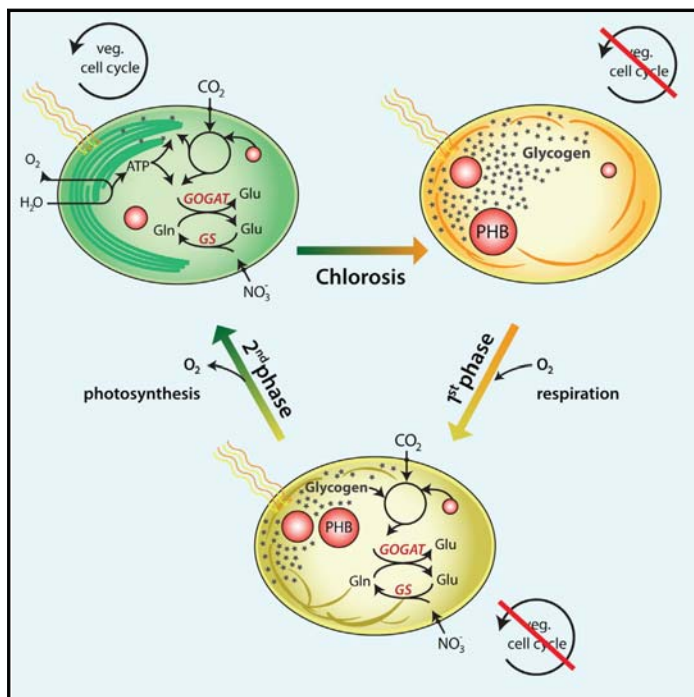
Klotz A, Georg J, **Bučinská L**, Watanabe S, Reimann V, Januszewski W, Sobotka R, Jendrossek D, Hess R W, Forchhammer K (2016).

*Curr Biol.* 26(21):2862-2872.

# Current Biology

## Awakening of a Dormant Cyanobacterium from Nitrogen Chlorosis Reveals a Genetically Determined Program

### Graphical Abstract



### Authors

Alexander Klotz, Jens Georg, Lenka Bučinská, ..., Dieter Jendrossek, Wolfgang R. Hess, Karl Forchhammer

### Correspondence

karl.forchhammer@uni-tuebingen.de

### In Brief

Klotz et al. present a detailed analysis of the cellular events during the awakening of a dormant bacterium. Resuscitation of a cyanobacterium from nitrogen chlorosis back to photosynthetically active life reveals a highly orchestrated program, with wide-ranging implications for our understanding of bacterial persistence and cellular aging.

### Highlights

- Awakening from nitrogen chlorosis is induced immediately upon the addition of nitrate
- Cells activate respiration/restore translational apparatus before photosynthesis begins
- Genes for major cellular processes are regulated in a highly orchestrated manner
- Microarray analysis reveals a major impact of regulatory RNAs

### Accession Numbers

GSE83363

# Awakening of a Dormant Cyanobacterium from Nitrogen Chlorosis Reveals a Genetically Determined Program

Alexander Klotz,<sup>1</sup> Jens Georg,<sup>2</sup> Lenka Bučinská,<sup>3,4</sup> Satoru Watanabe,<sup>5</sup> Viktoria Reimann,<sup>2</sup> Witold Januszewski,<sup>2</sup> Roman Sobotka,<sup>3,4</sup> Dieter Jendrossek,<sup>6</sup> Wolfgang R. Hess,<sup>2</sup> and Karl Forchhammer<sup>1,7,\*</sup>

<sup>1</sup>Interfaculty Institute of Microbiology and Infection Medicine Tübingen (IMIT), University of Tübingen, Auf der Morgenstelle 28, Tübingen 72076, Germany

<sup>2</sup>Faculty of Biology Genetics and Experimental Bioinformatics, University of Freiburg, Freiburg 79104, Germany

<sup>3</sup>Centre Algatech, Institute of Microbiology, Academy of Sciences of the Czech Republic, Třeboň 379 01, Czech Republic

<sup>4</sup>Faculty of Science, University of South Bohemia, České Budějovice 370 01, Czech Republic

<sup>5</sup>Department of Bioscience, Tokyo University of Agriculture, 1-1-1 Sakuragaoka, Setagaya-ku, Tokyo 156-8502, Japan

<sup>6</sup>Institute of Microbiology, University Stuttgart, Allmandring 31, Stuttgart 70569, Germany

<sup>7</sup>Lead Contact

\*Correspondence: [karl.forchhammer@uni-tuebingen.de](mailto:karl.forchhammer@uni-tuebingen.de)

<http://dx.doi.org/10.1016/j.cub.2016.08.054>

## SUMMARY

The molecular and physiological mechanisms involved in the transition of microbial cells from a resting state to the active vegetative state are critically relevant for solving problems in fields ranging from microbial ecology to infection microbiology. Cyanobacteria that cannot fix nitrogen are able to survive prolonged periods of nitrogen starvation as chlorotic cells in a dormant state. When provided with a usable nitrogen source, these cells re-green within 48 hr and return to vegetative growth. Here we investigated the resuscitation of chlorotic *Synechocystis* sp. PCC 6803 cells at the physiological and molecular levels with the aim of understanding the awakening process of a dormant bacterium. Almost immediately upon nitrate addition, the cells initiated a highly organized resuscitation program. In the first phase, they suppressed any residual photosynthetic activity and activated respiration to gain energy from glycogen catabolism. Concomitantly, they restored the entire translational apparatus, ATP synthesis, and nitrate assimilation. After only 12–16 hr, the cells re-activated the synthesis of the photosynthetic apparatus and prepared for metabolic re-wiring toward photosynthesis. When the cells reached full photosynthetic capacity after ~48 hr, they resumed cell division and entered the vegetative cell cycle. An analysis of the transcriptional dynamics during the resuscitation process revealed a perfect match to the observed physiological processes, and it suggested that non-coding RNAs play a major regulatory role during the lifestyle switch in awakening cells. This genetically encoded program ensures rapid colonization of habitats in which

nitrogen starvation imposes a recurring growth limitation.

## INTRODUCTION

Cyanobacteria are ubiquitous in the light-exposed biosphere, where they play major roles in global carbon and nitrogen cycles. In the course of evolution, they acquired sophisticated survival strategies that enable them to withstand unfavorable environmental conditions. A challenge that frequently limits growth in many terrestrial and aquatic ecosystems [1, 2] is the deprivation of usable sources of combined nitrogen, such as nitrate and ammonium. With respect to nitrogen use, cyanobacteria can be divided into two physiological groups: diazotrophic strains, which avoid nitrogen starvation by expressing nitrogenase to fix omnipresent gaseous N<sub>2</sub>, and non-diazotrophic strains, which stop growth in the absence of a combined nitrogen source and switch their metabolism from anabolism to maintenance [3]. This lifestyle switch starts with the degradation of photosynthetic pigments, known as chlorosis [4, 5], as the cells conspicuously change in color from blue-green to yellow (Figure 1) [6]. In the unicellular cyanobacterium *Synechococcus elongatus* PCC 7942 (hereafter *S. elongatus*), this process results in pale resting cells that are able to survive prolonged periods of starvation in a dormant-like state [7, 8].

Dormancy is widespread among prokaryotes, especially in nutrient-limited environments [9]. It has been proposed that dormant bacteria comprise a “seed bank,” i.e., a reservoir of cells that can be resuscitated by favorable conditions [10]. This mechanism contributes greatly to the fitness of bacterial populations and to the spreading of bacterial pathogens [11]. The molecular and cellular processes by which bacteria arrest growth, enter dormancy, and recover from the dormant stage are quite diverse among bacterial taxa, and they include the formation of endospores or exospores, encapsulated cysts, or apparently non-differentiated persister cells, as in

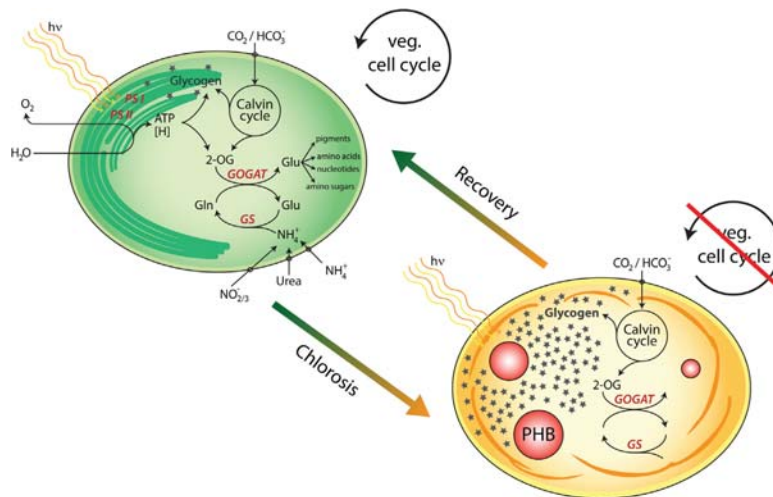


**Figure 1. Model of the Morphological and Metabolic Changes during Chlorosis Caused by Nitrogen Starvation**

During chlorosis, thylakoid membranes (green/yellow curved lines) are reduced and their composition changes, the vegetative cell cycle stops, and carbon polymers, e.g., glycogen (gray stars) and polyhydroxybutyrate (PHB, red dots), increase.

## RESULTS

### Resuscitation from the Chlorotic State Occurs in Two Phases

Prior to investigating the resuscitation of dormant *Synechocystis* cells from a chlorotic state, we first studied their viability and the accumulation of PHB and glycogen during prolonged nitrogen depletion for up to 42 days. For this, ni-

*Mycobacterium tuberculosis* [9]. To survive prolonged periods of starvation, non-differentiated resting cells maintain residual metabolic activity in a state occasionally termed quiescence [9]. Rapid resuscitation from dormancy is essential for ensuring the successful spread of bacterial populations, but this process is poorly understood.

The formation of dormant-like cyanobacterial cells has been studied in some detail in the non-diazotrophic freshwater strain *S. elongatus* [3, 7, 8] subjected to nitrogen starvation. The degradation of phycobiliproteins, the major light-harvesting pigments, is initiated by the *nbIA* product, whose expression is controlled by the *Nbl* regulatory system [12, 13]. While phycobiliproteins are degraded, the cells stop growth after a final cell division and concomitantly accumulate CO<sub>2</sub> fixation products as glycogen [4]. When nitrogen deficiency is prolonged, cells degrade the bulk of cellular proteins and the photosynthetic apparatus until they reach a final chlorotic stage. At this stage, they maintain a residual level of photosynthesis (~0.1% of initial activity) [8], which allows them to preserve full viability over at least 6 months.

A similar response specific to nitrogen deprivation also has been observed in the unicellular cyanobacterium *Synechocystis* sp. PCC 6803 (hereafter termed *Synechocystis*) [14, 15], which is a widely used model organism to study fundamental aspects of photosynthesis and cyanobacterial physiology. Under nitrogen deficiency, this strain produces a second carbon storage polymer, polyhydroxybutyrate (PHB), in addition to glycogen granules, and it was presumed that PHB might contribute in coping with chlorosis [16]. Preliminary results have indicated that *Synechocystis* also possesses the ability of long-term survival under nitrogen-deficient conditions, and chlorotic cultures are extremely efficient in recovering from chlorosis. This rapid recovery process provides a unique opportunity to study resuscitation of a dormant bacterium and thereby gain insights into a fundamental bacterial survival strategy. The aim of this study was to reveal the organization of resuscitation of chlorotic *Synechocystis* cells at the cellular and molecular level as an example of bacterial awakening from dormancy.

trate-grown cells were transferred into combined-nitrogen-free medium to initiate chlorosis. Of the two carbon reserves, glycogen started to accumulate almost immediately upon nitrogen depletion, and it reached a maximum of ~60% glycogen/cell dry weight after just 14 hr (Figure S1B). By contrast, accumulation of PHB proceeded much more slowly and only reached a maximum of 11%–13% PHB/cell dry weight after 14 days (Figure S1A). Nearly all cells remained viable for at least 42 days of nitrogen starvation and were able to rapidly recover following the addition of a nitrogen source, such as nitrate or ammonia (Figure S2).

Because the recovery of chlorotic cultures was highly reproducible, we investigated this process at the cellular and molecular levels to determine how dormant cells with only traces of residual photosynthetic activity can return to vegetative growth. Long-term chlorotic cells were resuscitated by adding nitrate to the medium. Typically, re-greening of chlorotic cells occurred within 48 hr, regardless of the lab strain used (three different strains were tested). No visual color change was observed during the first 12–16 hr. Thereafter, the color changed from yellow/orange to dark blue-green after 48 hr (Movie S1). Quantitatively, re-pigmentation, as shown by UV/Vis spectra of recovering cultures (Figure 2A), revealed that the absorbance at ~680/440 nm (indicative of chlorophyll *a/b*) and at 625 nm (indicative of phycobiliproteins) did not significantly increase during the first 8 hr of the recovery process. The first traces of chlorophyll and phycobiliproteins were detected after 15 hr. Complete pigmentation of exponentially growing cells was reached after 72 hr. Quantification of extracted chlorophyll (Figure 2B) confirmed the lack of significant increase during the first 12 hr of recovery. Cell density (optical density at 750 nm; Figure 3A) did not increase within the first 36 hr, which suggested that cells had not yet divided at that stage. Photosynthetic activity was initially estimated by pulse-amplitude-modulation (PAM) fluorometry, which measures chlorophyll fluorescence quantum yield from photosystem II (PSII) (Figure 2B) [17]. Fully developed chlorotic cells displayed only traces of PSII activity, as previously shown for *S. elongatus* [8]. Surprisingly, after the addition of

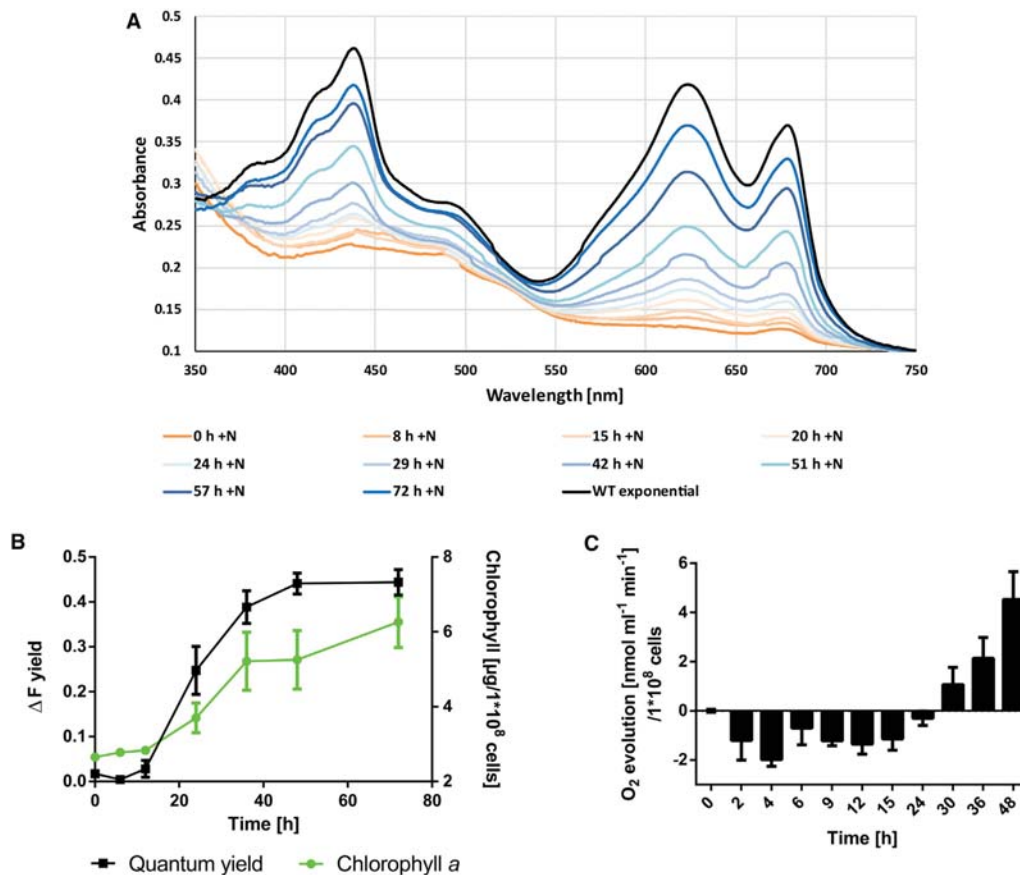


**Figure 2. Changes in Pigmentation, Photosystem II Quantum Yield, and Oxygen Consumption or Evolution during Resuscitation**

(A) Absorption spectra of a recovering *Synechocystis* culture during the course of resuscitation. Recovery was started by adding nitrate (0 hr). An exponentially growing culture (WT exponential) was used as a reference. Spectra were normalized to the same optical density at 750 nm of 0.1.

(B and C) Photosystem II quantum yield (B) as determined by pulse-amplitude-modulation (PAM) fluorometry and chlorophyll content (normalized to the cell density) and oxygen consumption/evolution (C, normalized to the cell density) during the course of recovery.

At least three biological replicates were performed and the SD was calculated. See also [Figure S2](#) and [Movie S1](#).

nitrate, quantum yields of PSII activity dropped to zero after 6 hr but resumed 6 hr later (12 hr of recovery). Subsequently, PSII quantum yield increased strongly until saturation at 48 hr of resuscitation.

To test whether respiration could support the recovery of chlorotic cells, we measured oxygen evolution or consumption of a culture starved for 1 month ([Figure 2C](#)). In chlorotic cells under standard illumination, traces of evolved oxygen due to residual photosynthesis were detected. However, 2 hr after nitrate addition cells began to consume oxygen despite illumination. After 4 hr cells reached maximal respiration, which they maintained at that level until 15 hr. Photosynthetic oxygen evolution was detected only after 24 hr, in agreement with the increase of PSII quantum yields and the re-appearance of photosynthetic pigments.

Chlorotic cells have two types of carbon reserves that could fuel initial respiration: PHB and glycogen. Previous studies have suggested that PHB could be important for recovery [16,

18], but we detected no significant decrease in PHB content during the first 24 hr of recovery, and PHB degradation did not start before the cells had resumed photosynthetic activity. We showed that PHB is indeed not required for the recovery of chlorotic *Synechocystis* cells by analyzing a PHB-free mutant deficient in the PHB biosynthesis enzyme PHB synthase ( $\Delta$ phaCE); the mutant recovered from a chlorotic state as quickly as the wild-type ([Figure S3](#)). Glycogen, which rapidly accumulates after nitrogen starvation and plays a major role in the transition to chlorosis [19], is the major source of carbon for respiration in the dark. Just 4 hr after the addition of nitrate, the glycogen content slightly but clearly decreased ([Figure 3B](#)) and continued to decrease while the cells were respiring. Glycogen consumption continued further from 24 hr on, as photosynthesis was activated, until the low glycogen level of exponentially growing cells was reached. These physiological studies revealed two phases of the resuscitation process. In the first phase, until ~16 hr, respiration is activated and is supported by glycogen. In the transition



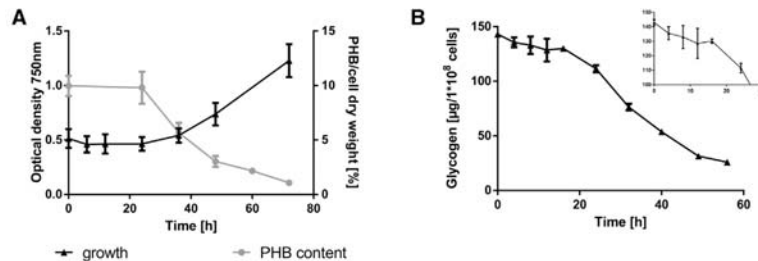


**Figure 3. Consumption of Carbon Polymers during Resuscitation**

Growth (optical density at 750 nm) and PHB content (normalized to cell dry weight; w/w) (A) and glycogen consumption (B) during resuscitation of a culture of chlorotic cells. The result of one of three biological replicates (each determined in technical triplicates) is shown. The inset shows a magnification of the first 30 hr of resuscitation. At least three biological replicates were performed, and the SD was calculated. See also [Figures S1–S4](#).

to the second phase, photosynthetic activity rises in parallel to the re-pigmentation of cells. In the second phase, glycogen continues to provide cells with carbon skeletons as photosynthesis takes over cellular energy supply.

### Structural Changes during Resuscitation

To visualize the morphological changes of cells during recovery, we took transmission electron micrographs of ultrathin cryosections of exponentially growing cells ([Figure 4F](#)), starved cells (>1 month; [Figure 4A](#)), and cells at different stages of resuscitation ([Figures 4B–4E](#); [Figure S5](#)). A major feature of fully developed chlorotic cells ([Figure 4A](#)), compared to growing cells ([Figure 4F](#)), is the almost complete absence of photosynthetic thylakoid membranes; the cells are instead completely filled with glycogen granules. These structures disappeared during resuscitation. In cells sampled after 24 hr of recovery ([Figure 4B](#); [Figure S5](#)), thylakoid membranes started to reappear in an amorphous cytosol. PHB granules were not yet degraded, and granules resembling cyanophycin (multi-L-arginyl-poly-L-aspartate, a transient nitrogen storage polymer [20, 21]) were occasionally observed during recovery ([Figures 4B and 4E](#); [Figure S5](#)). After 36 hr of recovery, cells had reconstituted thylakoid membranes in parallel stacks, but they still contained PHB, in agreement with its quantification. Glycogen granules mostly vanished, and carboxysomes (polyhedral microcompartments filled with ribulose-1,5-bisphosphate carboxylase/oxygenase [RuBisCO] and carbonic anhydrase [20]) became visible.

Ribosomes appear in transmission electron micrographs as electron-dense particles. The central part of the cytoplasm of vegetatively growing cells contains densely packed and evenly distributed particles resembling ribosomes, but only very few were visible in chlorotic cells. However, after just 24 hr, the number of ribosomes strongly increased, and after 36 hr, the central part of the cytoplasm seemed to be rich in ribosomes. Cells imaged after 48 hr of recovery had almost completely re-established thylakoid membranes, and a structure resembling lipid bodies was visible. After 66 hr of recovery, the cells resembled exponentially growing cells.

We continuously followed the re-formation of thylakoid membranes in recovering cells by taking advantage of the red chlorophyll autofluorescence of these membranes visualized by time-lapse fluorescence microscopy ([Movie S2](#)). *Synechocystis* cells, nitrogen starved for 14 days, were mounted on microscope slides and provided with nitrate as a nitrogen source. Almost no autofluorescence was visible until 12 hr of recovery. Thereafter, autofluorescence gradually increased like scattered clouds, distributing slowly over the entire cell. From 20 hr on,

autofluorescence increased dramatically until the entire cell was completely fluorescent red, i.e., until the thylakoid membranes had completely redeveloped.

Like most cyanobacteria, *Synechocystis* cells are polyploidic, with an estimated 4–20 chromosome copies per cell, depending on the lab strain and conditions [22, 23]. We followed the cell size ([Figure 5A](#)) and cellular DNA content ([Figure 5B](#)) during the recovery from chlorosis of cultures at different phases of growth using flow cytometry. In exponentially growing, non-chlorotic cells, the distribution of the number of chromosomes per cell was quite narrow, with most cells having five to six chromosomes per cell. In long-term chlorotic cells, i.e., nitrogen starved for 1 month, the distribution was broader, ranging from approximately two up to 16 chromosomes per cell and with most cells having approximately nine copies per cell. After 48 hr of recovery in the presence of nitrate, the distribution was still relatively broad, but the peak shifted toward six to seven copies per cell; after 92 hr of recovery, the distribution narrowed, with most cells having approximately five copies per cell and none having more than ten copies per cell. The cell size decreased correspondingly with the reduction in DNA content per cell. Apparently, initial cell division after recovery led to a reduction in cell size and partitioning of chromosomes, resulting in growing cells with an average of half the DNA content of chlorotic cells.

### The Transcriptome of Resuscitating Cells

To gain a deeper insight into the complex process of resuscitation, we analyzed the transcriptome of recovering cells using a high-density microarray ([Data S1, S2, and S3](#); GEO: GSE83363), with probes covering the entire chromosome and all seven plasmids with an orientation for the direct hybridization of total RNA, thereby avoiding the pitfalls of cDNA synthesis. The arrays were designed to include probes for all 8,916 transcripts previously detected in extensive transcriptome studies [24, 25]. Total RNA was extracted from exponentially growing cells and from cells nitrogen starved for 14 days and at four time points during recovery (4, 12, 24, and 48 hr after the addition of nitrate, three biological replicates each). All signals were normalized to that of exponentially growing cells, i.e., the fold changes in transcript levels were relative to the transcript abundance in exponentially growing cells.

During the process of resuscitation, the level of 1,570 transcripts, corresponding to 17.6% of the entire transcriptome, significantly changed by at least 1.8-fold ([Table 1](#); [Figure 6](#)). Of these, 780 transcripts increased in abundance and 790 transcripts decreased in abundance. According to the time course of the changes, these positively and negatively responding



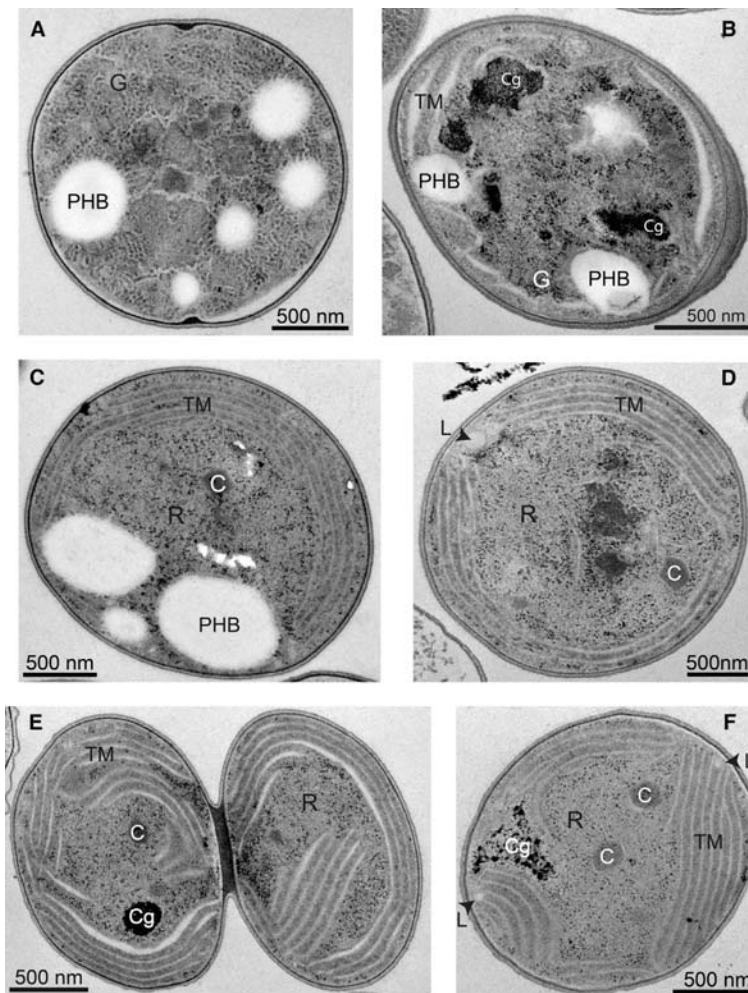


**Figure 4. Morphological Analysis via Transmission Electron Micrographs of *Synechocystis* Cells during Nitrogen Starvation and Resuscitation**

(A) Chlorotic cell starved for 1 month. (B–E) Cells during the course of resuscitation at 24 hr (B), 36 hr (C), 48 hr (D), and 66 hr (E). (F) Cell in the exponential growth phase. G, Glycogen granules; PHB, polyhydroxybutyrate granules; Cg, cyanophycin granules; C, carboxysomes; TM, thylakoid membranes; R, ribosomes; L, lipid bodies. See also [Figure S5](#) and [Movie S2](#).

[26]. Eighty transcripts encoded hypothetical or unknown proteins. Nearly the entire translational apparatus (all ribosomal proteins, translation factors, chaperones, and preprotein translocases) on 80 transcripts was induced early (P1) or over-induced after 4 and 12 hr. Other P1 transcripts included those for nitrate/nitrite assimilation factors, molybdopterin biosynthesis (*moa* cluster), ATP synthases, CO<sub>2</sub> fixation (carboxysome and RuBisCO), redox/electron transport, and sulfate assimilation.

P2 transcripts included those associated with the photosystems (primarily PSI), phycobilisomes, and chlorophyll biosynthesis, in agreement with the onset of photosynthetic activity. Others included those for glutamine synthetase-inactivating factors IF7 and IF17, putative transposases, and CRISPR-associated transcripts.

P3 transcripts included those associated with hypothetical proteins and cell division (*amiC* and *nlpD*).

As in the P1 group, asRNAs and non-coding transcripts were also the most abundant classes in groups P2 and P3.

transcripts could be classified into three major groups, reflecting the chronological order of transcriptome remodeling during resuscitation. Strikingly, the early-responding genes (4 hr after onset of recovery) comprised the largest group of both upregulated (425) and repressed genes (626), which impressively demonstrates that chlorotic cells are capable of immediate recovery. Since transcripts encoding hypothetical proteins comprise the largest category, their phylogenetic distribution was analyzed ([Data S4](#)).

The three major groups of positively responding transcripts were defined as those induced after 4 hr (P1), which could be further split into subgroups P1a and P1b, with P1b displaying a transient over-induction; those induced after 12 hr (P2); and those induced after 24 or 48 hr (P3). A clearly organized, step-wise restoration of defined cellular activities was reflected at the level of transcriptome dynamics.

The largest class of P1 transcripts, with a total of 106 transcripts, were antisense RNAs (asRNAs) and transcripts categorized as non-coding, although some of these might encode small peptides

This suggests that asRNAs and non-coding transcripts have important regulatory functions during the entire resuscitation process.

An even larger number of transcripts was downregulated during resuscitation and was likewise grouped into groups N1 and N2 according to their time course. N1 transcripts were subdivided into two subgroups: N1a (557 transcripts downregulated after 4 hr) and N1b (69 transcripts, rapidly but only transiently repressed after nitrate addition). N2 transcripts (164 transcripts) were downregulated only after 12 hr and none of the transcripts were downregulated later than after 12 hr. Most of the downregulated transcripts were abundant in chlorotic cells; therefore, the respective genes could have important functions during long-term starvation and might function in survival during “standby” dormancy.

The largest class of N1 transcripts (468 transcripts) was asRNAs, other non-coding transcripts, and those encoding hypothetical or unknown proteins. This impressive abundance of mostly non-characterized transcripts demonstrates our lack

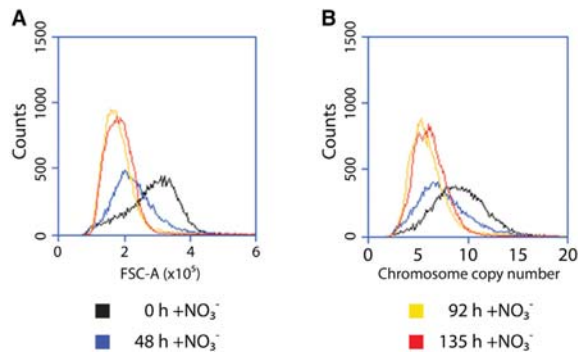


**Figure 5. Determination of Cell Size and Chromosome Number during Resuscitation**

Flow cytometry of chlorotic cells recovering from 1 month of nitrogen starvation to determine cell size (A) and chromosome copy number (B), measured as the amount of DNA. Recovery started with the addition of nitrate at 0 hr; cultures at 135 hr grew exponentially.

of knowledge of the biology of long-term-starved cells. Immediately after the initiation of resuscitation, the cells had to switch off expression of those transcripts that were abundant during chlorosis, as they might interfere with the resuscitation program. An intriguing example is asRNA *slr0653-as4*, which acts on the housekeeping sigma factor SigA. It is one of the most highly induced transcripts under chlorosis (>30-fold induced). Its level decreased 6.7-fold after only 4 hr, thereby releasing inhibition of *sigA* gene expression. Another interesting example is the highly repressed SyR7 asRNA, which is complementary to the *murF* 5' UTR and is possibly involved in the regulation of murein biosynthesis [27]. Other transcripts within this group encoded transposases, PHB-associated genes, and the proteolysis adaptor proteins NblA1/2. The majority of protease-encoding genes was induced during chlorosis and repressed during resuscitation; four of these belong to group N1 (see [Data S3](#)).

Similar to N1a, subgroup N1b mainly consisted of asRNAs, non-coding transcripts, and transcripts encoding hypothetical or unknown proteins. Moreover, glycolytic and oxidative pentose phosphate (OPP) pathway-associated transcripts were upregulated during nitrogen starvation and were transiently reduced during recovery.

Group N2 also was dominated by non-coding RNAs and transcripts encoding hypothetical or unknown proteins. Two identified non-coding RNAs with known function are NsiR4 and PsrR1. These RNAs were still highly expressed after 4 hr and were tuned down only after 12 hr. NsiR4 inhibits expression of *gifA*, which encodes the glutamine-synthetase-inactivating factor IF7 [28]. NsiR4 expression during nitrogen stress and 4 hr into resuscitation prevented *gifA* expression, thereby providing optimal glutamine synthetase activity for nitrogen assimilation. The high accumulation of the asRNA SyR1/PsrR1 during nitrogen stress, which remained high at least 4 hr into resuscitation, is consistent with its inhibitory function on the expression of genes encoding several photosynthetic and pigment biosynthesis proteins, including phycobiliproteins [29]. Its downregulation after 12 hr agrees with the subsequent transcription of PSI-related genes, and it fits with the delayed reappearance of

photosynthetic activity. Interestingly, the N2 group also included CRISPR1-associated transcripts and high-light-inducible (*hli*) polypeptides. The protein products are stress related, which indicates that the stress that caused and maintained enhanced CRISPR and *hli* expression was relieved after 12 hr. Transcript levels of the type 2 NADH dehydrogenase subunits *ndaA/B* significantly increased during chlorosis and decreased during recovery, which is indicative of metabolic rewiring.

## DISCUSSION

This study provides the first insights into an unexplored process, the resuscitation of a dormant cyanobacterium from chlorosis. Recovery of chlorotic cells appears to follow a strictly orchestrated and highly reproducible program. Evidently, *Synechocystis* is perfectly equipped with a response system that allows long-term survival under non-growth conditions. The majority of chlorotic cells remain viable and rapidly respond to the re-addition of a nitrogen source. The yield of extracted mRNA indicated that cells in chlorosis have an overall transcript abundance that is similar to that of growing cells. Therefore, reduced transcriptional activity might be compensated for by increased mRNA stability, a phenomenon observed in various growth-arrested microorganisms [9]. In the fully developed chlorotic state, the translational machinery is reduced to an absolute minimum, and these transcripts are among the most strongly repressed of the entire transcriptome. This finding agrees with the lack of ribosomes detected in electron micrographs, and it correlates with a previous study on long-term-starved *S. elongatus* cells, where labeling experiments demonstrated a barely detectable residual level of protein synthesis [8]. This indicates that most transcripts in chlorotic cells are translationally inactive. The highly abundant functionally characterized non-coding regulatory small RNAs, such as PsrR1 and NsiR4 [28, 29], as well as the asRNAs to *sigA* (*slr0653-as4*), the carboxysome operon (*sll1028-as* and *sll1029-as*), and the ATP-synthase operon (*sll1321-as2* and *sll1326-as*), were anti-correlated to their sense mRNAs. Therefore, they most likely play an important regulatory role in stabilizing this state. In comparison, transcript levels of the most classical global transcriptional regulators, such as sigma factors or certain response regulators, were only weakly changed compared to levels in growing cells.

When resuscitation starts with nitrate addition, a logical response was observed at the transcript level. Cells first reinstall the machinery for protein synthesis and nitrate assimilation (*narB*; *nir* operon; *moa* gene cluster for the molybdenum cofactor of nitrate reductase). The transcripts for all subunits of F<sub>1</sub>F<sub>0</sub>-ATPase were also turned on early, which implies that the entire F-type ATPase machinery was rebuilt de novo. In dormant cells in the absence of anabolic reactions and with low protein synthesis, almost no ATP is consumed. Therefore, the synthesis of ATP is reduced and the F<sub>1</sub>F<sub>0</sub>-ATPase is tuned down. During resuscitation, the need for ATP increases dramatically because the entire recovery process requires energy.

The first phase of resuscitation is energetically supported by respiration. Despite illumination, oxygen consumption started rapidly after the addition of nitrate, overcoming the Kok effect (inhibition of respiration by light). Glycogen catabolism appeared to contribute to a large part of the respiratory activity. Comparison

**Table 1. Overview of Transcripts that Responded Positively or Negatively during the Process of Recovery, Sorted into Functional Categories**

Transcript Category	Number of Transcripts
Early Positively Responding Transcripts (Group P1a)	216
AsRNAs and other non-coding transcripts	59
Hypothetical/unknown proteins	44
Carboxysome and RuBisCO associated	11
ATP synthase associated	9
Redox associated, electron transport	7
Translational machinery (ribosomal proteins, translation factors, etc.)	6
Tetrapyrrole biosynthesis	5
Photosystem associated	5
Glycolysis and pentose phosphate pathway associated	3
Nitrate/nitrite assimilation	3
Early Positively Responding Transcripts with Transient Over-induction (Group P1b)	209
Translational machinery (ribosomal proteins, translation factors, and such)	74
AsRNAs and other non-coding transcripts	47
Hypothetical/unknown proteins	36
Nitrate/nitrite assimilation and molybdopterin biosynthesis ( <i>moa</i> cluster)	13
Sulfate transport system	4
Tetrapyrrole biosynthesis	2
Slightly Delayed Positively Responding Transcripts (Group P2)	261
Hypothetical/unknown proteins	86
AsRNAs and other non-coding transcripts	44
Photosystem (primarily PSI) associated	21
CRISPR associated	14
Putative transposases	14
Phycobilisome associated	12
Tetrapyrrole biosynthesis	9
GS regulation ( <i>gif</i> genes)	2
Late Positively Responding Transcripts (Group P3)	94
AsRNAs and other non-coding transcripts	32
Hypothetical/unknown proteins	30
<i>amiC/nlpD</i>	2
Early Negatively Responding Transcripts (Group N1a)	557
AsRNAs and other non-coding transcripts	257
Hypothetical/unknown proteins	166
Putative transposases	35
CRISPR associated	13
PHB associated	5
<i>nblA1/2</i>	2
Early Negatively Responding Transcripts, Transiently Repressed (Group N1b)	69
AsRNAs and other non-coding transcripts	26
Hypothetical/unknown proteins	19

**Table 1. Continued**

Transcript Category	Number of Transcripts
Glycolysis and pentose phosphate pathway associated	5
Photosystem (primarily PSII) associated	3
Delayed Negatively Responding Transcripts (Group N2)	164
AsRNAs and other non-coding transcripts	65
Hypothetical/unknown proteins	39
CRISPR associated	31
High-light-inducible ( <i>hli</i> ) polypeptides	4

Positively responding transcripts (threshold: 1.8-fold increase compared to previous time point) are grouped as follows: P1, induced already after 4 hr of recovery (subdivided in P1a and P1b, with the latter subgroup containing transcripts that were transiently over-induced in the early phase of recovery); P2, responding after 12 hr of recovery; and P3, responding in the second phase of recovery (24 and 48 hr). In total, 780 transcripts were induced during resuscitation. Negatively responding transcripts (threshold: 1.8-fold decrease compared to previous time point) are grouped as follows: N1a, repressed already after 4 hr recovery time and decreasing to a basal level; N1b, transient repression after 4 hr recovery; and N2, repressed after 12 hr recovery time. In total, 790 transcripts were repressed during resuscitation as compared to chlorotic cells. See also [Data S1](#), [S2](#), [S3](#), and [S4](#).

of the respiration rate and glycogen degradation (see calculation in the [Supplemental Experimental Procedures](#)) revealed that glycogen consumption accounts for about half of the respiratory activity. By contrast, PHB seemed to be dispensable, which renders its physiological role in the survival of chlorotic cells elusive. Activation of respiration coincided with the disappearance of detectable PSII activity. In agreement, several PSII-related genes were transiently repressed early during resuscitation ([Data S3](#)). Remarkably, the level of the small regulatory RNA *PsR1*, which was high during chlorosis and specifically suppresses chlorophyll biosynthesis, PSI, and phycobilisome gene expression [29], remained high at 4 hr of recovery and was only later downregulated. Likewise, the transient 8-fold upregulation of the *slI0617-as* transcript (asRNA of the *VIPP1* transcript) and the concomitant downregulation of the *slI0617* transcript could specifically prevent photosystem biogenesis at the thylakoid membranes [30] during the first few hours of recovery.

Activation of glycogen degradation seems to be controlled mainly at the post-transcriptional level. Response regulator *Rre37*, a global activator of sugar catabolic genes [31, 32], showed inverse transcriptional dynamics to glycogen degradation; the *rre37* transcript was induced 9-fold during chlorosis, whereas this level decreased during resuscitation. Similarly, transcripts encoding the glycogen-degrading enzymes (*slI1356*, *slr1367*, *slI0158*, *slr0237*, and *slr1857*) decreased during recovery. A concordant behavior was observed for the transcripts required for glucose catabolism via the OPP, Entner-Doudoroff (ED) [33], and Embden-Meyer-Parnas (EMP) pathways. For example, transcripts for glucose 6-phosphate dehydrogenase (*zwf* and *opcA*), which leads toward OPP and ED pathways, as well as transcripts for phosphofructokinase *Pfk1* (*slI1196*) and *Pfk2* (*slI0745*), which lead toward the EMP pathway, decreased



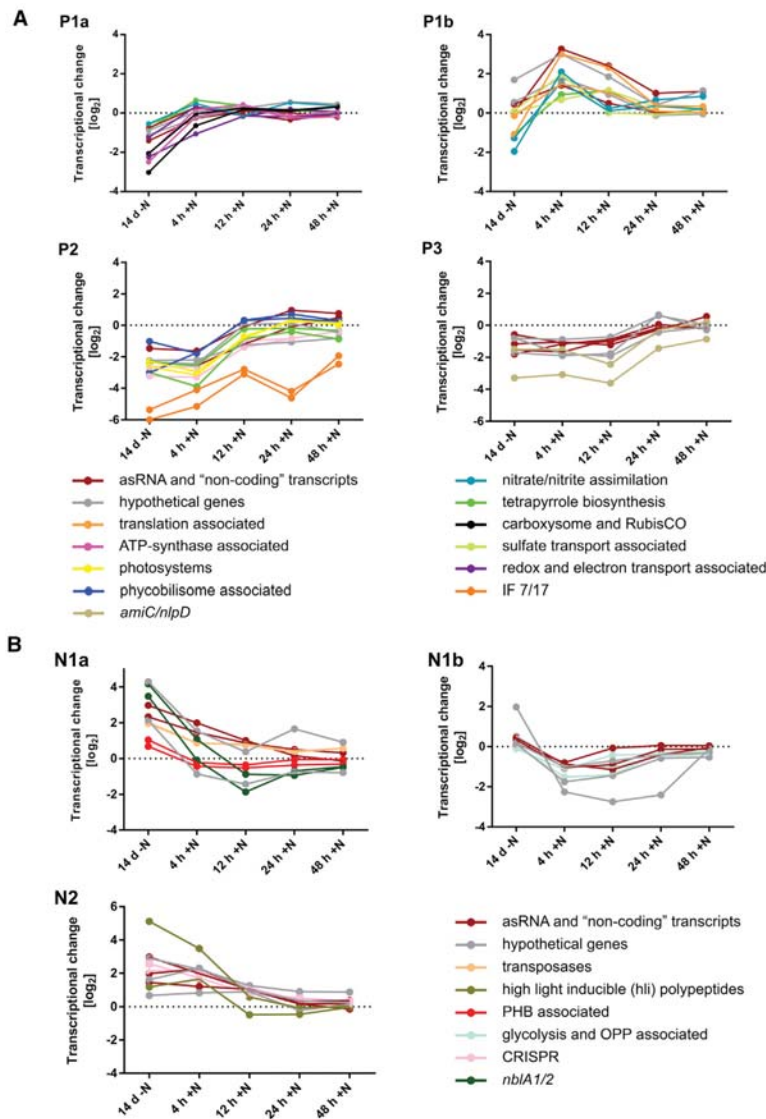


**Figure 6. Graphical Depiction of the Positively and Negatively Responding Transcripts Grouped According to the Time Course of Response**

(A) Representation of the major transcript groups responding positively during recovery from nitrogen starvation, sorted into functional categories. P1 transcripts increased at least 1.8-fold after only 4 hr and are divided into subgroups P1a and P1b. P1b transcripts transiently increased. P2 transcripts increased after 12 hr. P3 transcripts increased after 24 or 48 hr of recovery.

(B) Representation of the major transcript groups responding negatively during recovery from nitrogen starvation, sorted into functional categories. N1a transcripts decreased at least 1.8-fold after 4 hr and remained at the lower levels. N1b transcripts decreased early but only transiently. N2 transcripts decreased at least 1.8-fold after 12 hr.

In (A) and (B), the log<sub>2</sub> fold change of abundance of selected transcripts of the different functional categories is plotted against time of recovery. See also [Data S1](#), [S2](#), [S3](#), and [S4](#).

The sulfate assimilation operon (*slr1452-slr1455*) was turned on early, which reflects the need to synthesize the amino acids methionine and cysteine. In particular, methionine supply is critical for translation initiation. Overall, the first phase of resuscitation appears to be the re-installation of the central cellular processes revolving around protein biosynthesis that were strongly diminished during long-term chlorosis. Tight transcriptional repression of the protein biosynthesis machinery is a hallmark of the starvation-induced stringent response in bacteria, and its reversal seems to be key to the resuscitation program.

The second phase of resuscitation was characterized by the reconstitution of the photosynthetic apparatus. This was revealed at all levels of analysis, including the time course of re-pigmentation, reappearance of PSII activity and photosynthetic oxygen evolution, reappearance of thylakoid membranes, and expression of genes coding for components of the photosynthetic apparatus. Re-constitution of the photosynthetic apparatus creates a high metabolic burden to cells: they must synthesize the thylakoid membranes (which requires lipids), and they require large amounts of tetrapyrroles and all of the proteins of the photosynthetic apparatus, from reaction centers to peripheral antennae ([Data S3](#)). These processes can only start once the central machinery for protein synthesis and assimilatory reactions is fully functional. An increase in transcripts for phycobilisomes, PSI subunits, and most enzymes of the tetrapyrrole pathway at 12 and 24 hr of recovery explains the ensuing photosynthetic activity after 24-hr recovery.

in the first phase of recovery. This response implies that the enzymes for glycogen catabolism already accumulate during chlorosis, agreeing with a previous transcriptome analysis [5]. Apparently, cells prepare glycogen mobilization during its initial accumulation, which enables them to immediately start glycogen utilization when necessary. Notably, the genes encoding RuBisCo components were also among the early-induced genes, despite photosynthesis and net CO<sub>2</sub> fixation only being restored later. According to a reconstruction of *Synechocystis* primary metabolism, the amino acid glycine is produced from glyoxylate as a by-product of RuBisCo photorespiratory activity [34]. Therefore, oxygenation activity of RuBisCo might be immediately required for glycine biosynthesis, before its primary function for CO<sub>2</sub> fixation is needed when photosynthesis restarts.

thetic oxygen evolution, reappearance of thylakoid membranes, and expression of genes coding for components of the photosynthetic apparatus. Re-constitution of the photosynthetic apparatus creates a high metabolic burden to cells: they must synthesize the thylakoid membranes (which requires lipids), and they require large amounts of tetrapyrroles and all of the proteins of the photosynthetic apparatus, from reaction centers to peripheral antennae ([Data S3](#)). These processes can only start once the central machinery for protein synthesis and assimilatory reactions is fully functional. An increase in transcripts for phycobilisomes, PSI subunits, and most enzymes of the tetrapyrrole pathway at 12 and 24 hr of recovery explains the ensuing photosynthetic activity after 24-hr recovery.

The reconstitution of the PSII apparatus is subject to a complex regulation, with the expression of the assembly factors Ycf48 and PsbZ (P1 group) preceding the induction of the accessory PSII components L and J and the cyt *b559* components PsbE and PsbF. However, transcripts for large PSII core subunits did not decrease during chlorosis. The *psbD2* gene, which encodes a UV-stress-induced paralogue of the D2 protein in the PSII reaction center [35], was even 3-fold upregulated during chlorosis. This might reflect the intrinsic instability of the PSII reaction center, and, in order to maintain the minimum level of residual photosynthetic activity during chlorosis, permanent turnover has to be maintained. The biogenesis of thylakoid membranes requires a precise co-regulation between chlorophyll biosynthesis and translation and assembly of photosystems to prevent accumulation of free (phototoxic) tetrapyrroles. Ferrochelatase is the key regulator of the entire tetrapyrrole pathway, which includes heme and chlorophyll formation [36]. Heme, the product of ferrochelatase, controls the total flow through the pathway via a negative feedback loop. The ferrochelatase transcript (*hemH*) increases during nitrogen starvation and, during resuscitation, it decreases slowly. On the other hand, the transcript levels of light-dependent and light-independent protochlorophyllide reductase (*por* and *chlB*, *chlL*, and *chlN* genes), which leads to protochlorophyllide, were repressed during chlorosis and were induced only in the second phase. Repression of the *chlL/N* operon might be aided by the overlapping antisense 3' end of the *sl0733* transcript. Intriguingly, *chlL* expression was even further repressed at the early stage of resuscitation and activated only after 12 hr. This might ensure chlorophyll synthesis only during the second phase of resuscitation, simultaneously with the reappearance of chlorophyll-carrying proteins. Notably, ChlG, which converts toxic chlorophyllide into chlorophyll, is regulated similarly as ferrochelatase. This coherent regulation might ensure that toxic chlorophyllide cannot accumulate.

The assimilation of nitrogen through the GS-GOGAT cycle is mainly controlled by glutamine synthetase inhibitory factors IF7 and IF17 (*gif* genes), which are subject to a complex regulatory cascade [37, 38]. The IF1 and IF17 factors are among the most strongly repressed genes in chlorotic cells, in part caused by the detected high levels of the non-coding RNA NsiR4, which inhibits *gifA* expression [28]. This is reasonable because glutamine synthetase should not be repressed at all so that ammonia can be immediately scavenged from ambient nitrogen sources. In the course of resuscitation, *gif* transcript abundance gradually increased, which indicated a concomitant return to nitrogen homeostasis. This perfectly matches downregulation of NsiR4 after 12 hr, and it suggests that, at this time point, the transcription factor NtcA no longer activates NsiR4 transcription as it does during nitrogen limitation [28]. The activity of NtcA is activated by high 2-oxoglutarate levels [39–41], which suggests that at 12 hr this central metabolite, the precursor of glutamate synthesis, has returned to steady-state levels.

Forty-eight hours after the addition of nitrate, the majority of the cells had almost completely recovered the photosynthetic apparatus. Only at that time point did the cells begin to divide again, whereas as long as the photosynthetic machinery was not completely reinstalled, cell growth was suspended. Similarly, genes for the cell division proteins *amiC* and *nlpD* [42] were induced late during resuscitation. The results of flow cytometry

analysis of cultures indicated that cell division beginning at the end of resuscitation results in a diminished average cell size, which indicates a reductive cell division. The average ploidy level in chlorotic cells was almost double that of vegetatively growing cells, and in the DNA content did not increase during resuscitation. This suggested that chlorotic cells are arrested in a pre-divisional stage of the cell cycle in which DNA replication is complete, but cells have not yet divided. The transmission electron micrograph of a chlorotic cell (Figure 4A) is typical for the chlorotic state. It shows two invagination points at opposing positions of the cell periphery, where the cell septum is usually formed. The increased ploidy might serve as a reservoir of genetic information, similar to increased ploidy observed in akinetes (spore-like resting cells of filamentous cyanobacteria) [43]. This ensures the maintenance of intact genetic information in case of increased damage during dormancy [44], and, furthermore, it accelerates the restart of cell division. Intriguingly, the product of early-induced transcript *sl0505* shows homology to DNA integrity-scanning protein DisA from *Bacillus subtilis*, a checkpoint protein at the onset of sporulation [45]. Here it might control integrity of the chromosomes during resuscitation.

Altogether, the study of resuscitation from chlorosis provides an exceptional experimental system to address fundamental questions, such as how photosynthetic membranes are assembled de novo, how metabolic pathways are integrated under non-equilibrium conditions, and how non-coding RNAs orchestrate global gene expression during lifestyle transition. Furthermore, it sheds light on possible functions of unexplored hypothetical proteins. Gupta and Mathews [46] identified 39 signature proteins of cyanobacteria, and, notably, 13 of these (33%) were significantly regulated during resuscitation (Data S4). With the identification of major cellular processes and the transcriptional dynamics during resuscitation, this study sheds light on the existence of a sophisticated genetic program that guides the awakening of a dormant bacterium. Herewith it provides the framework for future investigations targeting the regulatory mechanisms executing this program.

## EXPERIMENTAL PROCEDURES

A detailed description of the experimental procedures is given in the [Supplemental Experimental Procedures](#).

### Cultivation Conditions

*Synechocystis* strains used in this study were propagated in BG11 medium supplemented with 5 mM NaHCO<sub>3</sub> [47], grown under continuous illumination with 40–50 μE at 27°C. Nitrogen starvation was induced as described previously [16], and the culture was adjusted to an optical density 750 (OD<sub>750</sub>) of 0.4. Recovery was initiated by transferring chlorotic cells into BG11 medium at an OD<sub>750</sub> of 0.4.

### Physiological Analysis

Glycogen was determined according to Gründel et al. [19] with some modifications [48]; intracellular PHB was quantified as described previously [16]. PSII quantum yield, respiration, and oxygen evolution were determined according to Dai et al. [49]. Methanol-extracted chlorophyll *a* was determined by fluorescence spectroscopy; fluorescence-activated cell sorting (FACS) analyses were performed according to [27].

### RNA Extraction

RNA was extracted via the PGTX method adapted from Pinto et al. [50]. The integrity of the resulting RNA was visually inspected on denaturing RNA

gels, and the quality of the experimental approach was verified by northern blot hybridizations targeting *cpcA*.

#### Transcriptomic Analyses

A high-resolution microarray manufactured by Agilent (format 8 × 60K; slide layout = IS-62976-8-V2) was used. The orientation of probes allows the direct hybridization of total RNA without conversion into cDNA. This array contains probes for all annotated genes as well as all other transcripts identified in the course of comprehensive RNA sequencing studies [24, 25]. The threshold for significant differentially expressed genes was  $|\log_2 \text{FC}| \geq 0.85$  and adjusted p value  $\leq 0.05$ .

#### Transmission Electron Microscopy

Cells were pelleted, cryofixed, and frozen under high pressure using a Leica EM Pact2 freezing device. Further preparation steps are described in the [Supplemental Experimental Procedures](#). Images were acquired using a transmission electron Jeol 1010 microscope equipped with a Mega View III camera (SIS) operated at 80 kV (Biology Centre Czech Academy of Sciences).

#### ACCESSION NUMBERS

The accession number for the microarray data reported in this paper is GEO: GSE83363.

#### SUPPLEMENTAL INFORMATION

Supplemental Information includes Supplemental Experimental Procedures, five figures, two movies, and four data files and can be found with this article online at <http://dx.doi.org/10.1016/j.cub.2016.08.054>.

#### AUTHOR CONTRIBUTIONS

A.K. performed physiological experiments and extracted RNA. J.G. and V.R. performed microarray analysis and analyzed data. W.J. designed the microarray. W.R.H. analyzed microarray data. L.B. and R.S. contributed transmission electron microscopy (TEM) analysis. S.W. conducted FACS analysis. D.J. assisted in time-lapse microscopy. A.K., J.G., W.R.H., R.S., and K.F. interpreted results. K.F. designed the study. A.K. and K.F. wrote the manuscript with input from all authors.

#### ACKNOWLEDGMENTS

This work was supported and funded by the RTG 1708 “Molecular principles of bacterial survival strategies” and by the Collaborative Research Center (CRC) 766, both granted by the German Research Council (Deutsche Forschungsgemeinschaft [DFG]), by the “Forschungsprogramm Bioökonomie Baden-Württemberg” (grant 7533-10-5-92A), as well as by EU FP7 Marie Curie ITN Design and Engineering of Photosynthetic Communities for Industrial Cultivation (PHOTO.COMM) 317184 (to W.J. and W.R.H.). R.S. was supported by the National Program of Sustainability (LO1416). We thank Waldemar Hauf and Björn Watzler for helpful discussions, Philipp Spät and Arne Mathews for experimental help, and Eva Nussbaum for technical assistance. We are indebted to Karen Brune for critically reading the manuscript.

Received: June 23, 2016

Revised: August 9, 2016

Accepted: August 22, 2016

Published: October 6, 2016

#### REFERENCES

1. Vitousek, P.M., and Howarth, R.W. (1991). Nitrogen limitation on land and in the sea: how can it occur? *Biogeochemistry* *13*, 87–115.
2. Kolzau, S., Wiedner, C., Rücker, J., Köhler, J., Köhler, A., and Dolman, A.M. (2014). Seasonal patterns of nitrogen and phosphorus limitation in four German lakes and the predictability of limitation status from ambient nutrient concentrations. *PLoS ONE* *9*, e96065.
3. Schwarz, R., and Forchhammer, K. (2005). Acclimation of unicellular cyanobacteria to macronutrient deficiency: emergence of a complex network of cellular responses. *Microbiology* *151*, 2503–2514.
4. Collier, J.L., and Grossman, A.R. (1992). Chlorosis induced by nutrient deprivation in *Synechococcus* sp. strain PCC 7942: not all bleaching is the same. *J. Bacteriol.* *174*, 4718–4726.
5. Krasikov, V., Aguirre von Wobeser, E., Dekker, H.L., Huisman, J., and Matthijs, H.C.P. (2012). Time-series resolution of gradual nitrogen starvation and its impact on photosynthesis in the cyanobacterium *Synechocystis* PCC 6803. *Physiol. Plant.* *145*, 426–439.
6. Allen, M.M., and Smith, A.J. (1969). Nitrogen chlorosis in blue-green algae. *Arch. Mikrobiol.* *69*, 114–120.
7. Görl, M., Sauer, J., Baier, T., and Forchhammer, K. (1998). Nitrogen-starvation-induced chlorosis in *Synechococcus* PCC 7942: adaptation to long-term survival. *Microbiology* *144*, 2449–2458.
8. Sauer, J., Schreiber, U., Schmid, R., Völker, U., and Forchhammer, K. (2001). Nitrogen starvation-induced chlorosis in *Synechococcus* PCC 7942. Low-level photosynthesis as a mechanism of long-term survival. *Plant Physiol.* *126*, 233–243.
9. Rittershaus, E.S., Baek, S.H., and Sasseti, C.M. (2013). The normalcy of dormancy: common themes in microbial quiescence. *Cell Host Microbe* *13*, 643–651.
10. Lennon, J.T., and Jones, S.E. (2011). Microbial seed banks: the ecological and evolutionary implications of dormancy. *Nat. Rev. Microbiol.* *9*, 119–130.
11. Lewis, K. (2010). Persister cells. *Annu. Rev. Microbiol.* *64*, 357–372.
12. Collier, J.L., and Grossman, A.R. (1994). A small polypeptide triggers complete degradation of light-harvesting phycobiliproteins in nutrient-deprived cyanobacteria. *EMBO J.* *13*, 1039–1047.
13. Baier, K., Nicklisch, S., Grundner, C., Reinecke, J., and Lockau, W. (2001). Expression of two *nblA*-homologous genes is required for phycobilisome degradation in nitrogen-starved *Synechocystis* sp. PCC6803. *FEMS Microbiol. Lett.* *195*, 35–39.
14. Richaud, C., Zabalun, G., Joder, A., and Thomas, J.-C. (2001). Nitrogen or sulfur starvation differentially affects phycobilisome degradation and expression of the *nblA* gene in *Synechocystis* strain PCC 6803. *J. Bacteriol.* *183*, 2989–2994.
15. Baier, A., Winkler, W., Korte, T., Lockau, W., and Karradt, A. (2014). Degradation of phycobilisomes in *Synechocystis* sp. PCC6803: evidence for essential formation of an *NblA1/NblA2* heterodimer and its codegradation by a *Cip* protease complex. *J. Biol. Chem.* *289*, 11755–11766.
16. Schlebusch, M., and Forchhammer, K. (2010). Requirement of the nitrogen starvation-induced protein *SlI0783* for polyhydroxybutyrate accumulation in *Synechocystis* sp. strain PCC 6803. *Appl. Environ. Microbiol.* *76*, 6101–6107.
17. Schreiber, U., Bilger, W., and Neubauer, C. (1995). Chlorophyll fluorescence as a noninvasive indicator for rapid assessment of in vivo photosynthesis. In *Ecophysiology of Photosynthesis*, E.-D. Schulze, and M.M. Caldwell, eds. (Springer), pp. 49–70.
18. Hauf, W., Schlebusch, M., Hüge, J., Kopka, J., Hagemann, M., and Forchhammer, K. (2013). Metabolic changes in *Synechocystis* PCC6803 upon nitrogen-starvation: excess NADPH sustains polyhydroxybutyrate accumulation. *Metabolites* *3*, 101–118.
19. Gründel, M., Scheunemann, R., Lockau, W., and Zilliges, Y. (2012). Impaired glycogen synthesis causes metabolic overflow reactions and affects stress responses in the cyanobacterium *Synechocystis* sp. PCC 6803. *Microbiology* *158*, 3032–3043.
20. Ziegler, K., Diener, A., Herpin, C., Richter, R., Deutzmann, R., and Lockau, W. (1998). Molecular characterization of cyanophycin synthetase, the enzyme catalyzing the biosynthesis of the cyanobacterial reserve material multi-L-arginyl-poly-L-aspartate (cyanophycin). *Eur. J. Biochem.* *254*, 154–159.
21. Forchhammer, K., and Watzler, B. (2016). Closing a gap in cyanophycin metabolism. *Microbiology* *162*, 727–729.



22. Labarre, J., Chauvat, F., and Thuriaux, P. (1989). Insertional mutagenesis by random cloning of antibiotic resistance genes into the genome of the cyanobacterium *Synechocystis* strain PCC 6803. *J. Bacteriol.* *171*, 3449–3457.
23. Zerulla, K., Ludt, K., and Soppa, J. (2016). The ploidy level of *Synechocystis* sp. PCC 6803 is highly variable and is influenced by growth phase and by chemical and physical external parameters. *Microbiology* *162*, 730–739.
24. Mitschke, J., Georg, J., Scholz, I., Sharma, C.M., Dienst, D., Bantscheff, J., Voss, B., Steglich, C., Wilde, A., Vogel, J., and Hess, W.R. (2011). An experimentally anchored map of transcriptional start sites in the model cyanobacterium *Synechocystis* sp. PCC6803. *Proc. Natl. Acad. Sci. USA* *108*, 2124–2129.
25. Kopf, M., Klähn, S., Scholz, I., Matthiessen, J.K.F., Hess, W.R., and Voß, B. (2014). Comparative analysis of the primary transcriptome of *Synechocystis* sp. PCC 6803. *DNA Res.* *21*, 527–539.
26. Kopf, M., and Hess, W.R. (2015). Regulatory RNAs in photosynthetic cyanobacteria. *FEMS Microbiol. Rev.* *39*, 301–315.
27. Watanabe, S., Ohbayashi, R., Shiwa, Y., Noda, A., Kanesaki, Y., Chibazakura, T., and Yoshikawa, H. (2012). Light-dependent and asynchronous replication of cyanobacterial multi-copy chromosomes. *Mol. Microbiol.* *83*, 856–865.
28. Klähn, S., Schaal, C., Georg, J., Baumgartner, D., Knippen, G., Hagemann, M., Muro-Pastor, A.M., and Hess, W.R. (2015). The sRNA NsiR4 is involved in nitrogen assimilation control in cyanobacteria by targeting glutamine synthetase inactivating factor IF7. *Proc. Natl. Acad. Sci. USA* *112*, E6243–E6252.
29. Georg, J., Dienst, D., Schürgers, N., Wallner, T., Kopp, D., Stazic, D., Kuchmina, E., Klähn, S., Lokstein, H., Hess, W.R., and Wilde, A. (2014). The small regulatory RNA SyR1/PsrR1 controls photosynthetic functions in cyanobacteria. *Plant Cell* *26*, 3661–3679.
30. Rütgers, M., and Schroda, M. (2013). A role of VIPP1 as a dynamic structure within thylakoid centers as sites of photosystem biogenesis? *Plant Signal. Behav.* *8*, e27037.
31. Azuma, M., Osanai, T., Hirai, M.Y., and Tanaka, K. (2011). A response regulator Rre37 and an RNA polymerase sigma factor SigE represent two parallel pathways to activate sugar catabolism in a cyanobacterium *Synechocystis* sp. PCC 6803. *Plant Cell Physiol.* *52*, 404–412.
32. Osanai, T., Oikawa, A., Numata, K., Kuwahara, A., Iijima, H., Doi, Y., Saito, K., and Hirai, M.Y. (2014). Pathway-level acceleration of glycogen catabolism by a response regulator in the cyanobacterium *Synechocystis* species PCC 6803. *Plant Physiol.* *164*, 1831–1841.
33. Chen, X., Schreiber, K., Appel, J., Makowka, A., Fährnrich, B., Roettger, M., Hajirezaei, M.R., Sönnichsen, F.D., Schönheit, P., Martin, W.F., and Gutekunst, K. (2016). The Entner-Doudoroff pathway is an overlooked glycolytic route in cyanobacteria and plants. *Proc. Natl. Acad. Sci. USA* *113*, 5441–5446.
34. Knoop, H., Gründel, M., Zilliges, Y., Lehmann, R., Hoffmann, S., Lockau, W., and Steuer, R. (2013). Flux balance analysis of cyanobacterial metabolism: the metabolic network of *Synechocystis* sp. PCC 6803. *PLoS Comput. Biol.* *9*, e1003081.
35. Viczián, A., Máté, Z., Nagy, F., and Vass, I. (2000). UV-B induced differential transcription of *psbD* genes encoding the D2 protein of Photosystem II in the cyanobacterium *Synechocystis* 6803. *Photosynth. Res.* *64*, 257–266.
36. Sobotka, R., Komenda, J., Bumba, L., and Tichy, M. (2005). Photosystem II assembly in CP47 mutant of *Synechocystis* sp. PCC 6803 is dependent on the level of chlorophyll precursors regulated by ferredoxin. *J. Biol. Chem.* *280*, 31595–31602.
37. García-Domínguez, M., Reyes, J.C., and Florencio, F.J. (2000). NtcA represses transcription of *gifA* and *gifB*, genes that encode inhibitors of glutamine synthetase type I from *Synechocystis* sp. PCC 6803. *Mol. Microbiol.* *35*, 1192–1201.
38. Saelices, L., Galmozzi, C.V., Florencio, F.J., and Muro-Pastor, M.I. (2011). Mutational analysis of the inactivating factors, IF7 and IF17 from *Synechocystis* sp. PCC 6803: critical role of arginine amino acid residues for glutamine synthetase inactivation. *Mol. Microbiol.* *82*, 964–975.
39. Vázquez-Bermúdez, M.F., Herrero, A., and Flores, E. (2003). Carbon supply and 2-oxoglutarate effects on expression of nitrate reductase and nitrogen-regulated genes in *Synechococcus* sp. strain PCC 7942. *FEMS Microbiol. Lett.* *221*, 155–159.
40. Espinosa, J., Forchhammer, K., Burillo, S., and Contreras, A. (2006). Interaction network in cyanobacterial nitrogen regulation: PipX, a protein that interacts in a 2-oxoglutarate dependent manner with PII and NtcA. *Mol. Microbiol.* *61*, 457–469.
41. Forcada-Nadal, A., Forchhammer, K., and Rubio, V. (2014). SPR analysis of promoter binding of *Synechocystis* PCC6803 transcription factors NtcA and CRP suggests cross-talk and sheds light on regulation by effector molecules. *FEBS Lett.* *588*, 2270–2276.
42. Stohl, E.A., Lenz, J.D., Dillard, J.P., and Seifert, H.S. (2015). The gonococcal NlpD protein facilitates cell separation by activating peptidoglycan cleavage by AmiC. *J. Bacteriol.* *198*, 615–622.
43. Sukenik, A., Kaplan-Levy, R.N., Welch, J.M., and Post, A.F. (2012). Massive multiplication of genome and ribosomes in dormant cells (akinetes) of *Aphanizomenon ovalisporum* (Cyanobacteria). *ISME J.* *6*, 670–679.
44. Stan-Lotter, H., and Fendrihan, S. (2015). Halophilic Archaea: life with desiccation, radiation and oligotrophy over geological times. *Life (Basel)* *5*, 1487–1496.
45. Bejerano-Sagie, M., Oppenheimer-Shaanan, Y., Berlatzky, I., Rouvinski, A., Meyerovich, M., and Ben-Yehuda, S. (2006). A checkpoint protein that scans the chromosome for damage at the start of sporulation in *Bacillus subtilis*. *Cell* *125*, 679–690.
46. Gupta, R.S., and Mathews, D.W. (2010). Signature proteins for the major clades of Cyanobacteria. *BMC Evol. Biol.* *10*, 24.
47. Rippka, R., Deruelles, J., Waterbury, J.B., Herdman, M., and Stanier, R.Y. (1979). Generic assignments, strain histories and properties of pure cultures of cyanobacteria. *J. Gen. Microbiol.* *111*, 1–61.
48. Klotz, A., Reinhold, E., Doello, S., and Forchhammer, K. (2015). Nitrogen starvation acclimation in *Synechococcus elongatus*: redox-control and the role of nitrate reduction as an electron sink. *Life (Basel)* *5*, 888–904.
49. Dai, G.-Z., Qiu, B.-S., and Forchhammer, K. (2014). Ammonium tolerance in the cyanobacterium *Synechocystis* sp. strain PCC 6803 and the role of the *psbA* multigene family. *Plant Cell Environ.* *37*, 840–851.
50. Pinto, F.L., Thapper, A., Sontheim, W., and Lindblad, P. (2009). Analysis of current and alternative phenol based RNA extraction methodologies for cyanobacteria. *BMC Mol. Biol.* *10*, 79.



## Curriculum vitae

Current as of December, 2018

**Name:** Lenka Bučinská

**Date of Birth:** 25.8.1985

**Nationality:** Czech

**Current address:** B. Smetany 25, České Budějovice 37001, Czech Republic

**Email:** bucinska@alga.cz

**Tel.:** + 420 384 340 444

### Academic qualifications and employment

- Ph.D. 2011 - present Ph.D. thesis: Biosynthesis of chlorophyll-binding proteins in cyanobacteria; Department of Molecular Biology and Genetics, Faculty of Science; University of South Bohemia, České Budějovice
- Bachelor (BSc.; 2007) and Master (MSc.; 2010) degree in Parasitology (Faculty of Science; University of South Bohemia, Č. Budějovice).
- Employed Apr 2011- present; Institute of Microbiology, Centre Algatech, CAS, Třeboň, Czech Republic
- 04/2008 – 12/2010 Technician in the Laboratory of Electron Microscopy, Biology Centre of CAS, České Budějovice.

### Courses and international research visit

- 2012 (18.3-23.3.) Cool runnings-cryo course, Rothamsted Research, Harpenden, UK (course of cryo techniques in electron microscopy)
- 2013 (18.09.-20.09) – DGE Course of on section immunolabeling for light and electron microscopy, Tübingen.
- 2013 (3 months), 2014 (2 weeks) and 2016 (3 weeks) research stay in the laboratory of Dr. I. Maldener (Tübingen University) and in the laboratory of Dr. H. Schwarz and Dr. M. Flötenmeyer (MPI for developmental biology, Tübingen).

### Teaching activity

- EMBO practical course in Electron Microscopy and Stereology in Cell Biology, České Budějovice. (Laboratory of electron microscopy, Biology Centre of CAS, ČB) 2008, 2012 and 2016 – The member of an organizing team
- Lectures and practical courses at Faculty of Science, University of South Bohemia

### Research interest and knowledge

Professional interests in biochemistry, electron microscopy and molecular biology in the field of photosynthesis, particularly the biogenesis of photosystems and thylakoid membrane. Employing the cyanobacterium *Synechocystis* PCC 6803 as the model organism.

- Biochemistry techniques: proteins' isolation (Flag and His affinity chromatography), separation (native-PAGE, SDS-PAGE; 1D and 2D system) and analyses (western blotting and immunolabeling)

- Molecular techniques: preparation of mutant strains of *Synechocystis* sp. (cloning, PCR)
- Microbiology techniques – cultivation work with cyanobacteria *Synechocystis* sp.
- Transmission electron microscopy (TEM): sample preparation by standard procedures, negative contrast, advanced cryo-techniques (HPF, FS), Tokuyasu method; ultra-thin, serial- and cryo-sectioning; basic operation with microscope Jeol 1010 and Tecnai G2;
- Immunocytochemistry: on section immunolabeling for TEM and fluorescence microscope
- Image processing (ImageJ; IMOD-3dmod, eTomo; Adobe Photoshop) and vector graphics (CorelDRAW)

### Grants

- 2014 – 2016 FEI grant for young scientists. Biogenesis of photosynthetic membrane in the cells of cyanobacteria.
- 2012 – 2013 Ph.D. student grant (South Bohemia university; 038/2012/P) Localization and purification of the complex important in the incorporation of chlorophyll into PS II subunits.

### Conferences:

- 15th International Symposium on Phototrophic Prokaryotes, August 2015, Tübingen, Germany (oral presentation).
- Conference of Czechoslovak microscopy society, May 2015 Lednice, Czech Republic (oral presentation)
- 18th International Microscopy Congress, October 2014, Prague, Czech Republic (oral presentation)
- Molecular Machines: Lessons from Integrating Structure, Biophysics and Chemistry May 2014, Heidelberg, Germany (poster presentation).
- Symposium - Endosymbiosis Meeting, October 2012 Munich, Germany (poster presentation).

### Publications:

- Mareš J, Strunecký O, Bučinská L, Wiedermannová J. (2019) Evolutionary patterns of thylakoid arrangement in cyanobacteria. *Front Microbiol.* Accepted.
- Bučinská L, Kiss E, Koník P, Knoppová J, Komenda J and Sobotka R (2018). The ribosome-bound protein Pam68 promotes insertion of chlorophyll into the CP47 subunit of Photosystem II. *Plant Physiol.* 176 (4): 2931-2942.
- Noda J, Mühlroth A, Bučinská L, Dean J, Bones A M, Sobotka R (2017). Tools for biotechnological studies of the freshwater alga *Nannochloropsis limnetica*: antibiotic resistance and protoplast production. *J Appl Phycol.* 29(2): 853–863.
- Klotz A, Georg J, Bučinská L, Watanabe S, Reimann V, Januszewski W, Sobotka R, Jendrossek D, Hess R W, Forchhammer K (2016). Awakening of a Dormant Cyanobacterium from Nitrogen Chlorosis Reveals a Genetically Determined Program. *Curr Biol.* 26(21): 2862-2872.

- Hollingshead S, Kopečná J, Armstrong D R, Bučinská L, Jackson P J, Chen G E, Dickman M J, Williamson M P, Sobotka R & Hunter C N (2016). Synthesis of Chlorophyll-Binding Proteins in a Fully Segregated  $\Delta ycf54$  Strain of the Cyanobacterium *Synechocystis* PCC 6803. *Front Plant Sci.* 7: 1-15.
- D'Haene S E, Sobotka R, Bučinská L, Dekker J P, & Komenda J (2015). Interaction of the PsbH subunit with a chlorophyll bound to histidine 114 of CP47 is responsible for the red 77K fluorescence of Photosystem II. *Biochim Biophys Acta-Bioenergetics.* 1847(3): 1327–1334.
- Linhartová M, Bučinská L, Halada, Ječmen T, Setlík J, Komenda J & Sobotka R (2014) Accumulation of the Type IV prepilin triggers degradation of SecY and YidC and inhibits synthesis of Photosystem II proteins in the cyanobacterium *Synechocystis* PCC 6803. *Mol Microbiol.* 93(6):1207–23.
- Kopečná J, Komenda J, Bučinská L, Sobotka R (2012). Long-term acclimation of the cyanobacterium *Synechocystis* sp. PCC 6803 to high light is accompanied by an enhanced production of chlorophyll that is preferentially channeled to trimeric photosystem I. *Plant Physiol.* 160(4): 2239-2250.